NASA Technical Memorandum 78526

Final Reports of U.S. Experiments Flown on the Soviet Satellite Cosmos 936

Susan N. Rosenzweig and Kenneth A. Souza

September 1978

NASA
National Aeronautics and
Space Administration

NASA Technical Memorandum 78526

Final Reports of U.S. Experiments Flown on the Soviet Satellite Cosmos 936

Susan N. Rosenzweig
Kenneth A. Souza, Ames Research Center, Moffett Field, California

National Aeronautics and
Space Administration

Ames Research Center
Moffett Field, California 94035

TABLE OF CONTENTS

PREFACE

On August 3, 1977, the Soviet Union launched Cosmos 936, an unmanned spacecraft carrying biological and radiaton physics experiments from nine countries, including seven from the United States. The launch marked the second time the Soviet Union has flown US experiments aboard one of its unmanned spacecraft, the first being Cosmos 782 launched November 25, 1975.

Cooperation between the US and USSR in the area of Space Biology and Medicine began in 1971 with the signing of the US/USSR Science and Applications Agreement. A Joint Working Group for Space Biology and Medicine was established and met periodically to exchange information obtained during spaceflights and to discuss problems and areas of mutual scientific interest. In October of 1974, during the fifth meeting of the Joint Working Group, the Soviets offered to fly US experiments aboard an unmanned spacecraft which was scheduled for launch during the winter of 1975. The US accepted this offer and submitted experiment proposals to the Soviets. A group of 11 experiments was selected and subsequently flown on Cosmos 782 which remained in orbit 19.5 days. Again, at the sixth meeting of the Joint Working Group for Space Biology and Medicine, in August 1975, the Soviets offered to fly additional US experiments on another unmanned spacecraft scheduled for launch during the summer of 1977. As before, US experiment proposals were submitted to the Soviets and a group of seven experiments was selected. These experiments, flown 18.5 days on Cosmos 936, August 3-22, 1977, are described in this volume.

Cosmos 782 and 936 contained experiments which were directed at determining the effects of spaceflight on a variety of biological specimens, including animals, plants, and insects. Although both of these Cosmos flights were unmanned, many of the experiments they contained focused on problems common to both man and animals during prolonged spaceflight. Rats, for example, were used to investigate alterations in normal bone chemistry, muscle structure, and general physiology resulting from spaceflight, alterations that have been observed in both astronauts and cosmonauts during and following stays in space. Rats were also used, together with a variety of other biological and nonbiological material, to measure cosmic radiation and assess its potential hazard to man during prolonged spaceflights.

As evidenced by the scientific results presented in this volume, the Cosmos 936 mission has made a substantial contribution to Space Biology and Medicine. In addition, the Joint US/USSR Biological Satellite Program has established a level of international cooperation rarely achieved in science or other fields. It has been a great pleasure to take part in this program and, on behalf of all members of the NASA and the scientific community who participated in the Cosmos 936 Mission, I would like to extend our sincere thanks to the Soviet government for making our participation possible and to our Soviet colleagues for their superb assistance in the execution of our experiments.

Kenneth A. Souza
Manager, Cosmos Project
NASA-Ames Research Center

72

N79-11672

THE COSMOS 936 MISSION

KENNETH A. SOUZA
MANAGER, COSMOS PROJECT
BIOSYSTEMS DIVISION
NATIONAL AERONAUTICS AND SPACE ADMINISTRATION
AMES RESEARCH CENTER
MOFFETT FIELD, CA 94035

ABSTRACT

On August 3, 1977, the Soviet Union launched Cosmos 936, an unmanned spacecraft carrying biology and physics experiments from 9 countries, including both the Soviet Union and the U.S. The launch marked the second time the Soviet Union has flown U.S. experiments aboard one of its unmanned spacecraft, the first being Cosmos 782 launched Nov. 25, 1975, which remained in orbit 19.5 days. Aboard Cosmos 936 were: 1) 30 young male Wistar SPF rats, 20 of which were exposed to hypogravity during flight while the remainder were subjected to a 1 x g acceleration by continuous centrifugation; 2) experiments with plants and fruit flies; 3) radiation physics experiments; and 4) a heat convection experiment. After 18.5 days in orbit, the spacecraft landed in central Asia where a Soviet recovery team began experiment operations, including animal autopsies, within 4.5 hr. of landing. Half of the animals were autopsied at the recovery site and the remainder returned to Moscow and allowed to readapt to terrestrial gravity for 25 days after which they, too, were autopsied. Specimens for U.S. experiments were initially prepared at the recovery site or Soviet laboratories and transferred to U.S. laboratories for complete analyses. An overview of the mission focusing on preflight, on-orbit, and postflight activities pertinent to the seven U.S. experiments aboard Cosmos 936 is presented.

INTRODUCTION

Cosmos 936 was the fourth in a series of Soviet Biological Satellite missions which began with Cosmos 605 in October 1973 (Table 1). As with its predecessors, the general objective of the Cosmos 936 mission was to determine the effects of spaceflight on a variety of biological specimens, focusing on biomedical problems observed during spaceflight in both men and animals, e.g., muscle atrophy, space nausea, calcium loss, and decreased total body red blood cell mass (1-4). While similar in its general objective, Cosmos 936 differed notably from previous biological satellites in that it contained two centrifuges which rotated rats throughout the flight, thus creating a unique artificial gravity environment. If the absence of gravity was responsible for some or all of the deleterious effects of spaceflight mentioned above, the artificial gravity created during centrifugation would be expected to counteract them. If, on the other hand, spaceflight-associated stresses, i.e., launch vibration, acceleration, and noise, were responsible, animals on the centrifuge would be expected to exhibit the same biomedical problems as those exposed to weightlessness.*

Nine countries participated in the Cosmos 936 mission. In addition to experiments from the US and USSR, the mission included experiments from Czechoslovakia, France, Hungary, Poland, Rumania, Bulgaria, and the German Democratic Republic. Every attempt was made to maximize the scientific return from the mission and, to this end, investigators from the nine participating countries examined virtually every organ and piece of tissue from all the specimens flown. Exemplifying such attempts were the wide variety of experiments performed on the rats. Over 70 experiments were conducted with the rats, involving over 100 scientists. A short descriptive title and the sponsoring country for these experiments is given in Table 2 which also includes other types of experiments aboard the spacecraft. Table 3 lists the participating institutions from each country.

*Although the term "weightlessness" is used here and in other reports of this volume, it is understood that complete weightlessness (the absence of all accelerations) was not achieved. The spacecraft rotated in orbit and imparted accelerations to experiments located at the edge of the spacecraft of 1.7×10^{-7} to 1.5×10^{-4} x g. Accelerations to rats were even lower because rat holding units were located near the center of the spacecraft. In any case, these accelerations are thought to be below the threshold of biological sensitivity.

TABLE 1

SOVIET BIOLOGICAL SATELLITE MISSIONS

MISSION PARAMETERS	COSMOS-605	COSMOS-690	COSMOS-782*	COSMOS-936*
LAUNCH DATE	31 OCT '73	22 OCT '74	25 NOV '75	3 AUG '77
RECOVERY DATE	22 NOV '73	12 NOV '74	15 DEC '75	22 AUG '77
MISSION LENGTH	22 DAYS	20.5 DAYS	19.5 DAYS	18.5 DAYS
PERIOD OF REVOLUTION	90 MIN.	89.6 MIN.	90.5 MIN.	90.7 MIN.
APOGEE	424 KM (261 MI)	389 KM (241 MI)	405 KM (251 MI)	419 KM (260 MI)
PERIGEE	221 KM (135 MI)	223 KM (137 MI)	226 KM (140 MI)	224 KM (139 MI)
ORBITAL INCLINATION	62.8°	62.8°	62.8°	62.8°

*U.S. PARTICIPATION IN MISSION

TABLE 2 DESCRIPTIVE TITLES AND SPONSORING COUNTRIES FOR THE EXPERIMENTS OF COSMOS 936

Title	Country
I. EXPERIMENTS WITH RATS	
Histological study of bones	USSR
Biochemical study of bone composition	USSR
Study of bone mineral composition	USSR
Determination of new bone growth and resorption; determination of bone strength and mineralization; morphological bone studies	USA
Study of mineral composition, histological structure, and growth of bone	Poland
Biochemical study of bone marrow	Czechoslovakia
Biochemical study of hydrolytic enzymes in bones	USSR
Study of chromosomal damage in bone marrow cells	Bulgaria
Histological study of bone marrow	USSR
Cytological study of bone marrow	USSR
Study of proliferative capacity of bone marrow stem cells	Czechoslovakia
Study of ectopic osteogenesis	USSR/USA
Histological, histochemical, and electron-microscopic muscle study	USSR
Biochemical investigation of protein composition, ATPase activity, and lipids in muscle	USSR
Muscle fiber analysis	USA
Biochemical study of carbohydrate metabolism and ionic composition of muscles	USSR
Study of amino acid composition of muscles, nucleotide content, glycolysis rate, acetylcholine, and cholinesterase activity	USSR
Electron-microscopic and histochemical study of muscles	Poland
Study of the mechanical properties of glycerinated muscle fibers	USSR

Table 2 Continued

Biochemical study of blood plasma	USSR
Assay of blood-plasma lipids	Czechoslovakia
Assay of catecholamines in plasma	Czechoslovakia
Biochemical study of nucleotides	Czechoslovakia
Random hemolysis and red blood cell life span	USA/USSR
Study of glycolysis and ATP in erythrocytes	USSR
Determination of hemoglobin structure	USSR
Histological study of lymphoid organs	USSR
Biochemical study of lipids and DNA in lymphoid organs	Czechoslovakia
Biological study of nucleic acids and enzymes controlling their metabolism in the spleen and thymus	USSR
Immunological studies	France
Cytochemical study of RNA and protein in spinal cord, brain, and intravertebral ganglia	USSR
Biochemical study of the cholinergic structures of the brain and spinal cord	USSR
Biochemical study of cholinesterase	USSR
Biochemical study of catecholamines and the enzymes involved in their metabolism in the hypothalamus	Czechoslovakia
Biochemical study of serotonin, histamine, catecholamines, and their precursors in the spleen, hypothalamus, and cortex of the brain	USSR
Histological study of hypothalamus	USSR
Cytochemical study of enzymes of energy metabolism in the brain	USSR
Histological study of hypophysis	USSR
Biochemical determination of cyclic AMP	Czechoslovakia
Histological study of epiphysis	Rumania
Histological and histochemical study of adrenal glands	USSR
Assay of catecholamines and the enzymes of their metabolism in the adrenal glands	Czechoslovakia
Assay of corticosterone in the adrenal glands	USSR

Table 2 Continued

Determination of corticosterone production and the response to corticotropin	Czechoslovakia
Histological study of the thyroid gland	USSR
Biochemical study of thyroid gland hormones	Czechoslovakia
Histological study of testes	USSR
Morphological and cytogenetic analysis of the testes	Bulgaria
Histological study of the kidneys and bladder	USSR
Biochemical study of the kidneys	USSR
Determination of osmotic gradient and sodium-potassium activity of ATPase	Czechoslovakia
Electron-microscopic study of the inner ear	USSR
Histological study of the lungs	USSR
Biochemical study of catecholamines and the enzymes of their metabolism in the myocardium	Czechoslovakia
Biochemical study of contractile proteins, their enzymatic activity, and lipids in the myocardium	USSR
Biochemical determination of the catecholamine content of the myocardium	USSR
Electron-microscopic study of myocardium	USSR/Poland
Electron-microscopic study of the retina	USA
Study of the enzymes which transform carbohydrates to lipids	USA
Biochemical study of lipid content of hepatic nucleic acids	Czechoslovakia
Biochemical study of the enzymes of catecholamine metabolism and other enzymes in the liver	Czechoslovakia
Biochemical study of protein synthesis in the liver	Hungary
Biochemical study of oxidative-metabolism enzymes in the liver	USSR
Biochemical study of the glycolysis rate and amino acid metabolism in the liver	USSR
Biochemical investigation of the nucleic acid content and the activity of the enzymes involved in controlling their synthesis	USSR

Table 2 Concluded

Histological study of the liver	USSR
Biochemical study of white and brown adipose tissue	Czechoslovakia
Biochemical, histological, histochemical and electron-microscopic study of submaxillary glands	USSR/Rumania
Biochemical, histological, histochemical, and electron-microscopic study of the pancreas	USSR/Rumania
Biochemical, histological, histochemical, and electron-microscopic study of the stomach	USSR/Rumania
Biochemical, histological, histochemical, and electron-microscopic study of the small intestine	USSR/Rumania
Morphological study of Fater-Pachinni bodies	USSR
II. PHYSICS EXPERIMENTS	
Heat-transfer experiment	USSR/Czechoslovakia
"Radiation" effects on a variety of biological material - "Bioblok" experiment	USSR/Rumania/France
Use of electrostatic and dielectric shielding techniques to deflect charged particles	USSR
Radiation dosimetry on-board the spacecraft - "ion dose" experiment	USA/USSR
III. EXPERIMENT WITH HIGHER PLANTS	
Morphologic and histologic studies with *Crepis capillaris* and *Zea mays*	USSR
IV. EXPERIMENT WITH LOWER PLANTS	
Morphogenesis and growth characteristics of *Phycomyces blakesleeanus*	USSR
V. EXPERIMENT WITH INSECTS	
Development, aging, and genetics of the fruit fly, *Drosophila melanogaster*	USA/USSR

TABLE 3 SCIENTIFIC INSTITUTIONS PARTICIPATING IN THE EXPERIMENTS OF COSMOS 936

Institution	Country
Ames Research Center, Moffett Field, CA	USA
Children's Hospital Medical Center, Oakland, CA	USA
Jet Propulsion Laboratory, Pasadena, CA	USA
University of Southern California Medical Center, Los Angeles, CA	USA
University of San Francisco, San Francisco, CA	USA
Veterans Administration Hospital, American Lake, WA	USA
Veterans Administration Hospital, Syracuse, NY	USA
Institute of Biomedical Problems of the Ministry of Health of the USSR	USSR
Central Scientific Research Institute of Traumatology and Orthopedics imeni Priorov of the USSR Ministry of Health	USSR
Central Scientific Research Institute of Stomatology of the USSR Ministry of Health	USSR
Institute of Evolutionary Physiology and Biochemistry of the USSR Academy of Sciences	USSR
Institute of Biochemistry imeni Bakh of the USSR Academy of Sciences	USSR
Institute of Physiology imeni Pavlov of the USSR Academy of Sciences	USSR
Central Scientific Research Institute of Gastroenterology of the Moscow Municipal Executive Committee	USSR
Institute of Medical Radiology of the USSR Academy of Medical Sciences	USSR
Institute of Nutrition of the USSR Academy of Medical Sciences	USSR
Central Scientific Research Institute of First Aid imeni Sklifasov of the RSFSR Ministry of Health	USSR
All-Union Scientific Research Institute of Electronic Standards	USSR
Institute of Aviation Medicine, Warsaw	Poland

Table 3 Concluded

Institute of Experimental Endocrinology of the Slovakian Academy of Sciences, Bratislava	Czechoslovakia
State University imeni P. Shafarik, Koshitse	Czechoslovakia
Institute of Physiology, Bucharest	Rumania
Institute of Nuclear Physics of the Atomic Energy Commission	Rumania
Curie National Scientific Research Institute of Radiobiology and Radiohygiene, Budapest	Hungary
Institute of X-Ray Technology and Radiobiology of the Medical Academy, Sofia	Bulgaria
Laboratory of Medical Biology of the Department of Medicine of Toulouse University	France
L. Pasteur Institute	France
Laboratory of Corpuscular Radiation of the Strasbourg Nuclear Research Center	France
University of Paris	France
Dosimetry Laboratory of the Fontenay-aux-Roses Center	France
Institute of Biophysics of the Czechoslovakian Academy of Science	Czechoslovakia

NOTE: Scientists from the German Democratic Republic also participated, but their institution and experiment title are not now known.

The participation in the mission of scientists from countries other than the USSR was much the same. In nearly all cases Soviet scientists were trained in the experiment-specific procedures which would be performed in the absence of the principal investigators, i.e., autopsies and tissue preparations performed by the recovery team. Following the flight, scientists from each country either analyzed their specimens in Soviet laboratories or returned to their own countries to complete their investigations. The activities performed by Soviet scientists in support of US experiments are identified and discussed below. A general description of mission operations, particularly those pertinent to US experiments, is also presented and will provide a foundation for understanding and interpreting the reports of US experiments contained in this volume. Those pre- and post-flight activities performed in support of non-US experiments and which had no impact on them, were not included.

THE SPACECRAFT

A modified Vostok spacecraft similar to that used for previous biological satellites, Cosmos 605, 690, and 782 as well as the early Soviet manned spaceflights, was used for the Cosmos 936 mission. It was a spherical craft approximately 8 feet in diameter with a 2000-lb payload and a gross weight of approximately 5000 lb (Fig. 1). During flight, most of the power required by the spacecraft was supplied by batteries. The atmosphere within the craft was maintained at approximate sea level conditions. Total pressure ranged during the mission from 745-815 mm mercury, with a pO_2 of 145-210 mm mercury and a pCO_2 of 2-4 mm mercury. Gaseous impurities generated within the cabin during flight, i.e., ammonia and methane, were kept at low levels by circulating cabin air through cannisters containing absorbent materials.

Within the spacecraft, biological specimens and experiments were contained in a variety of hardware. Of primary interest to US investigators were the rat holding units (Fig. 2). Rats were held throughout the flight in individual cages, each containing its own light, food, water, air circulation, and waste management systems. Each cylindrically shaped cage was approximately 8.2 inches deep and 3.75 inches in diameter (Figure 3). Light was regulated to a 12/12 hour light/dark cycle with a 2-lux intensity within each cage. Ten-gram quantities of a special paste diet were provided to the animals four times/day at 6-hour intervals throughout the flight. This same diet was provided to both flight and ground control animals. All animals were placed on this diet approximately 2 weeks before launch and kept on the diet throughout the flight and 25-day recovery phases of the mission. Water was provided ad libitum at all times. Cabin air was drawn through each cage from the rear and was dispersed from

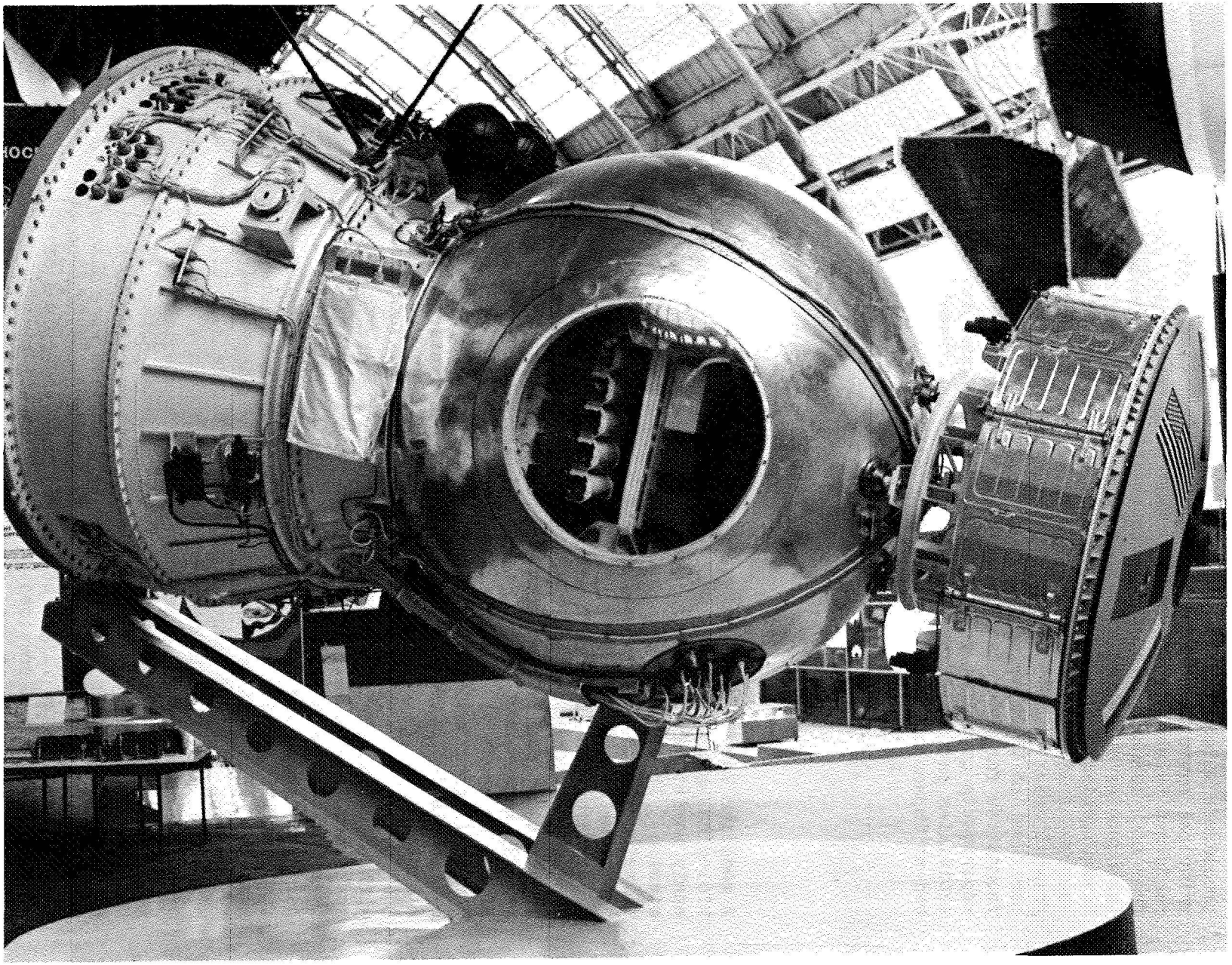

Figure 1 - Cosmos 782 spacecraft on display in the Space Museum, Astakeno, U.S.S.R. A circular viewport was installed in the spherical craft when placed on display.

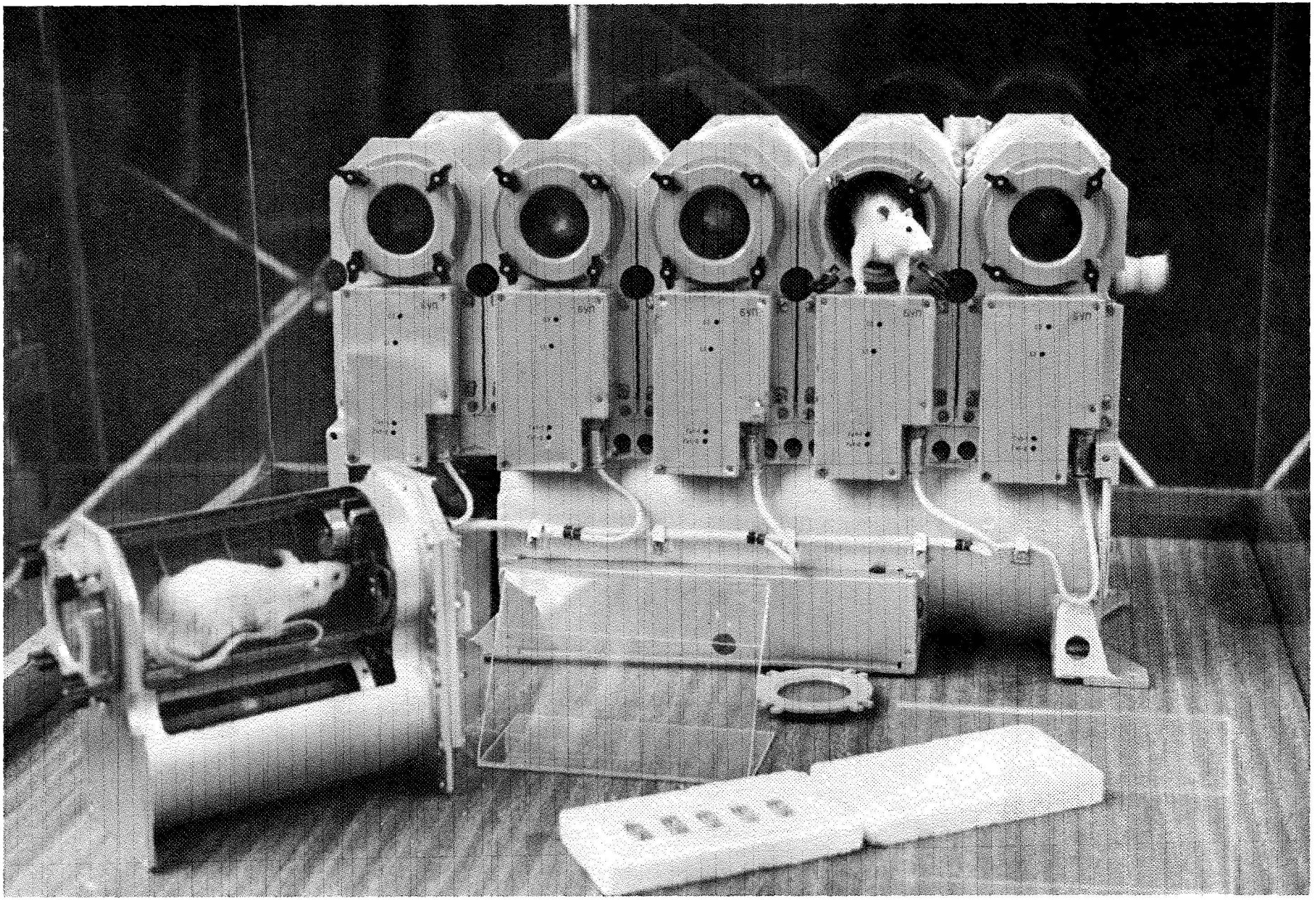

Figure 2 - Rat holding unit and individual rat cage. Four holding units were included in the Cosmos 936 spacecraft.

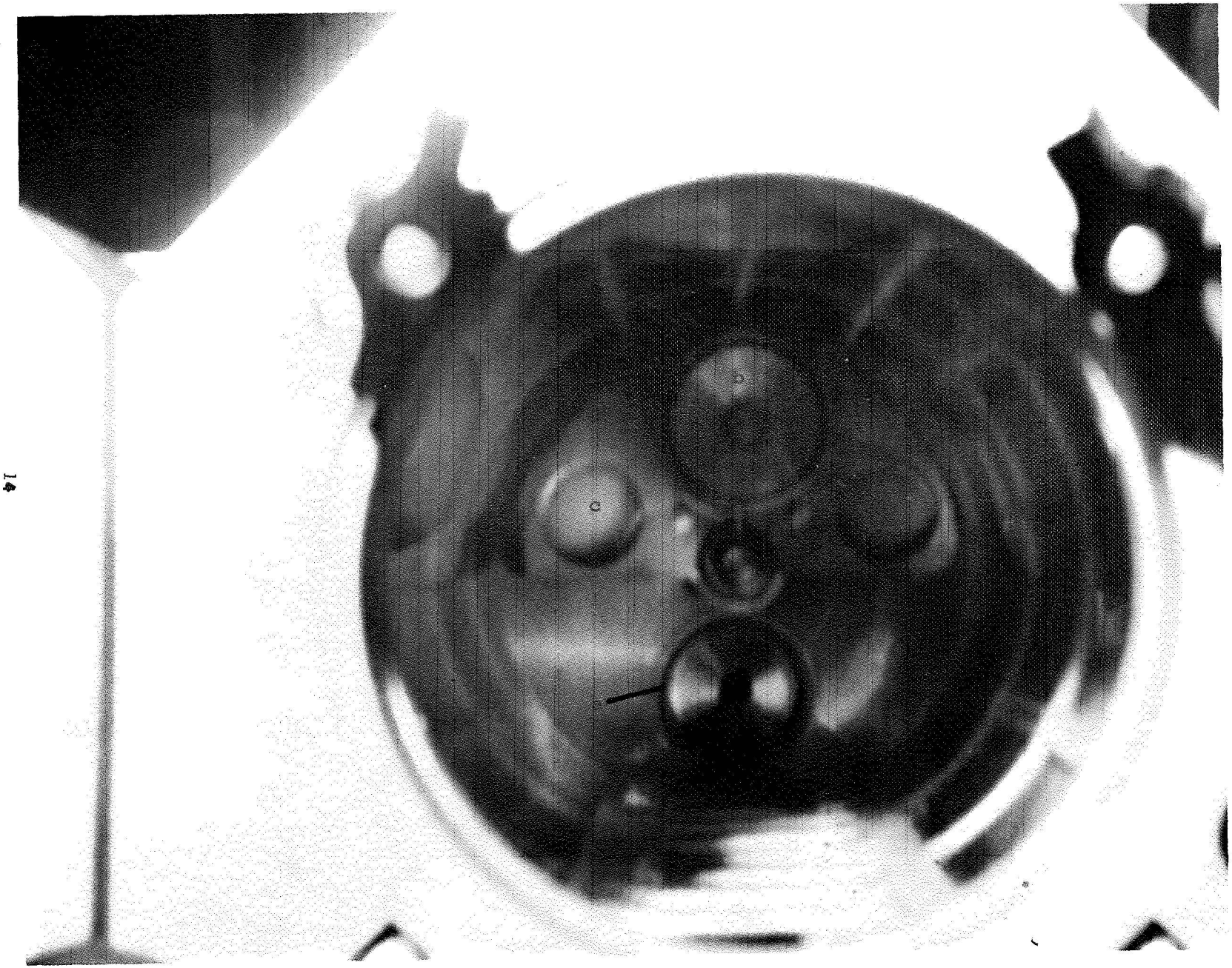

Figure 3 - Interior view of one of 5 rat cages which constituted the rat holding units on board Cosmos 782 and 936. The food, water and light sources are labeled a, b, and c, respectively.

the cage ceiling through a series of holes in a plastic cage liner. The air flow passed downward over the animal, forcing animal wastes and debris into a waste collection trap which rotated to present a clean trap to the animal at 2-day intervals. Air passing through the waste trap was then circulated through activated charcoal filters and returned to the cabin. Surrounding the plastic cage liner was a wire coil through which an electric current was passed and gross body movements of the animal could be measured.

The rat cages described above were arranged in groups of five, with each group sharing a common food and water reservoir. Only the quantity of food and water delivered to the group of five cages as a unit was measured and this only once, at the end of the experiment. Cosmos 936 contained four such units and the 20 rats housed within them constituted the group of animals exposed to weightlessness during the flight.

In addition to the 20 cages described above, the spacecraft contained 10 cages which were divided into two groups of 5 and each group placed on a centrifuge. The centrifuges were designed to provide an artificial gravity environment by rotating continuously during the flight. Each centrifuge had a radius of 32 cm as measured from the centrifuge center to the longitudinal axis of the animals during rotation. The centrifuges were switched on when the spacecraft reached its orbit and were switched off approximately 5 hours before landing. The rotation rate was 53.5 $\pm$3 rpm, which provided an acceleration of 1 x g to the animals. The five cages on each centrifuge were similar to the cages used for the weightless group of animals, differing only in that air flow through the cage was not from top to bottom, but rather, air entered the cage through holes in the cage door and depended on centrifuge rotation to force air through the cage.

PAYLOAD

The Cosmos 936 payload consisted of:

- Rats

Thirty male Wistar specific pathogen free (SPF) rats were obtained from the Institute of Experimental Endocrinology of the Slovakian Academy of Sciences, Bratislava, Czechoslovakia. The rats were approximately 62 days old and weighed an average of 215 gm at the start of the experiments. During the flight, 10 of the 30 animals were subjected to artificial gravity by continuous centrifugation; the remaining 20 were exposed to weightlessness for the full 18.5-day mission. The general objectives of the experiments with rats were to determine the effects of spaceflight on the general physiology and health of the animals and to evaluate artificial gravity, as provided by centrifugation during flight, as a means of reducing or eliminating the deleterious effects of spaceflight.

o Higher Plants

Sprouts of Zea mays and Crepis capillaris were used to study the effects of spaceflight on the duration of stages of the mitotic cycle, spontaneous mutation, and the ultrastructural organization of the basic organelles of meristem cells.

o Lower Plants

The fungus Phycomyces blakesleeanus was used to determine if spaceflight affected the growth and development of this organism.

o Insects

The effects of spaceflight on the development and aging of Drosophila melanogaster were investigated. Genetic studies were also conducted to determine if an increase in the mutation rate occurred as a result of spaceflight.

o Radiation Physics Experiments

Radiation physics experiments consisted of dosimetry experiments using biological and nonbiological materials to measure the radiation environment inside and outside the spacecraft, and radiation shielding experiments to evaluate electrostatic and dielectric techniques for reducing the level of cosmic radiation.

o Heat Exchange Experiment

An experiment was designed and flown to study the process of heat exchange between a heated surface and the spacecraft cabin air during spaceflight.

MISSION OPERATIONS

In support of the investigations aboard the spacecraft, three different types of ground control experiments were performed: the Synchronous Control, the Vivarium Control, and the Omega Bios Control. The Synchronous Control attempted to provide an environment as similar as possible to that experienced by the biological specimens during spaceflight. A spacecraft mockup was loaded with all of the experiments and specimens contained in the actual spacecraft (Figure 4). Control specimens were housed in the same type of hardware as the Flight specimens and food, water, lighting, and airflow were similar for both groups. Two centrifuges were included in the mockup and the 5 animals on each centrifuge were rotated at the same rate, 53.5 ± 3 rpm, as those centrifuged in orbit. Due to terrestrial gravity, the resultant acceleration applied to these animals was approximately 1.5 x g as opposed to the 1 x g administered to animals in orbit.

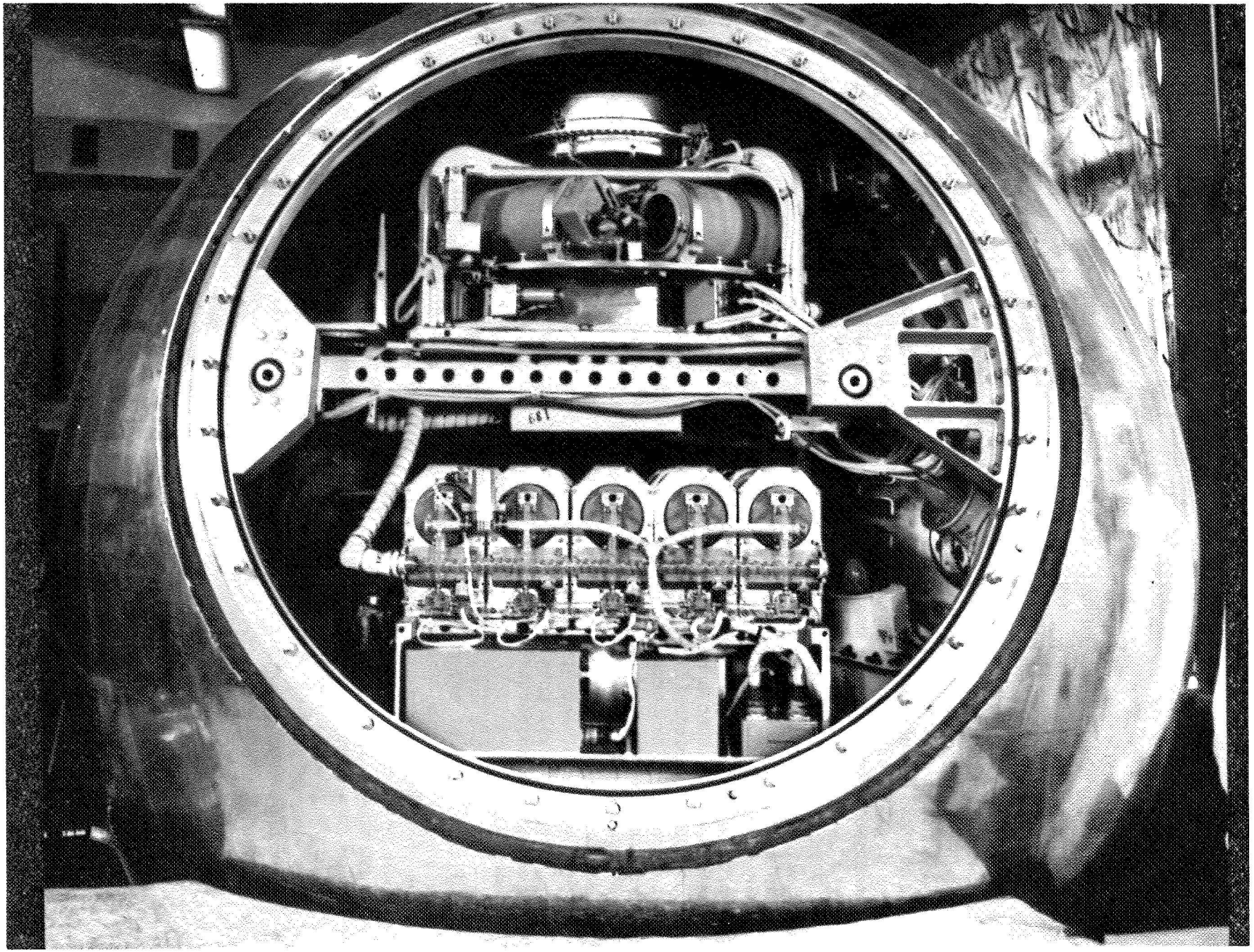

Figure 4 - Spacecraft mockup used for the Synchronous Control experiment during the Cosmos 936 mission.

Just prior to the initiation of the Synchronous Control experiment on August 7, 1977, animals were subjected to launch stresses similar to those experienced during the actual launch. The noise level was raised to 110 db and a vibration frequency of 50-70 Hz at an amplitude of 0.4 mm was applied to animal holding units for 10 minutes. Immediately following noise and vibration stresses, animals were subjected to acceleration for a period of 10 minutes with a plateau of 4 x g for 7 minutes. During the Synchronous Control experiment, the quality of the cabin air and the environmental temperature were regulated to simulate that of the orbiting spacecraft.

After completion of the control experiment on August 26, 1977, reentry stresses were applied to the animals. They were first accelerated for 5 minutes with a plateau of 6 x g for 3 minutes and subsequently subjected to an impact shock with a magnitude of 50 x g and a duration of 10 msec. Following the application of reentry stresses, the animals, as well as all other biological specimens, were handled exactly as the flight specimens.

A Vivarium Control experiment was also conducted during the mission. The purpose of this control was to provide a group of minimally stressed animals for comparison with the Flight and other Control groups. Animals were housed in standard polyvinyl cages (450 x 310 x 160 mm) in groups of 5 animals per cage and maintained in that arrangement throughout the flight and postflight periods (Figures 5, 6). A paste diet identical to that provided to the Flight and Synchronous Control animals was provided to the animals once per day in 40 gm/animal quantities during the preflight and on-orbit phases of the mission; 45 gm/animal was provided during the readaptation period. However, there was no attempt to ensure that each animal within a cage received the full portion of food allocated for each animal; thus some animals undoubtedly received more than others within the same cage.

The third control experiment, termed "Omega Bios," was designed to provide a group of animals that experienced centrifugation on the ground at the same rotation rate as those centrifuged in space, but differing from the group of animals centrifuged in the Synchronous Control experiment in that the radius of the centrifuge used for the Omega Bios experiment was 9.2 rather than 32 cm (Fig. 7). The shorter radius reduced the resultant acceleration to 1.04 x g rather than the 1.5 x g of the Synchronous Control centrifuge. The cages on both centrifuge types were identical.

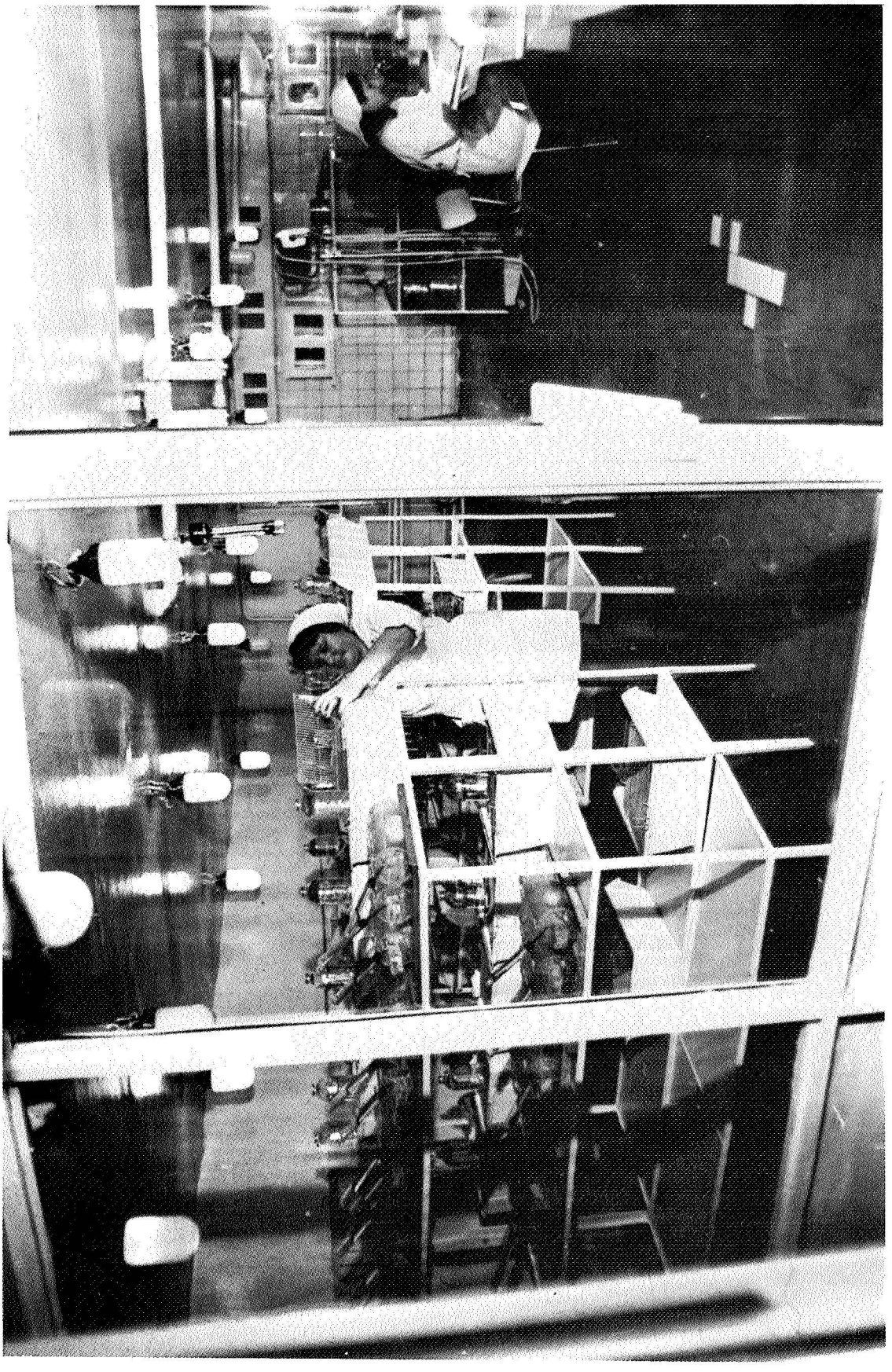

Figure 5 - Animal vivarium at the Institute of Biomedical Problems, Moscow.

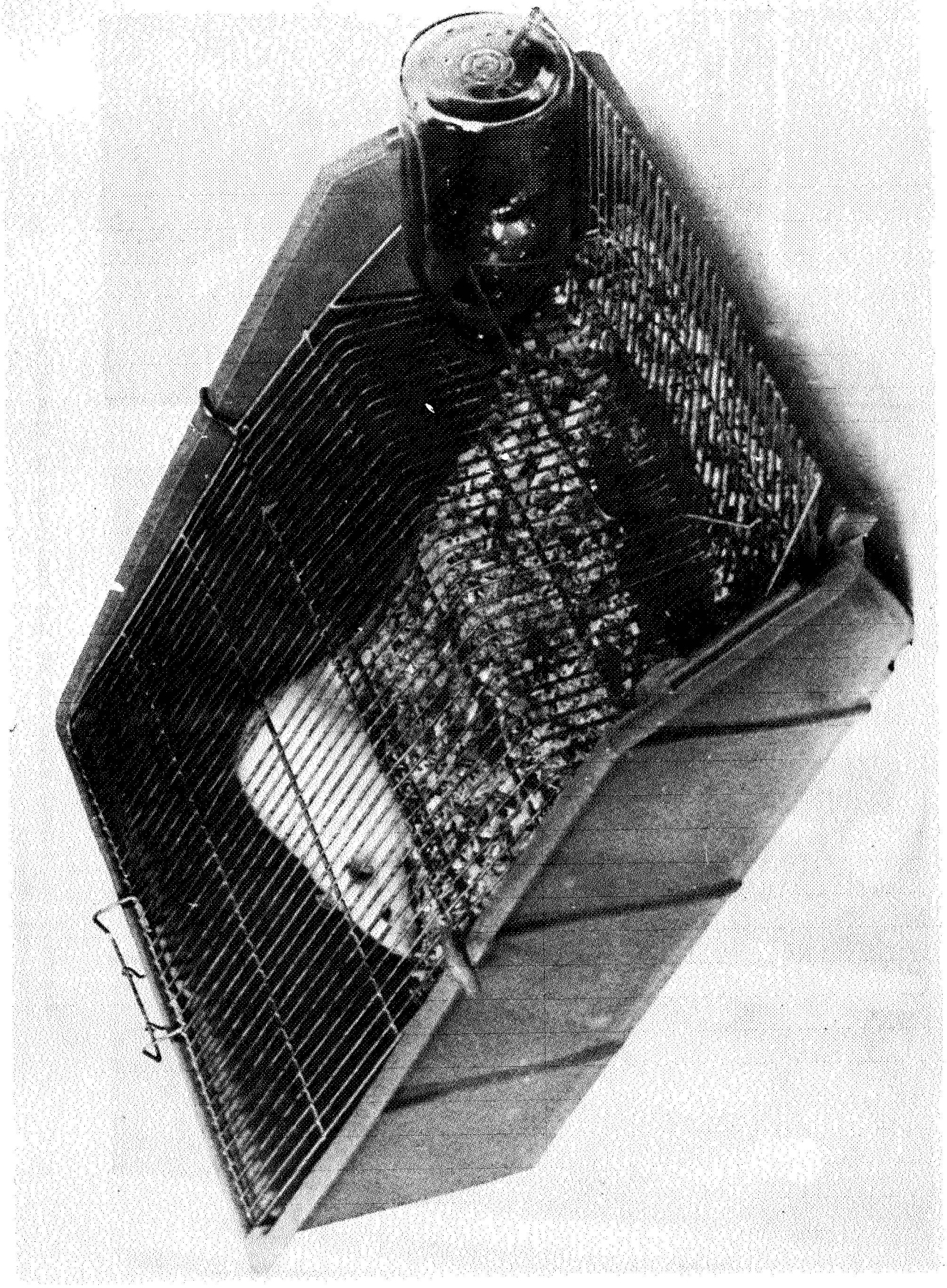

Figure 6 - Standard polyvinyl vivarium cage 450 x 310 x 160 mm.

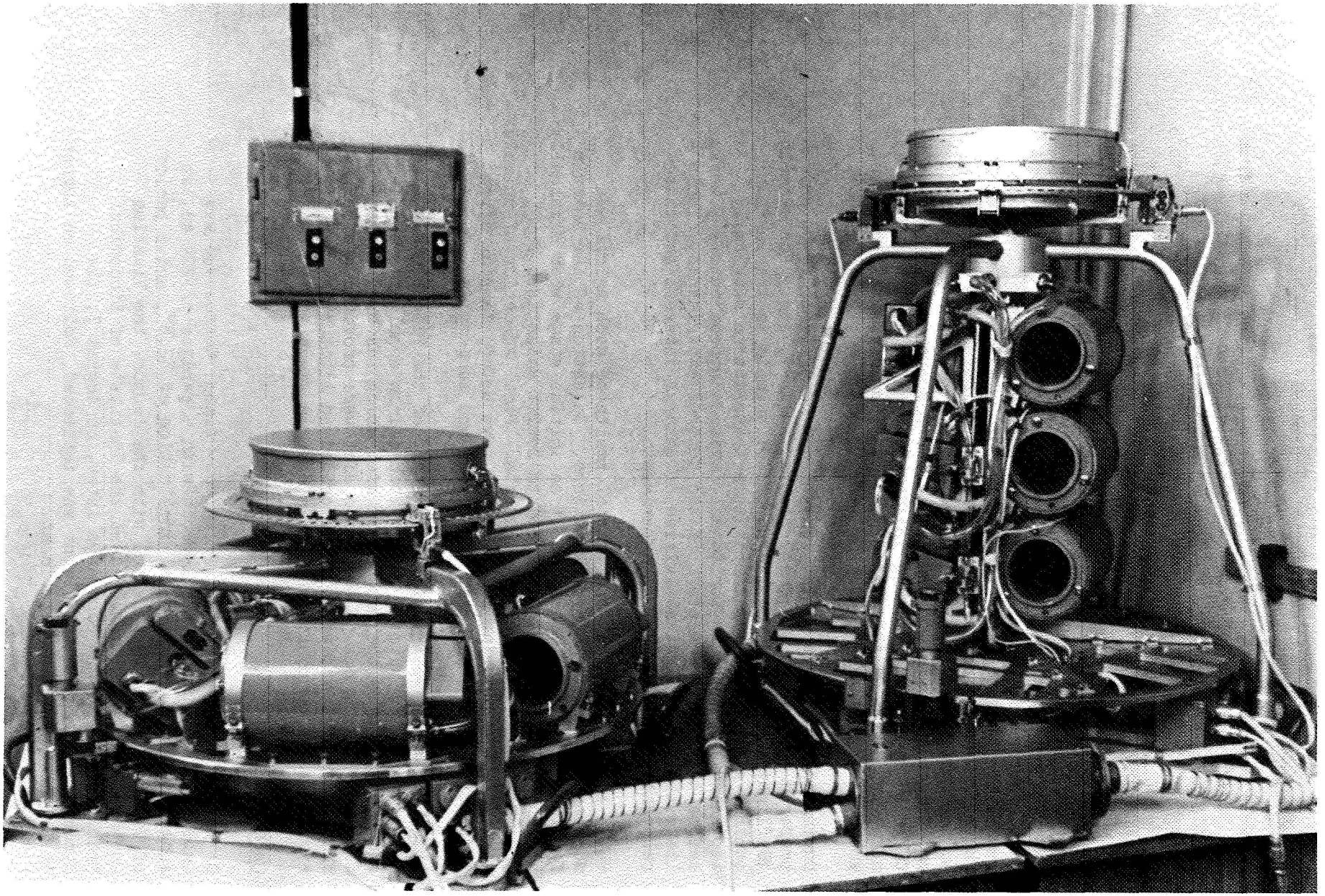

Figure 7 - Rat centrifuges used during the Cosmos 936 mission. Short radius centrifuge (on right) used for the Omega Bios Control experiment. The standard centrifuge used to provide a 1 x g acceleration to rats during spaceflight is also shown (on left).

Prelaunch Activities

On July 6, 1977, 300 Wistar SPF male rats arrived in Moscow from the Institute of Endocrinology, Slovakian Academy of Sciences, Bratislava, Czechoslovakia. The animals were placed in a vivarium at the Institute of Biomedical Problems in Moscow with 5 rats per cage, at an ambient temperature of 22 $\pm$ 2°C, relative humidity of 80 $\pm$ 5%, and a 12L/12D cycle. Of the 300 rats, 150 were born on June 1-2 and the remainder, on June 4-5, 1977. The 30 animals used for flight were taken from the older group as were most of the animals used for the Vivarium Control experiment. Animals used for the Synchronous Control and Omega Bios experiments were taken from the younger group. The main reason for the use of different ages of animals in Flight and Control experiments was the desire to use animals of approximately the same age and weight at the start of both Flight and Control experiments and, since the Synchronous Control and Omega Bios experiments were initiated 4 and 7 days, respectively, after the start of the Flight and Vivarium Control experiments, younger animals were used.

During the preflight period, Flight and Control specimens were prepared similarly, e.g., injections, surgery, etc. For example, 10 flight rats and a similar number of animals in the various control groups had body temperature transmitters surgically implanted within their peritoneal cavities approximately 3 weeks before the launch and start of the Control experiments. Table 4 lists those preflight activities of general interest and those relevant to one or more US experiments.

While in the vivarium, the general health of each animal was monitored through daily examinations. Selection of the animals for the experiments consisted of an initial stage when clinically healthy animals were transferred to Soviet scientists for preparation for specific experiments. Final selection of animals was carried out during the last few days before launch, after completion of all required injections and surgery.

Approximately 2 weeks before the start of the Flight and Control experiments, all animals were switched from a pellet/seed diet fed ad libitum to the same paste diet which was used during the flight. Forty grams of the paste diet were provided once a day for each animal and water was provided ad libitum throughout the mission. The composition of this diet is given in Table 5.

On-Orbit Activities

On August 3, 1977, at 5:00 PM (Moscow time), Cosmos 936 was launched into an elliptical orbit with a perigee of 224 km, an apogee of 429 km, an orbital inclination of 62.8°, and a period of 90.7 minutes. In parallel with the launch, the Vivarium Control experiment commenced at the Institute of Biomedical Problems in Moscow. Four days later, on August 7, the Synchronous Control experiment was initiated, followed on August 10 by the Omega Bios experiment.

Table 4 Prelaunch Experiment Activities

Date (1977)	Activity
June 1-2	Date of birth of Flight and most Vivarium Control rats
June 4-5	Date of birth of Synchronous Control and Omega Bios rats
June 28	US dosimeter package loaded into flight container
July 6	All rats placed in the Vivarium at the Institute of Biomedical Problems, Moscow
July 10	Temperature transmitters implanted intraperitoneally into appropriate Flight and Vivarium animals
July 12	Decalcified, lyophilized bone matrix implanted under the fascia of the anterior wall of the abdomen of appropriate Flight and Vivarium Control animals
July 14	Temperature transmitters implanted intraperitoneally into appropriate Synchronous Control and Omega Bios animals
July 15	^{14}C-glycine injected into appropriate Flight and Vivarium Control animals
July 18	Decalcified, lyophilized bone matrix implanted under the fascia of the anterior wall of the abdomen of appropriate Synchronous Control animals
July 19	^{14}C-glycine injected intraperitoneally into appropriate Synchronous Control and Omega Bios animals
July 20	Flight and Vivarium Control animals placed on flight diet
July 24	Synchronous Control and Omega Bios animals placed on flight diet
July 24	Approximate start of cage training; animals complete 30 hours of training before launch
July 31	Declomycin, injected intraperitoneally into all Flight, Synchronous Control, and Vivarium Control animals
August 1	Rats placed in flight cages (51 hours prelaunch)
August 1	Drosophila loaded into spacecraft (48 hours prelaunch)
August 3	Launch: 5:00 PM Moscow time, North Cosmodrome, Plesetsk, USSR
August 3	Start of Vivarium Control experiment
August 7	Start of Synchronous Control experiment
August 10	Start of Omega Bios experiment

Table 5 Composition of the Paste Diet Fed to Rats During the Cosmos 936 Mission

Constituents	Quantity, grams	Minerals	Quantity, mg/40 g of diet	Vitamins	Quantity, µg/40 g of diet
Casein	3.0	Sodium (Na^+)	82.6	B_1	64.8
		Chlorine (Cl^-)	20.4		
Corn starch	3.0	Potassium (K^+)	84.9	B_2	62.4
		Phosphorus ($P^{+3,5}$)	113.4		
Sucrose	6.7	Calcium (Ca^{++})	122.2	B_3	240
		Iron (Fe^{++})	2.1		
Sunflower seed oil	1.7	Iodine (I^-)	0.01	B_6	50.5
		Zinc (Zn^{++})	0.1		
		Copper (Cu^{++})	0.1	B_{12}	1.5
Dry brewers yeast	1.0	Cobalt (Co^{++})	0.02		
		Flourine (F^-)	0.002	E	1380
		Aluminum (Al^{+++})	0.01	A	20
Salt mixture	0.6	Magnesium (Mg^{++})	9.3	D	6
		Sulfur (S^{+6})	14.2	K	25
Water	24.0	Manganese (Mn^{++})	0.9		
				Biotin	5.0
				Folic acid	5.0
				Choline	?
				p-amino Benzoic Acid	?
				Nicotinic acid	493.6

During the 18.5-day mission, animals were fed and cared for as previously described. Total gross body movement of the Flight and Synchronous Control animals was monitored during 2-hour blocks of time every other day thoughout the 18.5 day "flight phase" of the experiments. Due to problems in the motor activity recording system, only a preliminary observation can be reported at present: the total body movement of animals in weightlessness was significantly greater than that of animals on the centrifuges.

Preliminary analysis of body temperature data from the rats showed that the lowest temperatures were recorded in the weightless group of animals. The body temperatures of the animals subjected to centrifugation during the flight tended to be slightly, but not significantly, higher than the corresponding ground control animals.

On the sixteenth day of the Synchronous Control experiment, the mockup was opened to investigate a problem which developed in the food distribution system of one of the two centrifuges. It was determined that the equipment could not be rapidly repaired and the five animals aboard the centrifuge were removed and excluded from the experiment. The hatch was replaced within 2 hours and the experiment continued for the remaining 2.5 days of the 18.5 day experiment.

Postflight Activities

On August 22, 1977, at 6:27 AM (Moscow time), Cosmos 936 touched down near the central Asian city of Kustanay. Within 45 minutes, a recovery team consisting of Soviet scientists and engineers arrived at the scene and began assembling a field laboratory (Figs. 8 and 9). The laboratory was fully deployed within 3 hours and autopsies begun at 11:00 AM. Each autopsy took about 30 minutes and approximately half the rats aboard the spacecraft were autopsied at the recovery site; the remainder were returned to Moscow and allowed to readapt to terrestrial gravity for 25 days. At 1:00 AM of the following morning, all scientific studies were completed and, at 8:07 AM, the recovery team, specimens, and equipment departed the recovery site. At 5:27 PM, August 23, experimental material and live animals arrived in Moscow.

During the return trip to Moscow, animals were kept individually in cages measuring 170 x 170 x 125 mm. The trip lasted approximately 9.5 hours and, during the trip, the animals were provided with 45 gm of the paste diet and an unlimited quantity of water. After arriving in Moscow, the animals remained in the shipping cages for an additional 19 hours, after which they were transferred to standard vivarium cages and housed in the vivarium at the Institute of Biomedical Problems (Figs. 5 and 6). Throughout the readaptation period, animals from the Flight, Synchronous Control, and Omega Bios groups were held individually in the standard cages and fed 45 gm of the paste diet supplied in

Figure 8 - Model of the field laboratory set up at the spacecraft recovery site. Electric generators and environmental control equipment provide the necessary conditions for the initial observation and examinations of biological specimens.

ORIGINAL PAGE
BLACK AND WHITE PHOTOGRAPH

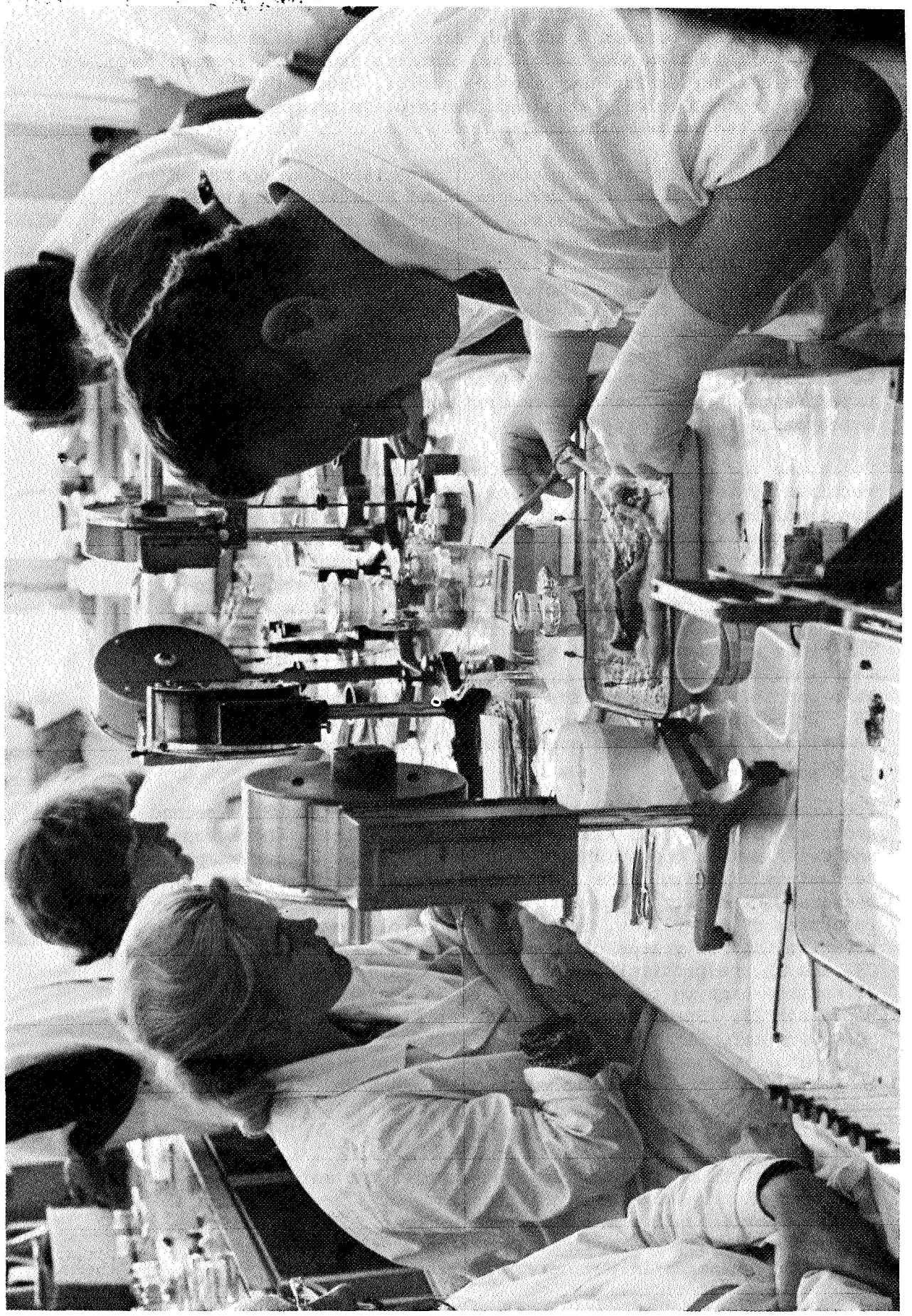

Figure 9 - Recovery team in the process of performing an autopsy and experimental procedures following the completion of the Synchronous Control experiment.

a single portion between 8 and 9 AM each day. The Vivarium Control animals also had their food quantity increased from 40 to 45 gm/animal/day during the recovery period. However, the Vivarium Control animals remained clustered in groups of five throughout the recovery period.

On August 26, the Synchronous Control experiment was completed and the same recovery team that processed Flight specimens also processed the Control specimens. Autopsies were begun at 11 AM as they were at the recovery site, and the experimental procedures employed at the recovery site were again followed. Animals used for readaptation studies were transferred to the vivarium and held for 25 days as described previously.

On August 29, the Omega Bios and Vivarium Control experiments were completed and the recovery team again followed the same experimental procedures as were used for the Flight and Synchronous Control experiments.

Following the autopsy of the rats and the unique operations required by the many investigators sharing the animals, the specimens were packed for shipment to the appropriate laboratories according to procedures worked out in advance between Soviet and US mission managers: specimens of bone, muscle, and liver were packed in dry ice for the return trip to the US; retinal tissue was immersed in a preservative in Moscow and shipped to the US at 4C in an insulated container; dosimetry materials were shipped in a specially constructed lead-lined case; and the fruit flies, Drosophila melanogaster, were hand-carried by US scientists who accompanied the shipment to the US. On September 2, US scientists and specimens arrived in San Francisco and transferred specimens to the laboratories of the US investigators.

Two weeks after the arrival of the specimens in the US, a second group of US scientists was sent to Moscow to attend the autopsies and experimental operations of the animals allowed to readapt to terrestrial gravity. The same autopsy procedures and team members were utilized for both recovery and readaptation studies. Autopsies of the Flight, Synchronous Control, Omega Bios, and Vivarium Control groups of animals occurred on September 16, 20, 23, and 23, respectively. Samples were again escorted by US scientists back to the US and arrived in San Francisco on September 25. Specimens for all US experiments, including dosimetry materials, arrived in the US in excellent condition. Temperature recorders contained in all shipping containers indicated that the temperature in each container remained within specifications throughout both trips. A summary of the above postflight operations is given in Table 6.

With the return of the experimental samples and materials on September 25, the mission operations phase was brought to an end. For the many investigators involved in the U.S. experiments aboard Cosmos 936, their work was just beginning, the results of which are contained in the seven reports which follow.

Table 6 Postflight Chronology of Events

Date	Time and Event
August 22	6:27 AM (Moscow time) - touchdown near Kustanay in central Asia
	7:15 AM - recovery team arrived and placed spacecraft in disassembly tent
	10:00 AM - field laboratory deployed
	11:00 AM - autopsies begun
August 23	1:00 AM - scientific studies end at recovery site
	8:07 AM - depart recovery site for base airport
	5:27 PM - biological specimens arrive in Moscow
August 23	US scientists arrive in Moscow
August 24	Approximately 12:30 PM, animals placed in Vivarium
August 26	11:00 AM - autopsies begun of Synchronous Control animals (4.5 hours after end of experiment, similar to flight)
August 29	11:00 AM - autopsies begun of Omega Bios and Vivarium Control animals
August 31	US Scientists and specimens depart Moscow
September 2	Scientists and specimens arrive in San Francisco
September 16	US Scientists arrive in Moscow
September 16	11:00 AM - autopsies begun of Flight animals
September 20	11:00 AM - autopsies begun of Synchronous Control Animals
September 23	11:00 AM - autopsies begun of Omega Bios and Vivarium Control animals
September 23	US Scientists and specimens depart Moscow
September 25	US Scientists and specimens arrive in San Francisco

ACKNOWLEDGEMENTS

A special thanks is owed to the many individuals who contributed to the success of the U.S. experiments flown on Cosmos 936 and particularly to: Samuel Abraham, Henry Asch, David J. Baylink, Eugene V. Benton, Kenneth R. Castleman, Lawrence P. Chambers, Luis A. Chui, William Crawford, Richard M. Farrell, Beulah P. Gossett, Lynn F. Hanold, Gladys Harrison, Rufus R. Hessberg, Joan Higgins, Emily M. Holton, Richard D. Johnson, Janice M. Kennard, Harold P. Klein, Stephen A. Landaw, Henry A. Leon, Chu Y. Lin, Robert W. Mah, Jaime Miquel, Arnauld Nicogossian, David D. Peterson, Delbert E. Philpott, Joseph C. Sharp, Richard C. Simmonds, Philip A. Thibideau, Joseph P. Van Der Meulen, Carol M. Volkmann, Darrain Waters, and David L. Winter.

REFERENCES

1. Ilyina-Kakueva, E.I., V.V. Portugalov, and N.P. Krivenkova. Spaceflight effects on the skeletal muscles of rats. Aviation, Space and Environmental Medicine. 47 : 700-703, 1976.

2. Johnston, R.S., and L.F. Dietlein (Editors). Biomedical Results from Skylab. Washington, D.C., National Aeronautics and Space Administration. SP-377. 1977.

3. Leon, H.A., L.V. Serova, J. Cummins, and S.A. Landaw. Alterations in Erythrocyte Survival Parameters in rats after 19.5 days aboard Cosmos 782. Aviation, Space and Environmental Medicine. 49 :66-69, 1978.

4. Morey, E.R., and D.J. Baylink. Inhibition of Bone Formation During Spaceflight Science, In Press.

EFFECTS OF WEIGHTLESSNESS ON THE GENETICS AND AGING PROCESS OF DROSOPHILA MELANOGASTER

Jaime Miquel, Ph.D. and Delbert E. Philpott, Ph.D.

NASA, Ames Research Center, Moffett Field, California 94035

ABSTRACT

The biological effects of space flight have been investigated on approximately 400 fruit flies (male Drosophila melanogaster Oregon R), in an experiment planned jointly with the USSR space biologist Dr. G. P. Parfenov.

The main purpose of the Soviet part of the experiment was to study the genetic effects of near-weightlessness, while our contribution was concerned with the developmental and aging processes.

Larval cultures and mature flies (imagoes) were exposed to the space environment for 18.5 days onboard the Cosmos-936 biosatellite and, after landing of the spacecraft, the containers housing various space-flown and ground control populations were sent to our laboratory.

Our studies on the Cosmos flies are in agreement with previous observations on the apparent lack of effect of hypogravity on the developmental processes of Drosophila. In effect, detailed investigation by scanning and transmission electron microscopy of flies which had developed in space showed that the external morphology and the internal fine structure of these insects was perfectly normal. This suggests that, at least in Drosophila, the mechanisms of cell division and differentiation associated with growth and morphogenesis are not appreciably influenced by the lack of gravity. On the other hand, the fly populations which had been exposed to near weightlessness during the young or middle age phases of their adult life span showed reduced vitality (expressed in negative geotaxis and mating) and a detrimental effect on longevity.

INTRODUCTION

A previous experiment from our laboratory, in collaboration with Dr.G.P. Parfenov, dealt with the effects of exposure to near-weightlessness on the embryonic development of Drosophila melanogaster of the Domodedovo strain. At launch, the flies were 4 days old, as estimated from oviposition time. The experimental Drosophila population was exposed to near-weightlessness during approximately 20 days, while an equal number of flies, which were housed in a centrifuge at approximately one-g onboard the Cosmos 782 vehicle, served as controls. After arrival to our laboratory, experimental and control flies were investigated using morphological, biochemical and behavioral techniques. As pointed out in a previous report (14), the results of that preliminary USSR-American experiment suggest that the development of Drosophila is not appreciably affected by the lack of gravity.

In the present follow-up experiment we have investigated the effects of hypogravity on the development of Drosophila melanogaster Oregon R, which is the strain routinely used in our environmental biology research. In addition, we have performed a preliminary investigation of the effects of exposure to the space environment on the aging process of Drosophila. Our results suggest that near-weightlessness may induce an acceleration of the aging process of flies which are exposed to that space condition during the adult phase of their existence. Thus, the effects of hypogravity on Drosophila aging may be similar to those of other life-shortening environmental parameters, such as moderately raised oxygen tensions (9, 17) and high ambient temperature (10).

MATERIAL AND METHODS

Exposure of Drosophila to hypogravity was performed onboard the Cosmos-936 biosatellite during approximately 18.5 days. The environmental conditions to which the flies were exposed during space flight were as follows: temperature, 21.5-24°C; illumination, 12/12, 2.0 lux; atmospheric pressure, 745-815 mm Hg; pO_2, 145-210 mm Hg; pCO_2, 1.8 mm Hg; RH, 80-90 %.

As in the previous Cosmos-782 experiment, the flies used in the development study were placed in the Soviet biosatellite, as larval cultures, in vials containing standard nutrient medium. On the other hand, the effects of hypogravity on the aging process were investigated on flies which had completed their development before launch. Two age groups of mature Drosophila were used in order to allow comparison of the effects of hypogravity on insects which are at the peak of their vitality, with others, which according to our previous studies, already show senescent loss of vigor (11,12,19) and tissue disorganization (1,5); Figures 1 and 2). The age of the various populations at launch, landing and arrival to our laboratory is shown in Table 1.

Young and middle aged flies, which hatched 4 days after the respective space-flown Drosophila were used as synchronous controls. These control flies were maintained in ground based facilities under environmental conditions as similar as possible to those of the biosatellite except for the absence of gravity and of the acceleration, vibration and shock associated with launch and landing of the spacecraft.

Table 2 shows the number of Drosophila which were delivered alive to our laboratory at the Ames Research Center at approximately 11 days after landing of the biosatellite.

On arrival, all flies were lightly etherized and weighed individually

DROSOPHILA MELANOGASTER (FRUIT FLY, X100)

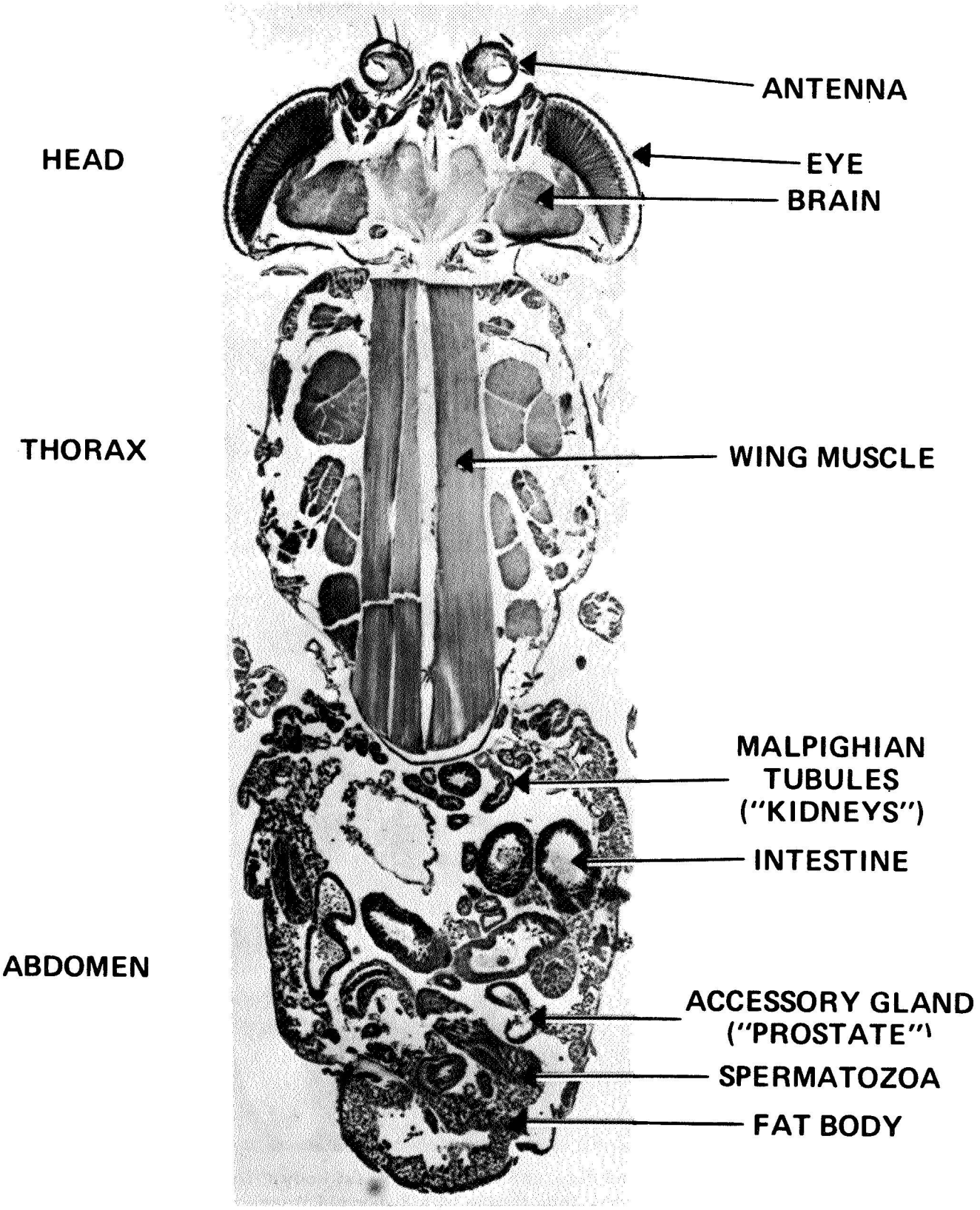

Fig. 1. Montage from our laboratory showing the perfect organization of the tissues in a young (7 day old) male imago of Drosophila melanogaster. Stain: basic fuchsin-amido-black-naphthol yellow method of Miquel et al.(7)

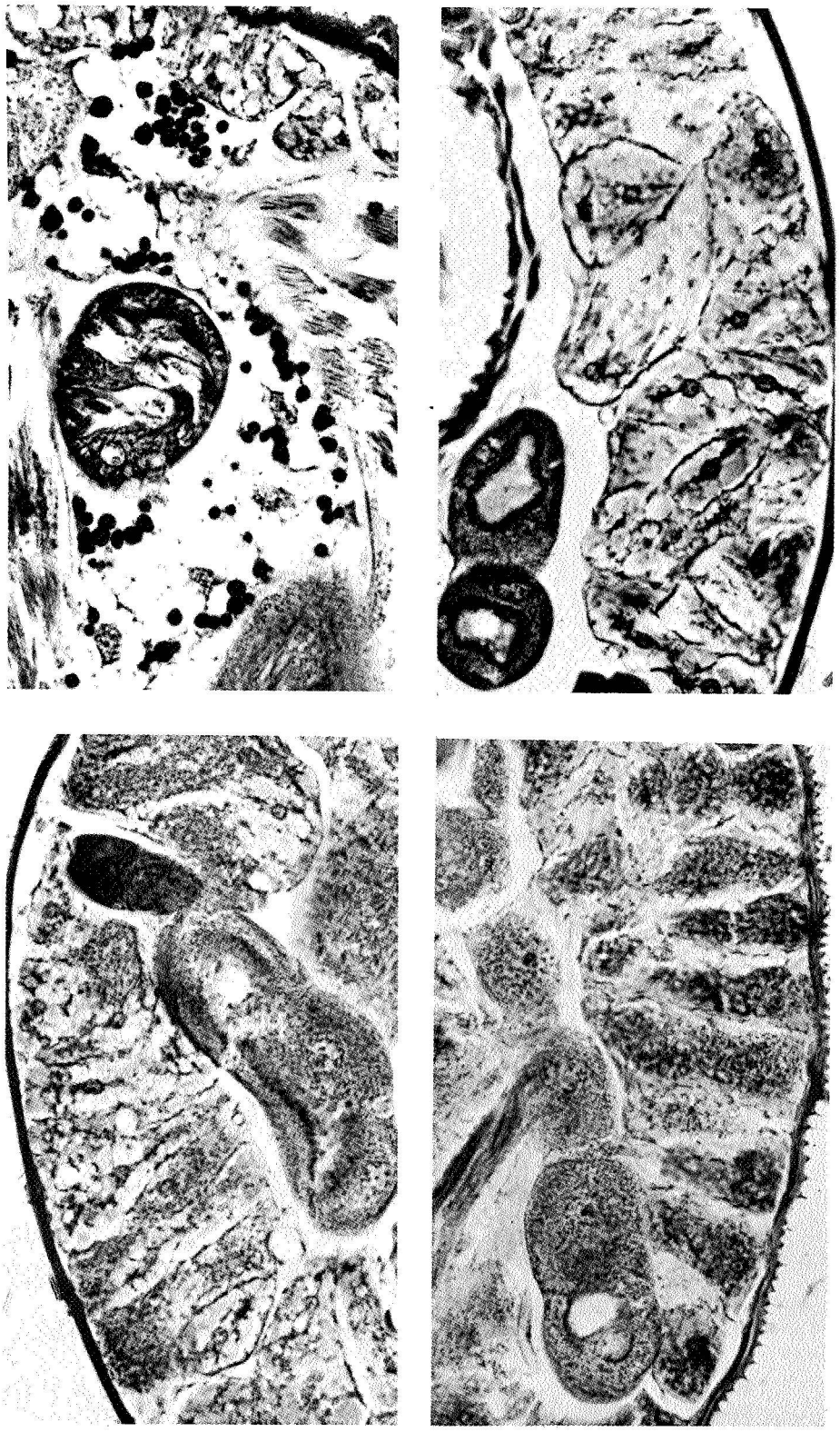

FIG. 2. Progressive age-related disorganization of the fat body ("liveradipose tissue") of control Drosophila. Upper row, left: tissue of a 2 day old imago showing the dense protein globules characteristic of immature fat body. Upper row, right: 7 day old fat body. The cells have the homogeneous appearance of the mature tissue. Lower row, left: 30 day old Drosophila. Lower row, right: 84 day old Drosophila. A comparison of these sections (stained with amido black for demonstration of proteins) shows a progressive granular disorganization of the cytoplasm. X700.

TABLE 1. Approximate age of the various Drosophila populations (days)*

	At launch	At recovery	On arrival to our laboratory
Cosmos-flown developing flies	3**	21**	32**
Young Cosmos-flown	7	25	36
Young synchronous controls	3	21	32
Middle aged Cosmos-flown	26	44	55
Middle aged synchronous controls	22	40	51

*For technical reasons, all flies with the exception of the developing population, were collected in Dr. Parfenov's laboratory in Moscow, over a five day period. Therefore, the values shown in this and the following tables for the young and middle aged flies represent mean age (±2 days).

**Age of the developing flies is given in days since oviposition. In all other populations age is indicated in days since eclosion of the imagoes.

TABLE 2. Number of flies which were found alive and body weights on arrival to our laboratory

	Number	Mean body weight (mg) ± S.E.	
Flies which completed their development onboard the biosatellite	130	730	9
Young Cosmos-flown	128	753	11
Young synchronous controls	121	758	9
Middle aged Cosmos-flown	127	734	8
Middle aged synchronous controls	130	808	9

in a Cahn electric balance. Thereafter, the flies were maintained in an air conditioned room at 24± 1°C, in half pint bottles containing 30-40 imagoes each. As in our previous studies (4-6,15) the nutrient medium, which was changed once weekly, contained corn meal, molasses and yeast in an agar base.

The space-flown and control flies were investigated as follows:

1. Determination of vitality, expressed in negative geotaxis and mating. Negative geotaxis was estimated using a glass stoppered volumetric cylinder of 250 ml fitted with a layer of soft plastic on its bottom. When shaken to the bottom by tapping the cylinder against a rubber mat, the young flies quickly run or fly to the upper region, while the old flies tend to stay on the bottom (Figure 3)). Approximately 70 flies were used for each measurement and the results were given as the percent of flies which were able to cross the 200 ml mark in 20 seconds (11). Mating competence was determined as in our previous work (12). Individual males were placed in empty vials (15 cm in length and 2.5 cm in diameter). Then, three 7-day old virgin females were placed in each tube, a cotton plug was pushed half-way into the tube and the mating behavior of the flies was observed for one hour, in order to determine the number of males able to mate in the allowed time.

2. Study of the external morphology (exoskeleton and its appendages) using a scanning electron microscope.

3. Investigation of age-associated changes in the muscle and other tissues, by transmission electron microscopy on material fixed in glutaraldehyde. As in our previous gerontological research, the emphasis was in the evaluation of mitochondrial and ribosomal changes (8, 10, 18) and age pigment increase (4, 9, 10, 13, 15, 19, 20).

4. Life span determination on approximately 70 flies from each Cosmos-flown and synchronous populations.

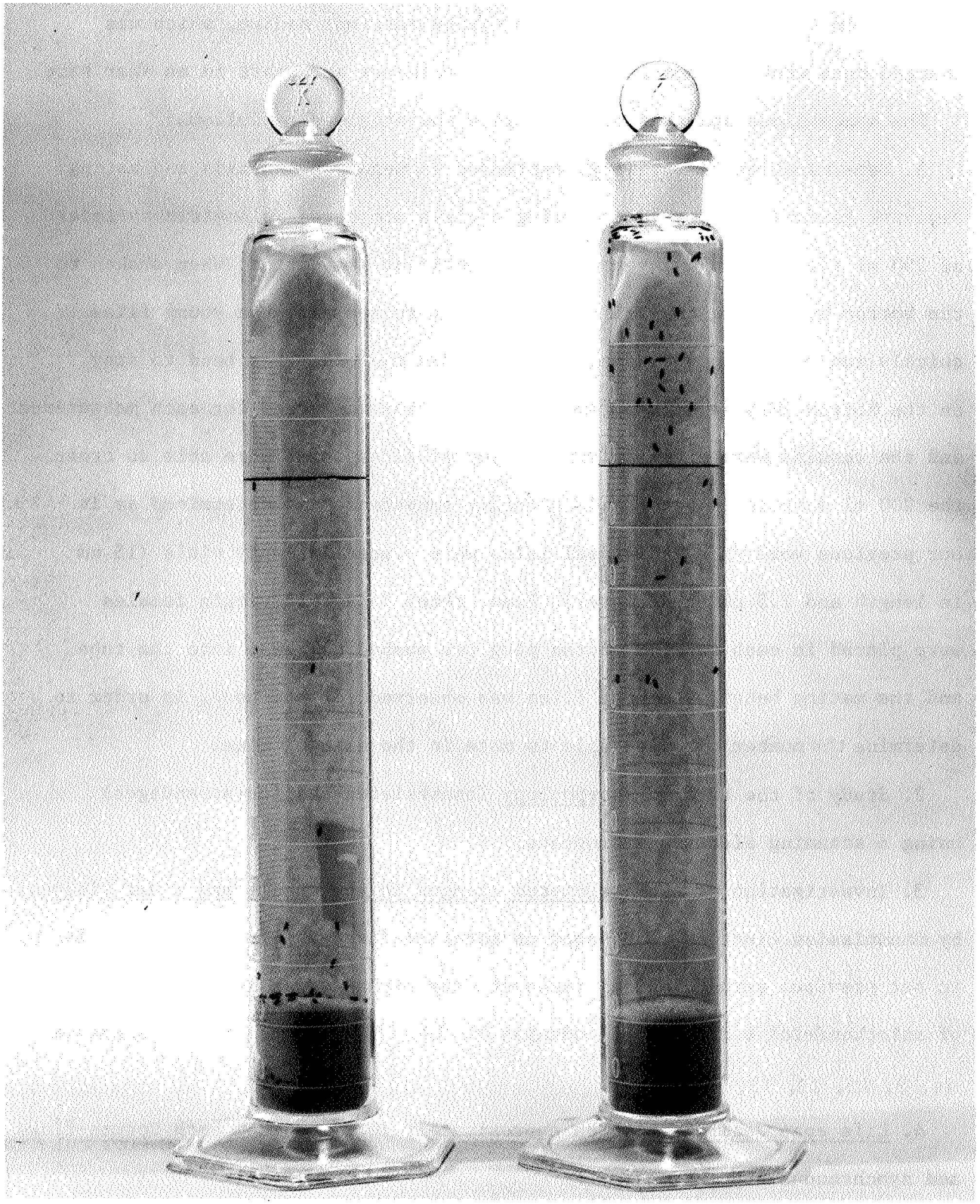

FIG. 3. Most insects, when placed in a vertical surface show an escape reaction negatively oriented with respect to earth gravity. This is illustrated by the localization of young control Drosophila in the right cylinder, following demonstration of vitality by our negative geotaxis technique (6). By contrast, the old controls in the left tube show a very diminished negative-geotactic drive.

RESULTS

Most flies from the initial population of 130 per group reached our laboratory alive and apparently in satisfactory condition. However, the lower body weights of the Cosmos-flown Drosophila as compared to the controls (Table 2) suggest that they suffered from exposure to some injurious environmental factor(s). This was particularly evident in the case of the middle aged flies.

That exposure to hypogravity or to other factors associated with space flight was somewhat detrimental to adult flies is also suggested by the lower vitality of the Cosmos-flown Drosophila as compared to the synchronous controls. This decreased performance was revealed both by the negative geotaxis and mating tests (Tables 3 and 4). Moreover, the life span of the flies which were exposed to hypogravity during the first days of their adult life ("young flies") was abnormally short (Table 5).

By contrast, our present observations by scanning electron microscopy (Figures 4-12) support our previous conclusion that insect development and morphogenesis proceed normally at near zero-g. A detailed study failed to shown any malformation of the exoskeleton or its appendages in the flies which developed in space. However, as illustrated in Figure 10, some flies (in all Cosmos-flown populations, but more frequently in the young group) showed evidence of wing injury.

Our transmission electron microscopic study has demonstrated the presence of normal mitochondria (Figure 13) both in the flies which developed in space and in those which were exposed to near zero-g as young and middle aged imagoes. On the other hand, the amount of glycogen granules in the wing muscle was strikingly lower in the Cosmos-flown young flies than in their ground controls. This was the only difference that we could detect between the fine structure of space-flown and control Drosophila. Otherwise, the histological and cytological characteristics of the flies which had been

TABLE 3. Negative geotaxis of Cosmos-flown and control Drosophila

	Age on the day of testing*	Number	Percent of "achievers"
Flies which completed their development onboard the biosatellite	31	76	28
Young Cosmos-flown	48	66	1
Young synchronous controls	44	80	38
Middle aged Cosmos-flown	67	71	5
Middle aged synchronous controls	63	79	34

*All ages are given in days since eclosion, including the estimated age for the flies which eclosed in space onboard the biosatellite.

TABLE 4. Mating competence of groups of 10 flies each of Cosmos-flown and control Drosophila*

	Age (days)	% of males able to mate
Young Cosmos-flown	41	70
Young synchronous controls	37	100
Middle aged Cosmos-flown	60	90
Middle aged synchronous controls	56	90

*The females used in this test belonged to our control Drosophila population. The age of all females was 7 days.

TABLE 5. Life span of Cosmos-flown and control Drosophila (days of imaginal life)

	Number of flies used	Mean life span ±S.E.	Maximum life span
Flies which completed their development onboard the biosatellite	78	63 1.4	89
Young Cosmos-flown	78	59 1.2	82
Young synchronous controls	77	84 1.3	106
Middle aged Cosmos-flown	73	83 1.3	102
Middle aged synchronous controls	84	91 1.4	117

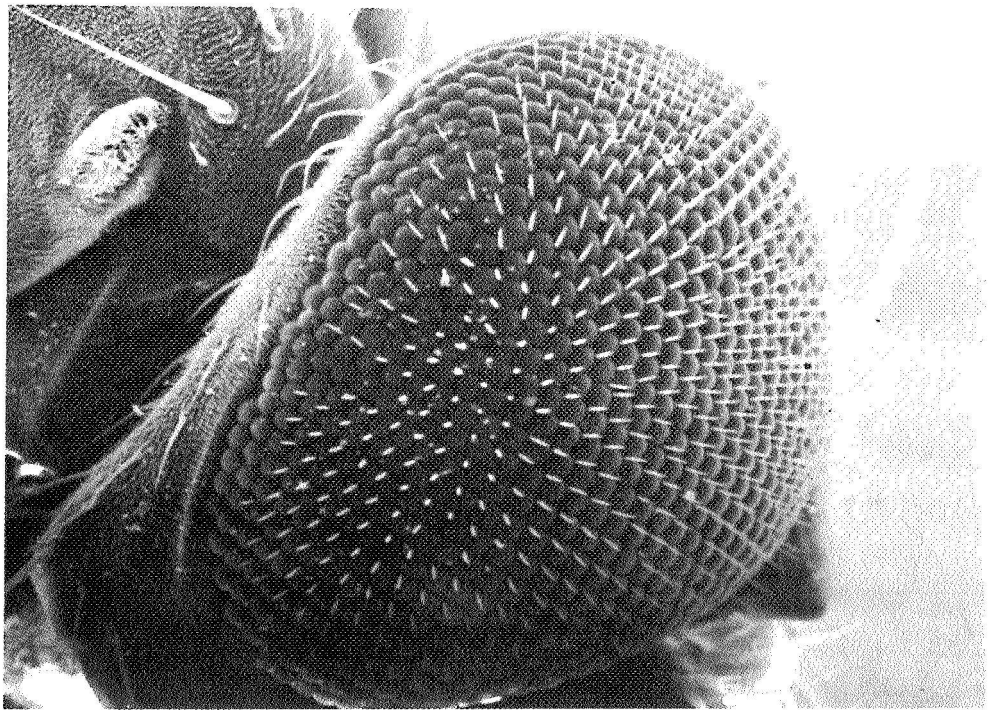

FIG. 4. Scanning electron micrograph of the head of a synchronous control fly. Notice the tracheal orifice in the thorax, immediately posterior to the compound eye. X200. The morphology of the Drosophila developed in space is identical to that in this figure.

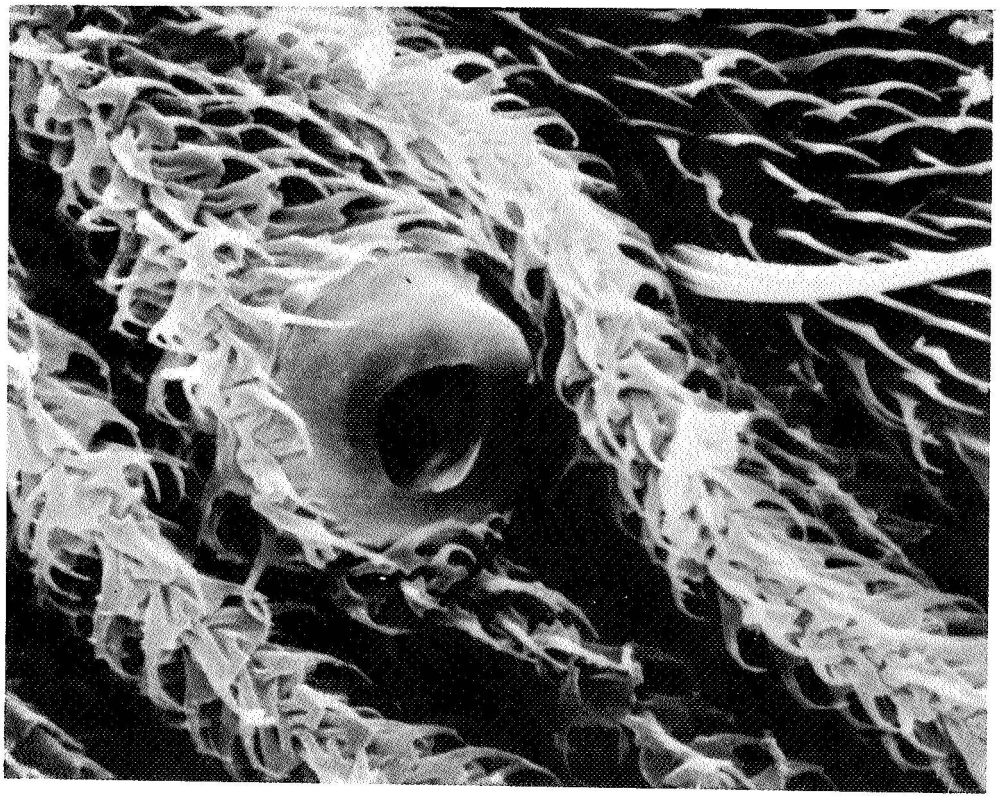

FIG. 5. External tracheal orifice from the thorax of a fly developed at near-weightlessness onboard the Cosmos-936 biosatellite. X7000.

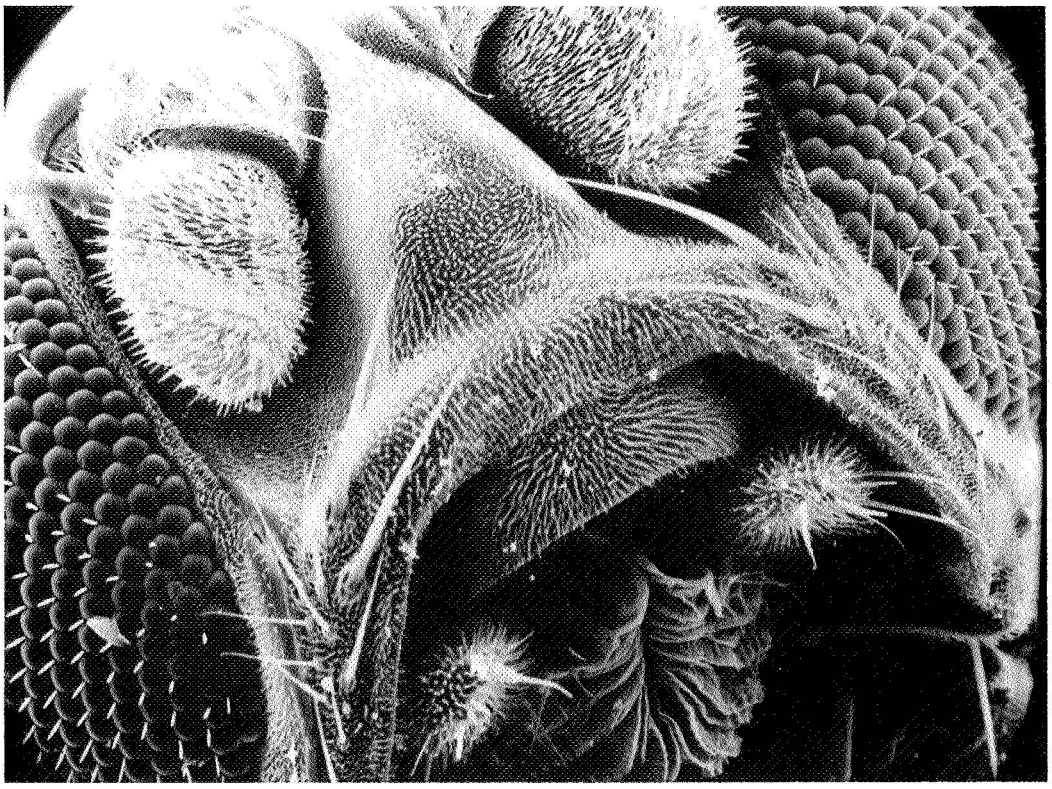

Fig. 6. Another aspect of the head of a synchronous control imago. X300.

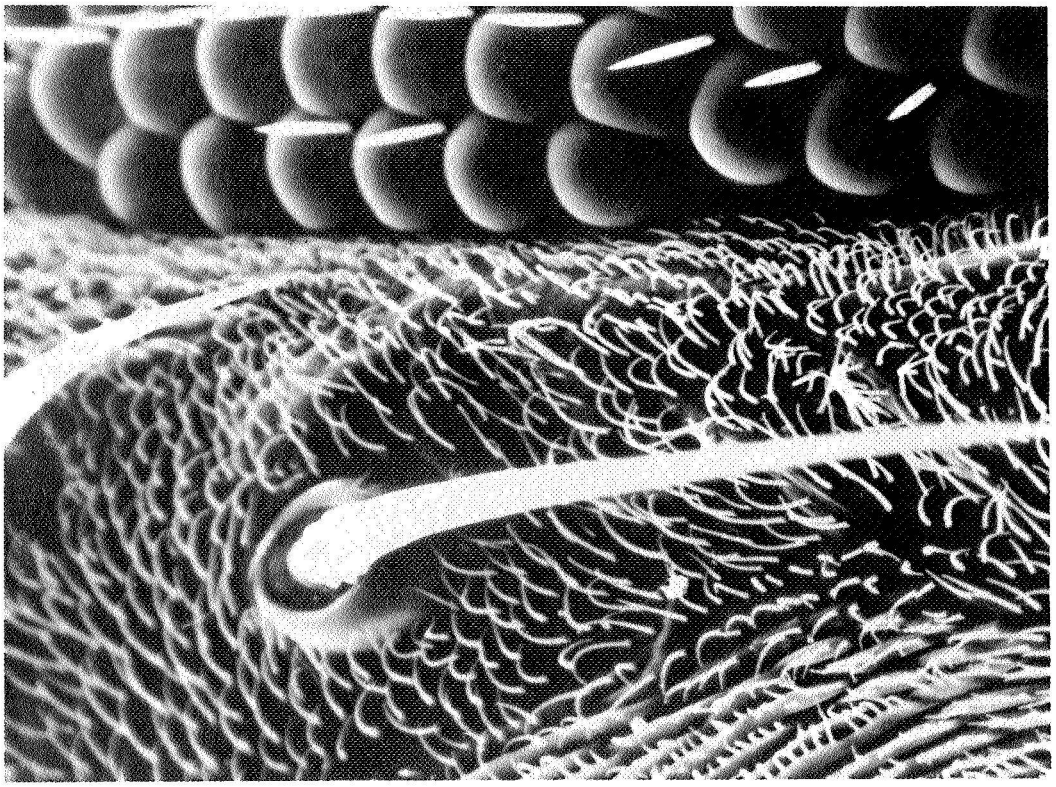

Fig. 7. Higher magnification of the external structures of the eye and adjacent exoskeleton from the same fly shown in the preceding figure. X1200.

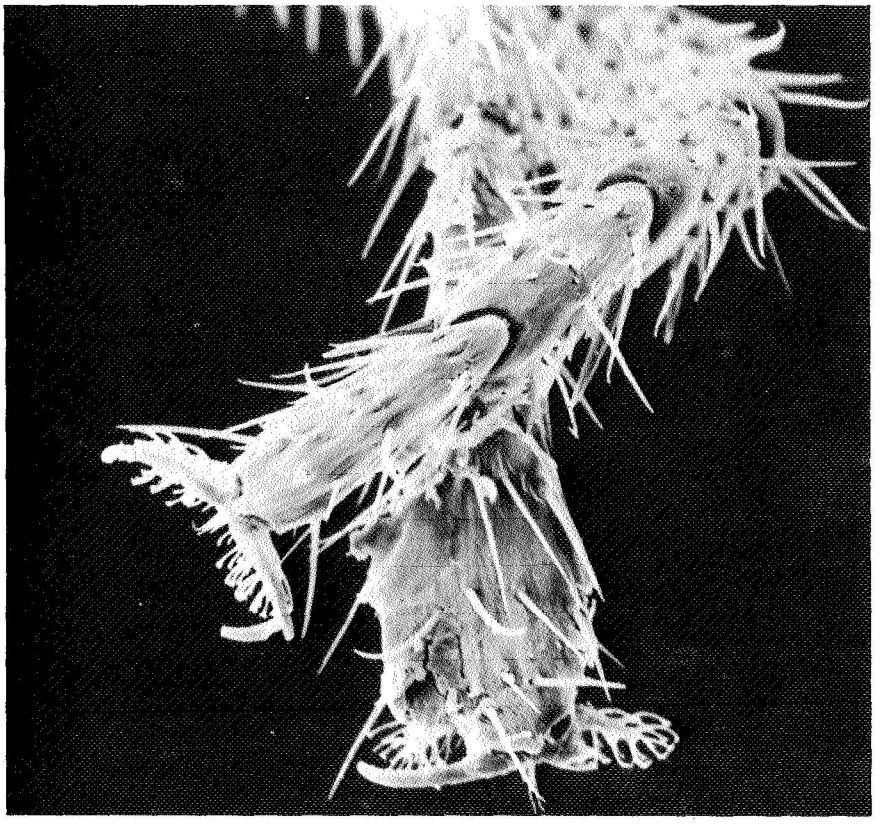

Fig. 8. Scanning electron micrograph of synchronous control Drosophila X500.

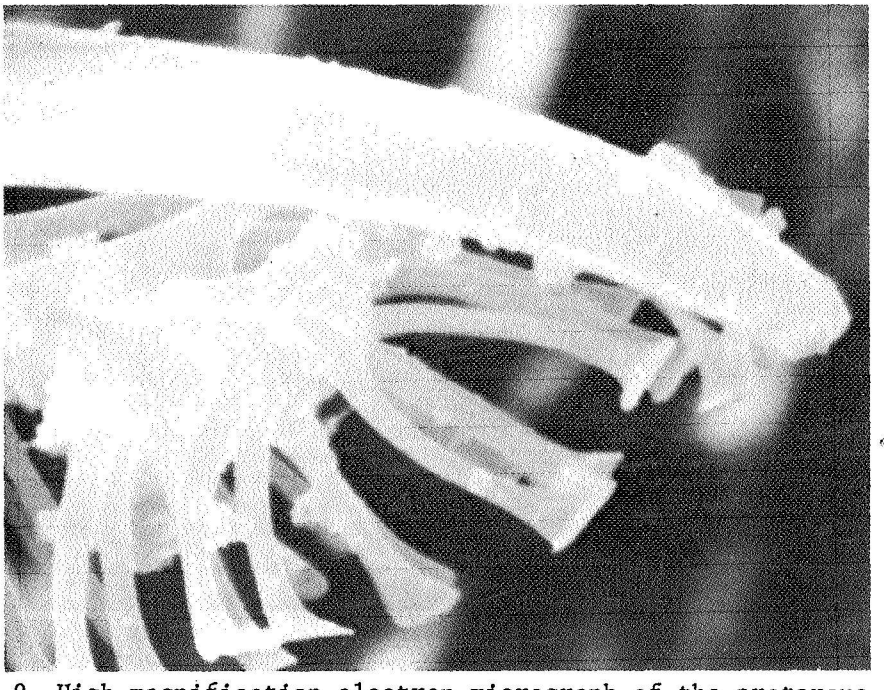

Fig. 9. High magnification electron micrograph of the pretarsus ("foot") shown in the preceding figure. X7000.

Fig. 10.Wing injury in a Cosmos-flown fly which was sent into space at 7 days of age. X1500.

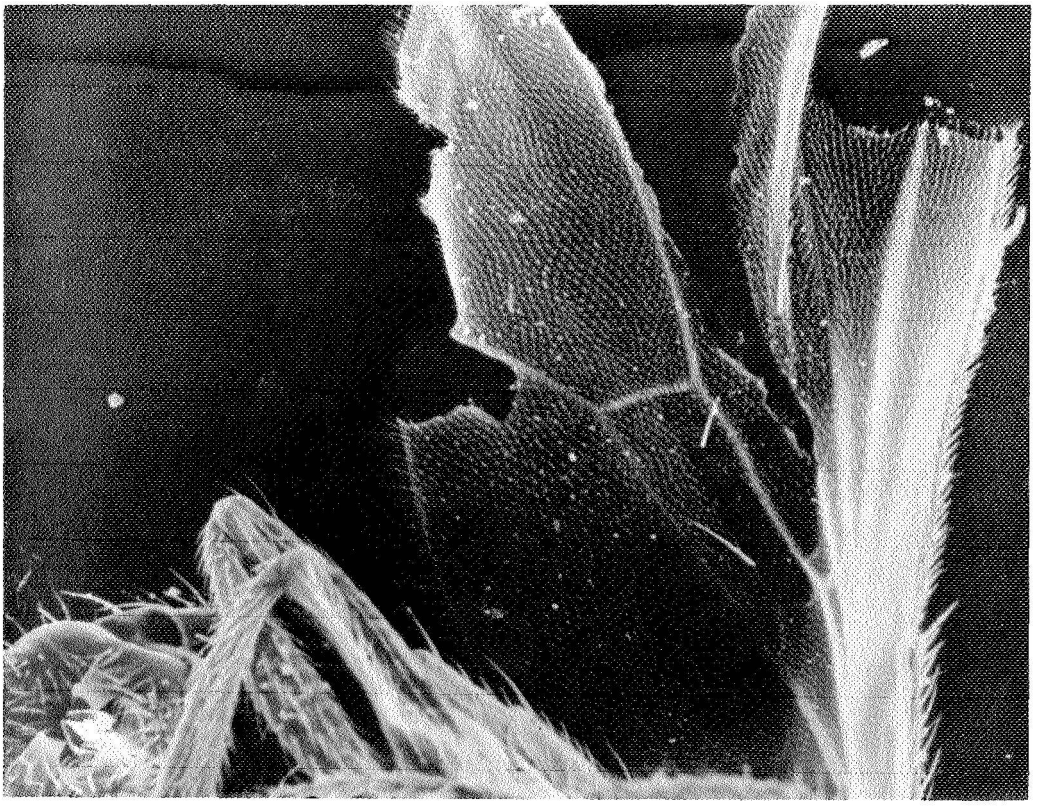

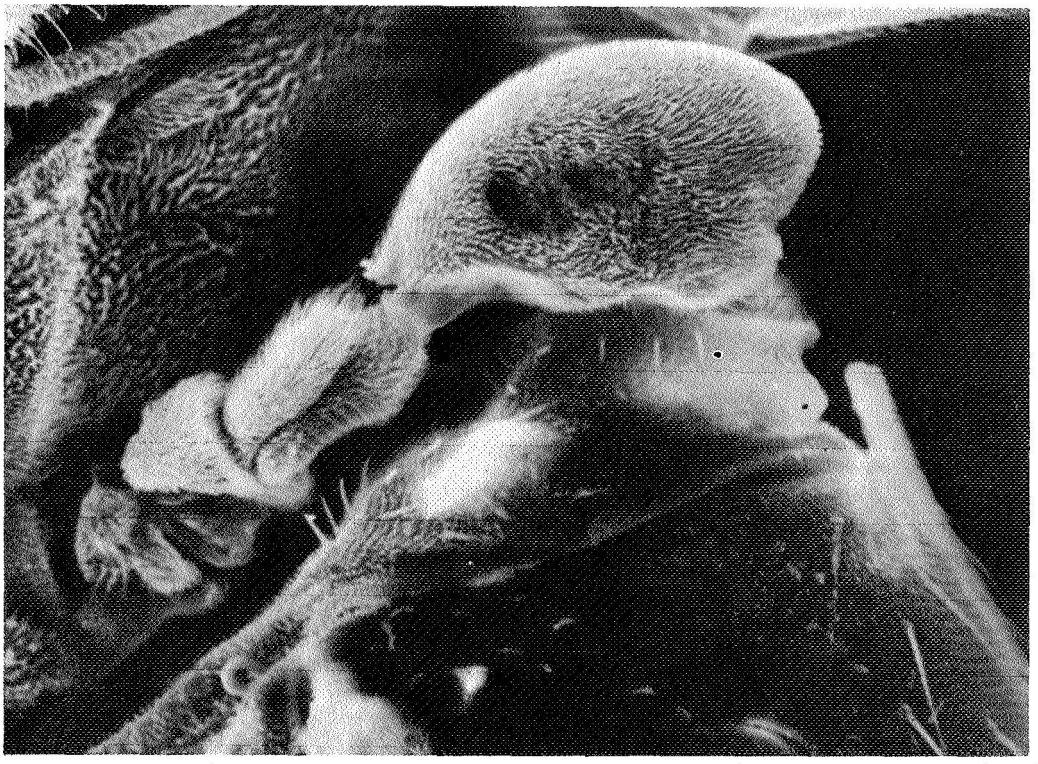

Fig. 11. Haltere (organ involved with postural control,acting as a mechanical gyrostabilizer during Drosophila flight) showing a perfectly normal morphology in a fly which developed in near-weightlessness. X300.

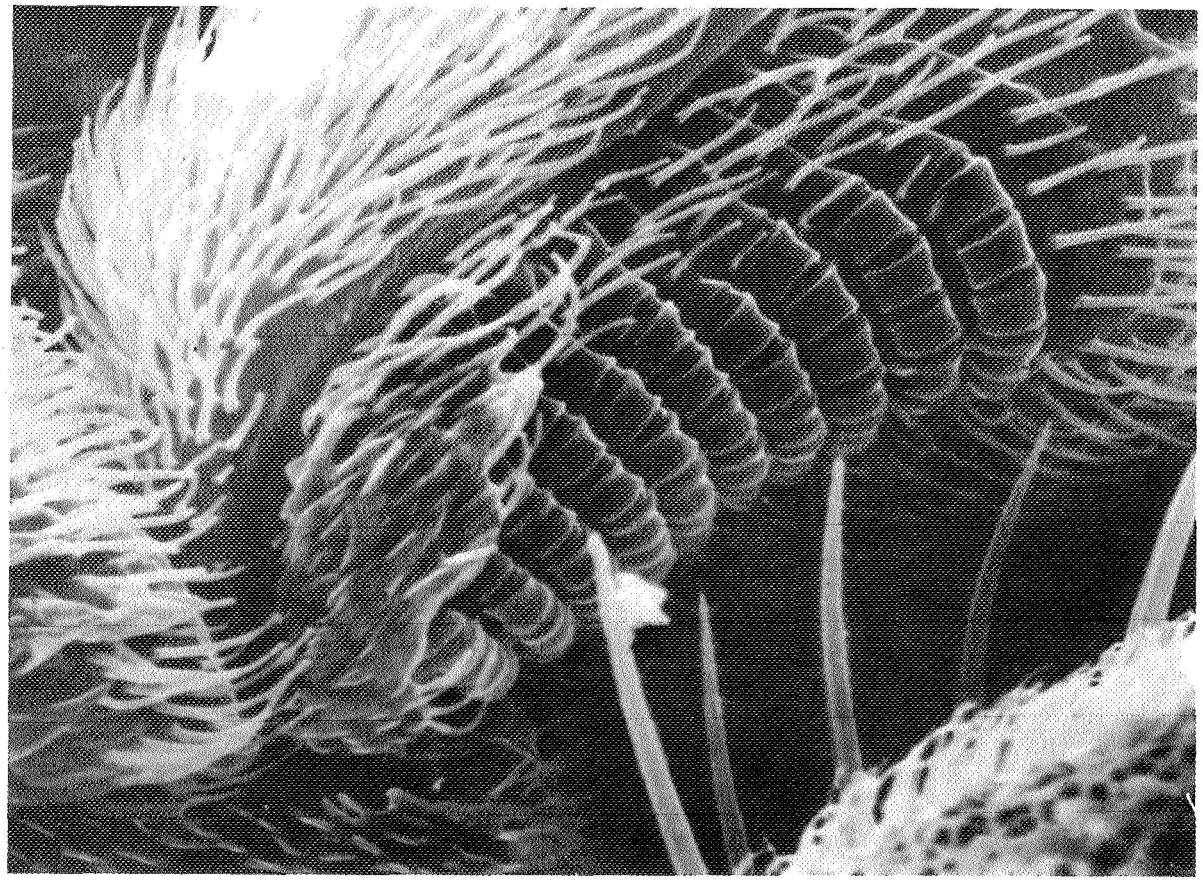

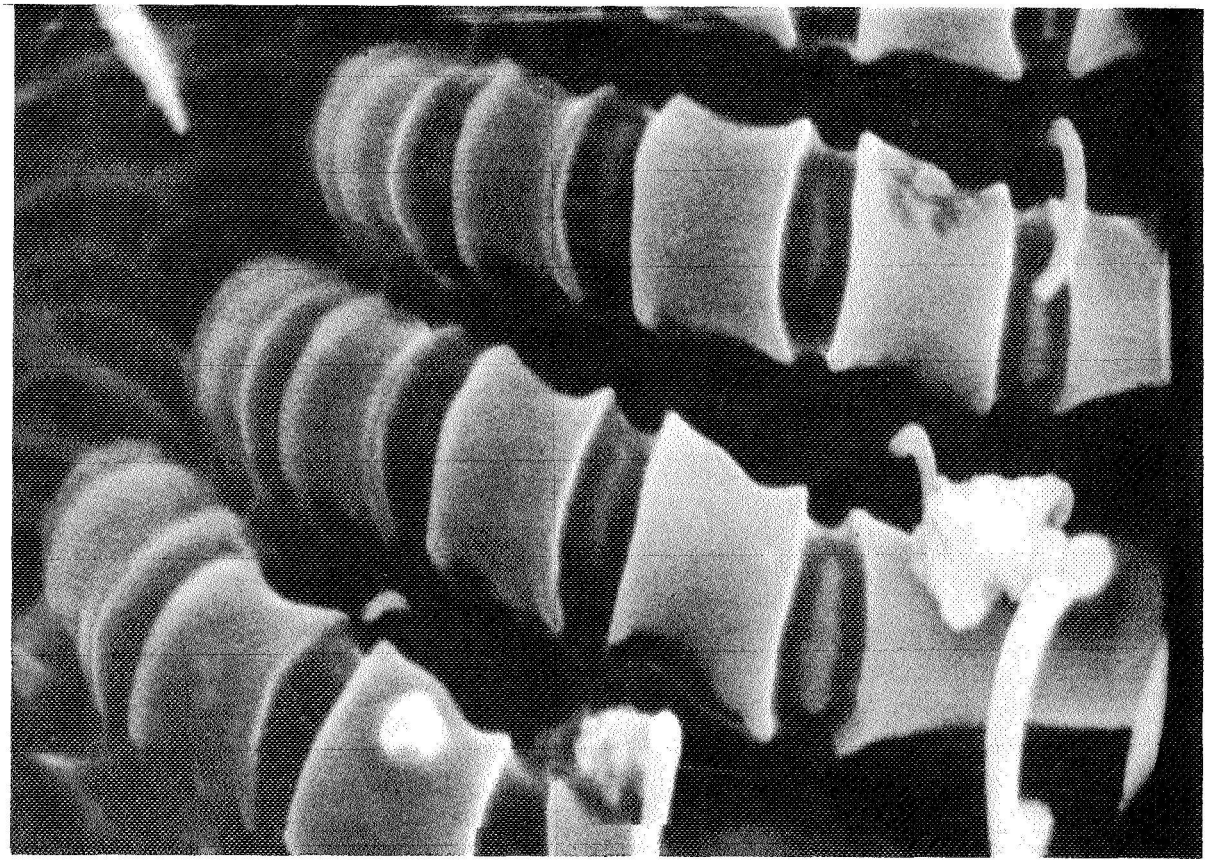

Fig. 12. Higher magnifications of the structures shown in the preceding figure. Above:X3000. Below: X7000.

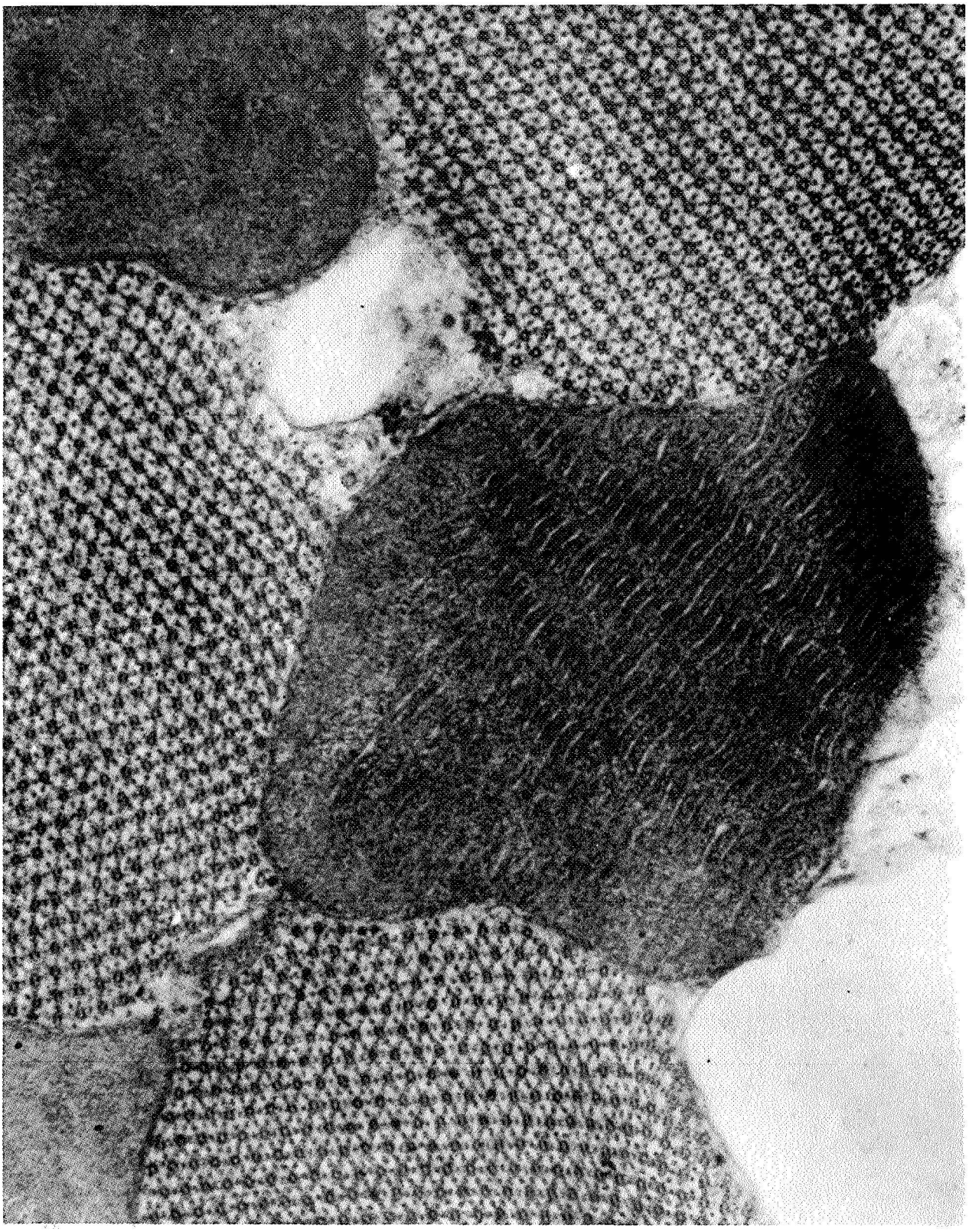

Fig. 13. Transmission electron micrograph of the wing muscle of a control *Drosophila* showing giant mitochondria and myofibrils in cross section. X170,000. These structures are well preserved in flies developed in space and in those exposed to near zero-g as imagoes, as well.

exposed to near zero-g were undistinguishable from those of ground controls of about the same age. This was ascertained in the case of the fat body ("liver-adipose tissue"), intestine (Figure 14) Malpighian tubules ("kidneys") and testes (Figure 15).

DISCUSSION

As regards embryonic development, our present findings are in perfect agreement with previous research by Antipov and Parfenov (cited by Wukelic, 21) and with our own observations on Cosmos-782 flies (14) suggesting that near-weightlessness does not seriously interfere with the developmental processes of Drosophila. On the other hand, the reduced vitality and the short life span manifested by the flies which were exposed to hypogravity during the first days of their imaginal life suggests that the aging process of Drosophila may be accelerated during space flight. In our opinion, the mechanism involved is a probable stress-associated increase in the level of activity of the flies, which would result in a raised O_2 utilization and a concomitant life shortening because of an accelerated senescence of the organs necessary to maintain life. This working hypothesis is supported by the presence of damaged wings in the Cosmos-flown Drosophila, which, in our opinion, probably result from disturbed fly behavior in the absence of gravity. Young imagoes placed in a near zero-g environment may be stressed by the inability to control flight, in agreement with previous observations on the behavior of butterflies during parabolic flights in aircraft. This disturbed behavior probably results in wing injury if the insects hit the container walls.

The above concept is in agreement with studies showing that gravity plays a fundamental role in the orientation of insects (3). In effect, it has been shown that ants and bees, when standing still on a vertical plane, react to every turn of their dorsoventral axis by turning in the opposite direction. This reaction does not take place when the gravity receptors have been

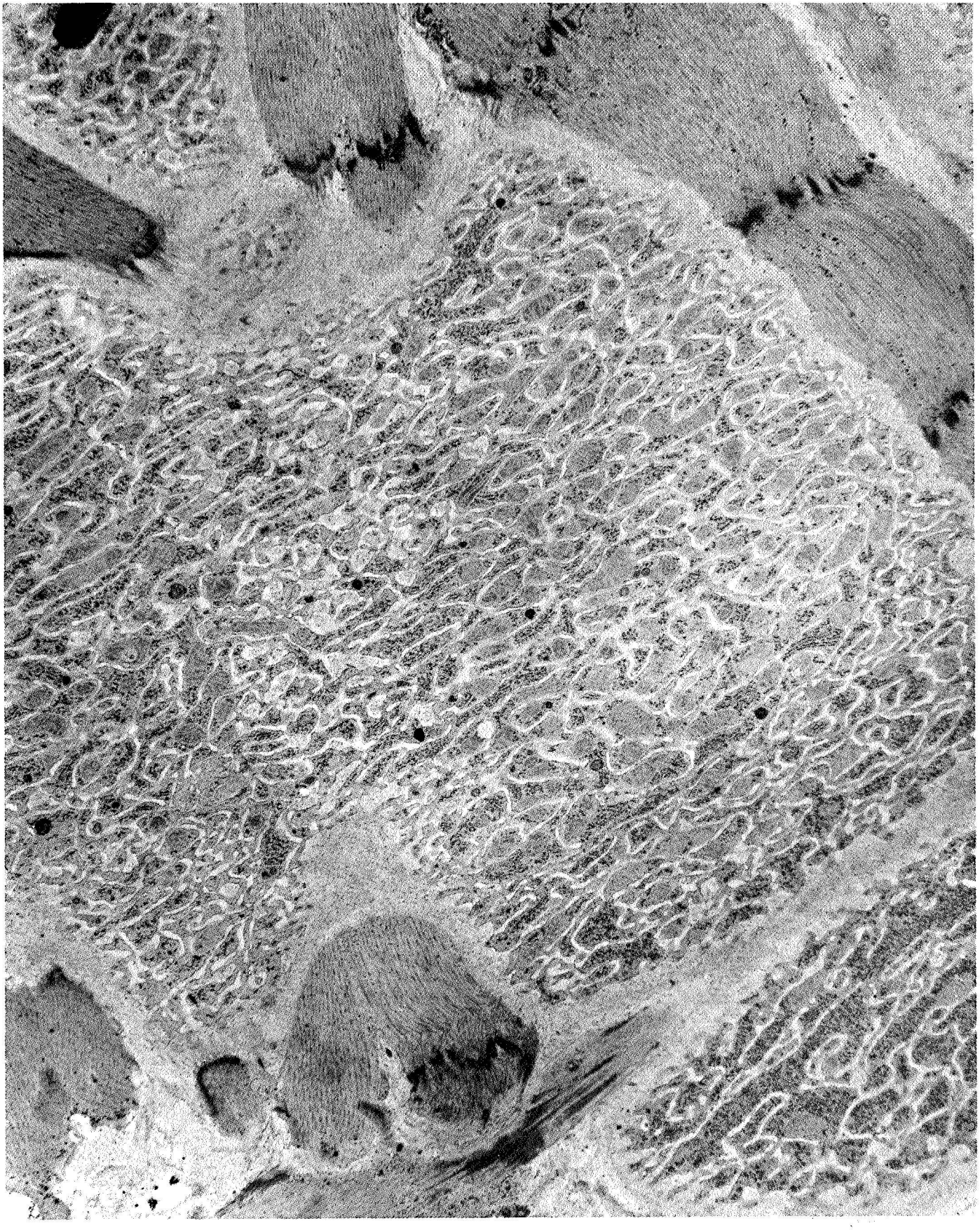

Fig. 14. Posterior intestine of a fly which developed in space, at 75 days of age. X13,650. The fine structure is identical to that of the intestinal cells of ground controls of the same age.

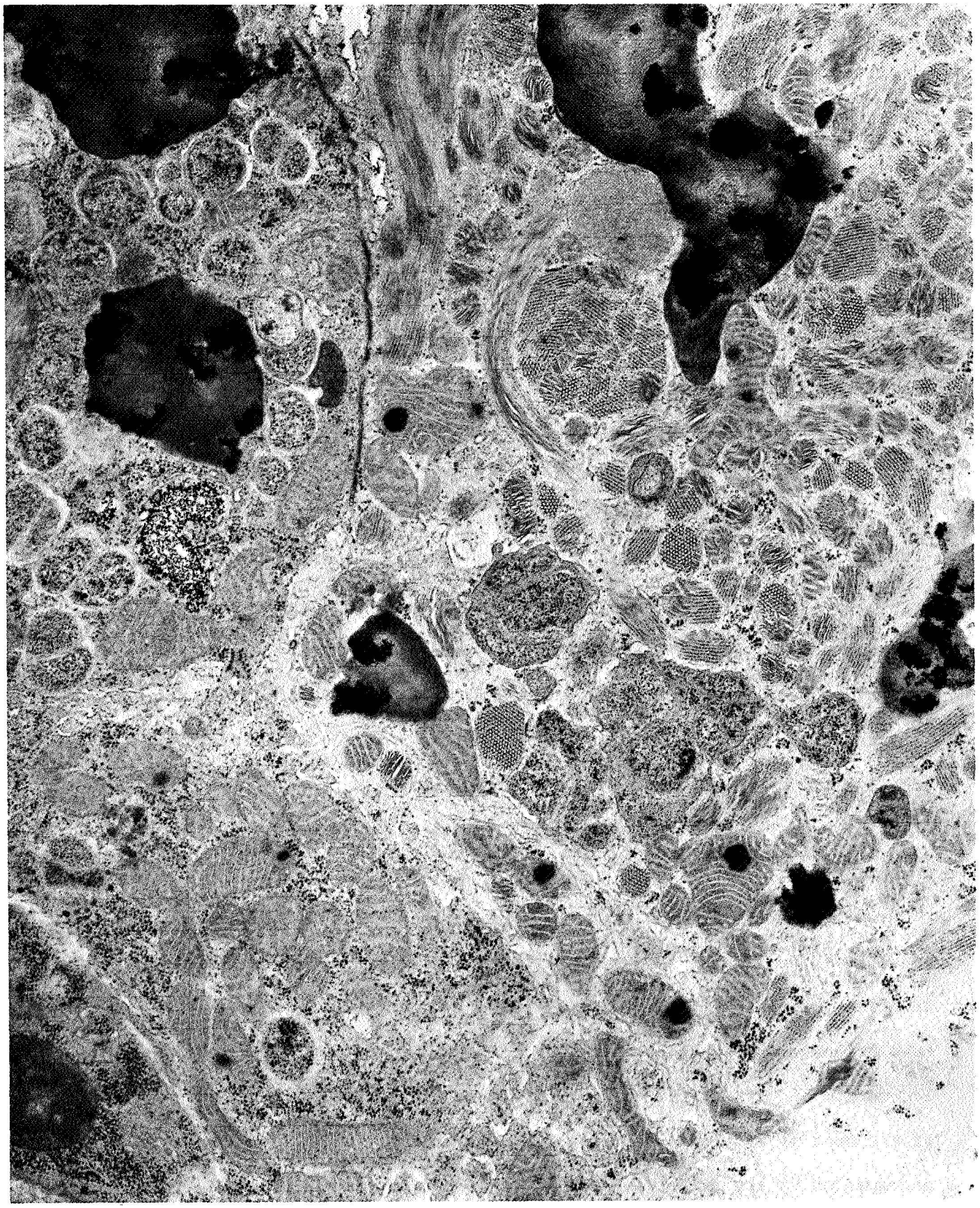

Fig. 15. Testis cells from the same Drosophila illustrated in the preceding figure, showing approximately the same amount of electron-dense lipopigment (lipofuscin) than ground controls of the same age. X30,780.

removed.

It seems that the position of the different parts of the body in relation to one another, which is changed by the effect of gravity when the insect moves, is controlled by groups of sensory "hair plates" located in the joints. These hair plates register the position of the body parts and act as measuring devices for proportionality feed-back mechanisms (3).

The above gravity sense organs, which are only found in insects, are quite sensitive, as shown by the fact that, for instance, ants can recognize the direction from which gravity acts on a sloping surface at only 2.5° inclination.

The gravity sensing mechanisms are even more refined in Drosophila, which excells in postural control, as demonstrated by its ability to maintain stability when flying in complete darkness.

Under normal earth conditions, gravity is distinguished from all other orienting stimuli in the organismic range of measurability by its unchanging intensity and direction (3). Therefore, we can assume that no adaptive mechanisms have evolved in insects to compensate for hypogravitational changes. Thus, exposure to near zero-g is likely to result in disturbed behavior and a stress-associated increase in motor activity similar to that shown by rats flown in the same Cosmos vehicle which housed the flies investigated by us (2).

Previous work from our laboratory has already shown that high levels of activity can induce an acceleration of the aging process of Drosophila. In effect, when adult flies were stressed by continuous rotation at 6 revolutions/minute in a horizontal clinostat, we could observe increased fly locomotion and a tendency to concentrate in the central area of the bottom of the housing bottle, i.e. along the axis of rotation. This behavior was accompanied by approximately 13 % life shortening, as compared to control flies which were rotated at the same speed in vertical clinostats.

An increased level of activity results in higher quotas of O_2 utilization

and this, as demonstrated by Pearl (16) and in full agreement with his rate-of-living theory of poikilotherm aging, results in premature senescence.

An alternative explanation for the wing injury and life shortening observed in the Cosmos-flown Drosophila could involve possible injurious effects of the accelerations and vibrations to which the flies were exposed during take-off and landing of the spacecraft. However, small insects such as Drosophila are very resistant to high-g loads. Thus, in our opinion, it is likely that the detrimental reactions observed in the Cosmos-flown Drosophila are the result of long term exposure to near zero-g, rather than an effect of accelerations and vibrations.

ACKNOWLEDGEMENTS

The essential contribution of Drs. G. P. Parfenov and K. A. Souza in making this study possible is gratefully acknowledged.

REFERENCES

1. Harman, M.M., J. Miquel, and M. Johnson. Viruslike particles and related filaments in neurons and glia of Drosophila melanogaster brain. J. Invertebr. Pathol. 17: 442-445, 1971.
2. Institute of Medical and Biological Problems, Ministry of Health USSR. Translation of "Predvaritel'nyye Rezul'taty Nauchnykh Eksperimentov na Biosputnike 'Kosmos-936"=(Preliminary results of the scientific experiments on the Kosmos-936 biosatellite), NASA TM-75071, 1978, p. 12.
3. Markl, H., and M. Lindauer, Physiology of Insect Behavior, in "Physiology of Insecta, vol. III, (ed. M. Rockstein), Academic Press, New York, 1965, pp. 3-122.
4. Miquel, J. Aging of male Drosophila melanogaster: histological, histochemical and ultrastructural observations. Advances in Gerontological Research 3: 39-71, 1971.
5. Miquel, J., K. G. Bensch, and D. E. Philpott. Virus-like particles in the tissues of normal and γ-irradiated Drosophila melanogaster. J. Invertebr. Pathol. 19: 156-159, 1972.
6. Miquel, J., K. G. Bensch, D. E. Philpott and H. Atlan. Natural aging and radiation induced life shortening in Drosophila melanogaster. Mech. Ageing Develop. 1: 71-97, 1972.
7. Miquel, J., W. Calvo, and L. J. Rubinstein, A simple and rapid stain for the biopsy diagnosis of brain tumors. J. Neuropath. exp. Neurol. 27: 517-523, 1968.
8. Miquel, J. and J. E. Johnson, Jr. Senescent changes in the ribosomes of animal cells in vivo and in vitro. In press in Mech. Ageing Develop.
9. Miquel, J., P. R. Lundgren and K. G. Bensch. Effects of oxygen-nitrogen (1:1) at 760 Torr on the life span and fine structure of Drosophila melanogaster. Mech. Ageing Develop. 4: 41-57, 1975.

10. Miquel, J., P. R. Lundgren, K. G. Bensch and H. Atlan. Effects of temperature on the life span and fine structure of Drosophila melanogaster. Mech. Ageing Develop. 5: 347-370, 1976.

11. Miquel, J., P. R.Lundgren and R. Binnard. Negative geotaxis and mating behavior in control and gamma-irradiated Drosophila. Drosophila Informat. Service 48: 60, 1972.

12. Miquel, J., and M. Johnson. Insect brain as a model for the study of aging. Age related changes in Drosophila melanogaster. Acta Neuropath. (Berl.) 19: 167-183, 1971

13. Miquel, J., J. Oro, K. G. Bensch, and J. E. Johnson, Jr. Lipofuscin: Fine structural and biochemical studies. In "Free Radicals in Biology", vol. III. (W. Pryor, ed.), Academic Press, New York, 1977, pp. 133-182.

14. Miquel, J., D. E. Philpott, P. R. Lundgren, R. Binnard, and C. E. Turnbill. Effects of weightlessness on the embryonic development and aging of Drosophila. Report on the Cosmos-782 Flight Experiment.

15. Miquel, J., A. L. Tappel, C. J. Dillard, M. M. Herman and K. G. Bensch. Fluorescent products and lysosomal components in aging Drosophila melanogaster. J. Gerontol. 29: 622-637, 1974.

16. Pearl, R, "The Rate of Living", University Press, London, 1928.

17. Philpott, D. E., K. G. Bensch, and J. Miquel. Life span and fine structural changes in oxygen-poisoned Drosophila melanogaster. Aerospace Med. 45: 283-289, 1974.

18. Rockstein, M., J. Chesky, D. E. Philpott, A. Takahashi, J. E. Johnson, and J. Miquel. An electron microscopic investigation of age dependent changes in the flight muscle of Musca domestica L. Gerontologia 21: 216-223, 1975.

19. Rockstein, M. and J. Miquel. Aging in Insects, in "Physiology of Insecta", 2nd Edition (M. Rockstein, ed.), Academic Press, New York, 1973, pp.371-478.

20. Takahashi, A., D. E. Philpott and J. Miquel. Electron microscope studies on aging Drosophila melanogaster. III. Flight muscle. J. Gerontol. 25: 222-228, 1970.

21. Wukelic, G. E. "Handbook of Soviet Space Science". Gordon and Breach Science Publishers, New York, 1968, p.62.

74

N79-11674

EFFECT OF WEIGHTLESSNESS AND CENTRIFUGATION (1XG) ON ERYTHROCYTE SURVIVAL IN RATS SUBJECTED TO PROLONGED SPACE FLIGHT

PRINCIPAL INVESTIGATOR:

Henry A. Leon, Ph.D.
Biomedical Research Division
National Aeronautics and Space Administration
Ames Research Center
Moffett Field, California 94035, U.S.A.

CO-INVESTIGATOR:

Stephen A. Landaw, M.D., Ph.D.
Veteran's Administration Hospital
Syracuse, New York 13210, U.S.A.

This work was done in collaboration with Luba V. Serova, Ph.D., of the Institute for Biomedical Problems, Moscow, U.S.S.R.

ABSTRACT

Rats were flown aboard the biosatellite Cosmos 936 for 18.5 days during August 1977. Five rats were subjected to near weightless space flight as with Cosmos 782 and five rats were subjected to a one g force via an on-board centrifuge. These rats, and 3 control groups were injected with 2-^{14}C glycine 19 days pre-flight. The flight rats were recovered from orbit after 18.5 days of space flight. Erythrocyte hemolysis and life span were evaluated in the five groups of rats by quantitation of radioactive carbon monoxide exhaled in the breath, which arises from the breakdown of the previously labeled hemoglobin. The results are supportive of our previous findings, wherein hemolysis was found to increase as a result of weightless space flight. A comparison to the centrifuged animals indicates that artificial gravity attenuates the effect of weightlessness on hemolysis and appears to normalize the hemolytic rate in the early post-flight period.

INTRODUCTION

With few exceptions the loss of a variable quantity of red blood cell (RBC) mass has been a consistent finding in humans subjected to space flight. A decreased RBC mass has been noted in astronauts in some Gemini and Apollo flights with a maximum loss of 20% after the eight-day Gemini V mission (1). This was attributed to the action of the pure hyperoxic environments in use during various phases of the flights, since in those Apollo flights where nitrogen was also present, minimal changes were observed (2). Accelerated hemolysis caused by the action of oxygen on RBC membranes was considered to be the predominant factor which caused the RBC mass reductions seen in the Gemini program (2). In Apollo, however, decreased production presumably caused by the inhibitory action of hyperoxia on erythropoiesis was considered to be the main cause for the decreased red cell mass (3,4). The results of the Skylab flights show that prolonged weightlessness in itself also causes a significant decrease in the RBC mass of astronauts. In the first manned Skylab mission which lasted 28 days, the average red cell mass loss immediately post-flight was 14.3%. The average loss 13 days post-flight as compared to pre-flight values was 15.5% indicating that the mechanisms causing the loss were still operative. Losses on the 59-day mission and the 84-day mission averaged 12.2% and 5.1%, respectively. No post-mission decrements were seen in these two flights (4). Similar findings have also been reported for cosmonauts (5). The Skylab atmosphere was nitrogen with a near-normal oxygen partial pressure (total pressure 260 torr, 0_2 170 torr) and Russian space cabin atmospheres are essentially air at sea-level pressure (4,5). Therefore, mechanisms other than oxygen-induced hemolysis must be operative to cause the decrease in RBC mass.

We have obtained direct evidence indicating increased destruction of RBC during space flight. Six rats were subjected to 19.5 days of near weightlessness space flight aboard the Soviet biosatellite, Cosmos 782. Based on the output of ^{14}CO arising from RBC prelabeled with 2-^{14}C glycine before the flight, survival parameters of this cohort of RBC was evaluated upon return from orbit. These were compared to ground control rats labeled with the glycine at the same time. Analysis of the data showed that random hemolysis was increased three-fold in the flight rats and the mean potential life-span was decreased about 5%. All conditions of the flight, except weightlessness, were largely excluded as causing these changes (6).

The present experiment was undertaken to verify the above alterations seen in Cosmos 782 and to ascertain if the alterations could be attenuated by artificial gravity via an on-board centrifuge. Such a finding would strengthen the contention that the mechanism of altered RBC survival is gravity-dependent.

MATERIALS AND METHODS

Male Wistar specific pathogen-free rats were used in this study. The test groups included:

1. Flight-Stationary Group (FS):

   Rats subjected to near weightless orbital flight, 5 each.

2. Flight Centrifuged Group (FC):

   Rats subjected to orbital flight but also subjected to a continuous compensatory 1xG load by means of an on-board centrifuge, 5 each.

3. Synchronous Stationary Group (SS):

   Ground control to the FS group above. These rats were subjected to a simulation of launch and recovery forces, nutritional and environmental conditions of temperature, pressures and humidity as experienced by the weightless flight rats, 5 each.

4. Synchronous Centrifuged Group (SC):

   Ground control to the FC group above. These rats were subjected to a simulation of launch and recovery forces, nutritional and environmental conditions of temperature, pressures and humidity as experienced by the centrifuged flight group. In addition, they were centrifuged about axis with a force of 1.07 x g, 5 each.

5. Vivarium Control Group (V):

   Rats maintained in the animal vivarium prior to and during flight, 6 each.

The rats were injected intraperitoneally with 500 μCi/kg of $2^{14}C$ glycine 19 days before the launch or the simulation. (Simulation of the SC group started 22 days post-injection).

At the time of the injection the flight groups averaged 146 g and the vivarium controls averaged 141 g. At the time of the injection they were 44 days old. Four days later, ground controls for both the stationary and centrifuged flight rats were injected. In all cases, the rats had been implanted with a temperature transmitter five days before the injection. These and other pertinent data are enumerated in Table 1.

TABLE I

ITINERARY

-5 Days	Implant temperature recorder
Zero Time	Inject 2-^{14}C Glycine FS, FC and V groups. Av. wt. 146, 146 and 141 g, respectively. Age 44 days
	SS and SC groups injected four days later. Av. wt. 128, 125 g, respectively. Age 44 days. Food consumption 40 g/day.
Injection + 19 days Launch, orbital flight or simulation	August 3 to August 22, 1977. Simulation of SC group started 22-day post-injection. Food consumption, g/day FS, 49.2; FC, 39.4; V, 40; SS, 45.4; SC, 39.3
Injection + 38 days	De-orbit - 18.5 days of flight or simulation
Injection + 40 days	First ^{14}CO collection Food consumption 45 g/day
Injection + 62 days	Last collection FS, FC, and SS groups
Injection + 64 days	Last collection for SC group
Injection + 68 days	Last collection for V group

The flight was launched August 3, 1977, aboard the biosatellite Cosmos 936 and lasted for 18.5 days. During the flight, the animals were housed in individual cylindrical capsules, 26 cm in length and 9.5 cm in diameter, which had automatic feeding and watering devices, and a waste management system attached. During the flight, the animals were fed a special paste-like diet at six-hour intervals (see Table 1 for total quantity). Water was given ad libitum. The temperature within the animal capsules varied between 21.5 - 24°C. The oxygen content ranged between 145 - 210 torr, the CO_2 content slowly increased but never exceeded 14 torr. The relative humidity was 80-90%. The rat capsules on the centrifuge were rotated around a radius of 32 cm at 53.5 RPM generating a force of 1.05 x G.

The controls for the stationary flight group, SS, and the centrifuged flight group, SC, were maintained in identical capsules under similar environmental conditions. The centrifuged control group was rotated around a 12 cm radius at 53.5 cm generating a force of 1.07 x G. The vivarium control rats were kept in a group of five in a cage measuring 45 x 31 x 16 cm. Both the flight and control rats were on a 12:12 day:night light cycle. Additional details on the conditions of the flight have been reported elsewhere (7).

Upon return from orbit, ^{14}CO arising from the degradation of the previously labeled RBC hemoglobin was evaluated in all the groups. The results are used to estimate the rate of hemolysis and RBC survival parameters (8). Determinations were started 40 days post-injection (2 days post-flight) and continued through day 62 post-injection for the flight groups and the stationary control group; day 64

for the centrifuged control groups; and day 68 for the vivarium control group.

Quantitation of respiratory ^{14}CO was performed as described previously (8). Briefly, each rat was placed in an individual chamber and flushed with air at a rate of 600 cc/min. Air exiting from the chamber was dried by passage through anhydrous $CaSO_4$. Carbon dioxide was removed by passage of the air stream through soda lime. The ^{14}CO was then oxidized to $^{14}CO_2$ by a Hopcalite cannister. The ^{14}CO thus generated was trapped in ethanolamine/2-Ethoxyethanol and aliquots were counted by liquid scintillation. Breath samples were taken for 3 hours at the same time each day to minimize potential circadian fluctuations.

The activity in ^{14}CO was expressed as dpm/hr. From these data, the following survival parameters relating to a cohort of labeled red blood cells can be obtained (8):

k, rate of random hemolysis (percent per day).

T, mean potential RBC life-span (days).

σ, spread of life spans about T (days).

%S, fraction of labeled RBC dying of senescence (%).

$\bar{T}$, mean overall RBC life-span (days).

C, fraction of injected glycine incorporated into RBC heme.

In the present experiment, C takes on a different meaning since actual determinations were not made for the initial or final portions of the survival curve. This will be discussed subsequently.

The protocol for this experiment did not permit observations of the entire ^{14}CO output curve. Although the final results could theoretically be changed if the entire curves were available for analysis, the

null hypothesis was offered that the selected portions of the curves in experimental and control groups should yield identical computer-determined values for RBC survival. That statistically significant differences were found between the groups strongly suggests that the limited data points do indeed reflect differences in RBC survival.

RESULTS

The RBC survival parameters for all rats are recorded in Table II. Rats SC16 and 18 had no or low counts, probably as a result of injection into the bladder. These two rats were excluded from all subsequent calculations.

Table III shows the averaged values and some of the statistical comparisons for the groups. The main thing to notice is that k, T, σ, %S, and $\bar{T}$ in all the control groups are essentially the same. This conformity occurred in spite of widely differing treatments for the three control groups.

The two flight groups show differing responses. The flight centrifuged group is essentially identical to the control groups for the above parameters. On the other hand, the flight stationary group, which, as in Cosmos 782, was subjected to near weightlessness for the flight period, shows evidence of increased hemolysis. Random hemolysis k, is up threefold as in Cosmos 782 and the %S, those dying of senescence, is down. These are of borderline significance statistically; however, mean overall life-span, $\bar{T}$, is decreased significantly. Since the mean potential life is essentially normal, $\bar{T}$ could only decrease as a result of increased random hemolysis.

As indicated in Table II, the large standard error of the FS group is due to the values from one rat, FS05 which was way out of line with

TABLE II

RED BLOOD CELL SURVIVAL PARAMETERS
FINAL COMPUTER VALUES FROM ALL ANIMALS

#	k	T	σ	C	# DATA POINTS	% S	$\overline{T}$
V21	.21	59.3	9.6	3633	13	88.4	55.7
22	.12	59.4	10.6	3917	15	93.2	57.3
23	.10	57.1	9.0	3824	15	94.5	55.5
24	.00	55.6	11.4	3335	11	100	55.6
25	.93	52.2	8.6	5255	12	61.9	41.2
26	.55	60.7	10.3	4660	16	71.8	51.4
SS11	.24	60.4	7.0	1555	16	86.6	56.2
12	.09	57.2	9.0	1732	15	95.0	55.7
13	.03	56.7	8.1	1610	16	98.3	56.2
14	.43	60.0	7.1	1483	15	77.4	52.8
15	.96	58.6	5.9	1790	13	57.2	44.8
SC 16	----------	----------	----------	no counts in samples	----------	----------	----------
17	.80	60.7	8.0	3867	13	61.8	48.0
18	----------	----------	----------	insufficient data	----------	----------	----------
19	.04	59.5	7.7	1590	16	97.7	58.8
20	.00	58.3	8.3	1280	16	100	58.3
FS01	1.65	58.5	5.2	4765	13	38.4	37.6
02	1.14	60.4	9.1	4992	12	50.7	43.5
03	0.50	53.2	7.5	4720	12	76.8	46.6
04	2.00	50.4	7.3	8051	13	37.1	31.7
05	.00	54.9	8.2	3110	13	100	54.9
FC06	.00	53.1	9.2	3565	14	100	53.1
07	.42	57.3	8.0	3169	15	78.7	50.9
08	.00	57.4	10.7	2630	15	100	57.4
09	.09	57.7	8.8	2618	13	95.0	56.2
10	.54	54.1	7.8	3495	13	74.8	46.8

RED BLOOD SURVIVAL PARAMETERS

TABLE III AVERAGE VALUES FOR THE GROUPS

	k	$\bar{T}$	σ	C	%S	$\overline{T}$
*V(6)	0.32 ± 0.14	57.4 ± 1.3	9.9 ± 0.4	4102 ± 292	85.0 ± 6.0	52.8 ± 2.5
*SS(5)	0.35 ± 0.17	58.6 ± 0.7	7.4 ± 0.5	1634 ± 56	82.9 ± 7.4	53.1 ± 2.2
*SC(3)	0.28 ± 0.26	59.5 ± 0.7	8.0 ± 0.2	2246 ± 816	86.5 ± 12.4	55.0 ± 3.5
*FS(5)	1.05 ± 0.37	55.5 ± 1.8	7.5 ± 0.6	5632 ± 809	60.6 ± 12.2	42.9 ± 3.9
*FC(5)	0.21 ± 0.11	55.9 ± 1.0	8.9 ± 0.5	2895 ± 204	89.7 ± 5.4	52.9 ± 1.9
FS vs FC	$0.1>p>0.05$	N.S.	N.S.	$p<.05$	$0.1>p>0.05$	$p=0.05$

* MEAN ± S.E.

the others in that group and showed no random hemolysis. It is now known that this rat suffered a broken femur on impact. Furthermore, in scrutinizing his growth pattern post-flight, we find that he was initially 9g heavier than the average of the other four rats in the group, but he became as much as 18g lighter indicating a highly suppressed growth rate. The fractured femur and the depressed growth rate may be interconnected; whatever the case, we feel that there is some justification for excluding this animal.

Calculations with this animal excluded in comparison to the FC and V groups are shown in Table IV. Random hemolysis is considerably and significantly increased over both the vivarium controls as well as the flight centrifuged group. Concurrently, both %S and $\bar{T}$ are significantly decreased. Again, T, the mean potential life-span is normal indicating that increased random hemolysis is the main cause of the decreased mean overall life-span, $\bar{T}$.

Referring to both Tables III and IV, the area under the curve, C, is high in the FS group and low in both the flight control groups SS and SC. The high value for C in the FS group is due largely to one high value.

The low values in the two control groups appears to be related to a depressed metabolism at the time of the injection of the glycine. All rats were injected five days after implantation of the temperature recorder. The growth rate of these two groups after the implantation was not as great as in the flight groups and the vivarium control suggesting a depressed metabolism which would result in a decreased incorporation. Growth rates appear to have picked up prior to the end of the simulation, thus normalization of RBC survival parameters except for C would

RED BLOOD SURVIVAL PARAMETERS

TABLE IV

F.S. GROUP - RAT FS-05 EXCLUDED

	k	T	σ	C	%S	$\overline{T}$
*FLIGHT STATIONARY	1.32 ± 0.32	55.6 ± 2.3	7.3 ± 0.8	5632 ± 809	50.8 ± 9.2	39.9 ± 3.3
F.S. vs F.C.	p<.01	N.S.	N.S.	p<.02	p<.01	p<.01
F.S. vs V.	p<.02	N.S.	p<.02	N.S.	p<.02	p<.02
F.S. vs S.S	p<.05	N.S.	N.S.	p<.01	p<.05	p<.02

* MEAN + S.E.

be expected.

DISCUSSION AND CONCLUSIONS

As with Cosmos 782, data was obtained only until day 24 post-flight for the flight rats (6). In Cosmos 782, 23 daily points were obtained for most of the flight rats, whereas with Cosmos 936, only 16 daily points were obtained. This undoubtedly had some effect on the precision of the calculated RBC survival parameters particularly since only a portion of the curve was available for analysis.

Nevertheless, when considered in total there is clear evidence that random hemolysis was again accelerated by near-weightlessness and artificial gravity attenuates this hemolysis of space flight. Considering only the output of ^{14}CO during the first three days post-flight, radioactivity was 60% higher in the near-weightless group (FS) than in the flight centrifuged group, FC. This latter group was slightly lower than the vivarium control group. Since this was well before the mean potential life-span, it could only indicate that hemolysis was highest in the FS group and hemolysis was equal in the FC and V groups. Calculations based on the values from the individual animals indicate the same relationship. Using all the 5 values for the FS group, random hemolysis is 3 times greater than the V group and the FC group is not appreciably different from the V group. The mean overall life-span is significantly shortened in the FS group as a result of increased hemolysis. The difference is even more pronounced if the one rat that suffered measurable injury is excluded from the data. These changes in hemolysis are also reflected in %S, the portion of RBC dying of senescence as well as mean overall life-span, $\bar{T}$.

No change was found in T, the mean potential life-span, or σ, the spread of life spans about T. This is in contrast to Cosmos 782 where T and σ were shortened in the FS group. Although shortening of T may occur as a result of weightlessness, it decreased only 5-6% in Cosmos 782, whereas random hemolysis increased 3 to 4-fold. Thus, the increased random hemolysis is biologically much more important than the shortened mean potential life-span.

The area under the curve C which is normally a measure of relative incorporation, did not show the same pattern that was seen in Cosmos 782 where C appeared to decrease in the FS group. The reasons for this are not clear. However, it should be pointed out that in view of the fact that C describes the area under the entire ^{14}CO output curve, calculated value for C based on a limited portion of the curve as we have done here and in Cosmos 782, it is perhaps the least reliable of all our calculations. On the other hand, random hemolysis which is indicated by the initial post-flight plateau of ^{14}CO output is the most reliable.

Clearly, attenuation of the hemolysis of space flight by artificial gravity excludes all extraneous factors such as radiation. The mechanism is therefore related to conditions brought into play by weightlessness or near weightlessness. One change known to occur in man during weightlessness and which may occur in rats also is the rapid shift in body fluid. Thus, in Skylab, measurements of leg volumes demonstrated that with weightlessness there is an immediate headward transfer of 1.8 liters of fluid and with continued weightlessness this was followed by another 0.4 liters. Thornton and Hoffler (9) suggest that certain body

sensors detect this abnormally large transposed volume and cause plasma to be reduced, thus leaving high hemoglobin and hematocrits in the circulating blood, both of which increased within a few days or less after initiation of the flights (10). Tissues sensitive to peripheral hemocrit changes inhibit erythropoiesis over a period of weeks such that red cell mass, via a normal destruction rate, becomes appropriate to the new volume.

Johnson, et al. (4) has presented a similar theory but also consider that these same fluid shifts could change splenic function leading to increased sequestration and hemolysis. This possibility is emphasized by the increase in the number of abnormally shaped cells found by Kimzey (10). We have suggested a similar theory and indicate that the reticulo-endothelial system may be involved (6). Hemolysis induced by a relative hemoconcentration has been considered as a normal physiological mechanism in the past. Thus, Merino (11) found that when humans who had developed a notable degree of polycythemia as a result of high altitude habitation were returned to sea-level, normalization of hemoglobin and cell count occurred within six weeks. The reticulocyte count fell indicating a suppression of erythropoiesis. However, he also found an increase of indirect plasma bilirubin and a distinct increase in fecal urobilinogen during the first week. On the basis of this evidence, he postulated that a dual mechanism wherein decreased production and increased destruction becomes operative when high altitude residents are returned to a sea-level environment. The stimulus for both of these responses was considered to be the removal of the hypoxic state, which, of course, can also be viewed as a hyperoxia relative to the previous environmental condition.

In conclusion, it appears that hemolysis in rats caused by weightlessness or near weightlessness is a consistent repeatable occurrence. It is unrelated to exogenous factors but is due specifically to weightlessness since it can be attenuated by artificial gravity created by centrifugation. A possible initiator of the hemolysis is a cephalid fluid shift and subsequent hemoconcentration caused by the weightlessness.

ACKNOWLEDGEMENTS

We extend our sincere appreciation to Kenneth A. Souza for his dedicated management of the Cosmos Project and to John Butte for his expert technical assistance.

REFERENCES

1. Fisher, Craig L., Philip C. Johnson, and Charles A. Berry. Red Blood Cell Mass and Plasma Volume Changes in Manned Space Flight. The Journal of The American Medical Association 200:579-583, 1967.

2. Berry, C. A. Summary of medical experience in the Apollo 7 through 11 manned space flights. Aerospace Med. 41(5):500-519, 1970.

3. Berry, C. A. Medical legacy of Apollo. Aerospace Med. 45(9):1046-1057, 1974.

4. Johnson, P. C., T. B. Driscoll, and A. D. LeBlanc. Blood Volume Changes. Ch. 26. Biomedical Results from Skylab. R. S. Johnston and L. F. Dietlein, ed. NASA SP-377, 1977.

5. Ushakov, A. S., S. M. Ivanova, and S. S. Brantova. Some aspects of energy metabolism in human blood erythrocytes under hypokinesia and during space flights. Aviat. Space Environ. Med. 48(9):824-827, 1977.

6. Leon, H. A., L. V. Serova, J. Cummins, and S. A. Landaw. Alteration in Erythrocyte Survival Parameters in Rats after 19.5 Days Aboard Cosmos 782. Aviat. Space Environ. Med. 49:66-69, 1978.

7. Ilyin, E. Preliminary Results of the Scientific Experiments on the Cosmos 936 Biosatellite. Institute of Biomedical Problems, Moscow, 1977. Unpublished Report.

8. Landaw, S. A. and H. S. Winchell. Endogenous Production of ^{14}CO: A method for calculation of RBC life-span *in vivo*. Blood 36:642-656, 1970.

9. Thornton, W. E. and G. W. Hoffler. Hemodynamic Studies on Legs Under Weightlessness. Ch. 31. Biomedical Results from Skylab. R. S. Johnston and L. F. Dietlein, ed. NASA SP-377, 1977.

10. Kimzey, S. L. Hematology and Immunology Studies. Ch. 28. Biomedical Results from Skylab. R. S. Johnston and L. F. Dietlein, ed. NASA SP-377, 1977.

11. Merino, C. F. Studies on Blood Formation and Destruction in the Polycythemia of High Altitude. Blood 5:1-31, 1950.

75

N79-11675

Cosmos 936, Experiment K204

FINAL REPORT

THE EFFECTS OF SPACE FLIGHT ON SOME LIVER ENZYMES CONCERNED WITH CARBOHYDRATE AND LIPID METABOLISM IN THE RAT

Principal Investigators:

Dr. S. Abraham* and Dr. H. P. Klein+

Collaborating Investigators:

Dr. C. Y. Lin* and Ms. C. Volkmann+

* Address: Bruce Lyon Memorial Research Laboratory, Children's Hospital Medical Center of Northern California, 51st and Grove Streets, Oakland, California 94609

+ Address: National Aeronautics and Space Administration, Ames Research Center, Moffett Field, California 94035

SUMMARY

We have examined, in rat liver, the activities of about 30 enzymes concerned with carbohydrate and lipid metabolism. In addition to the enzyme studies, the levels of glycogen and of the individual fatty acids in hepatic lipids were determined. The livers from flight and ground control rats at recovery (R_0) and 25 days after recovery (R_{25}) were used for these analyses.

It is evident from our data, that for virtually all of the parameters measured, the most meaningful comparisons are those made between the flight stationary (FS) and the flight centrifuged (FC) animals at R_0.

When these two groups of flight rats were compared at R_0, statistically significant decreases in the activity levels of glycogen phosphorylase, α-glycerol phosphate acyl transferase, diglyceride acyl transferase, aconitase and 6-phosphogluconate dehydrogenase were noted in the weightless group (FS). The significance of these findings was strengthened by the fact that all enzyme activities, showing alterations at R_0, returned to normal 25 days post-flight. Striking differences were also seen in the levels of the two liver constituents. When the liver glycogen and the total fatty acids of the two sets of flight animals were determined, significant differences that could be attributed to reduced gravity were observed. The weightless group (FS) at R_0 contained, on the average, more than twice the amount of glycogen than did the centrifuged controls (FC) and a remarkable shift in the ratio of palmitate to palmitoleate was noted.

These metabolic alterations, both in enzyme levels and in hepatic constituents, appear to be unique to the weightless condition. In addition, our data seem to justify the conclusion that centrifugation during flight is equivalent to terrestrial gravity.

INTRODUCTION

During early manned spaceflights, a specific physiological enigma was noted which concerned itself with caloric requirements. Theoretically, in the absence of gravitational force, less energy should be required for life-sustaining functions (39). However, on the initial flights where caloric intake was restricted, a marked inflight loss in body weight resulted (39). The available literature (11) on mammalian responses to spaceflight indicates that both in humans and in rats, caloric intake during spaceflight remains essentially the same as on the ground. Despite this, the organisms in flight generally lose weight, are in negative nitrogen balance and, in rats, lose body fat. During Skylab missions (11) when dietary intake was increased so that it was isocaloric with a 1 x G environment, a loss in body mass still occurred in spite of the increased food intake.

Several explanations for this unusual weight loss have been proposed. For example, it could be attributed to either a fluid imbalance, or an increased caloric demand caused by the stress of re-entry or, in some individuals, by the extravehicular activity. At the organ-tissue level, intestinal malabsorption or various alterations in carbohydrate-lipid metabolism could also account for body mass losses observed in space. Subtle changes which could occur at the cellular level include incomplete oxidation of substrates, enzyme alterations and/or changes in the efficiency of oxidative phosphorylation. The relationship between the caloric intake and the loss of body mass during weightlessness* is a problem which is, as yet, unresolved.

* We, of course, recognize that absolute "weightlessness" is very hard to establish. Thus, when we use the terms "weightlessness" or 0 x g, we recognize that such a condition was only approximated. Indeed, on the COSMOS 782 spacecraft, the actual g force ranged between 1.5×10^{-4} and 1.7×10^{-7} x g. At this writing, we do not have the precise values for this measurement aboard the COSMOS 936 spacecraft, but we believe it to be somewhere between those limits (Kenneth A. Souza, personal communication).

On COSMOS 605, the carbohydrate and lipid composition of rat liver tissue was examined (8) and it was found that whereas the total carbohydrate content was similar in flight and vivarium animals, an increase in total hepatic phospholipids could be attributed to weightlessness. In another communication, Yakovleva (44) reported that livers from rats aboard COSMOS 605 and 782 showed increased total lipids at recovery and that these slowly returned to normal levels by 25-27 days postflight. A detailed examination of rats flown in the COSMOS 690 flight also showed significant changes in the lipid concentrations of certain tissues had occurred (6). Evidence was obtained for increased rates of glycolysis in skeletal muscle, and changes were reported in the patterns of the lactate dehydrogenase (LDH) isoenzymes in this tissue (33). Despite overall losses in total body fat, flight rats showed increased plasma triglycerides and cholesterol, as well as elevated levels of phospholipids (6). In bone marrow and liver, triglycerides were found to be increased (6). Decreases in the phospholipid contents of the microsomal fractions of leg muscle tissues suggested to the USSR scientists that significant changes might take place in the membranes of this tissue as a result of spaceflight (42).

Some evidence is available from manned flights as well as from animal flights that bear on this problem. Data obtained during the Skylab program indicate that carbohydrate and fat utilization may well be affected. A loss in body fat stores, a mobilization of triglycerides, and an increase in plasma cholesterol were all observed postflight (11).

It is clear that additional data on gross total composition of various tissues of organisms after flight, while useful, are not likely to shed light on the dynamic processes that may be affected in spaceflight. We feel it is most important to study a key organ like the liver in order to determine whether any regulatable enzymes of carbohydrate and lipid metabolism have been affected; that is, whether the capabilities of the organ to produce these cellular constituents has, in fact, been altered.

Because of the many fragmented references documenting changes induced by weightlessness in tissue carbohydrate and lipid contents, we undertook a comprehensive survey of key hepatic enzymes of carbohydrate and lipid metabolism in rats carried on the COSMOS 936 biosatellite flight so as to shed additional light on this question.

MATERIALS AND METHODS

Tissue and Hemogenate Preparation Rats were sacrificed by decapitation, their livers removed as quickly as possible and immediately placed into ice-cold 0.25M sucrose solution. Two pieces of liver (about 100 mg each) were taken for glycogen and fatty acid analyses. These were wrapped in tin foil and frozen in dry ice. Four gram portions of each liver were minced and individually homogenized in a Potter-Elvehjem type tissue grinder with exactly 12.0 ml of fresh ice-cold 0.25M sucrose solution as given previously (1). All subsequent preparative procedures were carried out at 0-4°C.

Nuclei, cell debris and mitochondria were sedimented at 4500 x g for 30 minutes in a refrigerated centrifuge (Beckman). The mixed pelleted

fractions were discarded and the supernatant fractions (obtained with the aid of a disposable pipet from under the free floating fat) retained. These fractions were immediately frozen to -80°C in plastic tubes and shipped from the recovery site to our laboratories in the United States.

Upon arrival, the supernatant fractions (containing the cytosol and microsomal fractions of the liver) were slowly thawed out and subjected to centrifugation in a Spinco Ultracentrifuge at 100,000 x g for 60 minutes at 0-4°C. The cytosol (particle-free supernatant fraction) and the microsomes (pellet) were separated. The cytosol fraction from each rat liver was divided into many small aliquots which were placed into individual plastic test tubes, quick frozen, and stored at -80°C until used for enzymatic analysis. Once thawed out, the sample was immediately used for the assay of its enzyme activity and was not repeatedly frozen and thawed. The microsomal fractions were treated in a similar manner.

This entire effort was performed as a "double-blind" study in that all samples were initially coded so as not to reveal the specific identity of each sample. Subsequent to the completion of all analyses, the code was revealed to the experimenters.

Fatty Acid and Glycogen Analyses - Samples of frozen liver were thawed out, weighed (100 mg) and saponified in 1.0 ml of 3N potassium hydroxide in 50% methanol at 90°C for 12 hours under reflux. Isolation of the fatty acid fractions, preparation of the methyl esters and quantitative separation of each fatty acid by gas chromatography was performed as previously described (2).

Other samples of liver (ranging from 60 to 110 mg but precisely weighed out) were taken for analysis of glycogen content by the anthrone procedure as published previously (16).

Enzyme Assays - All enzyme assays, unless otherwise noted, were performed with either the 100,000 x g supernatant fraction (cytosol), or the pellet (microsomes) obtained from this centrifugation after removal of the mitochondria. Enzyme activities in the cytosol fractions were determined by following the changes in optical density of the reaction mixtures at 30°C with a Gilford automatic recording spectrophotometer. In all enzyme assays, concentrations of substrates and of added enzymes (where needed) were at least 10 times those required to yield maximal activities. Absorbancy changes were measured with reference to reaction mixtures, devoid either of substrates or of coenzymes. The reactions were started by additions of substrates, after a brief period of preincubation of the enzyme in the reaction mixture. Depending upon the assay, 0.0025 to 0.050 ml of the enzyme-containing fraction was used. Measurements of initial velocities were made under conditions in which kinetics were zero-order, and activity was proportional to enzyme concentration.

Specific activities of the cytosol enzymes are reported as nanomoles, either of pyridine nucleotide, oxidized or reduced, or of substrate converted to product, per milligram protein per minute, whereas those for the microsomal enzymes are given in the footnotes to the Tables. The following extinction coefficients were used in the calculations: reduced NADP (NADPH) and NADH (340 nm), 6.22×10^3 liter x $mole^{-1}$ x cm^{-1} (18); cis-aconitate (240 nm), 3.54×10^3 liter x $mole^{-1}$ x cm^{-1} (37).

Protein was determined by the method of Gornall et al. (15) or Lowry et al (25).

Enzymes were measured according to well-established methods or modifications of currently used techniques, as indicated below:

a) Cytosolic Enzymes - Glycogen synthetase by the spectrophotometric method coupled with pyruvate kinase and lactic dehydrogenase given in (27), glycogen phosphorylase (26), hexokinase and glucokinase (40), phosphoglucomutase (4), glucose-6-phosphate dehydrogenase (22), 6-phosphogluconate dehydrogenase (19), phosphofructokinase (4), fructose-1-6-diphosphatase (35), pyruvate kinase (13), lactate dehydrogenase with L-lactate as substrate (45), α-glycerophosphate dehydrogenase (40), glutamate oxaloacetate transaminase (9), glutamate pyruvate transaminase (10), citrate cleavage enzyme (40), malic enzyme (30), malate dehydrogenase with L-malate as substrate (31), fumarase with L-malate as substrate (17), isocitrate dehydrogenase (32), acetyl-CoA carboxylase (40), fatty acid synthetase (40), and aconitase (36).

b) Microsomal Enzymes - Palmitoyl-CoA synthetase was assayed according to the procedure described by Polokoff and Bell (34).

Stearoyl-CoA desaturase activity was measured as follows: The complete system contained in a total volume of 1.0 ml 30 nmoles stearoyl-1-^{14}C CoA, 0.3 μmoles NADH, 100 μmoles potassium phosphate buffer, pH 7.4, 6 μmoles Tris-$MgCl_2$ buffer, pH 7.4 and sufficient microsomal protein to yield a linear rate of desaturation. The enzyme and buffer mixture were equilibrated in air at 35°C for 2 min, and the reaction was started by the addition of substrate. At the end of a 5 minute incubation period, the reaction

was stopped by the addition of 0.5 ml of saturated potassium hydroxide. The samples were then saponified, and the fatty acids were extracted and methylated as reported previously (20). After methylation, methyl stearate and methyl oleate were separated by gas chromatography (21), and the radioactivity associated with each was counted. Enzyme activity was calculated as nanomoles of oleate produced per 5 minutes per mg protein as follows: [cpm in methyl oleate/cpm in methyl stearate + methyl oleate] times the nmoles of stearoyl-CoA added.

The glucose-6-phosphatase activity was assayed according to the method described by Nordlie and Arion (28). The orthophosphate liberated from glucose-6-phosphate was measured by a modification of the Berenblum and Chain method as described by Lindberg and Ernster (24).

α-Glycerol phosphate acyl transferase and diglyceride acyl transferase activities of hepatic microsomes were measured according to the procedures reported previously (23,41). α-glycerol-U-^{14}C-phosphate and palmitoyl-CoA were used as substrates for the former acyl transferase and sn-1,2,dilaurin and palmitoyl-1-^{14}C-CoA were the substrates for the latter acyl transferase. In the case of diglyceride acyl transferase, the synthesized ^{14}C-triglyceride was isolated from thin layer chromatography plates in which chloroform : acetone, 100:1.5 (v/v) was used as the solvent system (23).

Chemicals All chemicals were obtained from commercial sources and were of the highest purity available. AMP, ATP, glucose-6-phosphate dehydrogenase, glucose-phosphate isomerase, phosphoglucomutase, pyruvate kinase, α-glycerophosphate dehydrogenase, 6-phosphogluconate, glucose-1-

phosphate, phosphoenolpyruvate, α-D-glucose-1,6-diphosphate, lactate dehydrogenase and malate dehydrogenase were purchased from Boehringer Mannheim Corp., San Francisco, CA. Glucose-6-phosphate, fructose-1,6-diphosphate, NAD, NADH, NADP, NADPH, isocitrate, ethylene-diaminetetra-acetate (EDTA), coenzyme A, liver glycogen, and sodium pyruvate were purchased from Sigma Chemical Co., St. Louis, MO. Oxalacetate, L-malate, dithiothreitol, ADP, cis aconitate, DL-isocitrate, potassium citrate, α-keto-glutarate, UDP-glucose and glycerol-3-phosphate were purchased from Calbiochem., San Diego, CA. Acetyl-CoA and malonyl-CoA were purchased from P-L Biochemical, Milwaukee, Wisc. $Ba^{14}CO_3$, obtained from Oak Ridge National Laboratory, Oak Ridge, Tenn. Stearoyl-1-^{14}C-CoA, palmitoyl-1-^{14}C-CoA and α-glycerol-U-^{14}C-phosphate were purchased from New England Nuclear Corp., Boston, Mass. Sn 1,2-dilaurin was obtained from Supelco, Inc., Bellefonte, PA. Fructose-6-phosphate, free of glucose-6-phosphate, was prepared according to the method of Borrebaek, Abraham and Chaikoff (12).

RESULTS

Extensive preliminary experiments with rats of the same strain coming from the same source and fed the identical diet demonstrated that all of the activity of each enzyme assayed was stable under the conditions of storage used (i.e., at -80°C). In addition, these experiments also proved that all activities measured were retained in the proper cellular location, even after freezing of the post mitochondrial supernatant fractions for as long as two weeks. Thus, the data contained in Tables I through IV represent enzymatic activities and the amounts of specific

constituents in the liver of the rats at the time of sacrifice. It should be emphasized that all data contained in this report were obtained using a double-blind technique and, hence, the Tables contain two numbers. The first one is that designated by our Russian colleagues, and the second by our American Mission Manager, Mr. Kenneth Souza, who retained the code until the analyses were completed.

The data contained in Table I (A,B,C and D) were compiled from the liver fractions obtained from rats sacrificed at recovery (R_0) and those in Table II (A,B,C and D) from rats sacrificed 25 days later (R_{25}). They are presented as the average values ± their standard deviations for the various groups of rats in Tables III (A and B) and IV (A and B).

The results of the analyses of the various fatty acids in the livers of the rats sacrificed at R_0 are reported in Tables V A and V B and those for R_{25} in Tables VI A and VI B.

We have computed the significance (38) of all differences found between the liver constituents and enzyme activities determined from rats in the various groups of animals sacrificed at R_0 and R_{25}. The significance of these differences found when we compared the data from the individual groups of rats sacrificed at R_0 are given in Tables VII A, B and C. No significant differences were found between the various groups of experimental animals sacrificed at R_{25}. It should be noted that all alterations found between groups at R_0 were returned to normal at R_{25}. This latter finding adds to our confidence in the differences observed between groups sacrificed at R_0.

TABLE I A

INDIVIDUAL VALUES FOR RATS SACRIFICED AT R_0

	Rat No.		Weights at Sacrifice			Liver Constituent			
Group	USSR	USA	Carcass (grams)	Liver (grams)	Liver (% carc.)	Cytosol Protein (mg/ml)	Fatty Acid 16/16:1	Fatty Acid 18:2/20:4	Glycogen (% wet wt.)
Flight, Stationary	1	13	259	12.4	4.8	23.0	7.0	1.2	5.5
	2	14	281	12.4	4.4	19.8	11.1	1.5	5.4
	3	24	324	15.0	4.6	22.9	4.5	1.6	10.1
	4	1	371	16.4	4.4	19.4	5.5	1.5	8.6
	5	12	287	11.7	4.1	21.5	7.3	1.6	7.5
Flight, Centrifuged	16	6	273	10.8	4.0	21.8	12.0	1.4	4.5
	17*	-	103	2.0	1.9	-	132.0	0.5	0.5
	18	22	257	12.1	4.7	18.0	9.4	1.1	3.6
	19	4	253	8.6	3.4	22.5	11.9	1.1	2.3
	20	9	252	9.3	3.7	22.7	11.1	1.2	3.4
Synchronous, Stationary	26	2	280	11.0	3.9	20.3	19.4	1.2	4.9
	27	23	305	11.7	3.8	20.6	8.3	1.0	4.5
	28	7	295	10.9	3.7	20.9	10.4	2.1	3.8
	29	15	270	10.5	3.9	18.7	17.9	1.3	4.3
	30	21	290	11.3	3.9	23.8	9.3	0.9	2.8
Synchronous, Centrifuged	41	3	255	9.8	3.8	19.4	11.7	0.9	3.8
	42	16	275	10.2	3.7	18.5	14.9	0.9	2.7
	43	20	275	11.7	4.3	22.1	15.5	1.3	2.4
	44	19	270	9.7	3.6	18.8	36.8	0.9	2.6
	45	11	295	12.1	4.1	21.6	5.3	1.5	3.5
Vivarium	51	V-1	305	10.4	3.4	20.0	15.6	0.9	4.9
	52	V-2	320	11.2	3.5	18.4	23.0	0.9	4.1
	53	V-3	320	11.6	3.6	20.5	26.7	0.9	3.5
	54	V-4	285	9.8	3.4	20.6	16.7	1.2	4.2
	55	V-5	305	9.4	3.1	20.4	15.5	0.9	2.0
Omega Bios	61	8	310	11.0	3.6	22.8	12.9	1.3	4.1
	62	18	290	10.6	3.7	21.7	7.1	1.4	4.0
	63	10	270	10.2	3.8	19.9	12.0	0.9	3.6
	64	5	205	6.0	2.9	21.6	15.1	1.1	3.6
	65	25	320	11.1	3.5	22.1	12.5	2.1	3.4

* Data from this rat not used to calculate average as animal was severely fasted.

TABLE I B

INDIVIDUAL VALUES FOR RATS SACRIFICED AT R_0

Group	Rat No.		Enzyme Activity[a] (nmoles/min/mg Protein)									
	USSR	USA	GP	GS	HK	GK	PGM	GPDH	6PGDH	G6Pase[b]	PFK	FDP
Flight, Stationary	1	13	29.6	12.1	6.5	24.2	88	22.8	34.3	0.11	10.8	134
	2	14	36.0	12.3	6.6	28.6	107	39.0	45.3	0.11	12.2	190
	3	24	26.4	10.8	4.4	17.7	97	34.6	39.7	0.17	8.8	176
	4	1	30.4	10.1	5.5	28.0	99	10.8	35.1	0.17	11.7	174
	5	12	33.1	10.5	5.2	30.0	111	21.5	41.0	0.16	9.9	215
Flight, Centrifuged	16	6	39.5	14.0	5.8	28.2	101	19.6	43.6	0.14	9.1	166
	17	-	-	-	-	-	-	-	-	-	-	-
	18	22	33.2	14.6	4.9	29.9	119	39.4	51.2	0.11	13.1	197
	19	4	38.8	10.4	4.7	35.9	101	47.8	51.3	0.14	8.7	163
	20	9	38.1	10.6	5.2	31.8	114	55.1	58.0	0.13	7.6	192
Synchronous, Stationary	26	2	44.3	12.6	6.0	35.4	127	65.8	87.6	0.15	8.6	210
	27	23	36.8	14.8	5.5	33.6	115	41.0	50.4	0.12	10.3	225
	28	7	32.2	14.9	4.6	30.0	96	17.0	35.4	0.14	9.0	180
	29	15	38.0	17.2	5.5	31.5	119	30.8	44.3	0.16	10.0	226
	30	21	37.0	12.6	4.1	30.9	117	59.2	53.4	0.14	9.5	175
Synchronous, Centrifuged	41	3	38.5	14.4	5.2	33.4	123	66.8	65.8	0.16	8.0	217
	42	16	33.2	17.8	5.8	19.4	110	34.2	34.8	0.16	10.8	218
	43	20	34.4	13.0	5.0	30.9	109	28.6	41.9	0.17	9.0	186
	44	19	42.9	17.0	6.3	20.6	130	58.7	57.2	0.08	9.3	206
	45	11	45.7	12.4	4.3	36.9	110	51.2	49.8	0.11	8.4	194
Vivarium	51	V-1	34.6	24.7	5.8	24.8	124	136.0	54.7	0.13	11.8	203
	52	V-2	45.9	16.9	5.8	37.9	127	115.0	57.5	0.09	17.5	210
	53	V-3	45.1	13.4	5.5	35.3	140	129.0	65.2	0.08	12.5	196
	54	V-4	37.8	15.8	5.2	34.0	111	71.0	46.1	0.12	15.0	186
	55	V-5	40.5	15.4	5.2	31.6	128	143.0	74.7	0.10	9.7	206
Omega Bios	61	8	38.3	13.4	4.7	31.0	99	36.2	44.0	0.12	8.6	173
	62	18	35.5	15.3	6.5	34.0	117	51.9	46.4	0.14	9.3	228
	63	10	37.8	13.9	5.4	34.1	105	50.6	46.7	0.08	9.5	185
	64	5	40.0	14.0	4.3	35.6	104	25.3	46.4	0.13	16.4	179
	65	25	38.5	9.5	4.1	18.8	102	26.8	39.7	0.15	9.9	180

TABLE I C

INDIVIDUAL VALUES FOR RATS SACRIFICED AT R_0

	Rat No.		Enzyme Activity[a] (nmoles/min/mg Protein)											
						Trans-aminase					ICDH with Substrate:			
Group	USSR	USA	PK	LDH	αGPDH	GOT	GPT	CCE	ME	MDH	Cit	Acon	Isocit	FUM
Flight, Stationary	1	13	660	10114	487	477	665	19.3	39.2	6860	29.1	73.4	312	312
	2	14	862	10866	533	629	844	19.9	34.7	8172	33.0	78.3	406	450
	3	24	789	11319	526	454	697	23.2	34.5	8015	27.6	66.9	334	295
	4	1	836	11691	604	492	835	16.0	37.1	7552	27.7	68.7	322	299
	5	12	670	11272	568	771	996	14.1	23.3	8013	29.0	72.1	360	418
Flight, Centrifuged	16	6	676	9958	543	516	583	18.2	36.2	8272	38.6	94.0	398	407
	17	-	-	-	-	-	-	-	-	-	-	-	-	-
	18	22	695	10062	622	553	660	24.3	36.8	8095	30.5	81.2	384	293
	19	4	828	9216	546	450	642	26.5	42.2	6726	34.4	84.1	388	347
	20	9	821	10491	613	554	689	27.1	37.7	8015	35.1	86.3	368	369
Synchronous, Stationary	26	2	1329	12609	687	546	816	23.0	97.5	8843	38.1	93.3	375	356
	27	23	797	12142	552	685	979	14.9	27.5	7777	34.9	84.0	396	429
	28	7	815	10960	553	345	705	6.4	21.3	8012	30.9	71.3	360	259
	29	15	799	12406	593	662	966	8.0	29.1	8093	30.6	81.4	399	403
	30	21	810	11708	579	529	804	18.2	45.0	7712	33.2	80.9	366	316
Synchronous, Centrifuged	41	3	1100	12359	641	587	722	13.5	46.5	8216	36.9	95.3	393	387
	42	16	757	12627	660	532	926	8.9	16.1	9051	32.0	80.3	390	420
	43	20	876	10790	565	356	556	9.3	25.3	7577	29.8	74.9	355	333
	44	19	1032	13443	712	558	756	8.2	53.7	7922	39.6	91.0	405	388
	45	11	949	11700	576	446	691	13.5	40.9	8199	30.5	79.4	364	322
Vivarium	51	V-1	880	10530	575	426	584	23.0	106.0	7929	36.7	88.2	412	373
	52	V-2	840	11886	590	412	528	25.1	59.4	7858	38.3	88.8	458	451
	53	V-3	842	9752	595	460	491	23.5	80.5	6990	37.0	86.7	434	345
	54	V-4	713	11010	614	439	694	21.0	71.8	7972	30.8	82.1	368	342
	55	V-5	744	10880	556	505	656	31.3	101.0	6977	33.9	81.4	406	440
Omega Bios	61	8	790	9436	592	381	499	13.0	35.7	7556	35.2	80.2	383	328
	62	18	872	11348	667	627	887	26.2	32.8	8607	32.7	81.8	391	406
	63	10	862	10339	655	458	767	16.5	39.6	8495	32.7	82.2	390	316
	64	5	596	7155	516	491	126	24.6	22.5	7573	33.9	85.5	372	406
	65	25	600	9471	492	316	357	14.3	34.1	6455	33.7	82.2	324	331

TABLE I D

INDIVIDUAL VALUES FOR RATS SACRIFICED AT R_0

	Rat No.		Enzyme Activity[a] (nmoles/min/mg protein)								
			Acon with Substrates:					Pal CoA[d]		Acyl Trans.	
Group	USSR	USA	Cit	Acon	Isocit	AcCoAX[c]	FAS	Syn	Desat[e]	αGP	DG
Flight, Stationary	1	13	23.3	79.1	33.3	4.5	13.5	50.0	3.1	0.13	1.13
	2	14	25.6	95.0	38.9	9.8	16.6	42.4	1.2	0.03	0.51
	3	24	21.5	75.1	34.5	3.7	20.8	22.5	2.3	0.20	0.66
	4	1	27.9	72.6	35.6	2.7	17.4	25.8	5.4	0.04	0.61
	5	12	25.5	78.1	33.4	3.8	15.0	22.9	1.8	0.12	0.54
Flight, Centrifuged	16	6	32.2	94.8	47.4	3.6	10.4	11.5	2.3	0.18	2.25
	17	-	-	-	-	-	-	-	-	-	-
	18	22	27.6	89.1	37.2	4.5	12.8	19.2	0.7	0.10	1.05
	19	4	25.7	92.7	36.6	7.0	19.0	23.4	2.1	0.35	2.48
	20	9	30.1	93.3	44.3	5.1	19.0	27.1	2.0	0.33	2.07
Synchronous, Stationary	26	2	26.1	105.9	45.3	5.9	24.9	15.2	4.6	0.20	1.10
	27	23	26.9	93.8	40.2	2.7	10.8	40.8	1.7	0.20	1.68
	28	7	24.7	81.3	32.9	2.8	7.1	28.8	1.4	0.28	1.67
	29	15	27.6	83.4	37.1	4.1	10.1	30.3	0.6	0.24	1.33
	30	21	26.4	92.5	37.1	5.5	16.7	35.0	1.7	0.12	0.79
Synchronous, Centrifuged	41	3	35.4	102.6	45.0	5.1	16.1	13.2	2.4	0.20	1.55
	42	16	25.5	78.2	32.4	3.7	11.1	57.7	0.5	0.22	1.12
	43	20	26.0	75.5	31.9	2.6	12.9	31.6	0.7	0.15	1.38
	44	19	32.4	96.4	42.0	4.0	11.5	23.5	0.2	0.29	1.98
	45	11	26.0	89.5	33.1	2.5	19.3	26.6	1.8	0.22	1.67
Vivarium	51	V-1	29.9	97.6	41.0	6.9	21.4	83.3	2.3	0.14	1.63
	52	V-2	32.7	104.1	44.1	10.6	17.1	86.9	3.4	0.19	1.95
	53	V-3	37.9	105.4	45.0	5.6	16.0	62.8	2.3	0.16	1.55
	54	V-4	27.1	93.8	41.5	4.6	16.4	85	3.0	0.12	1.50
	55	V-5	26.8	94.5	44.3	8.1	18.9	100.7	4.3	0.15	1.82
Omega Bios	61	8	26.9	83.0	34.5	3.9	12.3	26.0	1.9	0.18	1.47
	62	18	26.3	84.0	34.5	5.2	26.5	50.9	2.7	0.18	1.53
	63	10	26.6	79.9	35.1	4.5	14.4	37.7	3.0	0.38	2.19
	64	5	29.3	87.6	37.4	4.1	13.0	13.2	0.7	0.13	1.55
	65	25	27.2	104.5	44.4	2.7	11.5	20.0	0.4	0.29	1.76

TABLE II A

INDIVIDUAL VALUES FOR RATS SACRIFICED AT R_{25}

Group	Rat No.		Weights at Sacrifice			Liver Constituent			
	USSR	USA	Carcass (grams)	Liver (grams)	Liver (% carc.)	Cytosol Protein (mg/ml)	Fatty Acid 16/16:1	Fatty Acid 18:2/20:4	Glycogen (% wet wt.)
Flight, Stationary	11	72	350	11.5	3.3	22.1	16.0	0.7	2.6
	12	51	320	9.7	3.0	20.7	17.3	0.6	1.6
	13	57	310	8.6	2.8	22.4	5.1	0.7	1.3
	14	74	330	9.0	2.7	23.0	28.7	0.5	1.9
	15	65	345	8.7	2.5	24.3	8.8	1.0	1.4
Flight, Centrifuged	21	52	380	12.9	3.4	20.9	10.9	1.0	3.7
	22	62	340	10.2	3.0	25.0	7.9	0.8	2.2
	23	67	340	10.6	3.1	22.0	9.6	0.7	2.4
	24	70	340	10.9	3.2	23.9	12.4	0.5	1.9
	25	59	350	10.1	2.9	24.0	17.1	0.6	2.3
Synchronous, Stationary	36	73	340	8.3	2.4	23.4	14.7	0.6	1.1
	37	69	335	10.7	3.2	22.5	12.1	1.0	2.5
	38	58	350	9.7	2.8	22.4	25.1	0.6	0.6
	39	66	315	9.1	2.9	23.2	24.3	0.6	1.4
	40	68	345	9.4	2.7	23.3	13.2	0.5	1.6
Vivarium	66	55	330	9.9	3.0	22.0	12.5	0.9	2.8
	67	56	325	9.4	2.9	20.9	15.8	0.8	1.4
	68	75	335	10.0	3.1	23.6	13.5	0.6	1.7
	69	53	325	10.2	3.1	21.3	18.4	0.7	3.6
	70	60	345	9.2	2.7	22.7	18.0	0.6	0.9
Omega Bios	76	54	310	9.1	2.9	21.5	21.1	0.6	0.8
	77	61	335	8.8	2.6	22.8	17.2	0.6	1.2
	78	63	350	8.7	2.5	22.3	26.7	0.4	2.5
	79	64	320	8.8	2.8	24.9	15.5	0.6	0.7
	80	-	-	-	-	-	-	-	-

TABLE II B

INDIVIDUAL VALUES FOR RATS SACRIFICED AT R_{25}

Group	Rat No.		Enzyme Activity[a] (nmoles/min/mg Protein)									
	USSR	USA	GP	GS	HK	GK	PGM	GPDH	6PGDH	G6Pase[b]	PFK	FDP
Flight, Stationary	11	72	39.1	10.7	5.4	27.6	104	97	62.5	0.12	10.2	198
	12	51	45.8	12.7	6.2	26.1	102	63	59.1	0.11	11.4	136
	13	57	48.4	15.0	6.2	36.5	96	138	43.3	0.15	7.4	187
	14	74	41.7	17.2	4.2	32.6	106	140	71.1	0.12	9.4	225
	15	65	46.8	14.4	5.1	34.4	109	144	62.1	0.13	8.5	196
Flight, Centrifuged	21	52	43.0	17.8	5.2	26.7	101	79	57.1	0.11	9.5	203
	22	62	45.0	16.2	4.9	31.5	102	123	65.7	0.11	7.8	212
	23	67	40.3	21.8	5.3	30.4	108	65	74.3	0.13	7.7	200
	24	70	44.2	16.8	5.1	33.2	113	86	73.8	0.11	8.8	199
	25	59	45.1	12.0	5.5	30.7	104	121	69.1	0.11	8.4	231
Synchronous, Stationary	36	73	42.1	15.5	5.0	26.0	107	70	58.6	0.14	8.5	194
	37	69	47.4	17.9	4.7	29.8	98	73	56.0	0.11	8.4	188
	38	58	45.6	13.2	6.6	24.6	104	74	49.0	0.10	14.6	184
	39	66	45.1	16.1	4.3	32.6	108	61	65.2	0.16	9.4	199
	40	68	52.1	15.1	4.0	47.4	121	190	84.4	0.14	9.5	213
Vivarium	66	55	44.0	14.2	5.5	27.9	104	97	62.8	0.09	9.5	197
	67	56	51.0	12.1	6.4	34.7	106	86	55.8	0.10	10.0	225
	68	75	43.0	24.3	4.5	29.9	113	114	62.6	0.11	7.4	220
	69	53	44.9	11.7	4.3	32.2	114	102	69.2	0.10	8.3	211
	70	60	54.0	13.4	5.5	30.7	104	121	69.1	0.12	8.4	214
Omega Bios	76	54	51.1	15.1	7.0	19.2	97	46	46.2	0.09	9.6	188
	77	61	46.5	11.2	4.4	25.2	98	47	43.6	0.12	8.4	221
	78	63	54.0	16.1	6.1	29.0	104	62	47.1	0.13	9.6	194
	79	64	46.8	17.7	4.0	34.2	117	89	56.7	0.17	7.8	204
	80	-	-	-	-	-	-	-	-	-	-	-

TABLE II C

INDIVIDUAL VALUES FOR RATS SACRIFICED AT R_{25}

	Rat No.		Enzyme Activity[a] (nmoles/min/mg Protein)											
						Trans-aminase					ICDH with Substrate:			
Group	USSR	USA	PK	LDH	αGPDH	GOT	GPT	CCE	ME	MDH	Cit	Acon	Isocit	FUM
Flight, Stationary	11	72	811	10952	544	451	767	13.0	39.0	6775	39.1	80.0	433	336
	12	51	854	12130	492	446	805	17.4	36.8	8167	33.2	74.7	377	276
	13	57	957	9113	523	442	750	27.0	41.3	7259	35.2	80.7	399	408
	14	74	799	10326	486	445	867	15.0	67.7	7280	37.2	83.8	428	436
	15	65	836	8480	542	470	885	18.6	54.7	6082	37.6	78.9	427	373
Flight, Centrifuged	21	52	801	10883	603	446	715	17.8	48.1	6856	39.4	78.1	416	407
	22	62	872	9785	491	516	879	30.7	70.8	5619	35.7	74.0	383	351
	23	67	1068	10560	582	456	856	14.2	34.6	6242	37.2	81.3	403	395
	24	70	1043	11089	536	546	877	22.9	37.3	8488	36.9	80.5	422	384
	25	59	873	10287	557	495	927	32.4	50.3	6843	31.5	71.0	377	327
Synchronous, Stationary	36	73	827	10689	538	485	850	10.2	32.0	7121	37.3	87.0	427	412
	37	69	902	10944	512	485	782	17.1	34.8	7299	36.3	74.5	416	294
	38	58	613	9127	490	451	516	12.6	23.3	7044	35.7	80.6	417	450
	39	66	746	10223	546	528	1245	29.3	48.4	6385	36.7	81.0	364	337
	40	68	971	10082	557	533	995	24.1	77.6	5756	37.7	84.5	430	361
Vivarium	66	55	999	9484	546	488	1036	19.5	49.2	6952	38.2	83.9	416	372
	67	56	878	10046	602	438	761	18.0	41.8	6417	40.0	86.9	424	329
	68	75	935	10297	575	490	947	28.7	49.5	7504	34.8	79.4	371	356
	69	53	995	10382	605	456	957	15.0	46.0	5896	36.9	75.9	383	427
	70	60	890	11918	594	498	780	13.8	46.0	6922	39.4	81.3	405	407
Omega Bios	76	54	813	9102	544	691	1122	8.9	21.1	7077	35.0	79.2	377	392
	77	61	659	11198	526	616	1073	6.7	19.1	6673	35.7	77.9	364	397
	78	63	691	12597	557	679	1319	13.3	26.5	7985	37.4	81.7	427	394
	79	64	865	11776	547	601	1285	14.2	37.4	8406	37.0	77.5	393	441
	80	-	-		-		-	-	-	-	-	-	-	-

TABLE II D

INDIVIDUAL VALUES FOR RATS SACRIFICED AT R_{25}

Group	Rat No. USSR	Rat No. USA	Enzyme Activity[a] (nmoles/min/mg Protein) Acon with Substrates: Cit	Acon	Isocit	AcCoAX[c]	FAS	Pal CoA[d] Syn	Desat[e]	Acyl Trans. αGP	DG
Flight, Stationary	11	72	32.7	114.1	48.0	5.9	21.1	35.7	1.4	0.18	1.74
	12	51	33.9	94.3	47.4	3.5	21.4	42.9	2.3	0.23	1.86
	13	57	31.5	93.3	47.6	8.0	28.3	57.1	3.7	0.24	2.04
	14	74	30.2	106.3	47.9	7.1	21.4	40.9	1.3	0.13	2.03
	15	65	34.6	100.5	45.5	4.5	24.0	31.8	1.5	0.38	2.55
Flight, Centrifuged	21	52	37.1	110.0	45.8	6.5	19.6	38.2	5.0	0.15	1.12
	22	62	35.2	95.8	52.1	8.2	28.0	40.9	4.4	0.23	1.86
	23	67	35.8	96.5	45.9	4.5	26.8	31.5	3.4	0.10	1.40
	24	70	32.8	93.6	47.8	11.0	27.3	49.4	2.9	0.19	2.01
	25	59	31.5	94.6	41.3	5.6	22.6	37.2	2.9	0.20	1.72
Synchronous, Stationary	36	73	31.6	101.1	43.1	6.2	15.7	63.8	0.7	0.21	2.14
	37	69	26.8	98.5	44.2	5.1	15.7	50.4	1.0	0.17	1.72
	38	58	34.2	102.0	47.0	4.7	15.6	34.0	0.6	0.22	2.62
	39	66	31.4	94.6	40.5	5.9	23.7	39.3	0.9	0.19	2.38
	40	68	35.8	109.2	49.5	-	31.4	25.2	1.6	0.23	2.17
Vivarium	66	55	33.2	102.4	49.9	7.3	23.2	35.5	1.2	0.16	1.51
	67	56	33.9	119.5	48.3	7.2	17.2	24.9	1.5	0.27	1.95
	68	75	27.8	101.1	45.4	8.4	25.8	38.8	1.7	0.22	1.82
	69	53	32.1	116.9	43.4	9.4	21.4	25.6	0.6	0.20	2.04
	70	60	36.0	92.5	41.9	5.6	14.0	48.2	1.0	0.36	3.26
Omega Bios	76	54	30.5	90.0	42.6	5.2	13.6	41.9	0.2	0.31	2.58
	77	61	31.1	93.3	41.3	4.1	12.6	40.9	0.2	0.33	2.39
	78	63	33.3	96.9	42.2	8.1	14.0	37.6	0.2	0.28	2.14
	79	64	31.0	95.9	45.6	5.9	23.7	37.0	1.0	0.27	2.39
	80	-	-	-	-	-	-	-	-	-	-

TABLE III A

AVERAGE VALUES† FOR RATS SACRIFICED AT R_0

Measurement††		Group					
		Flight		Synchronous		Controls	
Parameter	Units	Stationary	Centrifuged	Stationary	Centrifuged	Vivarium	Omega Bios
Weights							
Carcass	grams	304±44	259±10	288±14	274±14	307±14	279±46
Liver	grams	13.6±2.0	10.2±1.6	11.1±0.4	10.7±1.1	10.5±0.9	9.8±2.1
Liver/carc.	%	4.5±0.3	4.0±0.6	3.9±0.1	3.9±0.3	3.4±0.2	3.5±0.4
Liver Constit.							
Cyto. Protein	mg/ml	21.3±1.7	21.3±2.2	20.9±1.9	20.1±1.7	20.0±0.9	21.6±1.1
Glycogen	% wet wt.	7.4±2.0	3.5±0.8	4.1±0.7	3.0±0.6	3.7±1.1	3.7±0.3
Fatty acids							
16/16:1		7.1±2.5	11.1±1.1	13.1±5.2	16.4±12	19.5±5.9	11.9±2.9
18:2/20:4		1.5±0.2	1.2±0.1	1.3±0.5	1.1±0.3	1.0±0.1	1.4±0.5
Enzyme Activity[a]							
1. Carbohydrate							
GP	f	31.1±3.6	37.4±2.9	37.7±4.3	38.9±5.4	40.8±4.8	38.0±1.6
GS	f	11.2±1.0	12.4±2.2	14.4±1.9	14.9±2.4	17.2±4.4	13.2±2.2
HK	f	5.6±0.9	5.2±0.5	5.1±0.8	5.3±0.8	5.5±0.3	5.0±1.0
GK	f	25.7±5.0	31.5±3.3	32.3±2.2	28.2±7.8	32.7±5.0	30.7±6.9
PGM	f	100±9	109±8	115±10	116±10	126±10	105±7
GPDH	f	25.7±11.2	40.5±15.3	42.8±20.1	47.9±16.2	119±29	38.4±12.9
6GPDH	f	39.1±4.5	51.0±5.9	54.2±19.9	49.9±12.2	59.6±10.8	44.6±3.0
G6Pase	b	0.14±0.03	0.13±0.01	0.14±0.01	0.14±0.04		0.12±0.03
PFK	f	10.7±1.4	9.6±2.4	9.5±0.6	9.1±1.1	13.3±3.0	10.7±3.2
FDP	f	178±29	180±18	203±24	204±1.4	200±9	189±22
PK	f	763±94	755±81	910±234	943±134	804±71	744±137
LDH	f	11052±601	9932±530	11965±655	12184±999	10812±775	9550±1550
αGPDH	f	543±44	581±42	593±56	631±61	586±22	584±79

† Each value is presented as the mean ± its standard deviation.

†† See footnotes to Tables for individual units.

TABLE III B

AVERAGE VALUES† FOR RATS SACRIFICED AT R_0

Measurement††		Group					
		Flight		Synchronous		Controls	
Parameter	Units	Stationary	Centrifuged	Stationary	Centrifuged	Vivarium	Omega Bios
2. Krebs Cycle							
CCE	f	18.5±3.5	24.0±4.1	14.1±6.9	10.7±2.6	24.8±3.9	18.9±6.1
ME	f	33.8±6.2	38.2±2.7	44.1±31.1	36.5±15.5	83.7±19.6	32.9±6.4
MDH	f	7722±535	7777±109	8087±451	8193±54.5	7545±514	7737±871
FUM	f	355±73	354±48	352±68	370±41	390±52	357±45
ICDH							
a. Cit	f	29.3±2.2	34.7±3.3	33.5±3.1	33.8±4.3	35.3±3.0	33.6±1.0
b. Acon	f	71.9±4.4	86.4±5.5	82.2±7.9	84.2±8.6	85.4±3.5	82.4±1.9
c. Isocit	f	345 ±38	385±13	379±18	381±21	416±34	372±28
ACON							
a. Cit	f	24.8±2.4	28.9±2.8	26.3±1.1	29.1±4.6	30.1±4.6	27.3±1.2
b. Acon	f	80.0±8.8	92.5±2.4	91.4±9.8	88.4±11.6	99.1±5.4	87.8±9.7
c. Isocit	f	35.1±2.3	41.4±5.3	38.5±4.6	36.9±6.2	43.2±1.8	37.2±4.2
Transaminase							
a. GOT	f	565±134	518±49	553±135	496±94	449±36	455±118
b. GPT	f	807±132	644±45	854±117	730±133	591±85	674±360
3. Lipids							
AcCoAX	c	4.9±2.8	5.0±1.4	4.2±1.5	3.6±1.1	7.2±2.3	4.1±0.9
FAS	f	16.7±2.8	15.3±4.4	13.9±7.1	14.2±3.5	18.0±2.2	15.5±6.2
Pal CoA Syn	d	32.7±12.3	20.3±6.7	30.0±9.5	30.5±16.6	83.7±13.5	29.6±14.9
Desat	e	2.8±1.6	1.8±0.7	2.0±1.5	1.1±0.9	3.1±0.8	1.7±1.2
Acyl trans							
a. αGP	g	0.10±0.07	0.24±0.12	0.21±0.06	0.22±0.05	0.15±0.03	0.23±0.1
b. DG	g	0.69±0.25	1.96±0.63	1.31±0.38	1.54±0.32	1.69±0.19	1.70±0.29

† Each value is presented as the mean ± its standard deviation.

†† See footnotes to Tables for individual units.

TABLE IV A

AVERAGE VALUES† FOR RATS SACRIFICED AT R_{25}

Measurement††		Group					
		Flight		Synchronous		Controls	
Parameter	Units	Stationary	Centrifuged	Stationary	Centrifuged	Vivarium	Omega Bios
Weights							
Carcass	grams	331±17	350±17	337±14	-	332±8	329±18
Liver	grams	9.5±1.2	10.9±1.2	9.4±0.9	-	9.7±0.4	8.9±0.2
Liver/carc.	%	2.9±0.3	3.1±0.2	2.8±0.3	-	3.0±0.2	2.7±0.2
Liver Constit.							
Cyto. Protein	mg/ml	22.5±1.3	23.2±1.7	23.0±0.5	-	22.1±1.1	22.9±1.5
Glycogen	% wet wt.	1.8±0.5	2.5±0.7	1.4±0.7	-	2.1±1.1	1.3±0.8
Fatty acids							
16/16:1		15.2±9.1	11.6±3.5	17.9±6.3	-	15.6±2.6	20.1±5.0
18:2/20:4		0.7±0.2	0.7±0.2	0.7±0.2	-	0.7±0.1	0.6±0.1
Enzyme Activity[a]							
1. Carbohydrate							
GP	f	44.4±3.8	43.5±2.0	46.5±3.7	-	47.4±4.8	49.6±3.6
GS	f	14.0±2.5	16.9±3.5	15.6±1.7	-	15.1±5.2	15.0±2.8
HK	f	5.4±0.8	5.2±0.2	4.9±1.0	-	5.2±0.9	5.4±1.4
GK	f	31.4±4.4	30.5±2.4	32.1±9.1	-	31.1±2.6	26.9±6.3
PGM	f	103±5	106±5	108±8	-	108±5	104±9
GPDH	f	116±35	95±26	94±54	-	104±14	61±20
6GPDH	f	59.6±10.2	68.0±7.1	62.5±13.3	-	63.9±5.6	48.4±5.7
G6Pase	b	0.13±0.02	0.11±0.01	0.13±0.02	-	0.10±0.01	0.13±0.03
PFK	f	9.4±1.5	8.4±0.7	10.1±2.6	-	8.7±1.0	8.9±0.9
FDP	f	188±33	209±13	196±11	-	213±11	202±14
PK	f	851±63	931±117	812±139	-	939±57	757±9.8
LDH	f	10200±1453	10521±513	10213±700	-	10425±809	11168±1492
αGPDH	f	517±27	554±43	529±27	-	584±24	544±13

† Each value is presented as the mean ± its standard deviation.

†† See footnotes to Tables for individual units.

TABLE IV 'B

AVERAGE VALUES† FOR RATS SACRIFICED AT R_{25}

Measurement††		Group					
		Flight		Synchronous		Controls	
Parameter	Units	Stationary	Centrifuged	Stationary	Centrifuged	Vararium	Omega Bios
2. Krebs Cycle							
CCE	f	18.2±5.4	23.6±7.9	18.7±8.0	-	19.0±5.9	10.8±3.6
ME	f	47.9±13.1	48.2±14.3	43.2±21.2	-	46.5±3.1	26.0±8.2
MDH	f	7113±764	6810±1068	6721±641	-	6738±608	7535±799
FUM	f	366±63	373±33	371±61	-	378±39	406±24
ICDH							
a. Cit	f	36.5±2.3	36.1±2.9	36.7±0.8	-	37.9±2.1	36.3±1.1
b. Acon	f	79.6±3.3	77.0±4.4	81.5±4.7	-	81.5±4.2	79.1±1.9
c. Isocit	f	413±24	400±20	411±27	-	340±22	390±27
ACON							
a. Cit	f	32.6±1.8	34.5±2.3	32.0±3.4	-	32.6±3.0	31.5±1.2
b. Acon	f	47.2±1.0	46.6±3.9	44.9±3.5	-	45.8±3.3	42.9±1.9
c. Isocit	f	101.7±8.7	98.1±6.7	101.1±5.4	-	106.5±11.4	94.0±3.1
Transaminase							
a. GOT	f	451±11	492±42	496±34	-	474±26	647±45
b. GPT	f	815±60	851±80	878±269	-	896±120	1200±121
3. Lipids							
AcCoAX	c	5.8±1.8	7.2±2.5	5.5±0.7	-	7.6±1.4	5.8±1.7
FAS	f	23.2±3.1	24.9±3.6	20.4±7.1	-	20.3±4.7	16.0±5.2
Pal CoA Syn	d	41.7±9.7	39.4±6.5	42.5±15.0	-	34.6±9.7	39.4±2.4
Desat	e	2.0±1.0	3.7±0.9	1.0±0.4	-	1.2±0.4	0.4±0.4
Acyl trans							
αGP	g	0.23±0.09	0.17±0.05	0.20±0.02	-	0.24±0.08	0.30±0.03
DG	g	2.04±0.31	1.62±0.36	2.21±0.33	-	2.12±0.67	2.38±0.18

† Each value is presented as the mean ± its standard deviation.

†† See footnotes to Tables for individual units.

TABLE V A

HEPATIC FATTY ACID COMPOSITION OF RATS SACRIFICED AT R_0

Group	Rat No. USSR	Rat No. USA	Percent of Total Fatty Acids as: 14:0	16:0	16:1	18:0	18:1
Flight, Stationary	1	13	0.3	18.8	2.7	13.0	15.7
	2	14	0.3	16.7	1.5	13.9	12.2
	3	24	1.1	20.0	4.2	9.1	18.5
	4	1	0.5	19.9	3.6	12.0	17.0
	5	12	0.6	19.6	2.7	13.8	15.5
Average ± S.D.			0.6 ± 0.3	19.0 ± 1.4	2.9 ± 1.0	12.4 ± 2.0	15.8 ± 2.3
Flight, Centrifuged	16	6	0.9	19.2	1.6	13.4	16.3
	17*	-	0	13.2	0.1	30.6	5.5
	18	22	0.4	19.7	2.1	13.7	11.4
	19	4	0.2	19.1	1.6	17.3	12.0
	20	9	0.3	22.2	2.0	17.7	5.5
Average ± S.D.			0.5 ± 0.3	20.1 ± 1.5	1.8 ± 0.3	15.5 ± 2.3	11.3 ± 4.4
Synchronous, Stationary	26	2	0.3	17.5	0.9	15.9	12.2
	27	23	0.4	19.2	2.3	14.8	12.7
	28	7	0.8	17.7	1.7	11.8	16.6
	29	15	0.1	17.9	1.0	16.3	11.5
	30	21	0.4	19.6	2.1	11.5	12.6
Average ± S.D.			0.4 ± 0.3	18.4 ± 1.0	1.6 ± 0.6	14.1 ± 2.3	13.1 ± 2.0
Synchronous, Centrifuged	41	3	0.2	18.7	1.6	19.1	13.6
	42	16	0.3	19.4	1.3	15.8	9.5
	43	20	0.4	20.0	1.5	15.2	11.1
	44	19	0.1	18.4	0.5	19.1	8.5
	45	11	0.3	13.2	2.5	8.0	16.8
Average ± S.D.			0.3 ± 0.1	17.9 ± 2.7	1.5 ± 0.7	15.4 ± 4.5	11.9 ± 3.3
Vivarium	51	V-1	0.1	18.7	1.2	18.9	11.2
	52	V-2	2.4	18.4	0.8	14.2	11.6
	53	V-3	1.7	18.7	0.7	16.8	9.6
	54	V-4	0.2	20.0	1.2	13.7	11.8
	55	V-5	2.2	20.2	1.3	13.6	11.2
Average ± S.D.			1.3 ± 1.1	19.2 ± 0.8	1.0 ± 0.3	15.4 ± 2.3	11.1 ± 0.9
Omega Bios	61	8	0.2	19.3	1.5	15.3	13.8
	62	18	0.3	17.7	2.5	12.8	15.3
	63	10	0.1	18.0	1.5	15.5	13.2
	64	5	0.2	19.6	1.3	18.7	13.4
	65	25	0.5	18.6	1.5	11.4	16.2
Average ± S.D.			0.3 ± 0.2	18.6 ± 0.8	1.7 ± 0.5	14.7 ± 2.8	14.4 ± 1.3

* Data from this rat not used to calculate average as animal was severely fasted.

TABLE V B

HEPATIC FATTY ACID COMPOSITION OF RATS SACRIFICED AT R_0

Group	Rat No.		Percent of Total Fatty Acids as:				
	USSR	USA	18:2	18:3	20:2	20:3	20:4
Flight, Stationary	1	13	25.8	0.1	0.8	1.4	21.4
	2	14	29.7	0	0.6	1.0	20.3
	3	24	30.4	0.8	0.7	1.1	14.2
	4	1	26.8	0.1	1.1	1.8	17.3
	5	12	27.7	0.1	0.9	1.7	17.3
Average ± S.D.			28.1 ± 1.9	0.2 ± 0.3	0.8 ± 0.2	1.4 ± 0.4	18.1 ± 2.8
Flight, Centrifuged	16	6	27.2	0.1	0.6	1.3	19.4
	17*	-	15.6	0.3	0.9	0.6	33.2
	18	22	26.2	0.2	0.4	1.0	24.9
	19	4	24.8	0.1	0.6	0.8	23.5
	20	9	27.2	0.1	0.7	1.0	23.2
Average ± S.D.			26.4 ± 1.1	0.1 ± 0	0.6 ± 0.1	1.0 ± 0.2	22.8 ± 2.4
Synchronous, Stationary	26	2	27.4	0.1	1.0	0.9	23.8
	27	23	23.5	0.1	0.7	1.3	25.1
	28	7	33.4	0.2	1.0	1.0	15.7
	29	15	29.3	0.2	0.5	0.9	22.2
	30	21	28.5	0.1	0.5	1.0	23.8
Average ± S.D.			28.4 ± 3.6	0.1 ± 0.1	0.7 ± 0.3	1.0 ± 0.2	22.1 ± 3.7
Synchronous, Centrifuged	41	3	21.0	0.2	0.6	0.8	24.2
	42	16	23.6	0.1	0.6	0.7	28.7
	43	20	27.1	0.1	0.8	0.8	23.0
	44	19	23.9	0.8	0.4	0.7	27.6
	45	11	31.5	0.2	0.8	1.8	25.1
Average ± S.D.			25.4 ± 4.0	0.3 ± 0.3	0.6 ± 0.2	1.0 ± 0.5	25.7 ± 2.4
Vivarium	51	V-1	23.0	0.1	0.7	1.1	25.1
	52	V-2	24.3	0.1	0.8	1.2	26.4
	53	V-3	24.0	0	0.6	1.0	26.9
	54	V-4	27.9	0	0.6	1.2	23.2
	55	V-5	22.2	0	2.1	2.1	25.5
Average ± S.D.			24.3 ± 2.2	0 ± 0.1	1.0 ± 0.6	1.3 ± 0.4	25.4 ± 1.4
Omega Bios	61	8	27.3	0.1	0.7	1.2	23.5
	62	18	29.0	0.1	0.6	1.2	20.4
	62	10	23.3	0.2	0.8	1.4	26.0
	64	5	23.6	0.1	0.3	0.8	22.0
	65	25	33.9	0.4	0.5	0.6	16.5
Average ± S.D.			27.4 ± 4.4	0.2 ± 0.1	0.6 ± 0.2	1.0 ± 0.3	21.1 ± 3.4

* Data from this rat not used to calculate average as animal was severely fasted.

TABLE VI A

HEPATIC FATTY ACID COMPOSITION OF RATS SACRIFICED AT R_{25}

Group	Rat No. USSR	Rat No. USA	Percent of Total Fatty Acids as: 14:0	16:0	16:1	18:0	18:1
Flight, Stationary	11	72	0.2	17.6	1.1	20.1	9.2
	12	51	0.2	17.3	1.0	20.1	9.7
	13	57	0	19.8	3.9	20.6	11.5
	14	74	0.1	17.2	0.6	25.6	7.0
	15	65	0.2	19.4	2.2	18.6	10.5
Average ± S.D.			0.1 ± 0.1	18.3 ± 1.2	1.8 ± 1.3	21.0 ± 2.7	9.6 ± 1.7
Flight, Centrifuged	21	52	0.2	20.7	1.9	17.5	14.5
	22	62	0.4	18.9	2.4	17.3	14.4
	23	67	0.3	18.2	1.9	22.1	9.7
	24	70	0.2	17.3	1.4	21.6	9.6
	25	59	0.2	18.8	1.1	21.1	11.0
Average ± S.D.			0.3 ± 0.1	18.8 ± 1.3	1.7 ± 0.5	19.9 ± 2.3	11.8 ± 2.5
Synchronous, Stationary	36	73	0.2	17.6	1.2	20.0	9.3
	37	69	0.3	18.2	1.5	16.5	13.4
	38	58	0	17.6	0.7	23.8	7.7
	39	66	0	19.4	0.8	24.9	8.5
	40	68	0.3	18.5	1.4	23.5	9.9
Average ± S.D.			0.2 ± 0.2	18.3 ± 0.8	1.1 ± 0.4	21.7 ± 3.5	9.8 ± 2.2
Vivarium	66	55	0	18.8	1.5	21.2	10.8
	67	56	0.2	19.0	1.2	18.3	11.2
	68	75	0	18.9	1.4	21.0	8.2
	69	53	0.2	18.4	1.0	21.1	8.7
	70	60	0.2	18.0	1.0	21.8	7.6
Average ± S.D.			0.1 ± 0.1	18.6 ± 0.4	1.2 ± 0.2	20.7 ± 1.4	9.3 ± 1.6
Omega Bios	76	54	0	16.9	0.8	24.7	6.5
	77	61	0.2	17.2	1.0	21.6	8.6
	78	63	0.1	16.0	0.6	25.4	5.6
	79	64	0.2	17.0	1.1	23.5	8.7
	80	-	-	-	-	-	-
Average ± S.D.			0.1 ± 0.1	16.8 ± 0.5	0.9 ± 0.2	23.8 ± 1.7	7.4 ± 1.6

TABLE VI B

HEPATIC FATTY ACID COMPOSITION OF RATS SACRIFICED AT R_{25}

	Rat No.		Percent of Total Fatty Acids as:			
Group	USSR	USA	18:2	20:2	20:3	20:4
Flight,	11	72	21.6	0.4	0	29.8
Stationary	12	51	20.0	0.3	0.2	31.3
	13	57	17.7	0	0	26.5
	14	74	15.4	0	0	34.1
	15	65	23.7	0	0.6	25.0
Average ± S.D.			19.7 ± 3.3	0.1	0.2	29.3 ± 3.7
Flight,	21	52	22.5	0	0	22.7
Centrifuged	22	62	20.6	0.5	0.4	25.1
	23	67	18.8	0	0	29.1
	24	70	16.0	0.4	0.8	32.7
	25	59	18.4	0	0	29.5
Average ± S.D.			19.3 ± 2.4	0.2	0.2	27.8 ± 3.9
Synchronous,	36	73	19.8	0.3	0.2	31.5
Stationary	37	69	24.8	0.5	0.9	24.0
	38	58	18.7	0	0	31.6
	39	66	17.1	0	0	29.3
	40	68	15.9	0	0	30.6
Average ± S.D.			19.3 ± 3.4	0.2	0.2	29.4 ± 3.2
Vivarium	66	55	22.2	0	0	25.6
	67	56	22.9	0	0	27.3
	68	75	18.2	0	0	32.3
	69	53	21.5	0	0	29.1
	70	60	18.8	0	0	32.7
Average ± S.D.			20.7 ± 2.1	0	0	29.4 ± 3.1
Omega Bios	76	54	18.6	0	0	32.6
	77	61	19.7	0.2	0.4	31.1
	78	63	14.8	0.2	0	37.5
	79	64	17.6	0	0	32.0
	80	-	-	-	-	-
Average ± S.D.			17.7 ± 2.1	0.1	0.1	33.3 ± 2.9

TABLE VII A

DIFFERENCES FOUND IN R_0 RATS

Measurement	Difference Between*:			
	FS^+ vs. FC	FS vs. SS^+	FC^+ vs. SC^+	FC vs. SS
Weights				
Liver/carc.	+13% (>0.1)	+15% (<0.01)	none	none
Liver Constit.				
Fatty acids				
C16/16:1	-36% (<0.01)	-46% (<0.05)	-32% (<0.1)	none
C18:2/20:4	+25% (<0.05)	none	none	none
Glycogen	+111% (<0.01)	+80% (<0.01)	none	none
Enzyme Activity				
1. Carbohydrate				
GS	none	-22% (<0.01)	none	none
GP	-20.3% (>0.02)	-21.2% (<0.05)	none	none
HK	none	none	none	none
GK	-18% (<0.1)	-20% (<0.05)	none	none
PGM	none	none	none	none
GPDH	-37% (>0.1)	-40% (>0.1)	none	none
6PGDH	-23% (<0.02)	-28% (<0.2)	none	none
G6Pase	none	none	none	none
PFK	none	none	none	none
FDP	none	-12% (<0.2)	-12% (<0.05)	none
PK	none	-16% (<0.2)	-20% (<0.05)	none
LDH	+11% (<0.05)	-8% (<0.1)	-18% (<0.01)	-17% (<0.01)
αGPDH	none	none	none	none

* Values are presented as percent increase, +, or percent decrease, -, with the p values in ( ) calculated from the Student's t distribution (38). Those p values which are less than 0.05 are considered significant.

+ FS = Flight, Stationary; FC = Flight, Centrifuged; SS = Synchronous, Stationary; SC = Synchronous, Centrifuged.

TABLE VII B

DIFFERENCES FOUND IN R_0 RATS

Measurement	Difference Between*:			
	FS+ vs. FC	FS vs. SS+	FC+ vs. SC+	FC vs. SS
Enzyme Activity (Cont'd.)				
2. Krebs cycle				
CCE	-23% (<0.1)	none	+124% (<0.001)	+70% (<0.05)
ME	none	none	none	none
MDH	none	none	none	none
FUM	none	none	none	none
ICDH				
a. Cit	-16% (<0.05)	-13% (<0.05)	none	none
b. Acon	-17% (<0.01)	-13% (<0.05)	none	none
c. Isocit	-11% (<0.1)	-9% (<0.2)	none	none
ACON				
a. Cit	-14% (>0.05)	-6% (>0.2)	none	none
b. Acon	-14% (<0.05)	-12% (<0.1)	none	none
c. Isocit	-15% (<0.05)	-9% (<0.2)	none	none
Transaminase				
a. GOT	none	none	none	none
b. GPT	none	none	none	-25% (>0.01)

* Values are presented as percent increase, +, or percent decrease, -, with the p values in ( ) calculated from the Student's t distribution (38). Those p values which are less than 0.05 are considered significant.

\+ FS = Flight, Stationary; FC = Flight, Centrifuged; SS = Synchronous, Stationary; SC = Synchronous, Centrifuged.

TABLE VII C

DIFFERENCES FOUND IN R_0 RATS

Measurement	Difference Between*:			
	FS+ vs. FC	FS vs. SS+	FC+ vs. SC+	FC vs. SS
Enzyme Activity (Cont'd.)				
3. Lipids				
AcCoAX	none	none	none	none
FAS	none	none	none	none
Pal CoA Syn	none	none	none	none
Desat	none	none	none	none
Acyl trans				
a. αGP	-54% (>0.05)	-46% (<0.05)	none	none
b. DG	-65% (<0.01)	-48% (<0.02)	none	none

* Values are presented as percent increase, +, or percent decrease, -, with the p values in ( ) calculated from the Student's t distribution (38). Those p values which are less than 0.05 are considered significant.

+ FS = Flight, Stationary; FC = Flight, Centrifuged; SS = Synchronous, Stationary; SC = Synchronous, Centrifuged.

FOOTNOTES TO ALL TABLES

a - GS for glycogen synthetase (UDP glucose : α-1,4-glucan α-4-glucosyltransferase, EC 2.4.1.11);

GP for glycogen phosphorylase (α-1,4-glucan: orthophosphate glucosyltransferase, EC 2.4.1.1);

HK for hexokinase (ATP:D-hexose-6-phosphotransferase, EC 2.7.1.1);

GK for glucokinase (ATP:D-glucose-6-phosphotransferase, EC 2.7.1.2);

PGM for phosphoglucomutase (α-D-glucose-1,6-diphosphate: α-D-glucose-1-phosphate phosphotransferase, EC 2.7.5.1);

GPDH for glucose-6-phosphate dehydrogenase (D-glucose-6-phosphate: NADP oxidoreductase, EC 1.1.1.49);

6PGDH for phosphogluconate dehydrogenase (6-phospho-D-gluconate: NADP oxidoreductase, EC 1.1.1.44);

G6Pase for glucose-6-phosphatase (D-glucose-6-phosphate phosphohydrolase, EC 3.1.3.9);

PFK for phosphofractokinase (ATP:D-fractose-6-phosphate 1-phosphotransferase, EC 2.7.1.11);

FDP for hexosediphosphatase (D-fructose-1,6-diphosphate 1-phosphohydrolase, EC 3.1.3.11);

PK for pyruvate kinase (ATP:pyruvate phosphotransferase, EC 2.7.1.40);

LDH for lactate dehydrogenase (L-lactate: NAD oxidoreductase, EC 1.1.1.27);

αGPDH for glycerol-3-phosphate dehydrogenase (L-glycerol-3-phosphate: NAD oxidoreductase EC 1.1.1.8);

CCE for ATP citrate lyase (ATP: Citrate oxaloacetate lyase [CoA-acetylating and ATP-dephosphorylating], EC 4.1.3.8);

ME for malate dehydrogenase (decarboxylating) (NADP) (L-malate:NADP (L-malate: NADP oxidoreductase [decarboxylating], EC 1.1.1.40);

MDH for malate dehydrogenase (L-malate: NAD oxidoreductase, EC 1.1.1.37);

FUM for fumarase (L-malate hydro-lyase, EC 4.2.1.2);

ICDH for isocitrate dehydrogenase (NADP) (threo-D_s-isocitrate: NADP oxidoreductase [decarboxylating], EC 1.1.1.42);

Cit for citrate;

Acon for cis-aconitate;

Isocit for threo-D_s-isocitrate;

ACON for aconitate hydrotase (citrate [isocitrate] hydro-lyase, EC 4.2.1.3);

GOT for glutamic oxalacetic transaminase (L-aspartate: 2-oxoglutarate aminotransferase, EC 2.6.1.1);

GPT for glutamic pyruvate transferase (L-alanine: 2-oxoglutarate amino-transferase, EC 2.6.1.2);

AcCoAX for acetyl-CoA carboxylase (acetyl-CoA: carbon dioxide ligase [ADP], EC 6.4.1.2);

FAS for fatty acid synthetase;

Pal CoA Syn for acyl-CoA synthetase (Acid:CoA ligase [AMP], EC 6.2.1.3);

Desat for Acyl-CoA desaturase (stearyl CoA: oleoyl CoA desaturase); and

Acyl Trans. for acyl-CoA transferase (acyl-CoA: L-glycerol-3-phosphate acyltransferase, EC 2.3.1.15).

αGP for α-glycerol phosphate (glycerol-3-phosphate);

DG for diglyceride

b - μmoles of phosphate released per minute per mg microsomal protein.

c - nmoles of carbon dioxide fixed into malonyl CoA per 10 minutes per mg cytosol protein.

d - nmoles of palmityl CoA formed per minute per mg microsomal protein.

e - nmoles of oleate formed per 5 minutes per mg microsomal protein.

f - nmoles of substrate utilized per minute per mg cytosol protein.

g - nmoles of substrate converted to product per minute per mg microsomal protein.

An acceptable method to determine whether an enzymatic alteration is affecting the metabolic capacity of a tissue is to determine whether the level of the products or of the substrates of that particular enzyme are influenced by the conditions which have affected the enzyme. For this reason, we investigated two liver constituents in connection with the activities of the hepatic enzymes concerned with their anabolism or catabolism. We looked at the level of glycogen and of the activities of both glycogen synthetase and of glycogen phosphorylase. We also investigated the ratio of a pair of fatty acids, namely, palmitic (16:0) acid, a saturated fatty acid and palmitoleic (16:1) a monounsaturated fatty acid of the same chain length (16 carbons). This pair of fatty acids were singled out for special attention since the experimental diet did not contain appreciable amounts of this monounsaturated acid and we reasoned that the entire hepatic content of this acid must thus have come from its immediate precursor, palmitic acid, by the action of the enzyme desaturase.

We could show that there were statistically significant differences between the glycogen contents of the livers of rats in the group Flight Stationary (FS) and all other groups sacrificed at R_0 (Tables I A, III A). As a possible explanation for this, we have observed that although glycogen synthetase activity in this group was about the same as that in all other groups, its glycogen phosphorylase activity (an enzyme concerned with glycogen breakdown) was significantly less (Table III A and VII A). In the case of the ratio 16:0/16:1, we did observe a statistically significant difference between the FS group and all

other groups sacrificed at R_0 however, although hepatic desaturase activity was lower in this group, it was not of statistical significance (Table VII A).

DISCUSSION

Ideally, if one is to investigate the reasons why specific carbohydrates and lipids accumulate within, or are removed from, an organ during or following spaceflight, one should deal with whole, fresh tissues from animals (e.g., tissue slices or separated cells) and study both synthesis and degradation of the materials in question. However, due to the remote location in which the space vehicle was recovered, and because of logistical problems, sophisticated experiments of the type required to answer such questions were not feasible. Thus, a study of physiological responses to spaceflight using sensitive enzymatic markers, many of which are known to be affected by changes in diet, hormonal content, and general status of the animals, was chosen as the next best approach. With these techniques we were able to obtain important information that bears on the capacity of the liver to carry out both catabolic and anabolic reactions vital to the metabolism of the organism.

It is well known that the activities of certain hepatic enzymes concerned with the conversion of carbohydrates to lipids are affected by the nutritional as well as the hormonal status of the animal. Thus, for example, the activities of hepatic glucokinase, glucose-6-phosphate dehydrogenase, malic enzyme, citrate cleavage enzyme, acetyl-CoA carboxylase and fatty acid synthetase, among others, are reduced to low levels

in fasting normal and in diabetic rats, whereas these same enzymatic activities are elevated when the rats are fed diets high in carbohydrates (glucose, fructose or sucrose). Indeed, previous experiments have revealed that the levels of some hepatic enzyme activities are totally dependent upon diet, whereas others are controlled both by diet and hormones (3). Armed with this knowledge, we were very concerned about the nutritional status of the rats used in these experiments (COSMOS 936); for we did not want dietary influences to interfere with other physiological factors which might be encountered due to weightlessness. A very important consideration in drawing conclusions from data from our experiments is the question of appropriate controls. This was clearly recognized by the Soviet planners for this mission in that they provided four different control groups for the rats that were subjected to space flight.

Only those animals which were fed under identical conditions and had exhibited similar weight gains should be used for valid comparisons. The vivarium controls did not fulfill these criteria since their feeding regimen differed substantially from that of both the flight animals and the other ground control rats. This difference in dietary treatment clearly resulted in vastly different activities for many hepatic enzymes when compared to any of the other groups of rats (Table VII A,B and C).

For metabolic experiments of the type that were under investigation here, we feel that the most meaningful comparisons are those between animals in flight that were subjected to weightlessness and those that were centrifuged during flight. This contention is based on an assumption,

yet to be proven, that centrifugation in space adequately substitutes for the gravitational effects of the terrestrial environment. For this reason it was extremely important to compare the results obtained from the centrifuged flight animals with those from the synchronous ground controls. When this is done (Tables VII A, B and C), it is evident that for virtually all of the parameters measured in this experiment, the values for the flight centrifuged and the synchronous group control animals at R_0 were not significantly different. Therefore one conclusion that seemed justified from our data is that centrifugation during flight is equivalent to terrestrial gravity - at least for those parameters that we have measured.

If, indeed, centrifugation during flight is an adequate substitute for terrestrial gravity, then it is all the more important to compare the results from the two sets of flight animals because both sets of animals were subjected to all of the environmental factors, including diet, as well as the stresses of launch and recovery, associated with the space flight, and hence the two sets can be considered to be identical except for the gravity component.

When one compares the data from the two sets of flight animals, a number of significant differences are observed. One of the most striking differences is their respective contents of liver glycogen. As is seen in Fig. 1, the weightless group, at R_0, contained, on the average, more than twice the amount of glycogen of the centrifuged group. In turn, the centrifuged group contained about the same glycogen content as the synchronous ground controls. Finally, twenty-five days after recovery

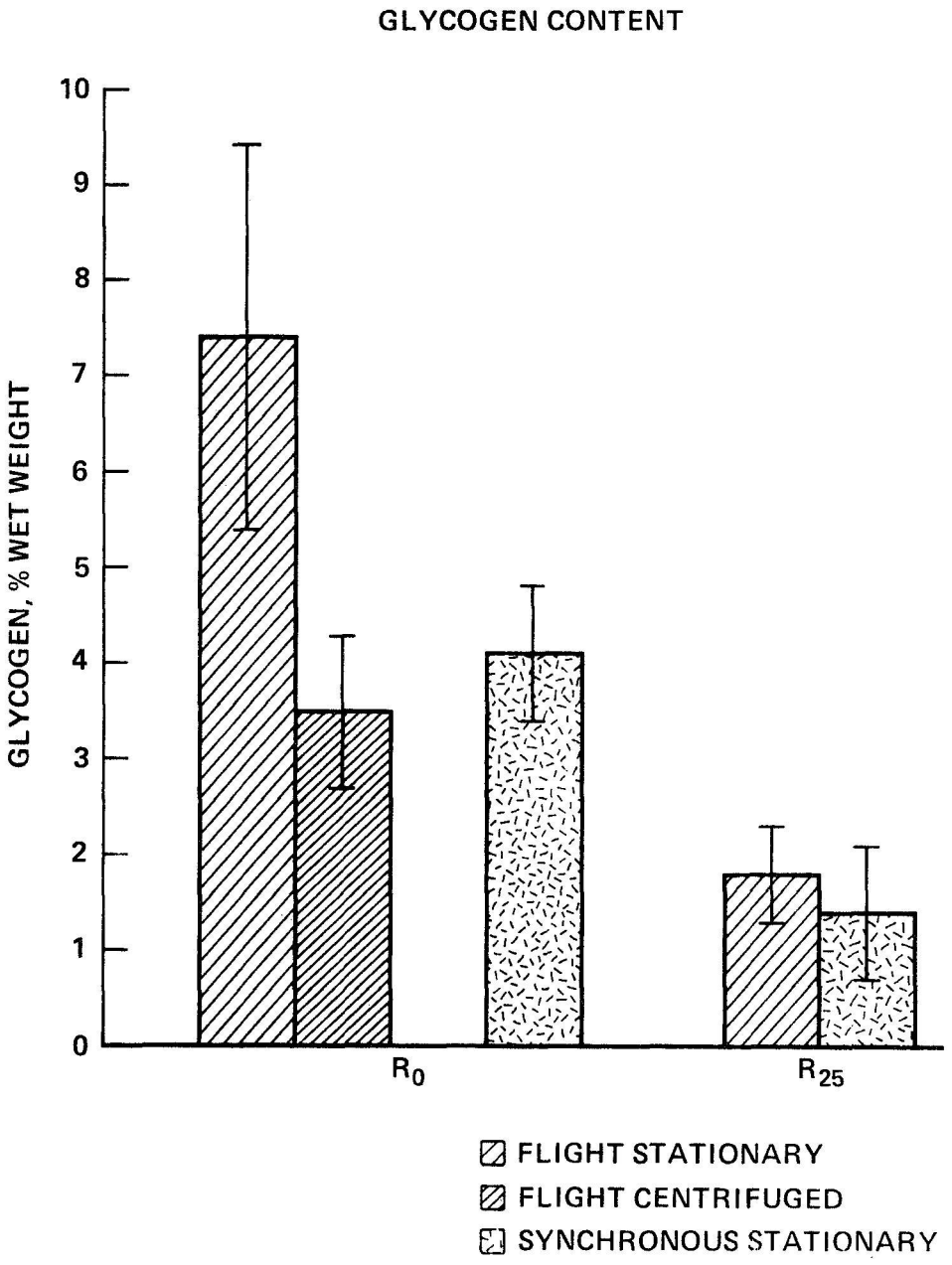

Figure 1. Liver glycogen levels in flight and synchronous control rats at recovery (R_0) and at 25 days postflight (R_{25}). A comparison of the mean values (the vertical lines indicate the standard deviations of the means) from flight rats and control rats sacrificed at R_0 showed statistically significant differences between the following groups:

Flight Stationary (FS) vs Flight Centrifuged (FC), $P < 0.01$

Flight Stationary (FS) vs Synchronous Stationary (SS), $P < 0.01$

(R_{25}), the content of glycogen in the livers of the flight animals had decreased and was now equivalent to the synchronous controls at R_{25}. In an attempt to understand this large glycogen content in the weightless group, we studied the principal enzymes concerned with the synthesis and breakdown of glycogen, namely glycogen synthetase and glycogen phosphorylase. The results of these analyses (Fig. 2) indicated no change in glycogen synthetase activity in the uncentrifuged animals and therefore suggest no modification in the synthesis of glycogen. However, the high level of glycogen in these animals' livers can be explained by the observed significant decrease in the activity of glycogen phosphorylase.

Another clear enzymatic difference between the weightless and centrifuged rats became evident in assays used to measure the conversion of citrate to α-ketoglutarate (an important series of reactions of the Krebs cycle [tricarboxylic acid cycle] in the extramitochondrial compartment of the hepatic cells). Using citrate as substrate, it was observed (Fig. 3) that the weightless group produced significantly lower amounts of α-ketoglutarate than the centrifuged group. In further tests, this time with aconitate as the substrate, this defect was maintained (Fig. 4), suggesting either a deficiency in aconitase or isocitrate dehydrogenase. However, when specific individual assays for these two enzymes were carried out, the data clearly showed no significant change in isocitrate dehydrogenase (Fig. 5) but did reveal a lowered activity of aconitase, using three different assay systems (Fig. 6). As with glycogen, the significance of these findings was strengthened by the fact that all of the observed changes in aconitase activity returned to normal twenty-five days after recovery.

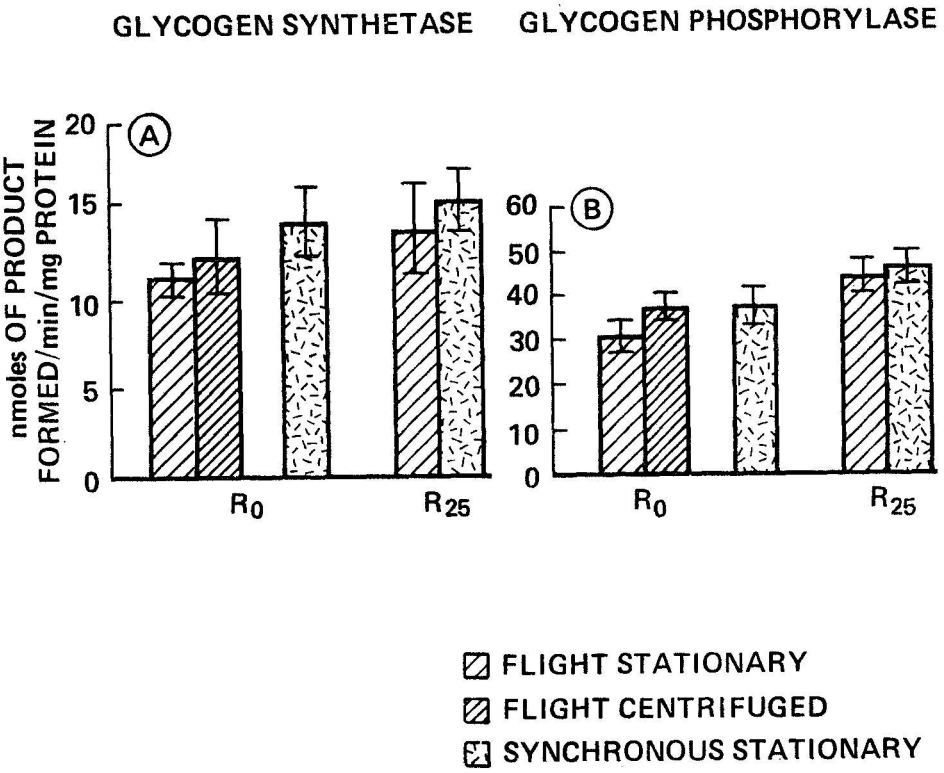

Figure 2A. Hepatic glycogen synthetase activity in flight and control rats at R_0 and R_{25}. Units of enzyme activity given as nmoles uridine diphosphate formed /min/mg protein. The vertical bars indicate the standard deviation for each group of rats.

B. Hepatic glycogen phosphorylase activity in flight and control rats at R_0 and R_{25}. Units of enzyme activity are given as nmoles of glucose-1-phosphate formed /min/mg protein. The vertical bars indicate the standard deviation for each group of rats. Statistical differences were noted between the following groups at R_0:

Flight Stationary (FS) vs Flight Centrifuged (FC), $P > 0.02$

Flight Stationary (FS) vs Synchronous Stationary (SS), $P < 0.05$

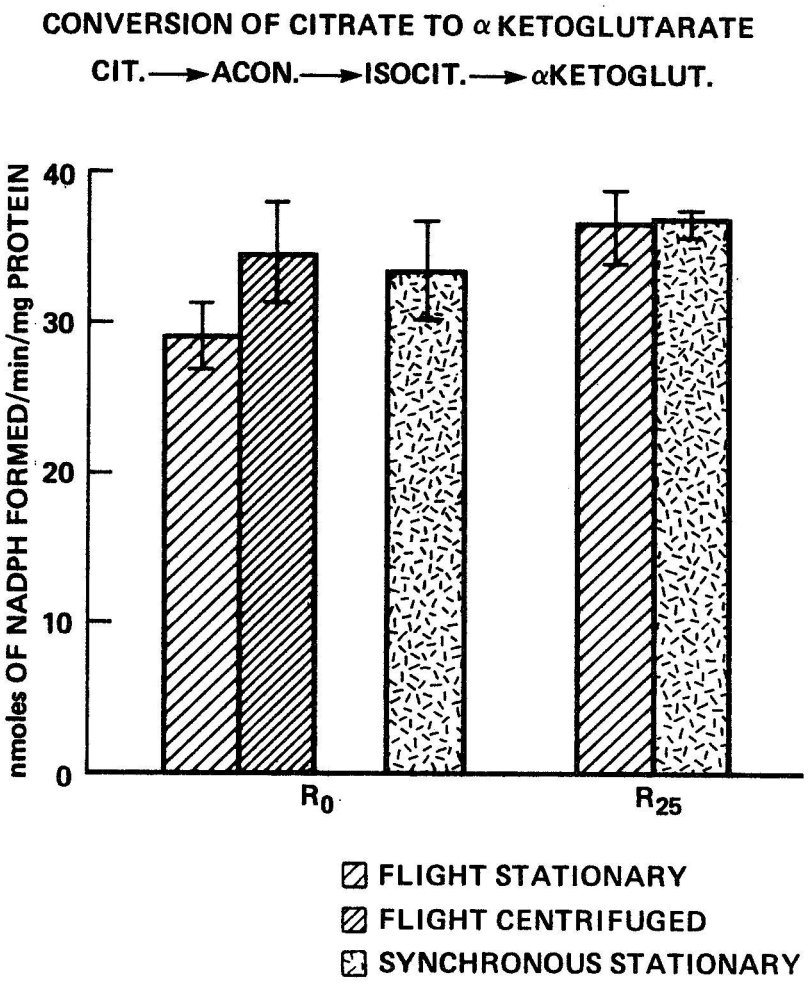

Figure 3. Hepatic aconitase and isocitrate dehydrogenase activities in flight and control rats sacrificed at R_0 and at R_{25}. Units of enzyme activity are given as nmoles of NADPH formed /min/mg protein when citrate served as substrate for aconitase and isocitrate dehydrogenase in the soluble (cytosol) portion of the hepatic cell. The vertical bars indicate the standard deviation from the mean values for rats sacrificed at R_0 and at R_{25}. Significant differences were only observed in the R_0 group between:

Flight Stationary (FS) vs Flight Centrifuged (FC), $P < 0.05$

Flight Stationary (FS) vs Synchronous Stationary (SS), $P < 0.05$

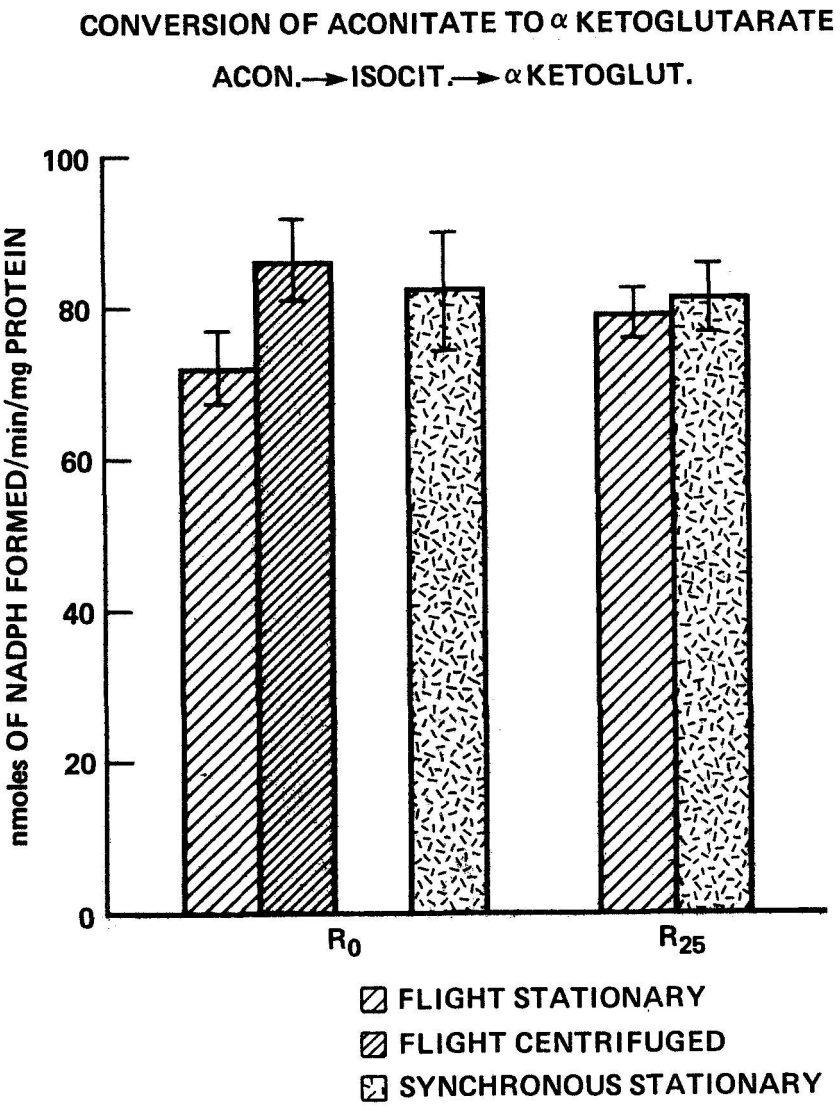

Figure 4. Hepatic aconitase and isocitrate dehydrogenase activities in flight and control rats with aconitate as substrate. Units of enzyme activity are given as nmoles of NADPH formed /min/mg protein in the soluble portion of the liver cells obtained from rats sacrificed at R_0 and R_{25}. Standard deviations from the mean values are given as vertical bars. Significant differences were only observed in the R_0 group between:

Flight Stationary (FS) vs Flight Centrifuged (FC), $P < 0.01$

Flight Stationary (FS) vs Synchronous Stationary (SS), $P < 0.05$

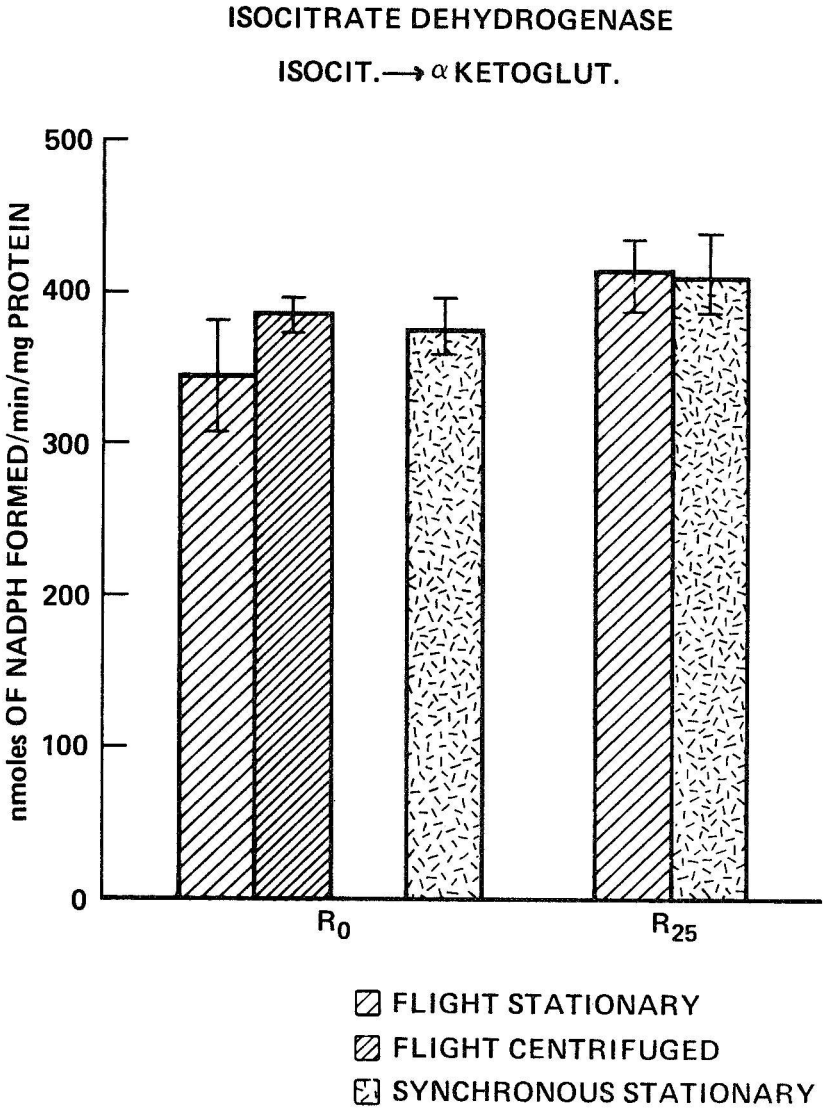

Figure 5. Hepatic isocitrate dehydrogenase in the soluble portion (cytosol) of the livers of rats sacrificed at R_0 and at R_{25}. See Figures 3 and 4 for units. No statistical differences between any of the groups of rats were observed.

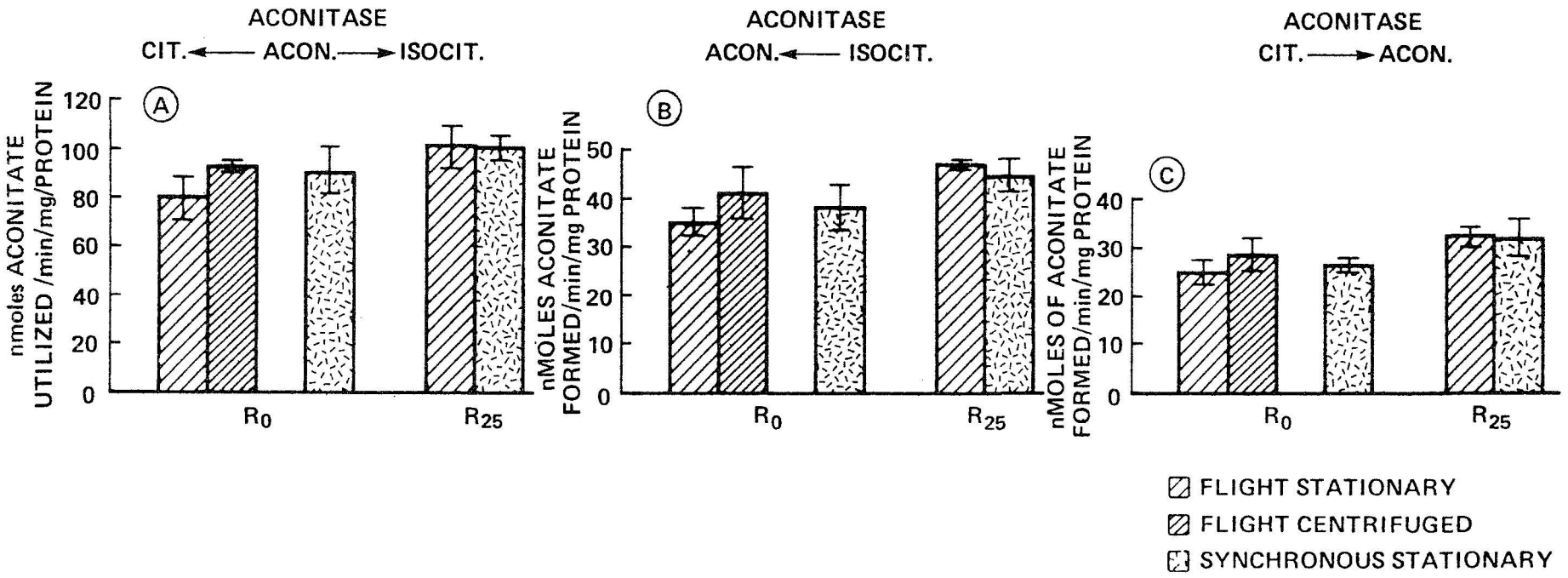

FIGURE 6 Soluble hepatic aconitase activities in flight and control rat livers sacrificed at R_0 and at R_{25} with (A) aconitate, (B) isocitrate or (C) citrate as substrate. The values are presented as the means and their standard deviations of either the disappearance (A) or appearance (B and C) of aconitate (nmoles) per min/mg protein. Significant differences were observed at R_0 in (A) between,

Flight Stationary (FS) vs Flight Centrifuged (FC), $P < 0.05$, and in (B) between,
Flight Stationary (FS) vs Flight Centifuged (FC), $P < 0.05$.

Since the generation of reducing power (NADPH) for biosynthetic purposes represents another potential focus for regulation, several enzymes involved in this process were assayed. Of these, 6-phosphogluconate dehydrogenase had statistically significant lower activity in livers from the weightless group (Fig. 7) as compared to any of the others, and it also returned to normal levels after twenty-five days. Glucose-6-phosphate dehydrogenase activity showed the same general pattern, but did not meet the test for statistical significance (38) (See Table VII). This was true for a small number of other enzymes that were tested (Table I) and, as such, point toward enzymatic targets that may warrant further study in future flights. It is noteworthy, however, that most of the enzyme activities did not show any significant differences between the weightless and centrifuged flight rats.

While we did not attempt to make a complete inventory of hepatic lipids, we were able to measure the pattern of fatty acids in the rat livers. These analyses (Table I A) revealed a remarkable shift in ratio of palmitic (16:0) to palmitoleic (16:1) fatty acids (Fig. 8). During the period of flight, substantial changes in the metabolism of fatty acids must have taken place in order to yield these results. However, our results on the activities of enzymes concerned with lipid synthesis do not identify the specific site of impairment in this process.

Several key enzymes of lipid biosynthesis, many of which are known to be regulatable, were studied in this experiment, including acetyl-CoA carboxylase, fatty acid synthetase, palmitoyl-CoA synthetase, and stearoyl-CoA desaturase. All of these enzymes, which are involved in the conversion

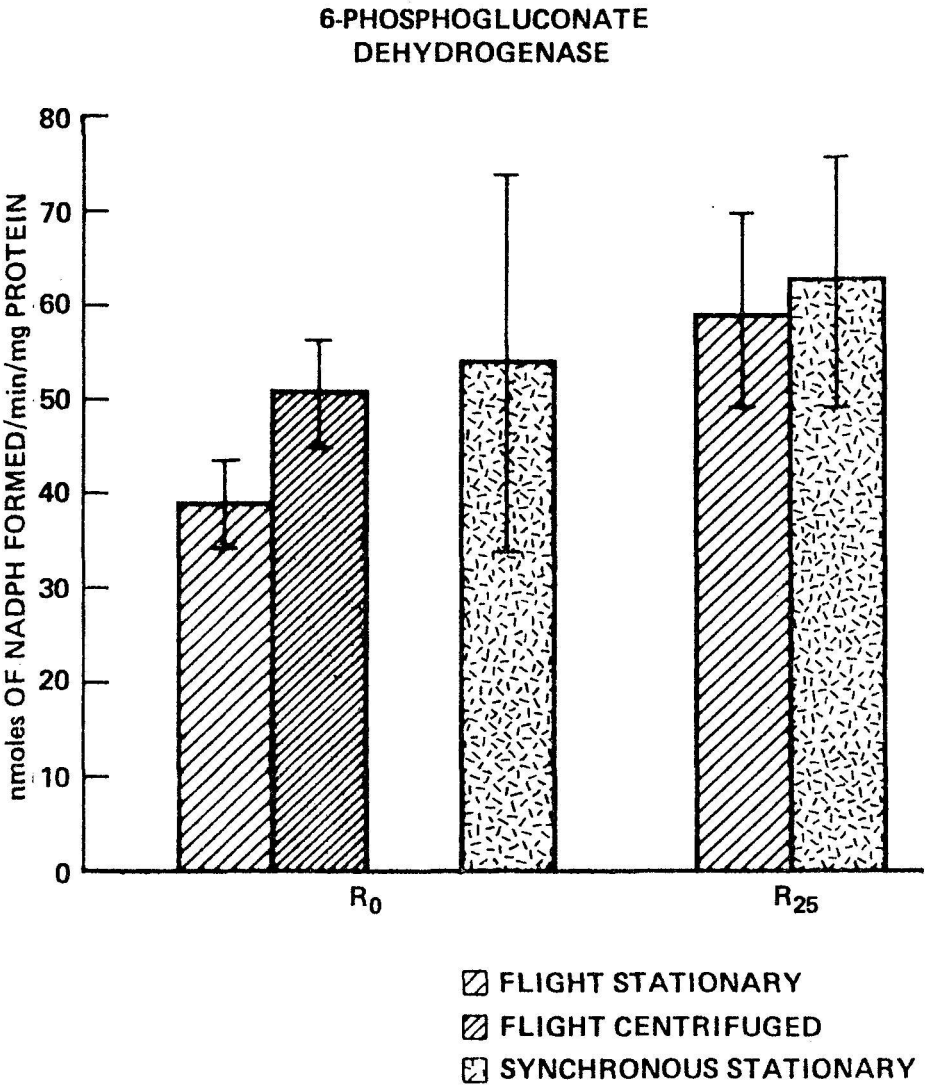

Figure 7. Hepatic 6-phosphogluconate dehydrogenase activities of the rats sacrificed at R_0 and at R_{25}. Statistical differences were only found in the rats at R_0 between, Flight Stationary (FS) vs Flight Centrifuged (FC), $P < 0.02$.

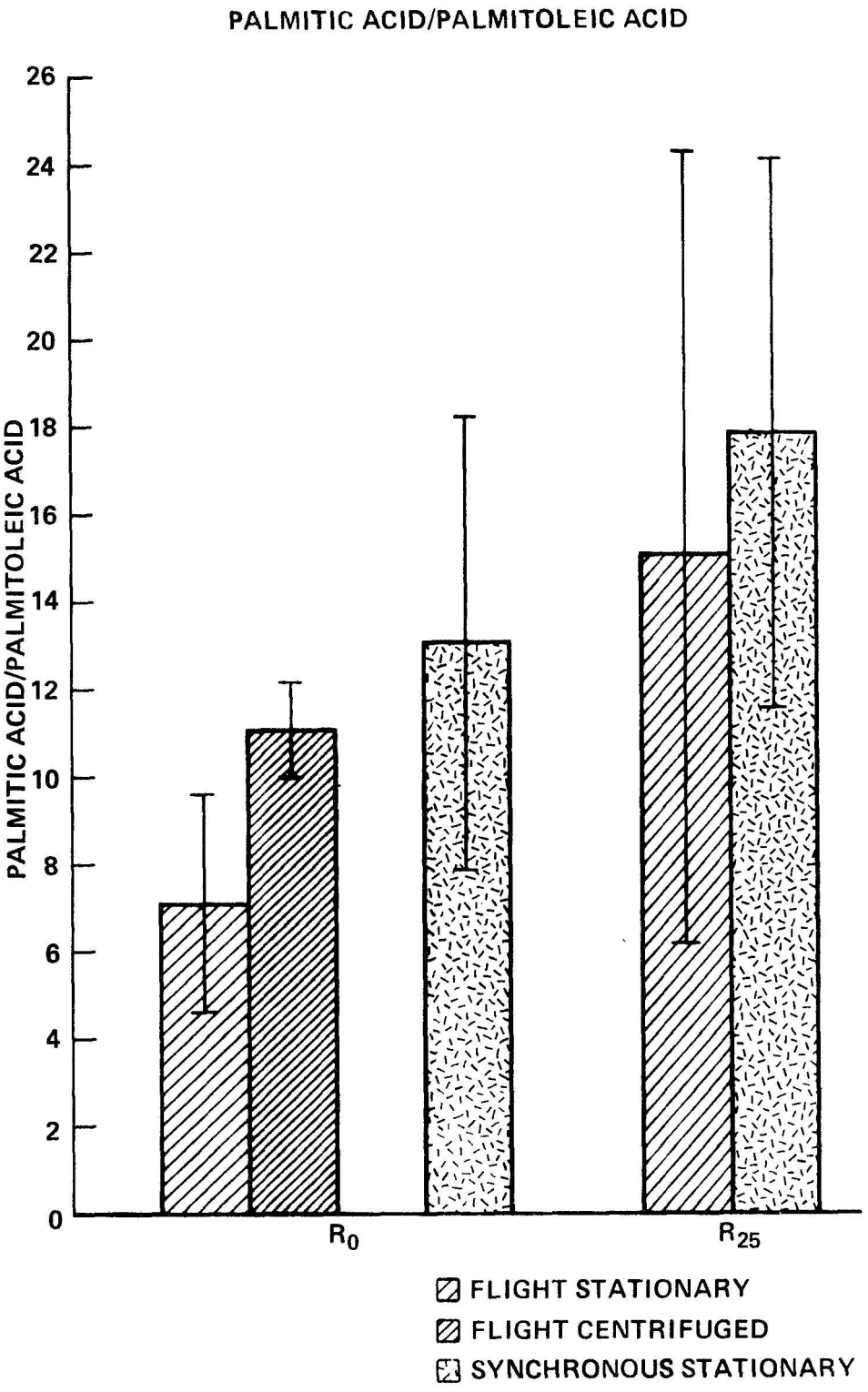

Figure 8. A comparison of the values for the ratios of hepatic palmitate/palmitoleate in rats sacrificed at R_0 and at R_{25}. Statistically significant differences were only observed between the R_0 groups:

Flight Stationary (FS) vs Flight Centrifuged (FC), $P < 0.01$

Flight Stationary (FS) vs Synchronous Stationary (SS), $P < 0.05$

of acetyl-CoA into long chain saturated and unsaturated fatty acids and their CoA esters, were found not to be affected by the weightless condition (Table VII C). However, in the subsequent ability of the livers to complex long-chain fatty acid esters, a severe reduction was observed in the livers of the uncentrifuged group of animals. As is seen in Fig. 9, the acyl transferases for both α-glycerol phosphate and diglyceride were reduced in activity when compared with the flight centrifuged animals (Table VII C). This severe enzymatic restriction (54% for α-glycerol phosphate acyl transferase and 65% for diglyceride acyl transferase) was alleviated completely after twenty-five days. The decreased activity of these two enzymes suggest an impaired ability of the liver to form triglycerides and phospholipids. Indeed, decreases in the content of these hepatic lipids were noted immediately after the COSMOS 690 flight (6), although in the earlier COSMOS 605 flight, Belitskaya (8) reported finding increases in the phospholipid content of rat liver after flight.

The results of our experiments, taken as a whole, do not, of course, resolve the issue of weight loss consistent with isocaloric food intake during spaceflight. However, they do focus upon metabolic changes in the liver at the enzyme level which may be involved in this process. The alterations that we have uncovered, particularly those that involve increased glycogen levels and decreased activities of the acyl transferases concerned with lipid synthesis, appear to be unique to the weightless condition. Generally conditions that lead to high glycogen levels invariably lead to increased levels of acyl transferase activity in the liver (14,29).

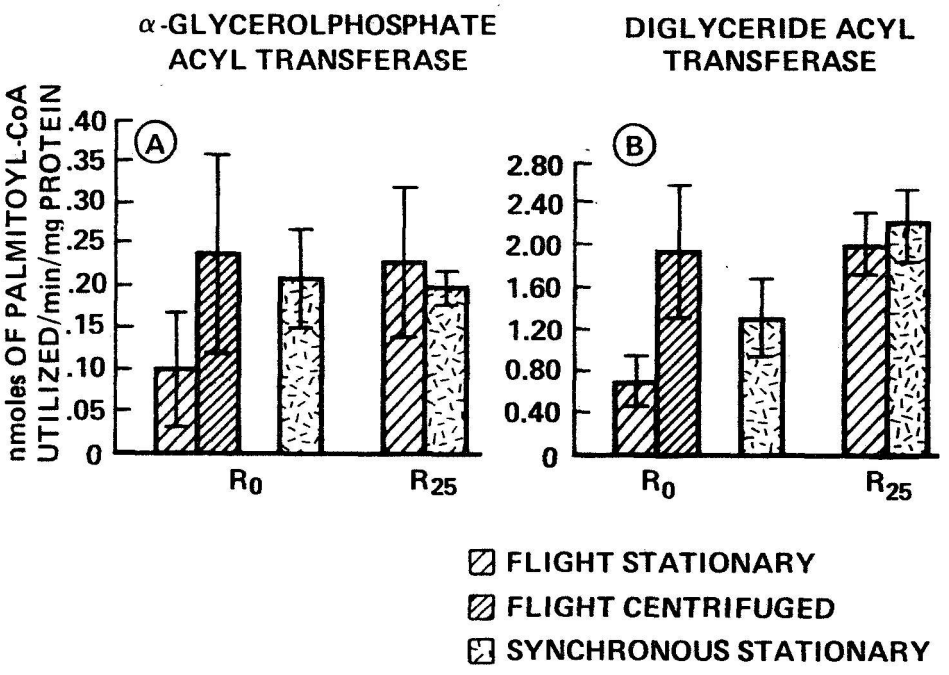

Figure 9. Hepatic acyl transferase activities of rats sacrificed at R_0 and at R_{25} with either α-glycerol phosphate (A) or diglyceride (B) as accepter for palmitoyl-CoA.

(A) α-glycerol phosphate acyltransferase activity in the liver microsomes of the Flight Stationary (FS) group was lower than that in the Flight Centrifuged (FC) group but the standard deviation precluded a statistical significance ($P > 0.05$). A statistically significant difference ($P < 0.05$) was observed between:

Flight Stationary (FS) vs Synchronous Stationary (SS), $P < 0.05$

(B) diglyceride acyl transferase activity in the livers of flight and synchronous control rats at R_0 showed the following groups to be significantly different:

Flight Stationary (FS) vs Flight Centrifuged (FC), $P < 0.01$

Flight Stationary (FS) vs Synchronous Stationary (SS), $P < 0.02$

ACKNOWLEDGEMENT

We would like to express our great appreciation for all of the efforts of our Russian colleagues which made this project possible. Special thanks are due to Drs. R. A. Tigranyan and Y. Kondratyev, as well as to Drs. E. A. Nosova and E. G. Vetrova. In addition, the efforts of our American associates, Ms. Hope McGrath, Ms. Linda Jahnke and Dr. Lewis Hillyard are also acknowledged.

Special thanks are due to Mr. Kenneth A. Souza, Manager, Cosmos Project (Ames Research Center), whose untiring energy helped with all logistical aspects of this investigation.

REFERENCES

1. Abraham, S., K. J. Matthes and I. L. Chaikoff. Fatty acid synthesis from acetate by normal and diabetic rat liver homogenate fractions. I. A comparison of cofactor requirements. J. Biol. Chem. 235:2551-2559, 1960.
2. Abraham, S., K. J. Matthes and I. L. Chaikoff. Factors involved in synthesis of fatty acids from acetate by a soluble fraction obtained from lactating rat mammary gland. Biochim. Biophys. Acta 49:268-285, 1961.
3. Abraham, S., L. Kopelovich and I. L. Chaikoff. Dietary and hormonal regulation of the hepatic citrate-cleavage enzyme. Biochim. Biophys. Acta 93:185-187, 1964.
4. Abraham, S., L. Kopelovich, P. R. Kerkof, and I. L. Chaikoff. Metabolic characteristics of preparations of isolated sheep thyroid cells. I. Activity levels of enzymes concerned with glycolysis and the tricarboxylic acid cycle. Endocrinology 76:178-190, 1965.
5. Anonymous. Results of scientific investigations on Cosmos 605 satellite, Preliminary Report, 1974.
6. Anonymous. Results of scientific investigations on Cosmos 690 satellite. Preliminary Report, 1975.
7. Anonymous. Preliminary results of the scientific experiments of the Cosmos 936 Biosatellite. Inst. of Medical and Biological Problems, Ministry of Health, USSR and the "Intercosmos" Council, Academy of Sciences, USSR, Moscow, Report 1977 p. 1-78, 1977.

8. Belitskaya, R. A. Carbohydrate and lipid content of rat liver tissue following a 22-day space flight. Space Biol. and Aerospace Med. 4:97-99, 1977.

9. Bergmeyer, H. and E. Bernt. Glutamate-oxaloacetate transaminase. In: Methods of Enzymatic Analysis (H. Bergmeyer, ed.), Academic Press, Inc., New York. 1963. pp. 837-845.

10. Bergmeyer, H. and E. Bernt. Glutamate-pyruvate transaminase. In: Methods of Enzymatic Analysis (H. Bergmeyer, ed.), Academic Press, Inc., New York. 1963. pp. 846-853.

11. Berry, C. A. Weightlessness. In: "Bioastronautic Data Book", 2nd ed., Chap. 8, pp. 349-415. Washington, D. C., NASA, 1973, (NASA SP-3006).

12. Borrebaek, B., S. Abraham, and I. L. Chaikoff. Enzymatic removal of glucose-6-phosphate from fructose-6-phosphate preparations. Anal. Biochem. 8:367-372, 1964.

13. Bücher, T., and G. Pfleiderer. In: Methods in Enzymology (S. P. Colowick and N. O. Kaplan, eds.), Vol. I, Academic Press, Inc., New York. 1955. pp. 435-440.

14. Fallon, H. J. and E. L. Kemp. Effects of diet on hepatic triglyceride synthesis. J. Clin. Invest. 47:712-719, 1968.

15. Gornall, A. G., C. J. Bardawill and M. M. David. Determination of serum proteins by means of the biuret reaction. J. Biol. Chem. 177:751-766, 1949.

16. Hassid, W. Z. and S. Abraham. Chemical procedures for analysis of polysaccharides. I. Determination of glycogen and starch. In: Methods in Enzymology (S. P. Colowick and N. O. Kaplan, eds.), Vol. III, Academic Press, Inc., New York. 1957. pp. 34-38.

17. Hill, R. L. and R. A. Bradshaw. Fumarase E.C. 4.2.1.2 L-Malate hydrolase. In: Methods in Enzymology (J. M. Lowenstein, ed.), Vol. XIII, Academic Press, Inc., New York. 1969. pp. 91-99.

18. Horecker, B. L. and A. Kornberg. The extinction coefficients of the reduced band of pyridine nucleotides. J. Biol. Chem. 175:385-390, 1948.

19. Horecker, B. L., and P. Z. Smyrniotis. 6-Phosphogluconic dehydrogenase. In: Methods in Enzymology (S. P. Colowick and N. O. Kaplan, eds.), Vol. I, Academic Press, Inc., New York. 1955. pp. 326-327.

20. Klein, H. P. Synthesis of lipids in resting cells of Saccharomyces cerevisiae. J. Bacteriol. 69:620-627, 1955.

21. Klein, H. P. Nature of particles involved in lipid synthesis in yeast. J. Bacteriol. 90:227-234, 1965.

22. Kornberg, A. and B. L. Horecker. Glucose-6-phosphate dehydrogenase. In: Methods in Enzymology (S. P. Colowick and N. O. Kaplan, eds.), Vol. I, Academic Press, Inc., New York. 1955. pp. 323-326.

23. Lin, C. Y., S. Smith and S. Abraham. Acyl specificity in triglyceride synthesis by lactating rat mammary gland. J. Lipid Res. 17:647-656, 1976.

24. Lindberg, O. and L. Ernster. Determination of organic phosphorus compounds by phosphate analysis. In: Methods of Biochemical Analysis (D. Glick, ed.), Interscience Publishers, Inc., New York. 1960.

25. Lowry, O. H., N. J. Rosebrough, A. L. Farr and R. J. Randall. Protein measurement with folin phenol reagent. J. Biol. Chem. 193:265-275, 1951.

26. Mendicino, J., H. Abou-Issa, R. Medicus and N. Kratowich. Fructose-1,6-diphosphatase, phosphofructokinase, glycogen synthetase, phosphorylase, and protein kinase from swine kidney. IV. Purification and properties of phosphorylase. In: Methods in Enzymology (W. A. Wood, ed.), Vol. XLII, Academic Press, Inc., New York. 1975. pp. 389-394.

27. Mendicino, J., H. Abou-Issa, R. Medicus and N. Kratowich. Fructose-1,6-diphosphatase, phosphofructokinase, glycogen synthetase, phosphorylase, and protein kinase from swine kidney. I. Isolation and properties of glycogen synthetase. In: Methods in Enzymology (W. A. Wood, ed.), Vol. XLII, Academic Press, Inc., New York. 1975. pp. 375-381.

28. Nordlie, R. C. and W. J. Arion. Glucose-6-phosphatase. In: Methods in Enzymology (S. P. Colowick and N. O. Kaplan, eds.), Vol. IX, Academic Press, Inc., New York. 1966. pp. 619-625.

29. Numa, S. and S. Yamashita. Regulation of lipogenesis in abnormal tissues. In: Current Topics in Cellular Regulation (E. R. Stadtman, ed.), Vol. 8, Academic Press, New York. pp. 197-246.

30. Ochoa, S. Malic enzyme. In: Methods in Enzymology (S. P. Colowick and N. O. Kaplan, eds.), Vol. I, Academic Press, Inc., New York. 1955. pp. 739-753.

31. Ochoa, S. Malic dehydrogenase from pig heart. In: Methods in Enzymology (S. P. Colowick and N. O. Kaplan, eds.), Vol. I, Academic Press, Inc., New York. 1955. pp. 735-739.

32. Ochoa, S. Isocitric dehydrogenase system (TPN) from pig heart. In: Methods in Enzymology (S. P. Colowick and N. O. Kaplan, eds.), Vol. I, Academic Press, Inc., New York. 1955. pp. 699-704.

33. Petrova, N. V. and V. V. Portugalov. Lactate dehydrogenase isozymes of rat skeletal muscles following a space flight and with hypokinesia. Space Biol. and Aerospace Med. 5:80-89, 1977.

34. Polokoff, M. A. and R. M. Bell. Millipore filter assay for long-chain fatty acid:CoASH ligase activity using ^{3}H-labeled coenzyme A. J. Lipid Res. 16:344-345, 1975.

35. Pontremoli, S. Fructose-1,6-diphosphatase. In: Methods in Enzymology (W. A. Wood, ed.), Vol. IX, Academic Press, Inc., New York. 1966. pp. 625-631.

36. Racker, E. Spectrophotometric measurements of the enzymatic formation of fumaric and cis-aconitic acids. Biochim. Biophys. Acta 4:211-214, 1950.

37. Rauen, H. M. Biochemisches Taschenbuch. p. 988, Springer Verlag, Berlin. 1956.

38. Snedecor, G. W. and W. G. Cochran. Student's t-distribution. In: Statistical Methods, 6th Edition, Iowa State Univ. Press, Ames, Iowa. 1967. pp. 59-61.

39. Smith, A. H. Principles of Gravitational Biology. In: Foundations of Space Biology and Medicine (M. Calvin and O. G. C. Gazenko, eds.), Vol. II, NASA, Washington, D.C. 1975. p. 148.

40. Smith, S., H. T. Gagné, D. R. Pitelka and S. Abraham. The effect of dietary fat on lipogenesis in mammary gland and liver from lactating and virgin mice. Biochem. J. 115:807-815, 1969.

41. Tanioka, H., C. Y. Lin, S. Smith and S. Abraham. Acyl specificity in glyceride synthesis by lactating rats. Lipids 9:229-234, 1974.

42. Tigranyan, R. A. Cosmos 782 post-flight biochemical studies of various organs and tissues of rats. 1976.

43. Webb, P. Weight loss in men in space. Science 155:558-560, 1967.

44. Yakovleva, V. A. Arkhiv. Anat. Gistologii i Embriologii 73:39, 1977.

45. Yoshida, A. and E. Freese. Lactate dehydrogenase from Bacillus subtilis. In: Methods in Enzymology (W. A. Wood, ed.), Vol. XLI, Academic Press, Inc., New York. 1975. pp. 304-309.

QUANTITATIVE ANALYSIS OF SELECTED BONE PARAMETERS

Emily Morey Holton
Biomedical Research Division
NASA-Ames Research Center
Moffett Field, CA 94035

Russell T. Turner
Mineral Metabolism
Veterans Administration Hospital
Tacoma, WA 98493

David J. Baylink
Mineral Metabolism
Veterans Administration Hospital
Tacoma, WA 98493

Running title: Space flight and bone

The effect of space flight on bone formation, bone resorption, bone length, bone density and pore size distribution, bone mechanical properties, and bone cell number in both flight and 1 G flight centrifuged rats was investigated and compared to ground countrol groups. The data obtained suggest that no gross change in endosteal bone resorption occurs during flight or postflight; that mean periosteal bone formation rate decreases about 45% and is not corrected by centrifugation; that the decrease in formation rate may be due, in part, to a cessation of bone formation which occurs sometime after the eleventh day of flight and continues until the second postflight day; that although centrifugation did not correct the defect in periosteal bone formation rate during flight, it appears to hasten the recovery following flight; that femor stiffness decreases about 30%; and that centrifugation did correct the defect in bone mechanical properties. All perturbations produced by space flight returned to or exceeded normal values by 25 days after flight.

INTRODUCTION

Changes in calcium homeostasis present a potential problem during prolonged space flight. Metabolic studies of the Skylab astronauts indicated that a significant increase in urinary calcium (21) similar to bed rest immobilization, occurred in flight (7,20). No change in hydroxyproline was observed (6). Bone density determinations in the Skylab astronauts showed a significant decrease in the os calcis after 84 days of flight while no change in the radius or ulna was detected (20). Such data suggest that loss of bone mineral is more prevalent in the weight bearing bones.

Microscopic examinations of the metaphysis of the long bones of young Wistar rats after a 22-day space flight aboard the Soviet biological satellite Cosmos 605 suggest that an inhibition of bone growth occurred during flight but returned to normal by 27 days postflight. No gross changes were observed in the diaphysis (22).

Following Cosmos 782, a significant inhibition of periosteal bone formation was noted in the rat tibial diaphysis (16). A significant decrease in femur length was found and was related to a decreased mass of primary cancellous tissue directly adjacent to the cartilage plate (17). A significant decrease in cross-sectional area and medullary area in the femoral diaphysis was also noted (17). The ash content of the femur epiphysis was decreased 13%, while the humeral epiphyseal ash content decreased 8% and no change was noted in the radius or ulnar ash content (19). $^{45}CaCl_2$, injected 4 hours prior to sacrifice of rats following Cosmos 782, showed an increase in uptake in the epiphysis of the femur and humerus with a decreased uptake in the diaphysis of the femur, ulna, and radius (19).

Since mechanical forces imposed by muscle utilization and gravity influence bone turnover (11), prolonged recumbency and/or prolonged weight-

lessness with continuous hypercalciuria and bone loss could ultimately result in osteoporosis. To better understand the effect of space flight and gravity on bone, the following parameters: bone formation and mineralization, bone resorption, bone length, bone density and pore size distribution, and bone mechanical properties were studied in stationary and centrifuged rats both immediately and 25 days after an 18.5 day flight aboard Cosmos 936.

MATERIALS AND METHODS

Specific pathogen-free male, Wistar rats from the Institute of Endocinology of the Slovakian Academy of Science were used.

The experiment consisted of two test periods: 1) the flight period and 2) the postflight period. All rats were injected intraperitoneally with a tetracycline derivative, demeclocycline (Declomycin), 1-mg/kg body weight, 3 days prior to the beginning of the flight period. Half the rats in each group were sacrificed immediately following the first period. A second tetracycline injection was given to the remaining rats 4 days postflight. At the end of the test period, rats were guillotined and the tibias and femurs removed and frozen. The bones were transported frozen to the United States and kept frozen until analyzed. The left femur was used for measurement of bone strength parameters, bone density and pore size distribution. The left tibia was used for measurement of differential cell counts, forming and resorbing surfaces, and bone formation and resorption rates.

Because a detailed treatment of the methods used in this study has been given in the Cosmos 782 final report and elsewhere (1-4), only a brief description of the parameters will be presented.

BONE PARAMETERS

1) Bone density and pore size distribution were measured in the left femur by mercury porosimetry (2) as was described in the Cosmos 782 final report.

2) Bone mechanical parameters were evaluated with the standard torsion test machine designed by Burstein and Frankel (4). The femur was maintained in a moistened condition at all times. The ends of the femur were embedded in an epoxy resin prior to testing. Data was displayed on a storage oscilloscope and the torque-angular displacement curve which resulted after specimen failure was reduced to obtain ultimate torque, deformation to failure, strain energy, and stiffness.

3) The rate of bone formation and resorption was determined in the left tibia by quantitative histological techniques described in the Cosmos 782 final report and elsewhere (1,3). In addition, osteoblast and osteoclast cell number was determined.

Each tibia was divided at right angles to its long axis at the fibular junction and three consecutive transverse sections, about 50μ thick, were sawed from the proximal segment using a Gillings Hamco thin-sectioning machine. The bone specimen holder was mounted on a goniometer to facilitate sawing sections which were perpendicular to the long axis of the diaphysis. The sawed sections were then hand ground to a final thickness of about 30μ. One left ground section was mounted unstained in Abopon (Valnor Corp., Brooklyn, NY), a water-soluble mounting medium, and used for measurements of area, width and surface length. These measurements were performed using a digitizer interfaced with a computer (PDP-8/E, Digital Equipment Co., Manor, MS). In principle, the method used to measure bone formation and

resorption relies on the fact that in the tibial diaphysis the periosteal circumference enlarges by bone formation and the endosteal circumference enlarges by resorption. Tetracycline is given to mark all periosteal bone formed during the experimental period. Bone resorption is determined by the change in medullary area and by measurement of total endosteal formation during the experimental period. Since endosteal formation is intermittent, a continuous tetracycline label is necessary to quantify this parameter. In this study, only measurement of the medullary area was possible.

To determine differential cell counts in the tibia, a diaphyseal bone segment immediately proximal to that used for the hand ground sections was fixed for 24 hours in cold buffered formalin, demineralized and then embedded in glycol methacrylate (18). Six 5μ thick cross-sections were cut (Zeiss Cut-All microtome). Section thickness was measured using a Mikrokator model 509-4 (Aktiebolaget C. E. Johansson). The sections were stained for acid phosphatase enzyme (18), counterstained with aqueous methyl green-thionine in citrate buffer and then mounted in Fluoromount (E. Gurr Ltd., London, S.W.N., England). Osteoblasts and osteoclast nuclei were counted at the endosteum. Osteoclasts were identified by their positive acid phosphatase reaction, while osteoblasts stained purple with thionine and had a negative circular Golgi apparatus.

The forming and resorbing surfaces were measured in both the ground sections and 5μ thick diaphyseal sections. In the ground sections, the smooth endosteal surface with osteoid backed by tetracycline label was considered to be forming. The remaining surface was either neutral or resorbing. In this study neutral surface could not be distinguished from

resorbing and therefore, was considered to be resorbing. In the diaphyseal sections forming surface was distinguished by osteoblasts lining the endosteal surface. Surface lined by osteoclasts, marrow or lining cells was considered to be resorbing.

RESULTS

Space flight had little effect on the bone porosimetry parameters measured (table 1). However, the flight control animals[1] did show a significant increase ($p<0.05$) in large canalicular volume when compared to all other flight period groups. Also, the lacunar-canalicular pore diameter was significantly smaller ($p<0.01$) in the vivarium animals than in the flight rats[1], but there was no difference between either flight group and its appropriate control. During the recovery period, no significant differences between groups in any of the pore size parameters were noted.

Space flight had a dramatic effect on the mechanical properties of the femur (table 2, figures 1 and 2). Immediately following flight, the flight animals show a significant decrease in torque as compared to the vivarium ($p<0.05$) and flight centrifuge ($p<0.005$) rats, in energy as compared to the flight centrifuge animals ($p<0.05$), and in stiffness as compared to all control groups (flight control centrifuge, $p<0.05$, while in all other group $p<0.005$). Twenty-five days postflight, the only significant value is the increase in torque when the flight rats are compared with the flight control group ($p<0.05$). The flight group is the only group which does not fall within the reference range in either experimental period (figures 1 and 2). The variance in the ground controls in most

[1]The following terms are used interchangeably: 1) flight control and synchronous stationary, 2) flight centrifuge control and synchronous centrifuge, 3) flight and flight stationary.

TABLE 1

EFFECT OF SPACE FLIGHT ON FEMUR DENSITY AND PORE SIZE DISTRIBUTION

GROUP	N	DENSITY (g/cc)	Lrg. CANAL. VOL. (10^{-3} cc/g)	Vasc. CANAL VOL. (10^{-3} cc/g)	L-C VOL.+	L-C PORE DIA. (μ)
BASAL						
Preflight control	6	1.42±0.03*	5.82±0.62	60.2±5.5	22.9±0.8	0.212±0.006
Preflight flight control	6	1.40±0.08	5.83±0.72	66.0±5.6	22.9±0.7	0.217±0.006
FLIGHT						
Vivarium	5	1.60±0.02	4.39±0.88	39.5±8.4	20.6±1.3	0.197±0.004
Flight control	5	1.60±0.01	5.70±0.80**	45.8±8.1	20.5±0.2	0.205±0.004
Flight control centrifuge	5	1.59±0.03	4.61±0.56	46.2±4.9	19.4±0.5	0.203±0.005
Flight	5	1.56±0.05	4.62±0.30	42.8±4.0	20.2±1.2	0.206±0.003**
Flight centrifuge	5	1.61±0.01	4.20±0.42	39.1±9.3	20.8±1.2	0.199±0.006
POST FLIGHT						
Vivarium	5	1.61±0.02	3.89±0.33	36.6±14.8	17.7±0.9	0.190±0.006
Flight control	5	1.62±0.03	4.03±0.45	31.6±3.5	18.2±0.8	0.191±0.004
Flight	5	1.63±0.03	4.21±0.07	30.5±11.1	18.5±1.5	0.194±0.003
Flight centrifuge	4	1.63±0.03	4.20±0.12	31.8±3.8	19.2±0.8	0.194±0.001

+ L-C is lacunar-canalicular (10^{-3} cc/g)
N = Number of rats/group
* = Mean ± S.D.
** = Significantly different from vivarium

TABLE 2

EFFECT OF SPACEFLIGHT ON FEMUR BREAKING STRENGTH

GROUP BASAL	N	TORQUE (10^5 cm-dynes)	DEFORMATION (degrees)	ENERGY (10^5 erg radians)	STIFFNESS (10^3 cm-dynes/ radian)
Preflight control	6	22.5±3.1*	14.2±4.1	2.9±1.0	3.18±0.78
Preflight flight control	6	20.6±4.2	12.4±4.0	2.4±1.2	3.10±0.59
FLIGHT					
Vivarium	5	32.2±9.6	11.4±3.3	3.7±2.0	4.82±0.72
Flight control	5	26.1±6.9	11.8±2.6	2.6±1.3	4.15±0.39
Flight control centrifuge	5	27.6±9.1	10.8±2.5	2.8±1.4	4.46±1.26
Flight	4	17.5±4.4**	10.3±2.2	1.8±0.9**	2.97±0.22**
Flight centrifuge	4	29.2±1.5	13.1±2.0	3.3±0.5	4.33±0.44
POST FLIGHT					
Vivarium	5	39.2±9.2	13.8±5.3	5.0±3.1	4.96±0.79
Flight control	5	35.9±4.4	13.5±2.7	4.2±1.3	4.76±0.72
Flight	4	43.9±3.6**	15.7±2.7	5.9±0.9	5.00±0.53
Flight centrifuge	5	37.9±7.6	12.7±3.0	4.6±2.2	5.37±0.49

N = Number of rats/group
* Mean ± S.D.
** Significantly different from controls (see text for details)

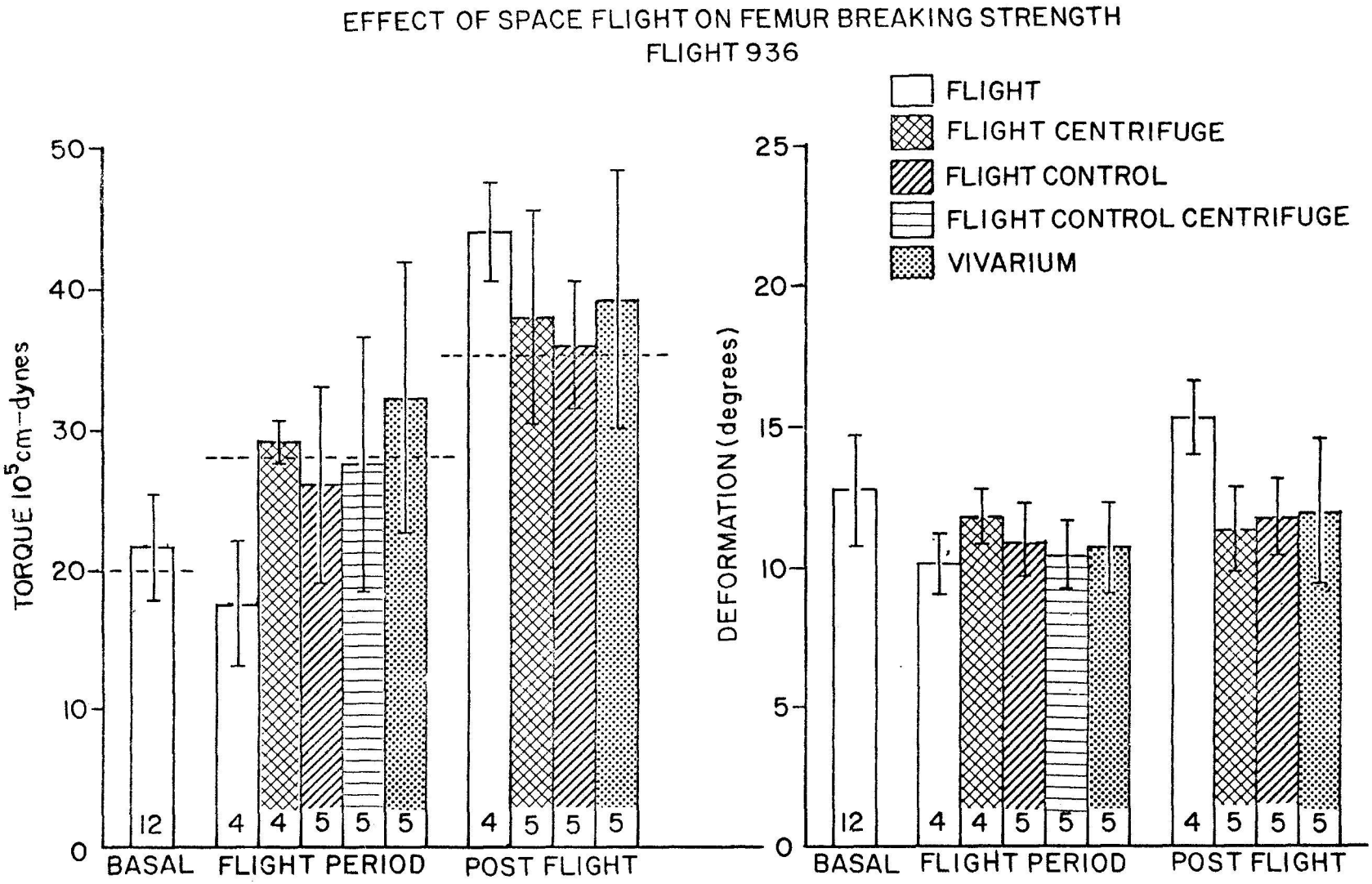

Figure 1. The effect of space flight on femur breaking strength - torque and deformation. Data are from the torque-angular displacement curve which is obtained during specimen failure. The vertical lines represent ± 1 S. D. The numbers in the bars are the number of animals in each group. The basal values are from animals sacrificed at launch. The dashed horozontal line represents reference data for torque which was obtained from rats of a similar weight used in other experiment. Space flight resulted in approximately a 40% decrease in torque. Note that the variance of the flight group in both the flight and postflight periods does not fall within the reference value. Deformation is a function of bone length. No significant differences were noted in deformation during the flight period.

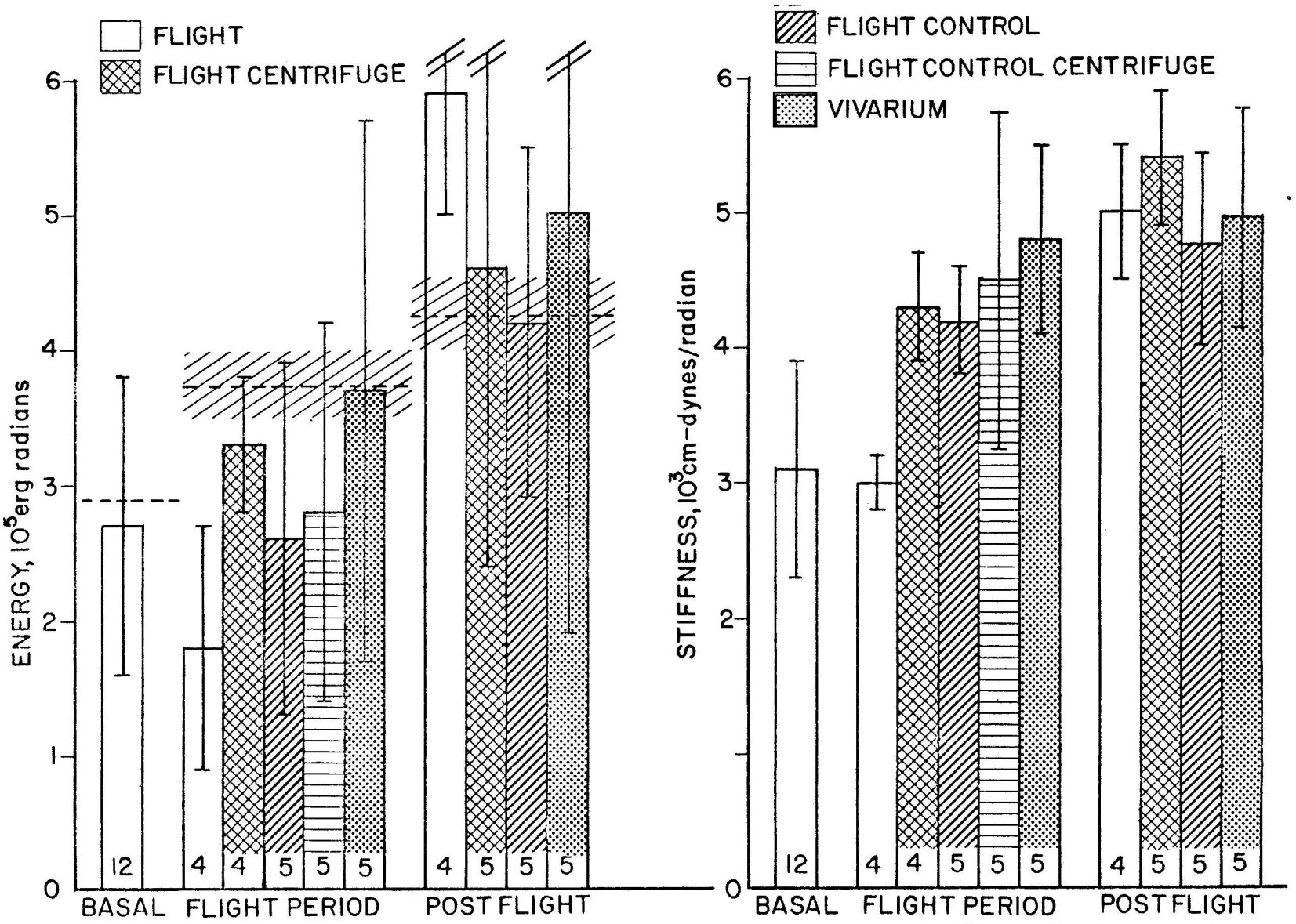

Figure 2. The effect of space flight on femur breaking strength - energy and stiffness. Strain energy is the energy absorbed to failure and is the area under the displacement curve. Stiffness is the slope of the curve. The hatched lines through the dashed horizontal line represent the range of reference data. For additional information see the legend to figure 1. Space flight appeared to cause about a 47% decrease in energy and a 31% decrease in stiffness. All defects in bone mechanical properties were corrected by centrifugation during space flight.

instances was notably higher than in the flight groups.

The body weights of the rats and the lengths of the left femurs and tibias are tabulated in table 3. The flight centrifuge rats weighed significantly less than the vivarium ($p<0.005$), the flight control ($p<0.025$), and the flight ($p<0.05$ when $n=5$) animals. Also, the femur and tibia lengths were significantly shorter in the flight centrifuge group as compared to the vivarium controls (<0.005 and 0.025, respectively). The only other value which was significantly different immediately following flight was the length of the femur in the flight control centrifuge group as compared to the vivarium rats ($p<0.025$). During the postflight period, no significant differences in weight or bone length were obvious. As depicted in figure 3, the femur and tibia lengths were closely correlated with body weight ($r=0.91$ and 0.89, respectively).

At the end of the flight period, the tibia cross-sectional area at the tibia-fibula junction, was significantly smaller in the flight and flight centrifuge than in the vivarium ($p<0.025$) and flight control ($p<0.05$) groups (table 3, figure 4). Following the recovery period no differences were found. In contrast, space flight appeared to have no significant effect on the rate of calculated longitudinal bone growth in the tibia or femur (table 4). During the postflight period, the rate of longitudinal bone growth in the tibia and femur in the vivarium rats was significantly decreased as compared to the flight control ($p<0.05$), flight ($p<0.01$ and 0.025, respectively), and flight centrifuge ($p<0.005$ and 0.025, respectively) animals. In addition, the vivarium and flight control groups exhibited a significant decrease in longitudinal growth of the tibia ($p<0.001$ and 0.010, respectively) and femur ($p<0.001$ and 0.005, respectively) in the postflight period as compared

TABLE 3

BODY WEIGHT AND BONE DIMENSIONS

GROUP	N	Weight (gm)	Left Femur Length (cm)	Left Tibia Length (cm)	Total Bone Cross-Section Area Left Tibia (mm^2)+
BASAL					
Preflight control	6	209±21*	3.12±0.10	3.39±0.09	2.90±0.14
Preflight flight control	6	235±15	3.17±0.08	3.41±0.08	2.96±0.23
FLIGHT					
Vivarium	5	289±9	3.51±0.08	3.74±0.06	3.68±0.40
Flight control	5	294±16	3.44±0.06	3.66±0.05	3.34±0.16
Flight control centrifuge	5	280±15	3.38±0.05**	3.68±0.05	3.40±0.27
Flight***	4F/5T	295±29/304±32	3.41±0.08	3.67±0.06	3.01±0.21**
Flight centrifuge ****	4	264±8	3.34±0.03**	3.59±0.08**	3.06±0.13**
POST FLIGHT					
Vivarium	5	332±8	3.59±0.03	3.82±0.03	3.65±0.34
Flight control	5	337±14	3.61±0.07	3.83±0.07	3.89±0.23
Flight	5	331±17	3.62±0.09	3.90±0.08	3.87±0.16
Flight centrifuge	5	351±17	3.62±0.09	3.86±0.08	3.94±0.26

+ At tibia-fibula junction; Total bone cross-section area=total cross-section area - medullary area
N Number of rats/group
* Mean ± S.D.
** Significantly different from control (see text for details)
*** One of five animals in this group suffered a broken femur on landing and therefore only 4 femurs (4F) and 5 tibias (5T) were available for study.
****One of the five animals in this group returned from space in an extremely cachectic state and was not used in this study.

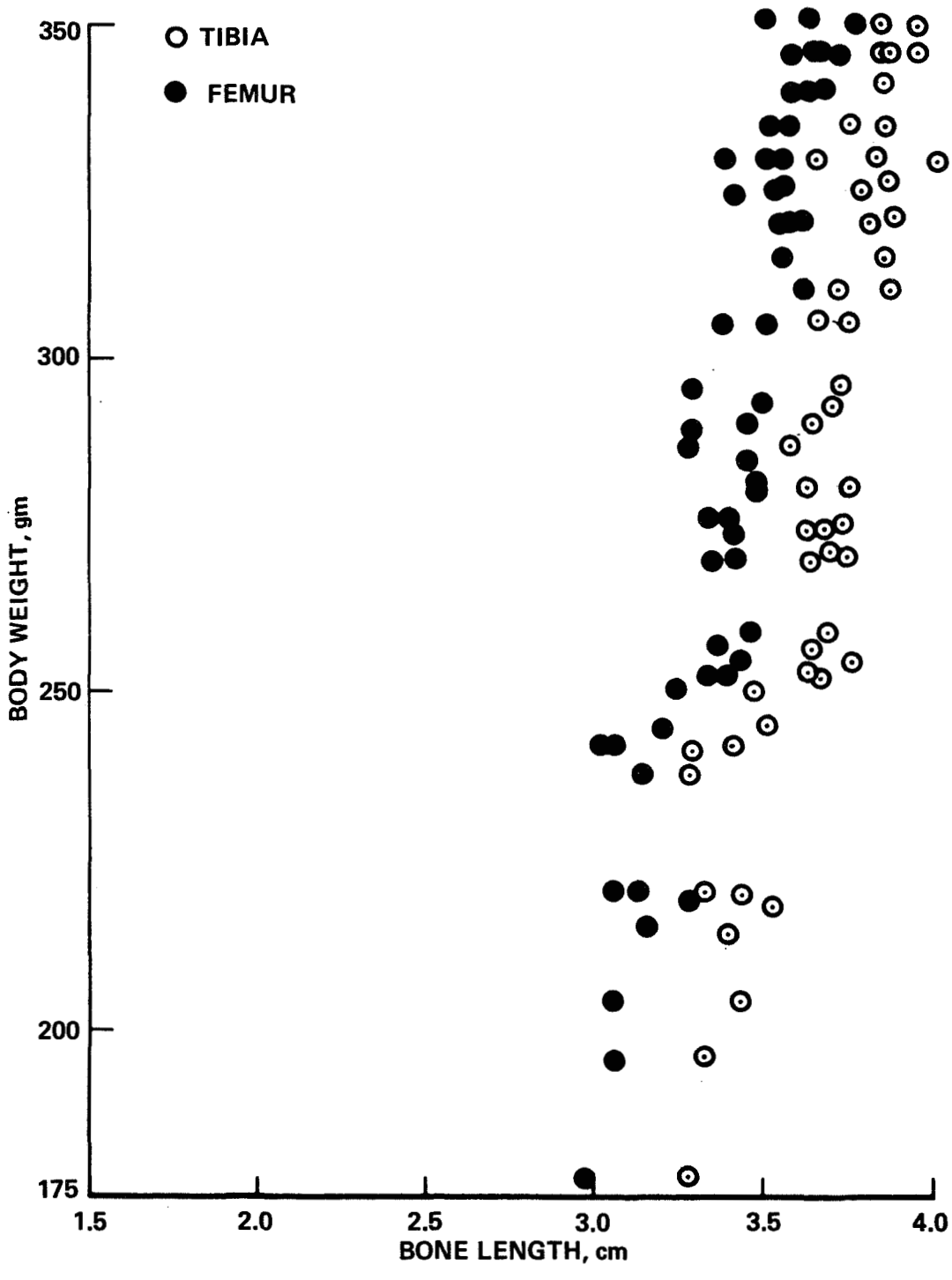

Figure 3. Body weight and bone length of all basal, flight period, and postflight rats. The body weight information is based on carcass weight. Notice that the units on the abscissa double more rapidly than those on the ordinate. All bones were measured with calipers by the same individual on the same day. As anticipated, body weight correlated well with bone length ($r \simeq 0.90$).

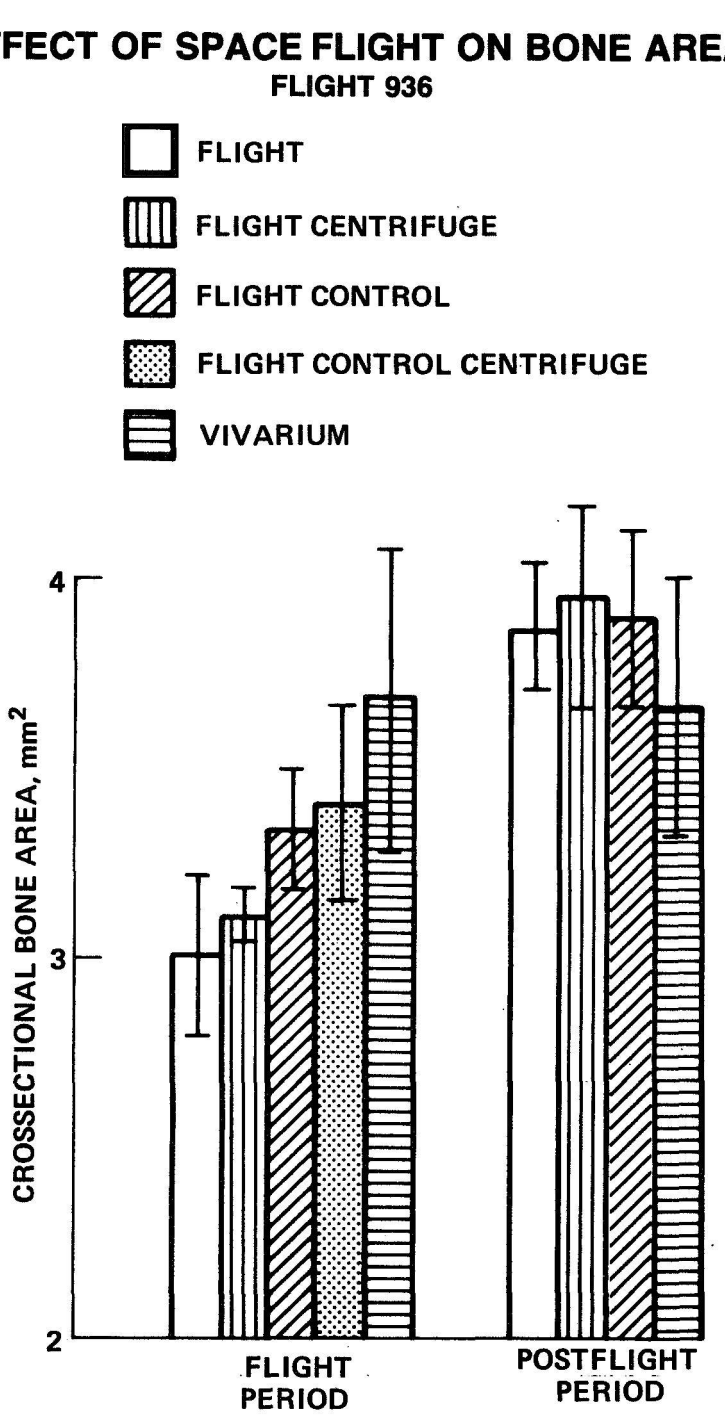

Figure 4. Effect of space flight on bone area. Cross-sectional bone area was calculated by subtracting medullary area from total cross-sectional area. Using this relatively insensitive measurement of linear bone growth, a significant decrease of about 10% was found in the flight groups as compared to the flight control groups. No differences were noted in the postflight period. The vertical lines represent ± 1 S.D.

TABLE 4

EFFECT OF SPACE FLIGHT ON THE RATE OF LONGITUDINAL BONE GROWTH (mm/day x 10^3)[1]

GROUP	TIBIA	FEMUR	HUMERUS+
FLIGHT			
Vivarium	13.7±2.3*	14.5±3.1	6.7±2.0
Flight control	13.6±2.8	15.3±3.2	4.1±0.8
Flight control centrifuge	14.5±2.6	12.2±2.5	ND
Flight	14.9±3.3	14.3±4.5	5.0±1.3
Flight centrifuge	12.6±4.6	13.1±1.6	ND
POST FLIGHT			
Vivarium	3.3±1.4	3.2±1.0	6.1±1.3
Flight control	6.8±2.6**	6.9±2.8**	7.8±1.6
Flight	9.4±3.1**	8.5±3.7**	6.4±1.9
Flight centrifuge	10.7±3.2**	9.1±3.6**	ND

+ Data from Cosmos 782
ND No centrifuge groups in Cosmos 782
* Mean ± S.D.
** Significantly different from vivarium

1 These values were calculated by taking the mean length of the basal bones, subtracting that value from the individual flight period rats, and dividing by the length of time between sacrifice of the basal rats and corresponding flight groups. For the postflight period, the mean values of the flight groups were subtracted from the corresponding postflight group and divided by the length of the post-flight period.

with the flight period. Another long bone, the humerus, did not show similar decreases in the postflight period (table 4).

Space flight resulted in a pronounced reduction in the periosteal bone formation rate at the tibia-fibula sampling site. During the flight period (table 5, figure 5), periosteal bone formation was significantly reduced in both the flight and flight centrifuge groups as compared to the vivarium and flight control animals ($p<0.001$ in all cases). In addition, bone formation was decreased in the flight rats as compared to the flight control centrifuge group ($p<0.025$) which, in turn, formed significantly less periosteal bone than did the vivarium animals ($p<0.05$). Similar results were obtained on Cosmos 782 (figure 5). The only significant difference in endosteal bone formation rate during the flight period was in the flight control centrifuge group which was decreased as compared to flight centrifuge ($p<0.005$), flight control ($p<0.01$), and vivarium ($p<0.025$) groups. The total bone formation rate in terms of significant differences, virtually reflected the periosteal bone formation rate.

Coincident with the decrease in formation rate was an arrest line at the periosteum of both the flight and flight centrifuge rats which was significantly more extensive than that occurring in flight control ($p<0.005$ and 0.05, respectively) and vivarium ($p<0.005$ and 0.01, respectively) groups. In addition, the arrest line was significantly longer in the flight group than in the flight centrifuge rats ($p<0.025$). The arrest line is depicted in figure 6 and the data are found in table 6. The data are similar to those found in Cosmos 782 (table 6) although about 25% less extensive.

TABLE 5

EFFECT OF SPACE FLIGHT ON BONE TURNOVER

GROUP		BONE FORMATION RATE ($mm^3/d \times 10^3$)				Medullary
BASAL	N	Periosteal	Endosteal	Total	N	Area (mm^2)
Preflight control	6	ND	ND	ND	6	0.78±0.36*
Preflight flight control	6	ND	ND	ND	6	0.80±0.36
FLIGHT						
Vivarium	10	26.2±3.7	4.2±1.4	30.6±3.7	10	0.96±0.14
Flight control	10	25.6±2.9	5.1±2.0	30.2±4.2	10	1.01±0.14
Flight control centrifuge	5	21.7±3.3**	2.6±0.8**	24.3±2.7**	5	1.03±0.11
Flight	10	16.0±3.2**	3.5±1.1	19.5±3.8**	10	0.97±0.15
Flight centrifuge	8	17.6±3.0**	4.7±0.9	22.3±3.5**	10	1.07±0.19
POST FLIGHT						
Vivarium	5	16.2±2.7	2.5±0.8	18.7±3.3	5	0.90±0.15
Flight control	5	25.5±3.1**	3.1±1.1	28.5±4.1**	5	0.88±0.14
Flight	5	26.0±5.1**	2.8±0.9	28.8±5.7**	5	1.07±0.14
Flight centrifuge	5	29.7±4.6**	3.9±0.6**	33.6±4.9**	5	1.01±0.24

ND Not determined due to absence of tetracycline label

N Number of rats/group

* Mean ± S.D.

** Significantly different from control (see text for details)

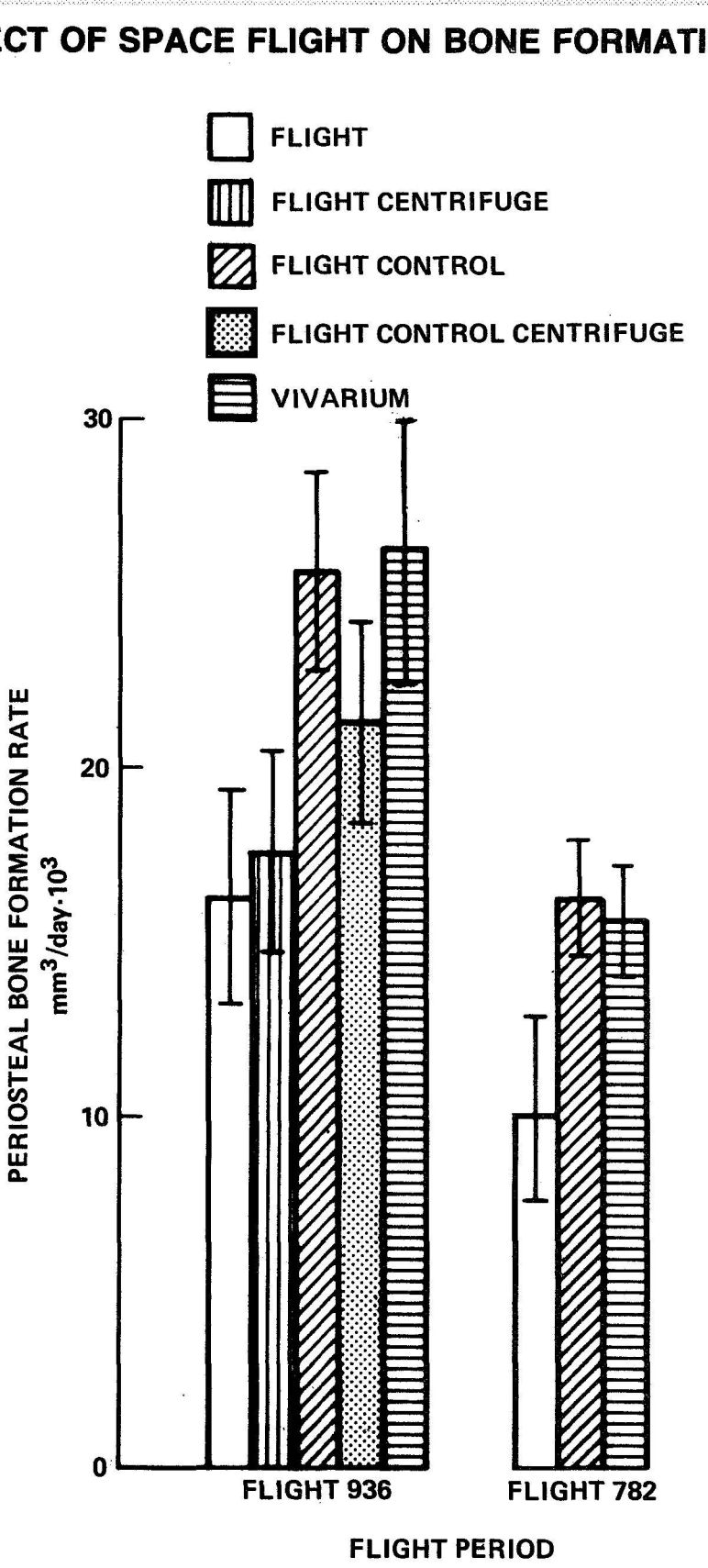

Figure 5. Effect of space flight on periosteal bone formation rate in Cosmos 936 and 782. A dramatic decrease in periosteal bone formation rate was noted in both flights. This defect was not corrected by centrifugation. The vertical lines represent ± 1 S.D.

TABLE 6

COMPARISON OF BONE PARAMETERS IN 782 AND 936

	782	936	
	FLIGHT	FLIGHT	FLIGHT CENTRIFUGE
PERIOSTEAL BONE FORMATION RATE			
FLIGHT PERIOD			
% DECREASE FROM CONTROL	41	37	31
(ADJUSTED FOR PREFLIGHT)	(47)	(43)	(36)
POSTFLIGHT PERIOD			
% INCREASE OVER VIVARIUM	53	60	83
% INCREASE OVER SYNCHRONOUS	NO DATA	2	16
FLIGHT TIME REQUIRED TO FORM TOTAL BONE VOLUME, days (TOTAL BONE VOL/FLIGHT CONTROL R_{BF}-3)			
R + 0	11.7	11.1	10.7
R + 3 (SECOND TETRACYCLINE INJECTION, 782)	11.2		
R + 4 (SECOND TETRACYCLINE INJECTION, 936)		12.8 (1.5)	15.8* (4.3)

	FLIGHT 782			FLIGHT 936			
	FLIGHT	SYNCHRONOUS	VIVARIUM	FLIGHT	FLIGHT CENT.	SYNCHRONOUS	VIVARIUM
ARREST LINE							
LENGTH, mm	5.3 ± 0.6[1]	2.1 ± 0.6	1.5 ± 0.7	4.0 ± 1.1	2.3 ± 0.4	1.6 ± 0.4	1.1 ± 0.4
% OF PERIOSTEAL SURFACE	73	29	19	52	30	22	15

*The total volume of bone formed in this group was significantly greater for the flight period (22.5 days) as compared with the flight rats sacrificed immediately after flight (18.5 days). The values in parentheses indicate the number of days required to form the volume of bone in the 4 days immediately following flight, i.e. total bone volume formed in the 22.5 days minus the volume formed in 18.5 days divided by the formation rate in the recovery period (see Discussion).

[1]Mean±S.D.

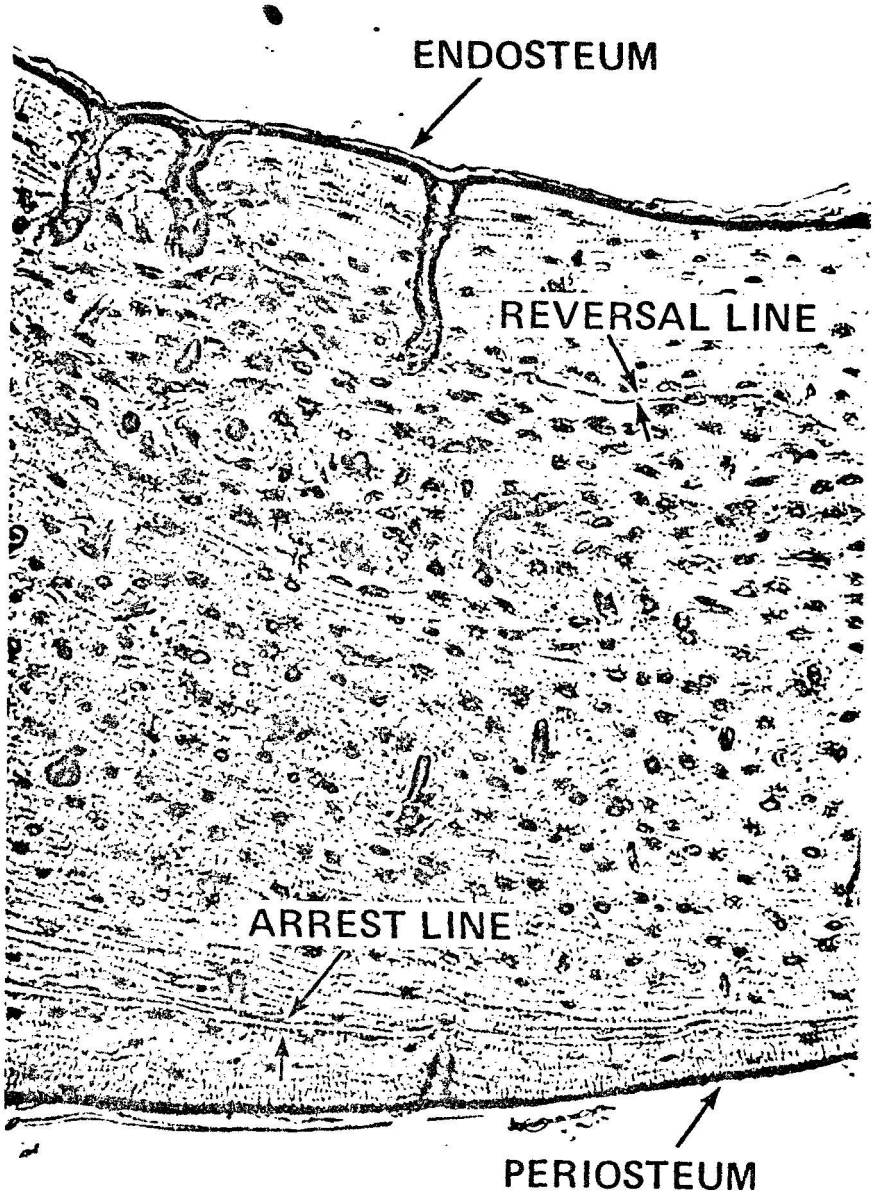

Figure 6. Higher power photomicrograph of a field from the tibial cross section of the Cosmos 782 rat in figure 12. This section was photographed under brightfield illumination. The difference in appearance between the arrest line and reversal line is apparent.

The defect in bone formation was corrected during the postflight period. Of importance is the finding that in all flight animals measured to date, less periosteal bone was formed during than after flight (figure 7). During the postflight period, the vivarium group exhibited significantly lower periosteal and total bone formation rates than the flight ($p<0.01$ and 0.025, respectively), flight centrifuge ($p<0.001$), and flight control ($p<0.005$ and 0.01, respectively) groups (table 5, figure 8). The vivarium rats also formed less endosteal bone than did the flight centrifuge animals ($p<0.025$).

No significant differences in medullary area were noted among any of the groups at either time period (table 5) similar to the data from Cosmos 782 (figure 9).

Space flight appeared to have little effect on the length of forming and resorbing surfaces. The only significant difference was a decrease in the length of forming surface in the flight group as compared with the flight control rats ($p<0.05$). The flight control centrifuge animals showed an increase in resorbing surface over the vivarium group ($p<0.05$). However, when expressed as a % of surface length, the flight rats were significantly lower than the vivarium ($p<0.05$) and flight control groups ($p<0.025$) in % forming surface and had less % resorbing surface that the vivarium animals ($p<0.05$). The flight control centrifuge animals demonstrated a decrease in % forming and resorbing surface when compared to the vivarium ($p<0.05$) or flight control ($p<0.025$) rats. During the postflight period, no significant differences were observed (table 7).

No significant differences in osteoclast nuclei/mm resorbing

EFFECT OF SPACE FLIGHT ON BONE FORMATION

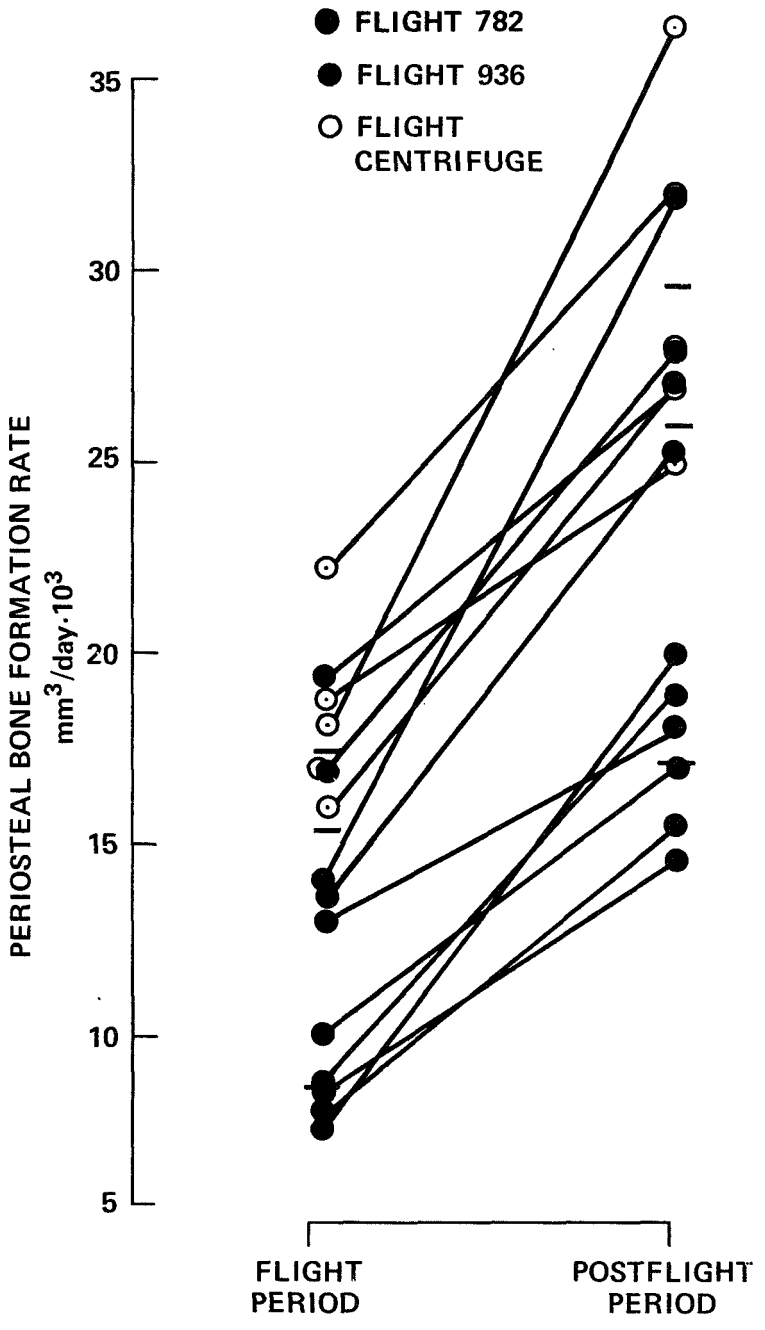

Figure 7. Effect of space flight on individual rats. The data in red are for Cosmos 782 while the other data are from Cosmos 936. The short horizontal lines represent the mean value for each group. Without exception, each rat formed less bone during than following flight. A similar graph for the vivarium animals would show a negative slope while that for the flight controls would exhibit no slope.

EFFECT OF SPACE FLIGHT ON BONE FORMATION

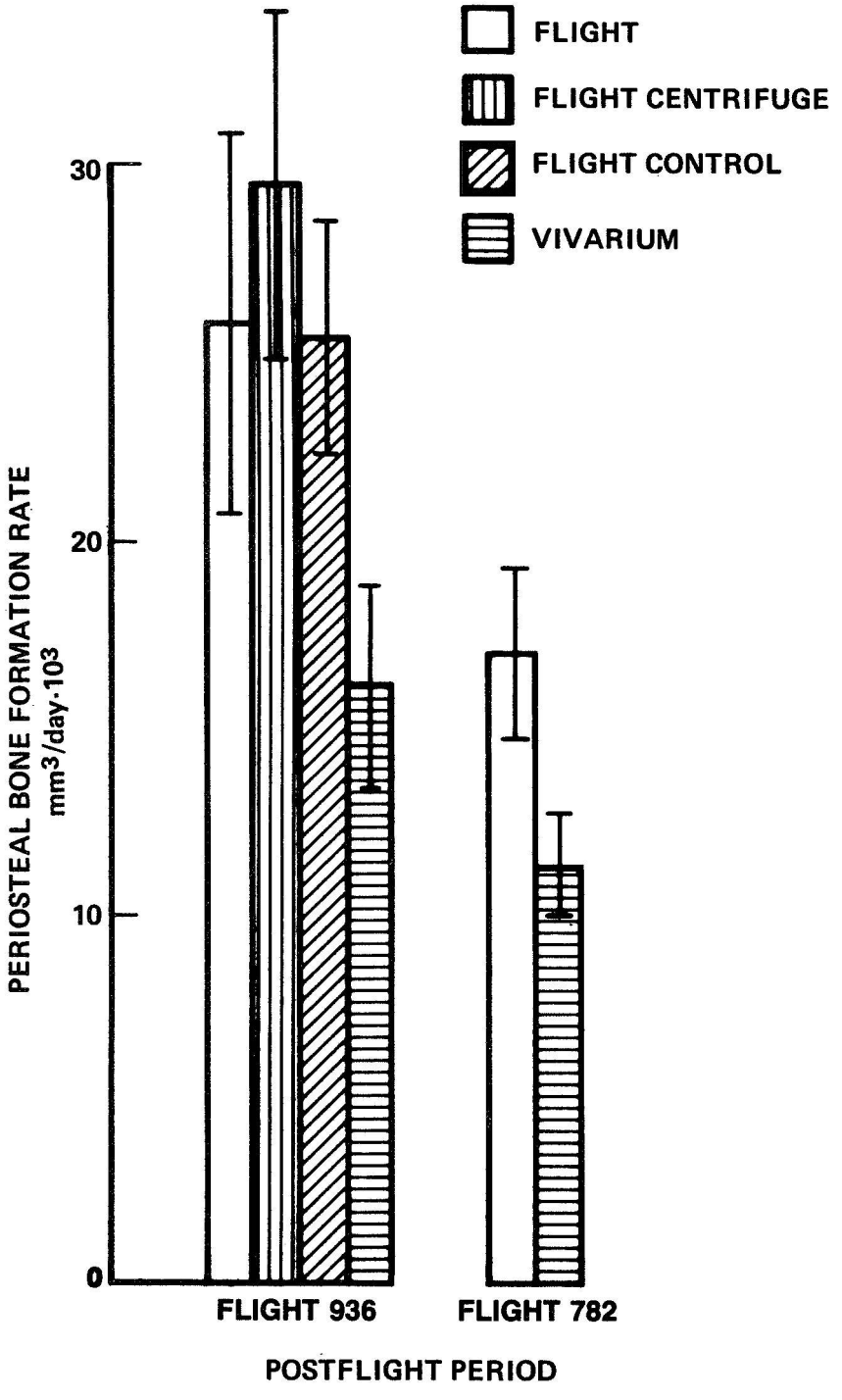

Figure 8. Periosteal bone formation rate during the postflight period. In both Cosmos 782 and 936, a significant rebound was noted in the flight groups as compared with the vivarium controls. No significant difference was found between the flight groups and the flight control rats during the postflight period. The vertical lines represent ± 1 S.D.

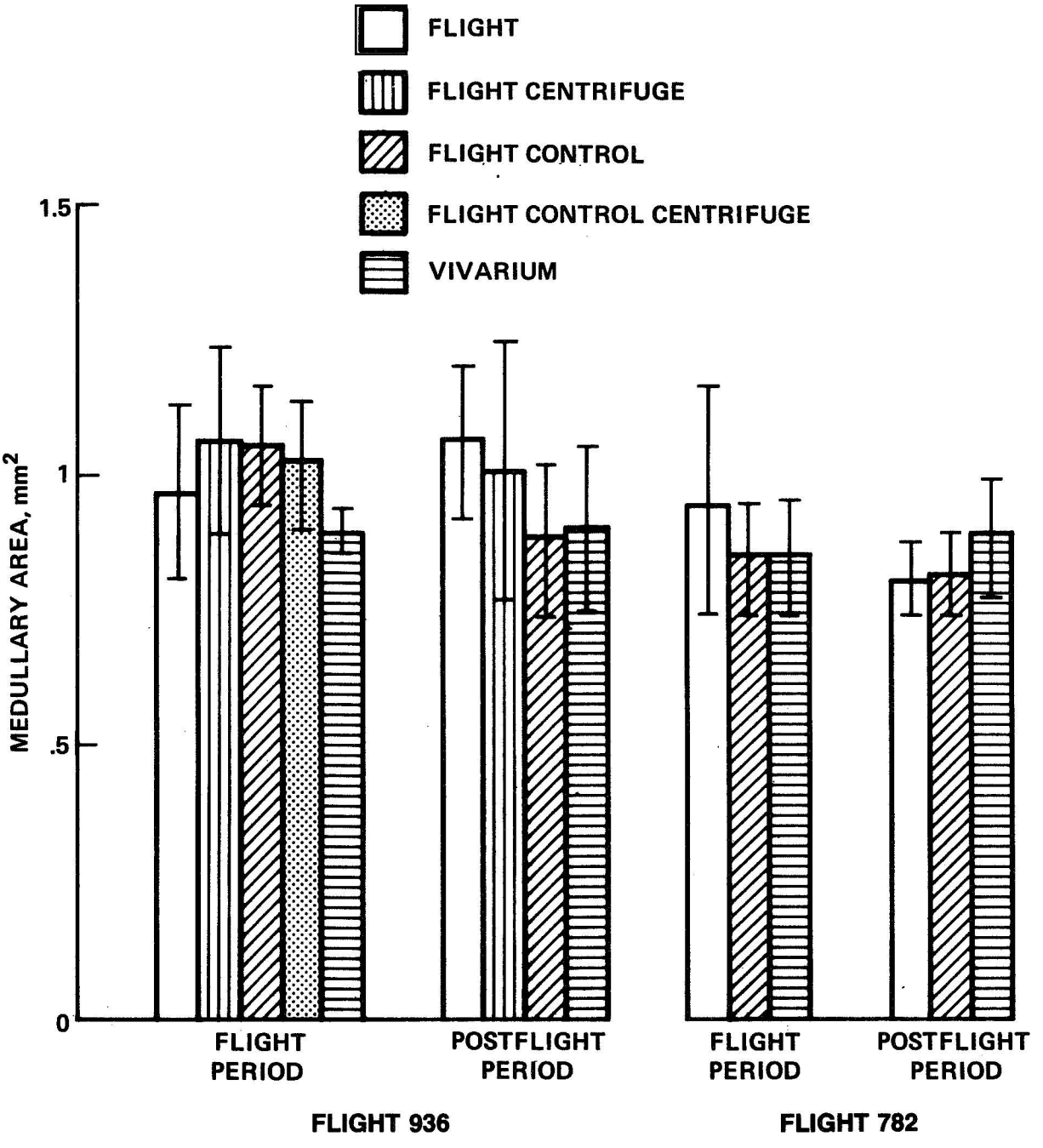

Figure 9. Effect of space flight on bone resorption. Medullary area is a relatively insensitive measurement of bone resorption. No significant intergroup differences occurred in the size of the medullary cavity in either flight during either experimental period. The vertical lines represent ± 1 S.D.

TABLE 7

EFFECT OF SPACE FLIGHT ON FORMING AND RESORBING SURFACES[1]

GROUP	N	Length Forming Surface (mm)	Length Resorbing Surface (mm)	% Forming Surface	% Resorbing Surface
BASAL					
Preflight control	6	2.73±0.24*	0.84±0.31	76.7±7.6	23.2±7.6
Preflight flight control	6	2.75±0.12	0.84±0.13	76.5±3.0	23.4±3.0
FLIGHT					
Vivarium	5	3.26±0.32	0.45±0.22	87.7±5.6	12.2±5.6
Flight control	5	3.34±0.25	0.45±0.24	92.7±8.1	7.3±8.1
Flight control centrifuge	5	2.91±0.61	0.99±0.36**	73.1±10.5**	26.8±10.5**
Flight	5	2.49±0.61**	0.95±0.43	71.9±11.9**	28.0±11.9**
Flight centrifuge	5	2.61±0.81	1.17±0.97	70.3±23.1	29.9±23.0
POST FLIGHT					
Vivarium	5	2.70±0.57	0.92±0.44	72.6±16.3	27.3±16.3
Flight control	5	3.04±0.30	0.51±0.24	88.4±8.9	11.5±8.9
Flight	5	2.68±0.71	1.08±0.51	70.5±15.1	29.4±15.1
Flight centrifuge	5	2.94±0.20	0.68±0.19	81.4±3.0	18.6±3.0

N Number rats/group
* Mean ± S.D.
** Significant difference from control (see text for details)
1 Measurements made at the endosteal surface on hand ground mineralized sections

surface or osteoblast number/mm forming surface were observed in the tibial diaphysis following space flight (table 8). In addition, no differences were found in forming or resorbing surfaces. However, the forming and resorbing surface values from demineralized, thin, diaphyseal sections were notably different, in most cases, from comparable measurements made on mineralized ground sections from the tibia-fibula junction (table 7 and 8).

Osteoclast nuclei show differences in mean values (table 9), but due to large scatter no significant differences were found.

DISCUSSION[2]

Although a decrease in the density of the humerus was noted in the flight animals following Cosmos 782, no change in femur density was found after Cosmos 936 (table 1). The negative results suggest that the density measurement may be too insensitive to detect changes in the femur or, more likely, that the mineral content of the femur is not proportionately different or, possibly, that differential effects are occurring within the bone which negate any significant change. Few changes in pore size distribution were noted in either Cosmos 782 or 936 indicating space flight has little effect on osteocytic size and number or on bone vascular volume.

Space flight resulted in signficant decreases in mechanical properties of the femur (table 2, figures 1 and 2). Interestingly, the flight animals, whether stationary or centrifuged, showed less variance than the ground control groups. Thus, even though the n

[2]To minimize biased statistical significance in this experiment due to a small n, all standard errors were calculated using (n-1) and a double-sided t-test for significance was performed.

TABLE 8

THE EFFECT OF SPACE FLIGHT ON OSTEOBLASTS AND OSTEOCLASTS[1]

GROUP	N	Length Forming Surface (mm)	Length Resorbing Surface (mm)	% Forming Surface	% Resorbing Surface	Osteoblasts/ mm Forming Surface	Osteoclast Nuclei/ mm Resorbing Surface
Flight control	4	2.15±0.21*	1.69±0.22	56.0±5.2	43.9±5.2	56.3±7.9	0.67±0.67
Flight control centrifuge	5	2.19±0.72	1.72±0.58	55.5±16.3	44.4±16.3	45.2±8.7	0.93±1.22
Flight	5	2.48±0.64	1.79±0.44	57.5±11.3	42.4±11.3	50.4±5.2	1.56±3.18
Flight centrifuge	5	2.02±0.45	1.96±0.61	51.3±13.1	48.6±13.1	54.5±13.4	0.51±0.51

N Number of rats/group
* Mean ± S.D.
1 Measurements made at the endosteal surface on demineralized diaphyseal sections

TABLE 9

THE EFFECT OF SPACE FLIGHT ON OSTEOCLAST NUCLEI

GROUP	N	Osteoclast Nuclei/mm Endosteal Surface
BASALS	12	0.88±1.29
FLIGHT		
Omega Bios	5	3.14±3.14
Vivarium	5	0
Flight control	4	0.34±0.34
Flight control centrifuge	5	0.42±0.55
Flight	5	0.65±1.33
Flight centrifuge	5	0.51±0.36
POST FLIGHT		
Vivarium	5	1.45±1.33
Flight control	5	0.71±1.33
Flight	5	0.54±0.47
Flight centrifuge	5	0.26±0.26

N = Number of rats/group
* Mean ± S.D.

was only 4 in the flight groups, significant differences were apparent immediately postflight. When compared with data for torque and energy from rats of a similar weight which were used in other experiments (dashed horizontal line in figures 1 and 2), the only group which falls completely outside the reference value is the flight group both in the flight and postflight periods. Thus, these parameters may actually decrease significantly after 18.5 days in space and rebound following recovery although the significance is somewhat obscured due to the large variance in the control groups. The decrease in breaking strength that occurred during flight cannot be attributed solely to the decreased rate of bone formation (table 3, figure 5) since the flight centrifuge animals also showed decreased formation but exhibited no defect in bone mechanical properties. A possible explanation is the length of the arrest line; the arrest line was significantly longer in the flight rats as compared to the flight centrifuge animals (table 6). If the arrest line is a cement line, it would act as a weak point or stress concentrator (14) and decrease the mechanical strength of the flight group.

The larger weight gain in Cosmos 936 as compared to Cosmos 782 can be attributed to an increased food intake. During Cosmos 782, the flight rats gained approximately 1.5 g/day while consuming about 14 g of food[3] per day and the flight control rats gained approximately 3.8 g/day while consuming about 14 g of food per day. During Cosmos 936, the flight rats gained weight at a rate of 3.3 g/day and ate about 19 g of food per day. The flight control animals gained more weight (3.7 g/day) while eating less food (16 g/day). These data suggest that the rat, like man,

---

[3]Food calculated in terms of dry weight assuming that 1 g dry weight of food ≃ 2.7 g of paste diet.

gain less weight per g of food consumed while in space.

Although space flight did not appear to significantly alter longitudinal bone growth (table 4), a significant decrease in cross-sectional bone area was found (table 3, figure 4). Cross-sectional bone area is a relatively insensitive measurement of circumferential bone growth. Interestingly, a decrease in linear bone growth could be shown by such a gross measurement while another similarly insensitive measurement, medullary area (table 4, figure 9), did not demonstrate any change in bone resorption.

Bone formation was decreased significantly during flight (table 5, figure 5) and was not corrected by centrifugation. Bone formation rate in the flight groups was decreased about 35% relative to either control group (table 6); however, if adjusted for the 3 day preflight period the rate decreased about 40%. If only the flight centrifuge rats sacrificed immediately following flight are used in the rate, about a 45% decrease is found. Similar changes were found in Cosmos 782 (table 6). The dramatic decrease in formation during flight was accompanied by an arrest line (figure 6). Arrest lines were evident in all other groups, but these lines were not as extensive as those in the flight rats (table 6). Centrifugation appears to at least partially correct the extent of the arrest line during space flight. Arrest lines seem to be a normal process in growing rats which are exaggerated by space flight. Arrest lines occur when formation ceases and is later reinitiated (9). The arrest line differs from a reversal line in several aspects (figure 6). The reversal line is created when resorption reverses to formation; it is characterized by an irregular appearance

and by acid phosphatase activity (figure 10). The arrest line, unlike the reversal line, is a smooth, distinct demarcation that does not stain for enzyme activity but does stain with thionine (figure 11). Thionine staining suggests acid polysaccharide or a basic substance which is not fat extracted; osteocyte lacunae and walls of canaliculi stain similarly. The arrest line is not an artifact caused by section preparation since the second tetracycline label consistently coincided with this line. Although the cause of cessation is not known, starvation was not a factor because almost all food was consumed during flight and the average weight of the flight group was not significantly different from controls. Also, immobilization was not a factor since flight rats, if anything, were more active than flight controls. Cessation of bone formation was probably due to either an inhibition in matrix formation or mineralization or both. Although the matrix parameters were not measured due to the absence of tetracycline labels in the basal groups, no significant difference was observed in osteoid width between the flight (11.0±3.6μ), flight control (11.7±2.1μ), or vivarium (9.8±3.3μ) groups. Hence, a defect solely in mineralization is unlikely. When arrest occurred is not known, but flight rats formed an average of 360×10^{-3} mm^3 of bone during the 18.5-day space flight, in 1 mm thick mineralized sections. If formation proceeded normally, i.e. 25.6×10^{-3} mm^3/day (table 5), until arrest, then the earliest that cessation could occur would be the 11th day of flight (table 6) (3 days of bone are formed prior to flight due to the labeling schedule). However, formation in flight rats may not have been constant prior to cessation but more likely was gradually decreasing.

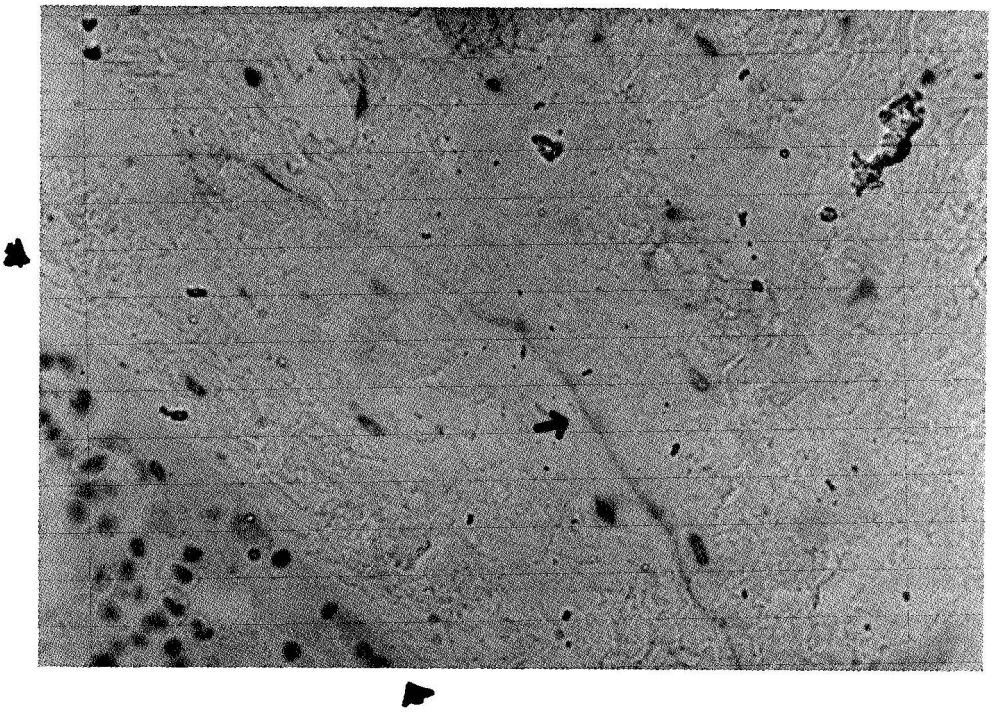

Figure 10. Reversal line stained with acid phosphatase. The arrow is pointing at the reversal line which has stained for enzyme activity indicating remanents of osteoclasts. The arrowhead indicates the endosteum. The marrow cavity is in the lower left hand corner. This photomicrograph is of a decalcified, 5μ thin section of tibial diaphysis taken from a Cosmos 936 flight rat.

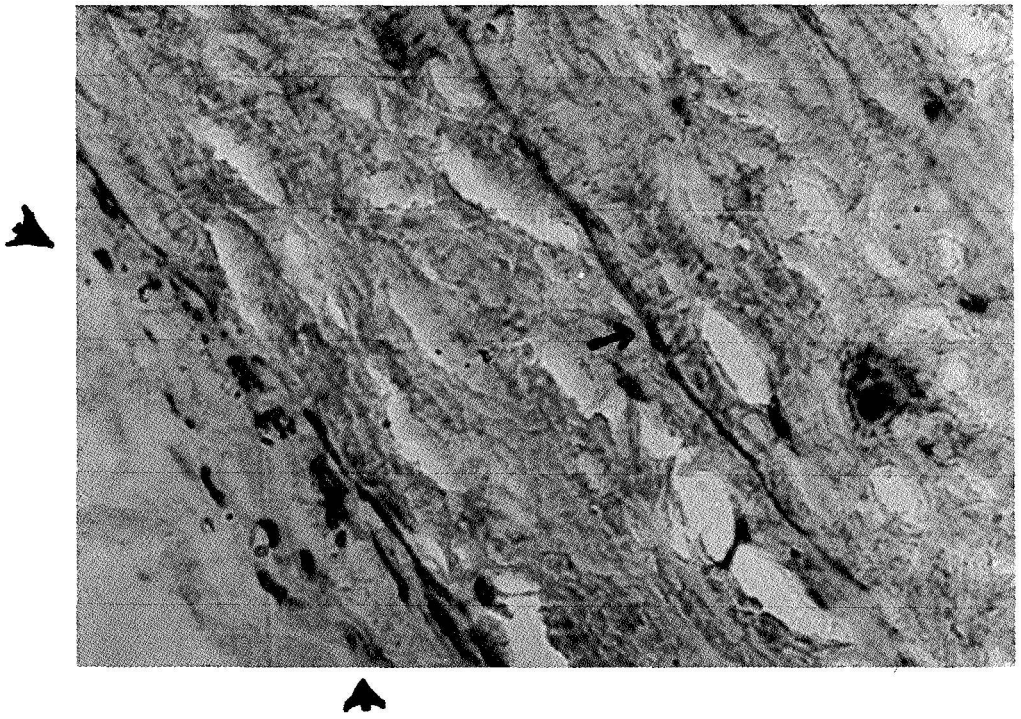

Figure 11. Arrest line stained with thionine. The arrow is pointing at the arrest line stained with thionine which suggests that the arrest line contains acid polysaccharide or a basic substance which is not fat extracted. The arrow head indicates the periosteum. The photomicrograph is of a decalcified, 5μ thin section of tibial diaphysis taken from a Cosmos 936 flight rat.

Two findings suggest that bone formation was reinitiated about the third day after flight. First, in Cosmos 782 both the group sacrificed immediately following flight and that receiving a second tetracycline label 3 days postflight formed the same volume of bone (232 and 224 x 10^{-3} mm^3, respectively) while in Cosmos 936, the group sacrificed immediately after flight formed about 40 x 10^{-3} mm^3 less bone than did the group that received a second tetracycline label 4 days after flight (363 vs 403 x 10^{-3} mm^3, respectively). If the Cosmos 936 rats were forming bone at the postflight rate (26.0 x 10^{-3} mm^3, table 5), then about 1.5 days of bone were formed suggesting that formation reoccurred around 2.5 days following flight. Second, the in vivo postflight label required active bone formation to entrap the tetracycline label and the second label in Cosmos 782 was less intense than that in Cosmos 936 (figure 12) suggesting that formation was reinitiated around the third postflight day.

If the flight animals are centrifuged, formation begins almost upon recovery. The flight centrifuge animals sacrificed immediately following flight formed 352 x 10^{-3} mm^3 of bone during the flight period while those labeled 4 days later formed 480 x 10^{-3} mm^3, a difference of 128. If this value is then divided by the postflight rate (29.7, table 5), 4.3 days of bone appear to have been formed in the 4 day period (table 6). Although centrifugation did not correct the defect in bone formation during flight, it apparently hastens the recovery postflight.

Changes in bone formation were consistent among the individual flight rats (figure 7). Without exception, all rats formed more bone following, than during, flight.

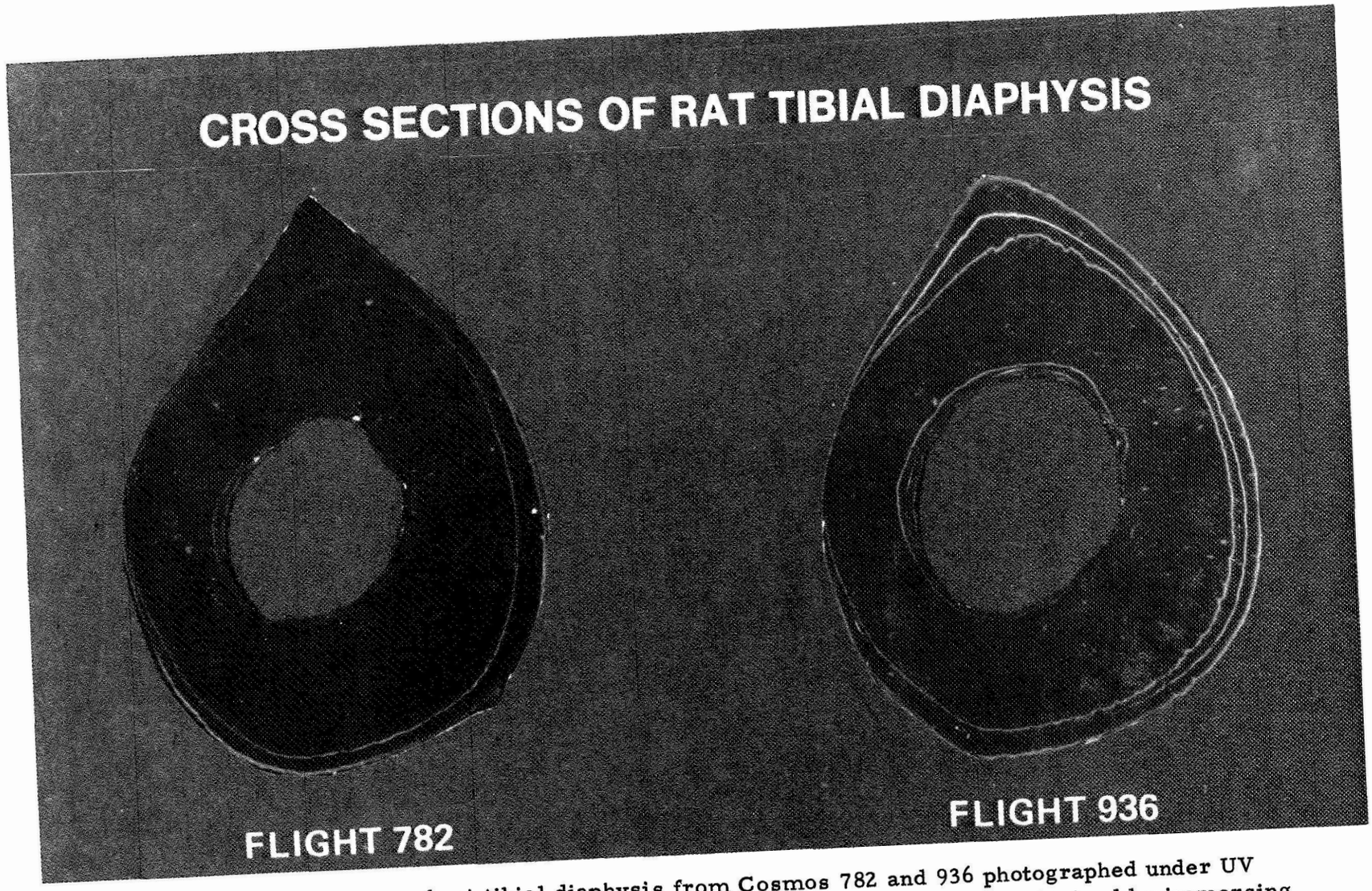

Figure 12. Cross-sections of rat tibial diaphysis from Cosmos 782 and 936 photographed under UV fluorescence. The fluorescent label at the periosteum (outer bone surface) was obtained by immersing the bone sections in tetracycline solution. The middle label is that given 3 days after flight in Cosmos 782 and 4 days postflight in Cosmos 936. This line is extremely faint in the Cosmos 782 flight rat as compared with the Cosmos 936 flight rat suggesting that bone formation was reinitiated just prior to the third postflight day. The innermost label is that given 3 days prior to launch. At the endosteum (the medullary area surface), the brighter label is that given 3 days prior to launch. The labels also indicate the shape of the bone at the beginning of the labeling period. Bone formation rates are measured by calculating the area between two labels and dividing this value by the length of the labeling period. These bone sections are hand ground mineralized sections about 30μ thick and are from the tibia-fibula junction.

During the postflight period, the flight groups and the flight control group showed a significant increase in bone formation when compared to the vivarium animals (table 5, figure 8). Since the flight and flight control animals were space restricted during the flight period, the rebound in bone formation may be due to increased activity after transfer to larger cages. The decrease in rate of bone formation in the vivarium group between flight and postflight periods (table 5) was not unexpected since these animals were about at the peak of their growth curve. The decrease in longitudinal bone growth in the postflight period (table 4) in these animals is also suggestive of a decreasing growth rate.

Space flight did not appear to have as dramatic an effect on bone formation at the endosteum (table 5), but these results were complicated by an unknown amount of resorption occurring concurrently with formation. Also, the endosteal formation rate is much less than the periosteal formation rate but the variance is not proportionally less. Although space flight did result in a decrease in forming surface of the endosteum at the tibia-fibula site (table 7), similar results were not seen at the diaphyseal sampling site (table 8). This discrepancy might be due to actual differences between the two sites, but the results are not strictly comparable since different criteria were used to evaluate forming surfaces on the ground sections (tibia-fibula sampling site) as opposed to decalcified, stained, thin sections (diaphysis). However, if the endosteum serves primarily as a mineral reservoir while the periosteum is associated with mechanical properties, a lack of space flight effect on the endosteum is not surprising.

Both osteoclast number and osteoclast nuclei/mm endosteal surface were estimated. Since the osteoclast nuclei were less variable (figure 13), only those data are presented (tables 8 and 9). Very few osteoclasts were present on the endosteal surface in these animals as compared with osteoblasts (table 8) suggesting that formation was predominant in these growing rats. Although the mean osteoclast values may suggest a slight increase in osteoclast nuclei in the flight group, no significant differences were found. Complementary to these data are medullary area values. Medullary area will enlarge to reflect any large changes in resorption. No significant intergroup differences occurred in the size of the medullary cavity during either experimental period (table 5, figure 9). Thus, no gross change in bone resorption was detected.

A decrease in bone formation or increase in bone resorption during space flight was expected since changes in bone mass have been reported in immobilized animals (12) and men (15), and in rats (22), monkeys (13), and men (20) following space flight. Because the greatest changes in bone mass during space flight occur in weight-bearing bones, changes in mechanical loading are undoubtedly important. Lack of such forces may also indirectly affect bone by causing changes in blood flow, neural transmission or hormonal levels. The reduction of mechanical stress is probably not sufficient to account for the decreased rate of bone formation since a comparable decrease in formation occurred in the 1G flight centrifuge group. However, the mechanical strength of the femur in the centrifuge rats was not reduced. In addition, bone formation was apparently reinitiated immediately upon recovery in the centrifuged rats whereas it was delayed 2-3 days in the flight rats (table 6).

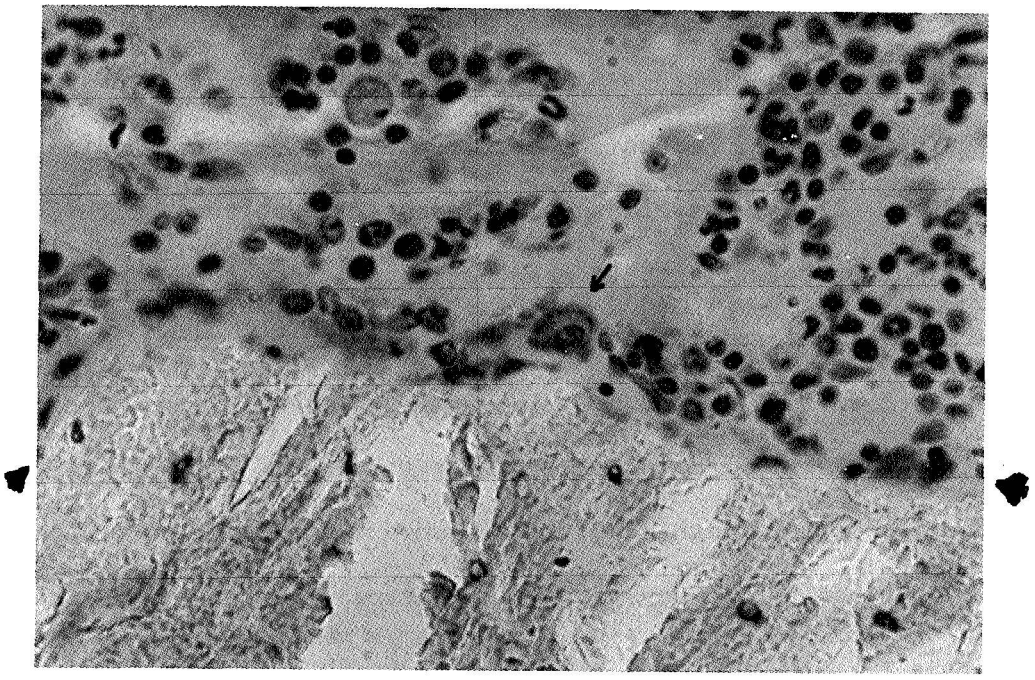

Figure 13. Acid phosphatase stained osteoclast with nucleus is indicated by arrow. The arrowheads point to the endosteum. Blood cells are seen in the marrow cavity which is the upper portion of the photomicrograph. Although osteoclasts/mm endosteal surface can be counted, less variance occurs when osteoclast nuclei are counted. So few osteoclasts were found in any of the experimental groups that no difference between groups could be determined. This photomicrograph is of a decalcified, 5μ thin section of tibial diaphysis from a Cosmos 936 rat.

Previous Cosmos data has shown no changes in parathyroid or thyroid gland histology or serum calcium. However, the flight rats did have significantly larger adrenal glands reflecting an increase in corticosterone content (19). Glucocorticoid treatment has been shown to decrease bone formation and the number of osteoblasts (8). Detection of glucocorticoid receptors in bone cells indicates that bone may be a target for direct glucocorticoid effects (5) such as inhibition of bone cell proliferation (10). Thus, glucocorticoids may also contribute to the bone changes noted during space flight.

Regardless of the mechanisms involved, the findings in this study demonstrate: 1) no gross changes in endosteal bone resorption occur during flight or postflight; 2) mean periosteal bone formation rate decreases about 45% and is not corrected by centrifugation; 3) the decrease in formation may be due, in part, to a cessation of bone formation which occurs sometime after the eleventh day of flight and continues until the second postflight day; 4) although centrifugation did not correct the defect in periosteal bone formation during flight, it appears to hasten the recovery following flight; and 5) bone mechanical properties, including torque, stiffness, and energy, are significantly decreased by space flight but are corrected by centrifugation. All significant differences produced by space flight on measured bone parameters returned to or exceeded normal values by 25 days after flight.

ACKNOWLEDGEMENTS

The authors thank the many Soviet scientists who assisted with the experiment by injecting rats, preparing samples, and expediting the shipment of biological specimens to this country. We also thank the NASA personnel who made this experiment possible. We are indebted to Patricia Halliday, Emily Thompson, Elmer Feist, and Bob Haller for preparing the bone sections and making the morphometric measurements, to Dr. Chung Liu and Charay Vatanaprida for the bone density and pore size distribution measurements, to Dr. Daniel Spengler and Dick Lee for the bone mechanical properties, to Joel Ivy for data processing, to Lucy Dillman for editorial assistance, and to Sandra Johnson for secretarial assistance.

REFERENCES

1. Baylink, D., E. Morey, and C. Rich. Effect of calcitonin on the rates of bone formation and resorption in the rat. Endocrinology. 84: 261-269, 1969.

2. Baylink, D., J. Sipe, J. Wergedal, and O. J. Whittemore. Vitamin D-enhanced osteocytic and osteoclastic bone resorption. Amer. J. Physiol. 224: 1345-1357, 1973.

3. Baylink, D., M. Stauffer, J. Wergedal, and C. Rich. Formation, mineralization, and resorption of bone in vitamin D-deficient rats. J. Clin. Invest. 49: 1122-1134, 1970.

4. Burnstein, A. H. and V. H. Frankel. A standard test for laboratory animal bone. J. Biomechanics. 4: 155-158, 1971.

5. Chen, T. L., L. Aronow, and D. Feldman. Glucocorticoid receptors and inhibition of bone cell growth in primary culture. Endocrinology. 100: 619-628, 1977.

6. Claus-Walker, J., J. Singh, C. S. Leach, D. V. Hatton, C. W. Hubert, and N. DiFerrante. The urinary excretion of collagen degradation products by quadriplegic patients and during weightlessness. J. Bone Jt. Surg. 209: 59A, 1977.

7. Donaldson, C. L., S. B. Hulley, J. M. Vogel, R. S. Hattner, J. H.Bayers, and D. E. McMillan. Effect of prolonged bed rest on bone mineral. Metab. 19: 1071-1084, 1970.

8. Feldman, D., R. Dziak, R. Koehler, and P. Stern. Cytoplasmic glucocorticoid binding proteins in bone cells. Endocrinology. 96: 29-36, 1975.

9. Frost, H. M. Bone modeling and skeletal modeling errors, Chas. C. Thomas, Springfield, Ill. pp. 74-77, 1973.

10. Jee, W. S. S., W. E. Roberts, H. Z. Park, G. Julian, and M. Kramer.

Interrelated effects of glucocorticoid and parathyroid hormone upon bone remodeling. In: Calcium, parathyroid hormone, and the calcitonins. R. V. Talmage and P. L. Munson, Eds., Excerpta Medica, Amsterdam, pp. 432-439, 1972.

11. Kummer, B. K. F. Biomechanics of Bone. In: Biomechanics. R. C. Fung, N. Perrowe, and M. Anliker, Eds., Prentice-Hall, Inc., New Jersey, pp. 237-271, 1972.

12. Landry, M. and H. Fleish. The influence of immobilization of bone formation as evaluated by osseous incorporation of tetracycline. J. Bone Jt. Surg. 46B: 764-771, 1964.

13. Mack. P. B. Bone density changes in a Macca Nemestrina monkey during the Biosatellite III project. Aerospace Med. 42: 828-833, 1971.

14. McElhaney, J. H. Dynamic response of bone and muscle tissue. J. Appl. Physiol. 21: 1231-1236, 1966.

15. Minaire, P., P. Meunier, C. Edouard, J. Bernard, P. Courpron, and J. Bourret. Quantitative histological data on disuse osteoporosis. Calc. Tiss. Res. 17: 57-73, 1974.

16. Morey, E. R. and D. J. Baylink. Inhibition of bone formation during space flight. Science, in press.

17. Portugalov, V. V. Personal communications.

18. Thompson, E. R., D. J. Baylink, and J. E. Wergedal. Increases in number and size of osteoclasts in response to calcium or phosphorus deficiency in the rat. Endocrinology. 92: 283-289, 1975.

19. Tigranyan, R. A. Personal communications.

20. Vogel, J. M., M. W. Whittle, M. C. Smith, Jr., and P. C. Rambaut. Bone mineral measurement-experiment M078. In: Biomedical results from Skylab.

R. S. Johnston and L. R. Dietlein, Eds., NASA SP-377, pp. 183-190, 1977.

21. Whedon, C. D., L. Lutwak, P. C. Rambaut, M. W. Whittle, M. C. Smith, J. Reid, C. S. Leach, C. R. Stadler, and D. D. Sanford. Mineral and nitrogen metabolic studies, experiment M071. In: Biomedical results from Skylab. R. S. Johnston and L. R. Dietlein, Eds., NASA SP-377, pp. 164-174.

22. Yagodovsky, V. S., L. A. Triftanidi, and G. P. Gorokhova. Space flight effects on skeletal bones of rats (light and electron microscopic examination). Aviat. Space Environ. Med. 47: 734-738, 1976.

FORMATION OF ECTOPIC BONE IN

IMPLANTED DEMINERALIZED BONE MATRICES

(US PORTION OF JOINT US/USSR EXPERIMENT)

Principal Investigator: Dr. Shvets, U.S.S.R.

Co-Investigators: D. J. Baylink
E. R. Thompson
E. Holton

American Lake Veterans Administration Hospital Tacoma, Washington 98493, U.S.A., University of Washington, Seattle, Washington, 98195, and Ames Research Center, Moffett Field, California 94035

INTRODUCTION:

Undenatured bone matrix, demineralized and lyophilized, induces bone formation when implanted in muscle or fascia of host animals. This model was employed by Dr. Shvets, U.S.S.R., to evaluate the effects of space flight on bone formation in implanted matrices.

Approximately half the implanted matrices recovered from basal, synchronous, vivarium control and flight groups of rats were sent by Dr. Shvets via NASA Ames Research Center to Mineral Metabolism Research Unit, American Lake V.A. Hospital for independent evaluation. These were accompanied by samples of unimplanted bone matrix.

MATERIALS AND METHODS:

Calcium Content: Representative samples of ectopic bone recovered from each host rat were dried, weighed, and digested in 6N HCl. Calcium content was determined on an aliquot by atomic absorption spectrophotometry and μg Ca/mg dry weight of sample was calculated.

Histological preparation: Specimens were prepared by a method which has been developed to preserve enzyme activity in mineralized bone, thus permitting the identification of osteoclasts as well as osteoblasts. Because cross sections are used for measurement of bone formation rate using a tetracycline time marker, and because bone formation does not occur uniformly throughout implanted matrix, specimens were cut into 2 to 4 segments and embedded for saggital sectioning. This resulted in the production of 57 tissue blocks, each containing from 1 to 3 segments of the specimen. Sections are cut with a Zeiss Universal

Cut-All microtome at 6μ for staining and 11.5μ (to be mounted in glycerol) for fluoresence microscopy.

Staining: Sections are stained by Goldner's modification of Masson's trichrome and by a method which differentiates osteoblasts and osteoclasts by taking advantage of the high RNA content of the former and acid phosphatase activity of the latter.

RESULTS AND DISCUSSION:

Calcium determinations demonstrate that calcium content is proportional to dry weight of specimens for all groups, including basal. These determinations were made to provide a referant for final analysis of data.

Forty-seven tissue blocks have been cut and representative slides from each group have been stained for the identification of bone cells. Sections of ectopic bone from all flight and vivarium control animals as well as representative slides from each of the other groups have been stained by the Goldner technique.

The general work plan is to review slides of each type and select the method or methods most likely to provide data which may demonstrate differences in response to the bone induction stimulus between flight and control groups. One potentially useful method would be counts of osteoblasts and osteoclast cell units, adjusted for bone suface area or bone volume if indicated.

A subjective study of slides suggests that the only areas stained green by the Goldner technique are mineralized bone. This is in contrast to what has been found in rat bone, in human bone, and in unimplanted bone matrix. In these, all "mature," or once mineralized matrix stains green even after being completely demineralized, and only newly formed osteoid stains red. If that were the case in the implanted matrices, all the old, implanted matrix except its normal borders of osteoid would be stained green as well as the mineralized bone formed during the time the matrix was implanted in the host rat. One would

then expect the red-stained area to be limited to the osteoid of the original matrix and the osteoid formed during the period of implantation which had not yet mineralized. Instead, it seems (but is not yet proven) that all the old matrix, whether once mineralized or not, is stained red. This suggests that a change occurs in the implanted matrix which cannot be demonstrated in the specimens of unimplanted matrix provided by Dr. Shvets, and which is reflected in a change in its tinctorial properties. Whether or not this change renders the old matrix mineralizable remains to be determined. Changes in implanted matrix have not previously been reported and therefore deserve study in order that the bone induction system be more fully understood.

If, as is suggested, only the mineralized bone formed during implantation is stained green by the Goldner stain, this would provide a means of obtaining data by measuring the mineralized areas in microscopic images projected on a digitizer tablet interfaced to a computer: equipment in use in this laboratory. Methods which can be used to verify the distribution of mineral in these complex specimens are Alizarin Red S, in vitro tetracycline, and, if necessary, autoradiography--or, more accurately, the chemography for which bone mineral is noted. A section should also be demineralized prior to staining and its tinctorial characteristics compared to an undemineralized serial section. Comparisons should be made in serial sections by photomicrography. A further photomicrograph using polarized light for collagen birefringence should help resolve the question of whether or not implanted matrix becomes re-mineralized. The collagen birefringence technique may be useful in determining the total amount of matrix formed in the ectopic bone specimens, whether mineralized or not.

It is hoped that the bone formation rate can be determined utilizing the tetracycline time marker. However, this would require that the labeled mineral has neither been resorbed nor has become a part of the exchangeable calcium pool

during the time between administration of tetracycline and sacrifice of the animal.

Note: The results reported above are preliminary in nature and represent the US portion only of the joint US/USSR Ectopic Bone experiment. A final report containing the combined results of US and USSR investigators will be released at a later date.

77

N79-11677

SPACE RADIATION DOSIMETRY ON BOARD COSMOS 936

US Portion of Experiment K—206

E.V. Benton, R. Cassou, A. Frank, R.P. Henke,

and D.D. Peterson

Physics Research Group

University of San Francisco

San Francisco, California 94117

ABSTRACT

Investigation of the space radiation environment was carried out in a joint US-USSR experiment on board the Cosmos 936 biosatellite. Results reported here were derived from measurements made in a variety of passive radiation detectors including plastic nuclear track detectors, fission foil detectors, thermoluminescence dosimeters, and nuclear emulsions. Measurements were made of HZE particles, neutrons, protons, and the total radiation dose. The mean observed HZE particle flux, as measured in cellulose nitrate plastic detectors, was 1.75/cm^2·day (±20%) on Cosmos 936, compared with 4.05/cm^2·day (±17%) on Cosmos 782. The charge spectrum of HZE particles was measured in the region $6 \leq Z \leq 18$. The fluences of thermal neutrons (<0.3 eV), resonance neutrons (0.3 eV–1 MeV), and high-energy neutrons (>1 MeV), were, respectively, 3.64×10^5/cm^2 (±20%), 9.5×10^5/cm^2 (–30% to +50%), and 2.1×10^6/cm^2. The total dose, as measured in TLD chips located at two sites in the US-25% part of the K-206 container, was 424 mrad (±9%) and 523 mrad (±11%). The mean tissue equivalent proton ender density, as measured in nuclear emulsions located in the US-25% part, was 2.72×10^5/cm^3·tissue. The physical parameters of the radiation environment reported here help specify important dosimetric information required to assess the potential radiation hazards to life systems in space.

INTRODUCTION

Life systems in space experience a unique and complex environment including radiation which presents hazards to life systems that may impair normal physiological processes and thereby create limitations to their natural functions. Worldwide interest in the effects of space environment has grown in relation to man's increasing endeavors in space, and has led to a wide variety of investigations in space and on Earth. These investigations have yielded valuable information about the effects of space on man, as well as on other life systems.

As a part of these investigations, joint US-USSR studies in space were initiated in 1974 with an offer by the Soviets to have US scientists participate in a biosatellite mission. The joint experiment was carried out on Cosmos 782 in late 1975. It focussed on the effects of weightlessness on a variety of physiological functions in plants and animals, and also included measurements of physical parameters of high-charge and -energy HZE particles on board the Vostok satellite.

The Cosmos 936 joint US-USSR space radiation dosimetry experiment, K-206, was designed mainly to determine physical parameters of the different components of the radiation in space. It included comparison of results between US and Soviet investigators with the objective to elucidate results from the Cosmos 782 mission which contained an unexplained difference in HZE particle flux values measured by US and Soviet investigators. The experiment also included ground-based studies of the calibration and the measurement of the response of various detectors. These studies are being carried out at the

Berkeley and Dubna accelerator facilities.

The K-206 experiment consisted of three separate parts: a US-25% part which was located at one end of the experiment container, a USSR-25% part located at the opposite end of the container, and a joint-50% part in the central region of the container. Detector materials from the joint-50% part were shared equally by US and USSR investigators. The joint-50% part was designed to determine the flux, LET spectrum, and charge spectrum of HZE particles. It contained two thick plastic stacks which were capped with nuclear emulsions, and twelve thin dosimeter packets attached in pairs to the six faces of a foam cube located in the central region of the joint-50% part. The US-25% part was designed to determine physical parameters of HZE particles, fluence and spectrum of neutrons, proton fluence, and total radiation dose. A schematic drawing of the K-206 experiment is shown in Fig. 1.

The following sections describe the details of the analysis and results obtained from the US detectors in the joint-50% part and the US-25% part of the K-206 experiment for HZE particles, neutrons, and protons on board Cosmos 936.

HZE PARTICLES — FLUX, INTEGRAL LET SPECTRUM, AND SPATIAL DISTRIBUTION

Measurements in spacecraft of HZE particles have been carried out by our research group at the University of San Francisco over the past decade. Plastic nuclear track detectors flown aboard Gemini IV and VI (1) registered tracks of heavily ionizing particles. This demonstrated that plastic detectors could provide a simple and effective method of measuring the integrated flux of HZE particles inside spacecraft. Plastic films are especially effective in this kind of measurement because they do not record the more abundant lightly ionizing particles such as electrons and protons but, instead, register tracks only of the relatively fewer heavy cosmic-ray nuclei that exist in

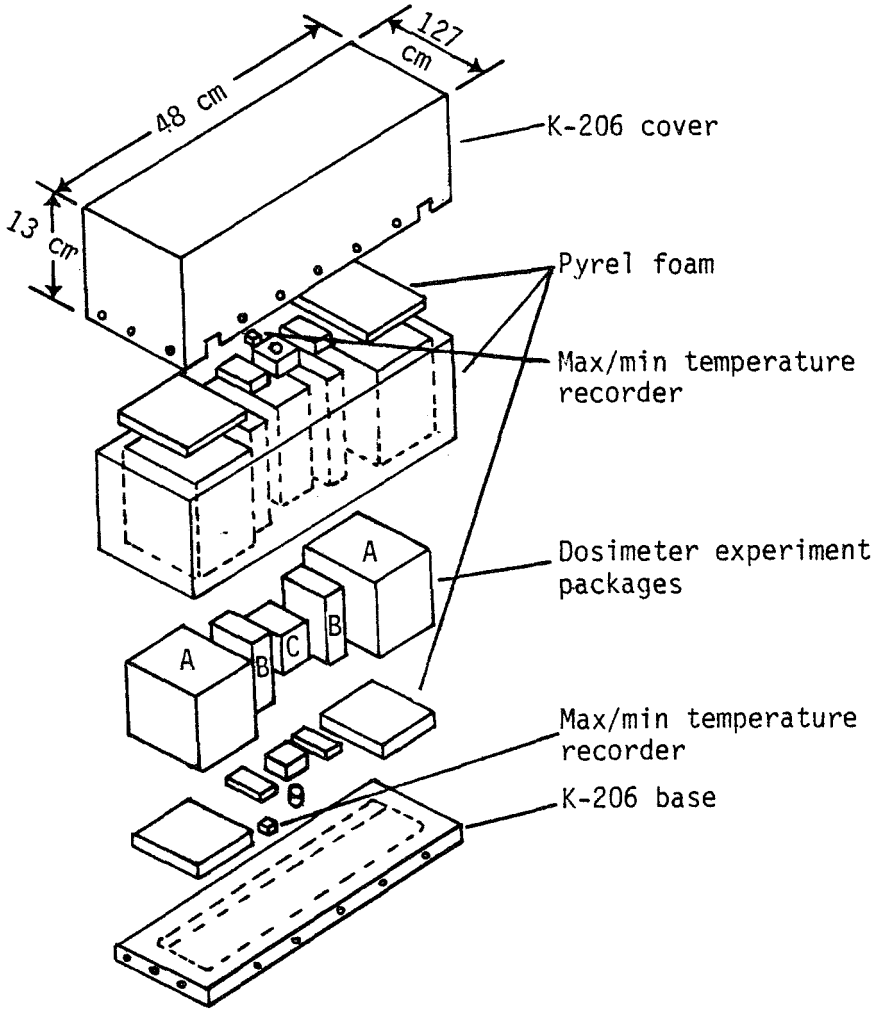

Figure 1

Diagram of K-206 experiment configuration. Dosimeter experiment packages show US-25% parts (A), and the joint-50% part thick plastic stacks (B) and orthogonal detectors (C).

space. Measurements of HZE particle radiation on Apollo, Skylab, and ASTP space missions using plastic detectors has recently been reviewed (3).

Consequences of astronaut exposure to HZE particles has been discussed in a report by the US National Academy of Sciences, with specific recommendations given for continued and improved dosimetry of this type of radiation using plastic detectors. Concern over HZE particle effects was dramatically intensified after Apollo 11 astronauts reported observing light flashes, presumably caused by heavy nuclei.

The radiobiological effects of energetic, heavy nuclei are only recently being studied in the laboratory, facilitated by high-energy heavy-ion accelerators such as the Berkeley-Bevalac in California. Until at least the knowledge of the effects of these particles on life systems is more complete than at present, the results of measurements of the physical parameters of HZE particles is important information to be recorded as part of man's activities in space.

The following sections describe details of our measurements of physical parameters of HZE particle radiation on board Cosmos 936.

Materials and Methods

The flux, integral LET spectrum and spatial distribution of HZE particles is determined through the analysis of plastic nuclear track detectors located in the joint-50% part of the K-206 experiment. The HZE particle detector contained thin films of cellulose nitrate (Kodak-Pathé, CA 80-15), polycarbonate (General Electric — Lexan) plastics and nuclear emulsions. Two films of each type of plastic were layered together and sealed, along with three nuclear emulsion films sealed in plastic, inside a black polyethylene envelope. The area of the plastic films is 4.5 × 6 cm.

A total of eighteen detectors were located inside the K-206 flight con-

tainer. Twelve detectors were attached in pairs to each of the six faces of a pyrel foam cube (7.7 × 7.7 × 7.7 cm) centrally located in the joint-50% part of the flight package. Six detectors were attached to each face of the US package located in the US-25% part of the container.

Flight exposed plastic detectors are stored at 5°C in polyethylene bags.

Standard techniques are used to develop the plastic detectors. Table 1 lists the details of the etchants, temperatures, and times used in these procedures. Column one lists the sample designation. For example, 1FB refers to flight (F) sample number 1, layer B. The four plastic layers within a detector are designated A, B, C, and D. Layers A and D are polycarbonate plastic, and layer A is adjacent to the nuclear emulsions. Layers B and C are cellulose nitrate plastic. Orthogonals 1F-US-6F-US were located in the joint-50% part of the flight package; 7F-US–12F-US in the US-25% part.

Scanning for HZE particle tracks in the developed plastic detectors is carried out with optical microscopes at ∿200X magnification. A central area, 3 × 3 cm, of each detector is scanned. The scanning procedure in a given orthogonal detector consists of attaching layer C to the microscope stage and then aligning and attaching layer B over the top of layer C. Layer C was etched until the thickness was reduced by ∿60%, yielding many etched-through holes that corresponded with measurable double-cone, or tapered-cylinder, events in layer B, the primary measurement layer. This scanning technique increases the efficiency of finding small track etch pits, with a decrease in the strain and duration of the scanning procedure.

Two small fiducial holes were drilled through the four plastics in each orthogonal prior to disassembly. The x and y coordinates of all HZE particle tracks found in the scanning procedure are specified with respect to the fiducial holes by mechanical encoders connected to the x and y stage drives of the microscope.

TABLE 1. DEVELOPMENT PARAMETERS FOR US PLASTIC DETECTORS

Sample	Plastic	Etchant	Time (hr)	V_B (μm/hr)
1FB-12FB	CN*	a	10.0	1.07 ± 0.05
1FC	CN	a	39.0	0.92
3FC-6FC	CN	a	30.0	1.01 ± 0.02
2FC, 7FC-12FC	CN	a	29.0	1.19
1FA-7FA, 11FA	Lexan†	b	44.0	0.15 ± 0.02
1FA-7FA, 11FA§	Lexan	b	24.0	0.55 ± 0.01

a) 2.5*N* NaOH, 40.0°C, solution stirred

b) 6.25*N* NaOH + 1 g/ℓ polycarbonate monomer + 0.05% surfactant (Dowfax 2A1), solution stirred

*thickness 90 μm/CN film

†thickness 190 μm/ Lexan film

§pre-etch UV treatment of samples

Measurement of etched track parameters is carried out with oil immersion objectives at 1000X magnification with a precision of ±0.5 μm. Measured parameters include depth, projection and surface minor axis of the track etch pit, and depth and width of the narrowest point in the case of tapered cylinder tracks. The etch rate of the bulk plastic is determined by measuring the thickness change of the film. The bulk etch rate of the Kodak-Pathé cellulose nitrate is very sensitive to the etch products concentration in the etchant, 2.5*N* NaOH at 40°C. The track etch rate in Pathé-CN is affected very little by etch product concentration.

Track etch rate is calculated with measured track parameters and analytical expressions based on track geometry which assume constant etch rate over the length of the etched track.

A unique relationship exists for each type of plastic track detector between track etch rate and restricted energy loss (2). This relationship is the basis for evaluation of restricted energy loss from track etch rate. Preliminary calibration curves used in data analysis in this work are given in Fig. 2 for plastics Kodak-Pathé cellulose nitrate and Lexan polycarbonate (with and without the ultraviolet light sensitization process). The graph in Fig. 2 is a plot of track etch rate, V_T, versus LET_{350} (the subscript denotes that only secondary electrons with energy ≤350 eV are included in calculation of restricted energy loss). The curves in Fig. 2 represent least-squares fits to data obtained with accelerator-produced ions of known atomic number and energy.

A requirement of particle track etchability in plastic detectors is that the vertical component of track etch rate must be greater than the bulk etch rate of the plastic film. A minimum value of LET_{350} is implied from the curves in Fig. 2 which depends on type of plastic and development, or pre-de-

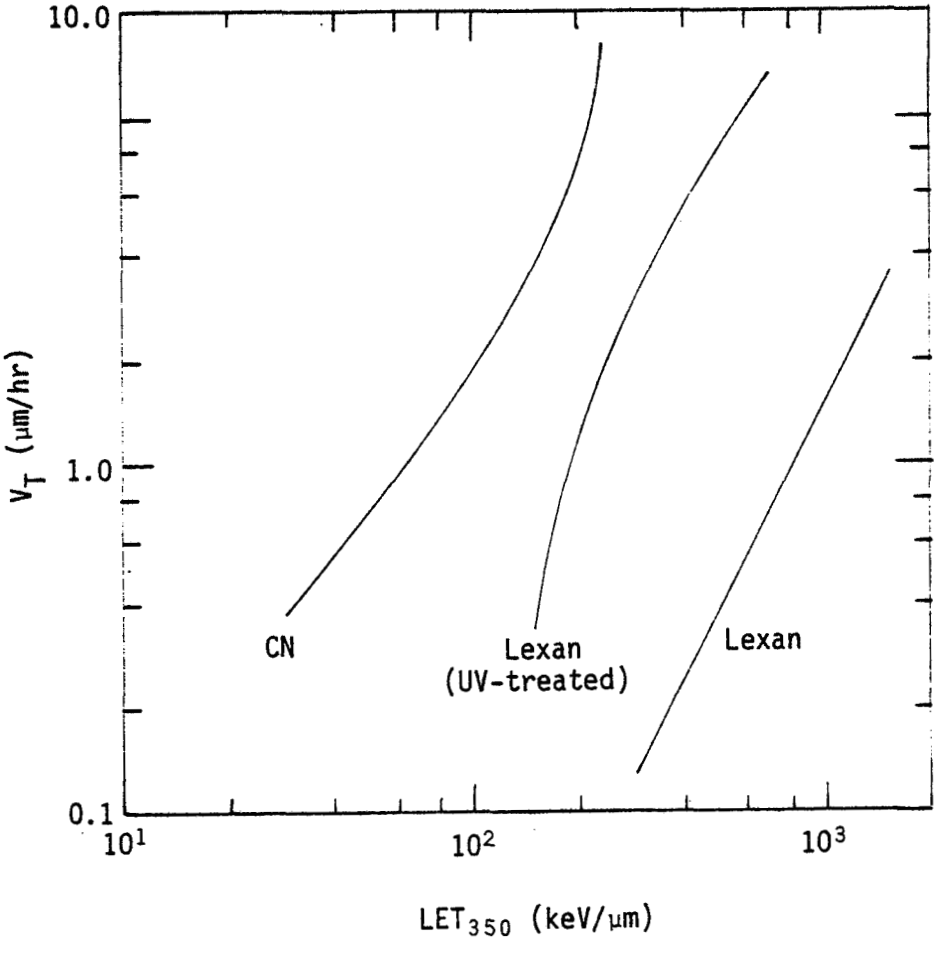

Figure 2

Calibration relationships used for Kodak-Pathé cellulose nitrate and Lexan polycarbonate plastic detectors.

velopment, treatment. Also, the requirement implies a critical dip angle (measured from the surface of the film) for particle registration at a fixed value of LET_{350}. A correction factor, dependent on track dip angle and LET_{350} value, is applied to the observed tracks in order to obtain the absolute fluence. For example, the integral LET_{350} spectrum is calculated by the summation of the product of each LET_{350} value (corresponding to a given track) multiplied by the correction factor for all tracks with LET_{350} value greater than a given value. The integral particle flux for a given value of LET_{350} is calculated by dividing the summation by $2\pi At$, where A and t are, respectively, the sample area and flight time.

The spatial distribution of incident HZE particles is determined by particle fluence values recorded in the six detectors attached to each face of the foam cube in the central region of the joint-50% part of the experiment container. An orthogonal set of detectors is achieved by this arrangement which can assess the fluence in the three mutually perpendicular directions, x, y, and z, in space

Results

The observed fluence and flux of HZE particles recorded in eight detectors from the joint-50% part and the US-25% part are listed in Table 2. The first column in Table 2 lists the detector and location, and the second column lists observed number of tracks found in a 9 cm^2 area of the detector. The values in column two correspond to HZE particles that registered on all four surfaces of the two adjacent CN layers B and C. Columns three and four list the observed fluence and flux, respectively. The flux values are based on the 18.5 day mission of Cosmos 936.

The integral LET spectra for detector 1F-US is plotted in Fig. 2. Orthogonal detector 1F-US registered the maximum HZE particle fluence in the six orthogonal detectors located in the joint-50% part.

TABLE 2. HZE PARTICLE DATA FOR US PLASTIC DETECTORS

	Observed*		
Detector/Location	Tracks	Fluence (tracks/cm^2)	Flux $\left(\frac{\text{tracks}}{\text{cm}^2 \cdot \text{day}}\right)$
1FB-US/joint part	361	40.1 ± 2.1	2.17 ± 0.11
2FB-US/joint part	230	25.6 ± 1.7	1.38 ± 0.09
3FB-US/joint part	319	35.4 ± 2.0	1.92 ± 0.11
4FB-US/joint part	221	24.6 ± 1.7	1.33 ± 0.09
5FB-US/joint part	279	31.0 ± 1.9	1.68 ± 0.10
6FB-US/joint part	335	37.2 ± 2.0	2.01 ± 0.11
7FB-US/US-part	354	39.3 ± 2.1	2.13 ± 0.11
11FB-US/US-part	188	20.9 ± 1.6	1.13 ± 0.08

*HZE particles with $Z \geq 3$ and a registration range ≥ 180 μm.

Discussion

HZE particle flux. Table 3 presents a comparison of results obtained in the Cosmos 936, Cosmos 782 (5), and Skylab (4). The maximum, minimum, and mean flux values listed in Table 3 are derived from the six orthogonal detectors in the joint-50% part in the Cosmos 936 mission, the twelve detectors in the Cosmos 782 mission, and from the nine astronaut personnel dosimeters in the Skylab SL2, SL3, and SL4 missions.

The mean HZE particle flux in the Cosmos 936 mission was a factor of 2.3 less than in the Kosmos 782 mission. Consideration of factors that can effect HZE particle flux, for example, orbital flight parameters, spacecraft shielding distribution and solar modulation and type of plastic detection, indicates that shielding differences and type of detector are the most probable causes of the flux difference in these missions. The effects of shielding are indicated by the results of measurements in the Skylab mission (4). The flux of HZE particles inside the heavily-shielded film vault was a factor 10X smaller than the flux received by the astronauts. The calculated equivalent spherical shielding thicknesses for the astronauts sleep compartment and the film vault were, respectively, $\sim$6 g/cm^2 and $\sim$50 g/cm^2.

The effect of the plastic detector type on particle registration efficiency is presently being studied at the Berkeley accelerator. The objective of the studies is to determine the efficiency of the different types of cellulose nitrate plastics used on the Cosmos 936 and Cosmos 782 missions.

Solar modulation effects can account for at most only a 10% decrease in cosmic-ray intensity for the Cosmos 936 mission over the Cosmos 782 mission. Cosmic-ray intensity is indirectly measured by ground-level neutron monitors which continuously record the secondary neutron production rate in the atmosphere. The Mt. Washington neutron monitor recorded only a 1% lower counting rate over the duration of the Cosmos 936 mission (3 August-22 August 1977) versus the Cosmos 782 mission (25 November-15 December 1975).

TABLE 3. HZE FLUX IN COSMOS 936, COSMOS 782, AND SKYLAB MISSIONS

Mission	HZE flux* (particles/cm^2·day) (max)	(min)	(mean)
Cosmos 782	5.15	3.28	4.05†
Cosmos 936	2.17	1.13	1.75§
Skylab	3.75	1.9	2.71

*HZE particles with $Z \geq 3$ and registration range ≥ 180 μm

†mean of detectors F1-F12

§mean of orthogonal detectors 1F-US to 6F-US in joint-50% part

**mean of nine astronaut personnel dosimeters in Skylab missions SL2, SL3, and SL4

Orbital flight parameters (i.e. period, inclination, perigee, and apogee) were essentially identical for the Cosmos 782 and Cosmos 936 missions. These factors cannot therefore be the cause of a difference in particle flux. Also, the Soviet Vostok-type satellite was used in each mission.

Integral LET spectrum. The integral LET spectrum, which specifies the number of HZE particles with LET greater than a given LET value, is an important dosimetric parameter required for assessing the potential radiobiological hazards to life systems in space. It can be used, for example, to calculate the radiation quality factor.

An example of the integral LET_{350} spectrum of HZE particles on Cosmos 936 is displayed in Fig. 3. The results are derived from measurements in detector 1F-US, located in the joint-50% part of the K-206 experiment container. Other measured spectra are shown for comparison in Fig. 3 for Cosmos 782 (5), Skylab astronauts and the Skylab film vault (4), and Apollo-Soyuz (ASTP) astronauts (3). A calculated integral LET_{350} spectrum for cosmic-ray nuclei at solar minimum (4) is also displayed in Fig. 3.

The integral LET_{350} spectrum of HZE particles on board Cosmos 936 exhibits a sharp decrease with increasing LET_{350} value as observed in past missions. The maximum flux of HZE particles with $LET_{350} \geq 80$ keV/μm·CN (i.e. $LET_{\infty} \simeq 106$ keV/μm·tissue) is 5.1×10^{-6}/cm^2·sec·sr for the Cosmos 936 mission. This value lies between the flux value for the Cosmos 782 mission (8.7×10^{-6}/cm^2·sec·sr) and the Skylab astronauts (4.5×10^{-6}/cm^2·sec·sr).

Spatial distribution. Results from the six detectors in the joint-50% part of the experiment package indicate that a target located at the center of the Pyrel foam cube (to which the detectors were attached) would receive a nearly isotropic fluence of HZE particles.

The magnitude of the fluence of HZE particles was the same within statistical limits on the top, bottom, and sides of the foam cube, as recorded in,

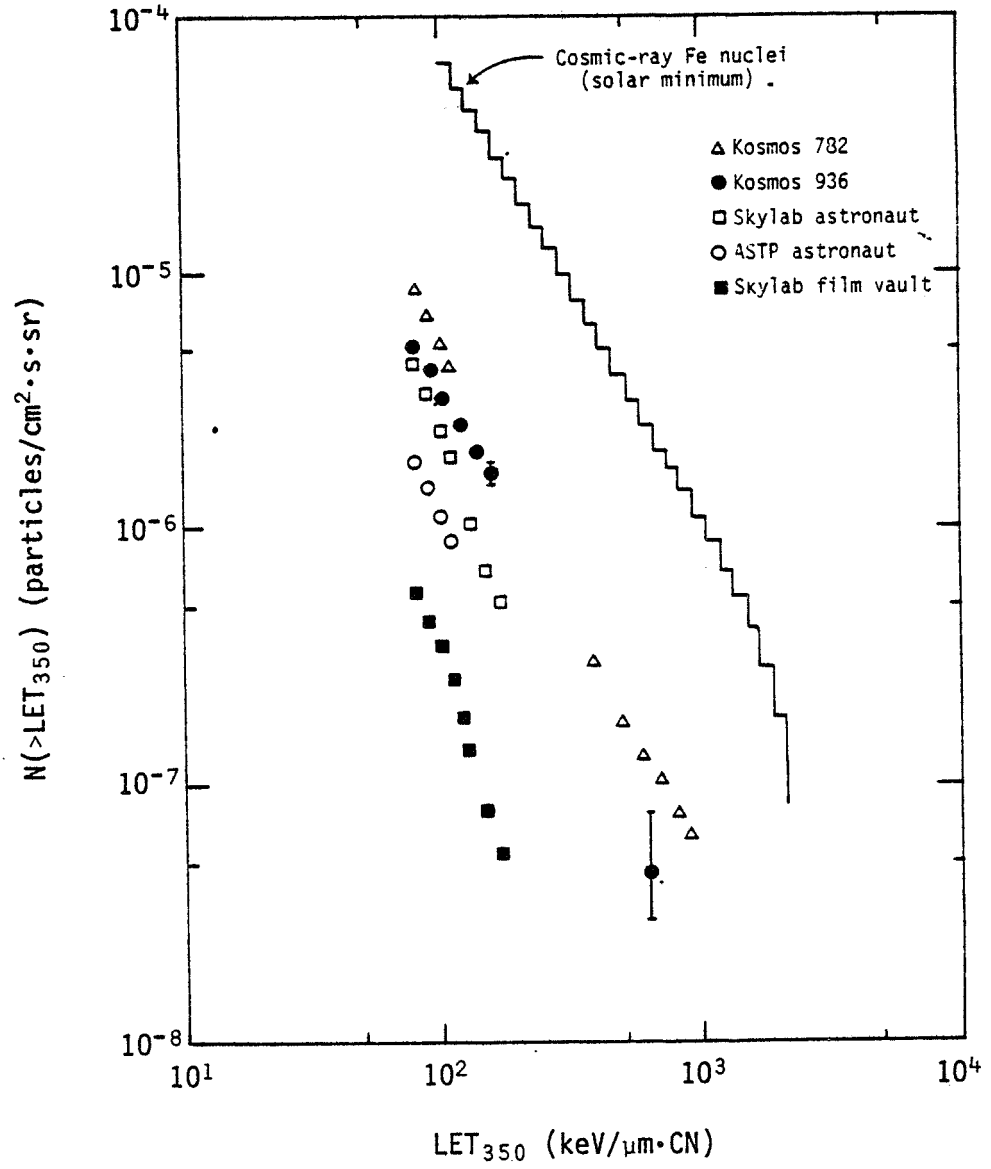

Figure 3

Integral LET spectra for HZE particles measured with plastic track detectors on different space missions.

respectively, detectors 1F-US, 3F-US, 5F-US, and 6F-US (see Table 2). The fluence in detector 5F-US was slightly less than statistical deviation would allow. The attachment of detectors on the cube was such that detectors 1F-US and 3F-US faced, respectively toward the top and bottom of the container, 2F-US and 4F-US faced, respectively, the "USSR"-end and the "US"-end of the container, and 5F-US and 6F-US faced the sides of the container.

Detectors 2F-US and 4F-US, which faced the ends of the container, were shielded by the thick plastic stacks in the joint-50% part, and also shielded by the block of material in each 25%-part end of the K-206 container. The equivalent of $\sim$22 g/cm^2 of aluminum shielded detectors 2F-US and 4F-US in a direction normal to the detector surface. As indicated by results from the Skylab film vault (4), the flux of HZE particles is reduced by $\sim$2X behind $\sim$20 g/cm^2·Al shielding. The consequence of the shielding of detectors 2F-US and 4F-US by the thick plastic stacks, both in the joint-50% part and the end-25% parts, is that the recorded fluence in these detectors should be multiplied by a factor of the order of $\sim$2X. Carrying this out then, the fluence of HZE particles in detectors 2F-US and 4F-US would be approximately equal to the fluence recorded in the other four detectors. The "absolute" incident fluence (i.e. normalized to the same shielding) is then approximately the same magnitude for each face of the cube.

HZE PARTICLES — Z SPECTRUM

In the traditional approach to Z analysis, stacks of plastic track detectors are processed by etching them in heated alkaline solutions, which gradually removes detector material from each detector surface and preferentially attacks the trail of damage left by each highly ionizing particle. The rate of this preferential attack is governed by the LET of the particle, so the

final length of the conical track formed about the particle trajectory is a measure of the LET. Usually 5-20% of the original thickness of the plastic is removed in the etch process.

Detector scanning and measuring are normally performed in two steps. 1) One or more layers are scanned at a relatively low magnification. There are also several alternatives to scanning including the use of sparks or vapor passage through etched-through holes to locate very widely spaced tracks. 2) The tracks found in the low-magnification scan are then measured at higher magnification and traced to other layers which may not have been scanned. In the measurement process, the positions and lengths of the cones on the two detector surfaces are measured. These measurements establish the particle trajectory and two values of LET along that trajectory.

In the data reduction process, there are two fairly distinct phases. In the first phase, the individual particle parameters are computed from the measured positions, LET values, and hopefully a measurement of the x,y,z position of the rounded track end that reflects the stopping point of the particle. Altogether, 7 parameters are required to specify the character of a stopping particle. One set of parameters is the three coordinates of the particles stopping point, the two space angles of the particle trajectory, and the identification of the particle type by the atomic number, Z, and atomic mass, A. In practice, it is usually not possible to achieve isotope resolution so either the most abundant isotope is assumed for each value of Z and only Z is determined, or an effective Z, which is assumed to be a continuous variable, is defined by combining the effects of Z and A. Thus the number of parameters per particle is reduced to 6.

In the second phase of the data analysis, the individual particle measurements are collected into statistical results. These statistical results are the distribution of particles in one or more variables. A common form

taken by these results is the particle Z spectrum, which is the distribution of the particles in Z value and usually one or more of the other parameters used to specify the individual particles. A logical form to be taken by the statistical results obtained in plastic detectors is the number of particles stopping per Z per volume (or mass) per solid angle $\frac{d\rho_Z}{d\Omega}$ The integral of $\frac{d\rho_Z}{d\Omega}$ over all 4π steradians of solid angle is the ender density-Z spectrum, ρ_Z. This distribution is somewhat in contrast with the Z-energy spectrum usually obtained by detectors which register high-energy, non-stopping particles. The ender density-Z spectrum is consistent with the response of plastic track detectors since they only register particles which are relatively near their stopping points. If $\frac{d\rho_Z}{d\Omega}$ is expressed as a function of position over all of space, it is fully equivalent to the energy spectrum expressed as a function of energy over the domain of all possible energies except for nuclear fragmentation effects. In practice, for small stacks it is reasonable to assume that $\frac{d\rho_Z}{d\Omega}$ is independent of position. With such an assumption, it is possible to compute other quantities and distributions of interest such as the LET spectrum.

The traditional methods of Z analysis have been employed many times in many different contexts. An extensive bibliography can be found in the book by Fleischer *et al.* (7). Most often the Z values are computed using what is known as the L-R plot. In this method the measured values of the track length, L, is plotted as a function of the particle residual range, R. This set of points, either individually or collectively, is compared with theoretically generated curves for the different possible values of Z. The approach used by Henke and Benton (unpublished data) for the Apollo 14 and 17 missions differs somewhat in that the comparison between the measurements and the theoretical model is accomplished entirely in an analytic rather than graphical fashion, using a least-squares technique. Using this approach, it is also possible to

process the track measurements from particles which do not have a measured stopping point.

The results presented in this current report are derived using the method which markedly differs from the traditional methods in that the measurements of track position and etch rate are made automatically with a Quantimet 720 image analyzing system. The detectors are etched to remove a large fraction of their original thickness. This results in large tracks which are etched completely through the plastic layers. The track etch rate is obtained through the measurement of the projected areas of these holes. This method has previously been employed in the measurement of a stack of Lexan detectors flown on the joint Apollo-Soyuz (ASTP) mission (Benton and Henke, unpublished data).

Materials and Methods

The Z spectrum here to be reported was derived from the joint section of the Cosmos dosimetry package (stack 1F-US). The stack was composed of 97 μm thick layers of Kodak-Pathé cellulose nitrate, CN, and 188 μm thick layers of GE Lexan polycarbonate. The layer sequence was 10 layers of CN, 200 layers of Lexan, 65 layers of CN, 200 layers of Lexan, and 10 layers of CN.

The cellulose nitrate layers have all been processed by etching them in a 2.5*N* NaOH solution at 40°C. This solution was saturated with camphor to improve and make constant its etching properties. The etching time of 112 hours has reduced these layers to a final thickness of 27 μm or 28% of the original thickness. With the largest fraction of the layers removed, most of the particles registering in the stack have left holes etched all the way through the plastic layer. The largest of these holes have opening areas of approximately 4000 μm^2.

The Lexan layers have been etched in a 6.25*N* NaOH solution at 70°C. The solution contained 0.5% Benax surfactant and 1 g/ℓ of 4,4'-iso-propylidene-

diphenol to simulate the effects of Lexan etch products in the solution. The etching time of 43.67 hours has reduced the layers to a final thickness of 36.6 μm or 20% of their original thickness.

A 9.75 cm^2 portion of each of the processed cellulose nitrate layers has been scanned and measured semi-automatically using our Quantimet image analyzing computer. For each of the etched holes produced by the intersection of a particle with one layer of the plastic, the position and opening area has been measured.

The measured track positions have been analyzed by a track-tracing computer code to evaluate the trajectories for particles having 3 or more measured tracks per particle. The trajectories were obtained by making linear regressions to the measured x positions as a function of z and the y positions as a function of z. The particle trajectory parameters determined from the regressions are the intersection of the trajectory with the z = 0 surface, (x_0, y_0), and the azimuthal and dip angles given by α and δ in Eq. (1). The

$$\frac{dx}{dz} = \text{ctn } \delta \cos \alpha$$
$$\frac{dy}{dz} = \text{ctn } \delta \sin \alpha \qquad (1)$$

parameters of the tracing program were adjusted so that all particles with $\delta > 30$ deg were accepted. Particles with smaller dip angles had such rapidly varying positions from layer to layer that including them would have led to ambiguity because of the relatively high track fluence of 54 tracks/cm^2.

The particles were then identified and the stopping point computed in a second least-squares computer code.

Since the tracks were automatically measured, it was not possible to measure the actual stopping point of each particle. Therefore, the measured values of the track area as a function of position along each trajectory were

used to evaluate both the particle's atomic number Z and the stopping point of the particle. This was accomplished by minimizing the expression

$$\mathcal{M} = \sum_{\text{track}} \left(\frac{A_c - A}{\sigma_A} \right)^2 \qquad (2)$$

with respect to both Z and the particle stopping point. Here A_c is the computed value of the area based on Z, the particle stopping point, a measured relationship between the track etch rate and the particle LET, and the trajectory of the particle from the tracking program. A is the "measured" area of the particle as previously described, and the weighting factor, $\frac{1}{\sigma_A^2}$, is obtained from the residuals about the fit. Since $\frac{1}{\sigma_A^2}$ is assumed to be a constant, it can be placed in front of the summation in Eq. (2). In this way σ_A is evaluated by setting the minimum value of $\mathcal{M} = \chi^2$ = the number of degrees of freedom $\left(\frac{\text{the number of measured tracks}}{\text{particle}} - 2 \right)$. Since A_c is not a linear function of the unknown quantities, Z and stopping point, Eq. (2) is linearized by expanding it in a Taylor series in the corrections to Z and the stopping point. Then the solution for the corrections to an original approximation are obtained by a normal linear least-squares fit in two variables. The final solution is obtained by iterating until the corrections go to acceptably small values. With the linearized system, it is also possible to obtain the uncertainties in Z and the stopping point as well as the correlation in these errors from the normal linear least-squares procedures. In the Z analysis, the dependences on Z and A were combined into a dependence on Z alone by replacing A with the approximate expression for the most abundant isotope, $A = 1.776\ Z^{1.059}$.

The statistical analysis of the computed Z values results in $\frac{d\rho_Z}{d\Omega}$ as approximated by the expression $\frac{\Delta N}{\Delta Z \Delta V \Delta \Omega}$ where ΔN is the number of events falling

in the intervals ΔZ, ΔV, and $\Delta\Omega$. The solid angle intervals, $\Delta\Omega$, are chosen to divide the measured solid angle region from $\delta = 30$ deg to $\delta = 90$ deg and from $\delta = -30$ deg to $\delta = -90$ deg into ten equal parts. Equation (1) can be satisfied using only positive values for δ, however negative values of δ have been used to designate particles with one sense of travel in the stack (downward in the stack) and positive values to designate the other sense of travel (upward in the stack). The actual regions used are enumerated in the results section. For each $\Delta\Omega$ region, the acceptable volume within which an acceptable particle can stop, ΔV (in water equivalence, since the detectors have a larger stopping power than water) is determined using the criteria 1) that the detection efficiency be nearly 100% and 2) the stopping point be sufficiently near the measurement region to ensure an acceptably small error in Z, σ_Z. The derived value of $\frac{d\rho Z}{d\Omega}$ is obtained by dividing the number of particles acceptable according to the above described criteria by the corresponding values of $\Delta\Omega$ and ΔV. The interval of ΔZ used in the derived spectrum is variable and will be discussed in the Results section.

Results

All of the measured track positions from the 85 CN layers are shown in Fig. 4. The position for each of the 45,072 hole openings is shown by a dot. The area shown is 4.14 cm wide by 2.35 cm high. It can be seen that there are many isolated dots produced by low-Z particles which only register in one layer, and there are also many long lines of dots produced by heavier particles which register in layer after layer. From these measured positions, 1834 particles with 4 or more tracks per particle were derived using the tracing program. The selection criteria in the tracing program also excluded the majority of the particles with $\delta < 30$ deg.

The accuracy of track position measurements can be assessed from the RMS

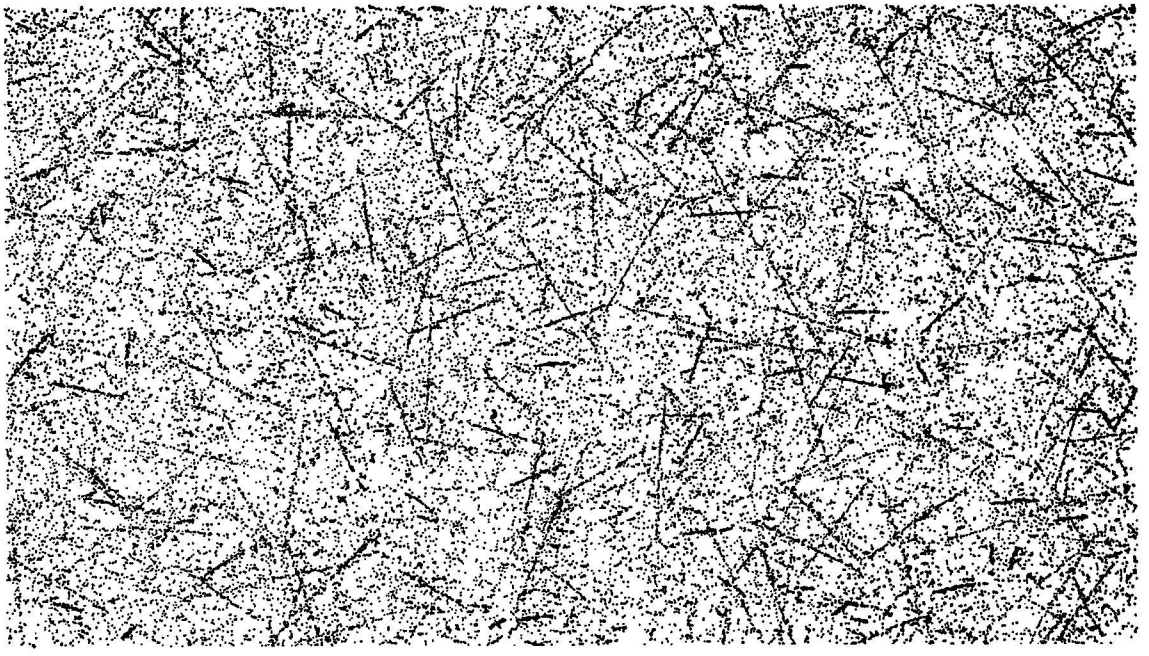

Figure 4

Positions of all of the measured tracks in the CN layers of the HZE stack.

(root mean square) deviation of the measured positions about the fit-line trajectories. The average value of this error was found to be 0.0023 cm or 23 μm. From the positional error, it is also possible to determine the error in the measured dip angle for each particle trajectory. Considering that approximately 50% of the trajectories had fewer than 7 tracks/particle, it can been seen that the particle trajectories were quite accurately determined since the median value of σ_δ is 0.92 degrees.

The measured Z spectrum is given in Table 4 and in Figs. 5 and 6. Table 4 gives the angular dependence of the Z spectrum. The particles have been integrated over all values of Z to achieve sufficient statistics to allow the angular distribution to be seen. Even with the detected solid angle divided into 10 equal regions of 0.2π steradians each, sufficient statistics remain to show the anisotropy of the beam. Of the original 1834 traced particles, 625 remained after all of the selection criteria had been applied.

Figure 5 gives the differential Z spectrum for Z treated as a continuous variable. In this spectrum, each selected particle has been represented as a gaussian distribution about the measured Z value with area $\frac{1}{\Delta V \sum \Delta\Omega}$ and with a standard deviation of 0.15 atomic number units. The sum of these gaussians is the spectrum. The integral form of the Z spectrum is shown in Fig. 6.

Although the accuracy of many of the measured values of Z is poorer than ±1, a sufficient number of particles have Z values which are accurate enough for some of the individual peaks of the Z spectrum to be resolved. The portion of the Z spectrum with Z below approximately 7 has not been determined with 100% efficiency because of the insensitivity of the detectors and the requirement that the tracks be seen in 4 layers.

Discussion

The automated approach used in the determination of the reported Z spec-

TABLE 4. ANGULAR DEPENDENCE OF THE PARTICLE STOPPING DENSITY

Dip angle interval (degrees)	Azimuthal angle interval (degrees)	Stopping density for all selected particles (particles/cm^3·ster with $Z \geq 7$)
$-90 \rightarrow -64.16$	$0 \rightarrow 360$	10.6 ± 1.3
$-64.16 \rightarrow -30$	$0 \rightarrow 90$	8.3 ± 1.2
	$90 \rightarrow 180$	3.9 ± 0.8
	$180 \rightarrow 270$	5.9 ± 1.0
	$270 \rightarrow 360$	4.6 ± 0.9
$3 \rightarrow 64.16$	$0 \rightarrow 90$	14.1 ± 1.5
	$90 \rightarrow 180$	9.6 ± 1.3
	$180 \rightarrow 270$	8.8 ± 1.2
	$270 \rightarrow 360$	11.8 ± 1.4
$64.16 \rightarrow 90$	$0 \rightarrow 360$	24.5 ± 2.0
	Average	10.2 ± 0.4

$\frac{d^2\rho}{dZd\Omega}$ (particles/cm^3 water·ster·atomic number units)
2
1.5
1
0.5
0
6
8
10
12
14
16
18
20
Z

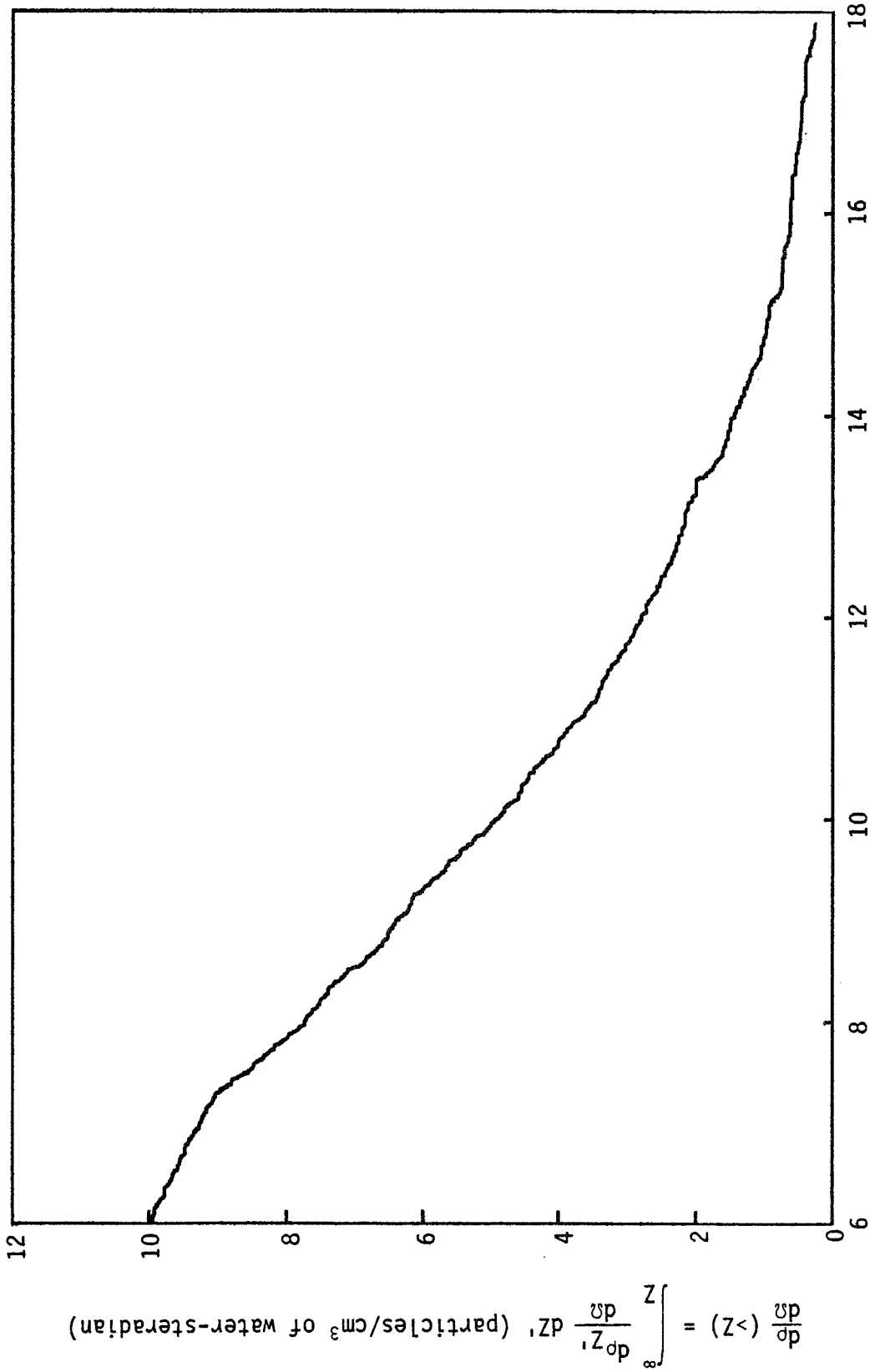

Figure 6
Integral Z spectrum.

trum has very great advantages and some disadvantages as compared to the manual methods of the past. The main advantages are the saving of large amounts of scanning and measuring time and the ability to accumulate very large amounts of data without an inordinate expense for scanning and measuring. This advantage is reflected in the large number of particles included in the Z spectrum analysis.

There are also disadvantages to the automated analysis of stacks. Most of the disadvantages result from the inaccuracies in the method in its present state of development. Most of these inaccuracies can be overcome with improvements in the stack configuration, processing, and measurement methods. The main limitations in the present data are the somewhat low Z resolution and the apparent inability to resolve particles with Z greater than approximately 18. Both of these problems apply to the cellulose nitrate stack and will be eliminated to a great extent when the Lexan polycarbonate portion of the stack has been read out. A limitation of the present experiment which can be avoided in the future is the division of the low and high sensitivity materials into distinct sections in the combined detector stack. Interleafing the Lexan and CN layers should result in a much more homogeneous stack which will eliminate the large gaps in the trajectories of particles which cross the low-sensitivity section at low LET. This will make the particle tracing process much more straightforward and less subject to ambiguities.

NEUTRONS

Neutrons ranging in energy from thermal to hundreds of MeV are present in orbital spacecraft. The spectra of the neutrons can be resolved into three divisions; thermal (<0.3 eV), resonance (0.3 eV < E_n < 1 MeV) and high energy (>1 MeV). This is due to the cross sections of the available reactions which

can be used in detection. Assumptions must necessarily be made concerning the neutron spectra within these energy regions. The neutron fluences calculated from induced nuclear decay measurements can vary significantly as the incident spectrum is assumed "harder" or "softer". The sensitivity to spectral shifts depends on the magnitude of reaction cross section differences within the energy regions. In the high-energy region, the measurements are further complicated by the fact that in addition to the (n,f) reactions used for neutron detection, the radiator foil nuclei possess (p,f) reaction cross sections of similar magnitudes. The high fluences of energetic protons present in Earth orbits create relatively large background track densities on the mica detectors. Uncertainties in proton spectra and fluences introduce inaccuracies into the subtraction of the proton-induced fission fragment tracks. Proton spectra have been measured during previous orbital spaceflights so that a good basis for approximating the shape of the Cosmos 936 spectrum exists. Less is known of neutron spectra in space, but the neutrons can be assumed to have been produced by spallation reactions between energetic charged particles--mainly protons--and the nuclei of atoms within the spacecraft and the earth's outer atmosphere. This allows some reasonable estimations to be made regarding spectral shapes.

Several types of detectors were flown in the detector packet US-25% part in order to measure neutron fluxes present in the spacecraft. These were all passive integrating devices and employed either thermoluminescent detectors (TLDs) or track etch detectors as the sensitive recording medium. In the first case, the high cross section of the $^{6}Li(n,T)^{4}He$ reaction in LiF TLDs is used. In the second case, various radiator foils are sandwiched against cellulose nitrate plastic or moscovite mica which record the tracks of either ^{4}He particles or fission fragments, respectively.

Materials and Methods

Detectors having particle radiators composed of ^{6}LiF, ^{181}Ta, ^{209}Be, ^{232}Th and ^{238}U were included in the detector packet. The first of these employed cellulose nitrate plastic to register the ^{4}He particles from the $^{6}Li(n,T)^{4}He$ reaction. The remainder contained mica to register fission fragments from the (n,f) reactions. Other detectors of these types which were intended to be flown were not available due to procurement problems. The thickness of the ^{6}LiF radiator foils were 4.5 mgm/cm^2. The thicknesses of the fission foils varied but all were thicker than the ranges of the fission fragments produced. This gave the fission foil detectors their maximum efficiency, since there is little attenuation of the detected neutrons through the foils. The ^{6}LiF detectors require a self-shielding correction.

The TLDs were of both the ^{6}LiF and ^{7}LiF types. The dimensions of the chips were 0.635 cm by 0.635 cm by 0.089 cm. The chips were composed of pure extruded LiF. Discrimination on the basis of the high neutron cross section of ^{6}Li can be made from the measurement differences between the two materials. Neutron measurements can be made in the presence of relatively large absorbed doses from other particles by this method.

The relevant cross sections in the thermal energy range are shown in Fig. 7. When detectors are shielded by 1-mm-thick cadmium sheet, the neutrons below about 0.3 eV are absorbed out before reaching the detector. Therefore, when paired detectors, with and without cadmium shielding, are used together, the measurements can be separated into those fractions due to neutrons of thermal and higher-than-thermal energies. This method was used to measure the thermal neutron contribution to track densities measured with the ^{6}LiF/cellulose nitrate plastic detectors. Half of these detectors flown were shielded with cadmium.

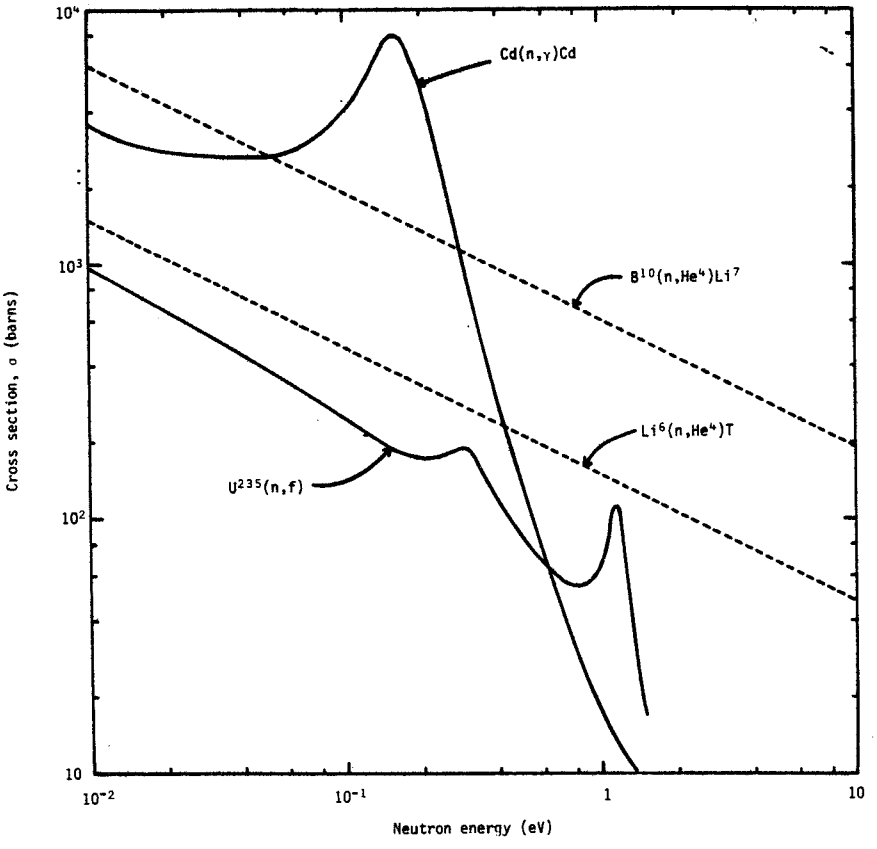

Figure 7

Some nuclear reaction cross sections in the thermal neutron energy region which are used in detectors.

The gamma ray from the $Cd(n,\gamma)Cd$ reaction makes this material unsuitable as a thermal neutron shield for the TLDs. Shields of 0.3 gm/cm^2 of ^6LiF were used instead. This arrangement does not provide the sharp energy cutoff of the previous detectors but an effective cutoff of about 1.5 eV is achieved. The responses of thermal and higher-than-thermal neutron energies were separated on this basis. Half of the TLDs of each type flown were shielded in this way.

The neutron detectors were arranged in two separate packets for the flight. The packets were 0.9 cm thick and composed of two slabs of Lucite. The thicker slab (0.6 cm) had holes milled into it to accommodate the detectors. The USF stack in the Cosmos 936 flight package was sandwiched, top and bottom, by the #1 and #2 neutron detector packets. The #1 packet was directed out through the spacecraft walls and was less shielded from space radiation than was the #2 packet. In packet #1 were three ^{209}Bi and four ^6LiF radiator detectors and nine ^6LiF TLDs. There were also background samples of mica and cellulose nitrate plastic. In packet #2 were two ^{209}Bi, two ^{181}Ta, three ^{232}Th and three ^{238}U radiator detectors and twelve each of ^6LiF and ^7LiF TLDs. The ^{209}Bi radiators were 1.27 cm by 1.27 cm in dimensions. Those radiators of ^{181}Ta and ^6LiF were 1.8 cm in diameter and those of ^{232}Th and ^{238}U were 1.27 cm in diameter. The ^6LiF material was plated on a backing. Therefore, a single cellulose nitrate detector on the active side of the foil was used. The other foils were self supporting and mica detectors were placed against both sides.

Before detector assembly the mica discs were stripped of a surface layer to ensure an undamaged surface, then etched for 16 hours in 50% HF solution at room temperature. The fossil fission fragment tracks in the surface of the mica were etched out to a large size by this treatment. After disassembly, the discs were etched again for 50 minutes under the same conditions. Those tracks registered during the Cosmos flight were etched out to a size where

they were easily recognizable under 350X while being much smaller than the fossil tracks. The exposed surfaces of the mica discs were then scanned completely for Cosmos tracks. Track densities were calculated for each detector and mean track densities plus standard deviations were calculated from the multiple individual measurements for each detector type. The individual measurements were corrected for background tracks which were not due to recent fission fragments by counting tracks on mica surfaces not in contact with fission foils during the flight. In addition, there was a background to be subtracted from the ^{238}U/mica detectors which was due to spontaneous fissioning of ^{238}U nuclei. After disassembly of packet #2, it was reassembled with fresh mica in these detectors. After 92.78 days, they were removed and etched to determine the contribution to track density of spontaneous fissioning. Tracks were found to have accumulated at a rate of 1.710 ± 0.085 tracks/cm^2-day.

The cellulose nitrate plastic used in the detectors was Kodak-Pathé Ca-80-15. In preparation for counting, the samples were washed clean in room temperature water, then etched for 1 hr 40 min in 6.25*N* NaOH solution at 40°C. The tracks of the low-energy (≤2.05 MeV) ^4He particles were observed as short cylinders at 430X magnification. The detector samples, plus a flight background, were counted to determine track densities.

Prior to readout, the TLD chips were washed in ethyl alcohol. They were then read out in a standard TLD reader. The reader heats the chips at a predetermined rate to a maximum temperature of 240°C. This causes radiation-induced glow peaks to be emitted by the dosimeter chips. The amount of light emitted is proportional to the absorbed dose of radiation received by the chip. The light emission is recorded by means of a photomultiplier tube and integrating picoammeter. The dosimeter chips were individually calibrated with ^{137}Cs gamma rays from a source of known intensity. The integrated cur-

rent output from the reader was converted to equivalent gamma-ray exposures by this means.

The TLD chips in packet #2 were also corrected for a spurious background during the post-flight reassembly. The ^{238}U and ^{232}Th foils emit gamma rays which contributed a small dose rate to the TLDs during the period the packet was assembled. The chips were annealed after the flight readout and reassembled in the packet to measure this background. In the worst case, the background contribution was less than 8% of the total measured absorbed dose. For most of the TLDs, it was less than 3%. Between the two packets was the plastic HZE stack and 0.32 cm of brass, so that the background dose in packet #1 was negligible.

Results

The results of the track counting and TLD measurements are given in Tables 5, 6, and 7. In Table 5 the ^{6}LiF/cellulose nitrate plastic detector measurements are given in tracks/cm^2. The associated errors are the standard deviations calculated from counting statistics. The TLD readout is given in Table 6. The errors given are the standard deviations calculated from the scatter in the individual chip readings. The fission foil detector results are given in Table 7. The standard deviations due to counting statistics are also given. The counting errors in the ^{238}U measurements were multiplied because of the high spontaneous fission background. Because of logistics, it was necessary that the detector packets be assembled for 87 days so the build-up of the spontaneously induced tracks became very significant. The neutron fluences were calculated from the above measurements and the corresponding detectors' responses.

Thermal neutrons. From the track densities measured with the ^{6}LiF/cellulose nitrate plastic detectors in Table 5, it can be seen that the thermal neu-

TABLE 5. TRACK DENSITIES COUNTED FROM THE ^{6}LiF/CELLULOSE NITRATE PLASTIC DETECTORS IN DETECTOR PACKET #1

Detector #	Tracks/cm^2	Shielding
1	2172 ± 66	none
2	2268 ± 68	none
3	444 ± 22	1 mm Cd
4	431 ± 22	1 mm Cd
Background	167 ± 16	none
E_n < 0.3 eV	1783 ± 62	
E_n > 0.3 eV	271 ± 31	

TABLE 6. READOUT OF THE TLD CHIPS

Detector packet	Detector type	Equivalent gamma-ray exposure (mR)
#1	^{6}LiF-unshielded	628 ± 8
	^{6}LiF-shielded	569 ± 12
#2	^{6}LiF-unshielded	485 ± 7
	^{6}LiF-shielded	462 ± 6
	^{7}LiF-unshielded	439 ± 10
	^{7}LiF-shielded	418 ± 4

TABLE 7. RESULTS OF THE TRACK COUNTING FROM THE FISSION FOIL/MICA DETECTORS

Detector packet	Radiator	Track recorder	Tracks/cm^2
#1	^{209}Bi	top	5.3 ± 2.3
		bottom	—
	^{209}Bi	top	7.2 ± 2.6
		bottom	9.5 ± 2.8
	^{209}Bi	top	5.9 ± 2.4
		bottom	11.7 ± 3.1
	background		0.8 (2 tracks)
#2	^{209}Bi	top	11.3 ± 3.0
		bottom	6.0 ± 2.4
	^{209}Bi	top	10.6 ± 3.0
		bottom	12.2 ± 3.2
	^{181}Ta	top	0.4 (1 track)
		bottom	0.4 (1 track)
	^{181}Ta	top	0.8 (2 tracks)
		bottom	0.4 (1 track)
	^{232}Th	top	62.9 ± 8.1
		bottom	60.2 ± 7.6
	^{232}Th	top	55.4 ± 7.4
		bottom	79.7 ± 8.9
	^{232}Th	top	56.7 ± 7.4
		bottom	71.6 ± 8.3

(continued)

TABLE 7. continued

Detector packet	Radiator	Track recorder	Tracks/cm^2
	^{238}U	top	221 ± 14
		bottom	251 ± 15
	^{238}U	top	271 ± 16
		bottom	243 ± 15
	^{238}U	top	256 ± 15
		bottom	238 ± 15
	background		0
Reassembly	[^{238}U spontaneous		176 ± 12
	fission background]		165 ± 12
	All ^{209}Bi		8.9 ± 2.6
	All ^{181}Ta		background
	All ^{232}Th		64.4 ± 8.6
	All ^{238}U		77 ± 24

tron component was found to be 1783 ± 62 tracks/cm^2 which was 80% of the total track density. Since the ^{6}LiF films were 4.5 mg/cm^2, which is more than three times the range of 20.5 MeV ^{4}He particles, the detectors had the maximum possible sensitivity to the thermal neutrons incident within the 2π solid angle on the side with the cellulose nitrate plastic. Those incident on the opposite side had a reduced sensitivity due to self shielding in the ^{6}LiF. A calculation of self shielding yields a factor of 0.75 for the track density reduction for thermal neutrons. In order to calculate the total neutron fluence during the flight, it is necessary to assume an isotropic incidence. A total 4π self-shielding correction factor of 1.143 was therefore used for the track density. The 2π response of a similar detector with a thick ^{6}LiF layer has been measured to be 5.6×10^{-3} tracks/thermal neutron (16). From these factors, a fluence of 3.64×10^5 thermal neutrons/cm^2 is calculated.

The thermal neutron fluence can also be found from the TLD measurements. From Table 6, the dose equivalent due to neutrons less than 1.5 eV is the difference between the shielded and unshielded ^{6}LiF TLD measurements. This is seen to be 59 ± 20 and 23 ± 13 mR equivalent for detector packets #1 and #2, respectively. The large errors are due to the subtraction of two large numbers. The TLD measurements were dominated by the charged particle absorbed doses. The two numbers cannot be said to be significantly different so the average, 41 mR equivalent, was used. A conversion factor between thermal neutron fluence and gamma-ray exposure has been reported for ^{6}LiF chips (17). It was found that 10^{10} thermal neutrons/cm^2 gave a thermoluminescent output equivalent to 900 ± 90 R of ^{137}Cs gamma rays. The thermal neutron fluences were calculated using this factor. This yields a value of 4.56×10^5 thermal neutrons/cm^2. This is 25% higher than found with the ^{6} LiF/cellulose nitrate plastic detectors. The errors in the TLD measurements of this component can account for this difference. The greater energy cutoff, 1.5 eV to 0.3 eV, is also a contributing factor.

The errors involved in the two determinations are those due to statistical variations in the readout, the absolute calibrations, the neutron conversion factors and those due to the unknown spectral shape and isotropy of the neutrons. The low-energy neutrons are unlikely to be well thermalized. With a hardened spectrum, the thermal fluence would be underestimated. The efficiencies could be substantially different if the neutrons are non-isotropic. The latter uncertainties are difficult to estimate but the method of production of the neutrons, spallation reactions in the spacecraft and the Earth's atmosphere, should impart no striking deviations from 4π or 2π geometries. A reasonable estimate of errors is ±20% for the ^{6}LiF/cellulose nitrate plastic detectors and −50% to +100% for the TLDs.

Resonance neutrons. The resonance neutrons (0.3-1 MeV) are measured with the same detectors as were the thermal neutrons. The $^{6}Li(n,T)^{4}He$ reaction cross section drops off with increasing energies so that there is little contribution from neutrons above 1 MeV. Measurements made with thermal-neutron-shielded detectors are therefore mainly due to resonance neutrons. The response of the detectors varies greatly over the wide neutron energy range involved. The $^{6}Li(n,T)^{4}He$ reaction has a cross section of 950 barns for thermal neutrons and follows the relationship

$$\sigma = \frac{150.2}{E_n^{\frac{1}{2}}}$$

in the neutron energy region below 1 keV. At 1 MeV it is down to about 0.3 barns. In order to derive fluence from the track density measurements an assumption of the spectral shape of the neutrons must be made. A "soft" spectrum will yield a smaller value for fluence than will a "hard" spectrum. A spectrum proportional to $\frac{1}{E_n}$ is a reasonable estimate in this region, since this is approximately the shape that a moderated neutron spectrum assumes.

Another factor to be considered is the increase in the energies and ranges of the ^4He particles emitted in the $^6Li(n,T)^4He$ reaction over this neutron energy range. This results in an increase in detector efficiency per reaction. For thermal neutron interactions, the ^4He particles carry off 2.05 MeV. For 1 MeV neutrons, they carry off 2.48 MeV. This represents a 22% increase in particle range in the LiF radiator and about a 30% increase in track counting efficiency. A correction factor of $(1 + 0.3 \times 10^{-6}\ E_n)^{-1}$ was applied to the ^6LiF/cellulose nitrate plastic detector efficiency calculations and a factor of $(1 + 0.21 \times 10^{-6}\ E_n)^{-1}$ to the TLD efficiency calculations.

For the ^6LiF/cellulose nitrate plastic detectors the response as a function of neutron energy is

$$R(E_n) = R_{Th}\ (1 + 0.3 \times 10^{-6}\ E_n)^{-1} \left(\frac{\sigma_{E_n}}{\sigma_{Th}}\right)$$

where R_{Th} is the thermal neutron response and σ_{E_n} and σ_{Th} are ^6Li neutron interaction cross sections. To simplify the calculations, the $^6Li(n,T)^4He$ cross section was approximated by

$$\sigma_{E_n} = 0.75 + \frac{150}{E_n^{\frac{1}{2}}}$$

The ratio becomes

$$\frac{\sigma_{E_n}}{\sigma_{Th}} = 7.9 \times 10^{-4} + \frac{0.158}{E_n^{\frac{1}{2}}}$$

The response of the detectors to the resonance neutrons is then

$$R_{Re} = R_{Th} \frac{\int_{0.3}^{10^6} \left(\frac{7.9 \times 10^{-4} + 0.158}{E^{\frac{1}{2}}}\right)(1 + 0.3 \times 10^{-6}\ E)^{-1}\ E^{-1}\ dE}{\int_{0.3}^{10^6} E^{-1}\ dE}$$

This expression was numerically integrated to get

$$R_{Re} = 2.86 \times 10^{-4} \text{ tracks/neutron}$$

From Table 5 it is seen that 271 ± 31 tracks/cm^2 were measured above the cadmium cutoff. This converts to a neutron fluence of 9.5×10^5 per cm^2 in the resonance region.

The calculation of the resonance neutrons from the TLD measurements is subject to greater error than in the above case. It is necessary to use the difference between two large numbers, as with the thermal neutron calculations. Also the neutron energy cutoff characteristics of the 0.3 gm/cm^2 ^{6}LiF shields make the response determinations more subject to error. A numerical integration similar to that above was carried out to find the detector response to a $\frac{1}{E}$ resonance neutron spectrum. A calibration factor of 5.8×10^8 neutron/cm^2-R equivalent was found for neutrons between 1.5 eV and 1 MeV in energy. From Table 6, the difference between the shielded ^{6}LiF TLDs and the shielded ^{7}LiF TLDs is the dose-equivalent due to these neutrons. In packet #2, this is 44 ± 10 mR equivalent. This yields a fluence of 2.5×10^7 neutrons/cm^2. This value is 26 times higher than that measured with the ^{6}LiF/cellulose nitrate plastic detectors. The TLD measurements must be considered the major source of error, despite the good agreement between the individual chips--as seen in the small statistical fluctuations. In comparing the TLD measurements, it is seen that the difference in the unshielded ^{6}LiF and ^{7}LiF detectors is 47 ± 17 mR equivalent. This should be the measure of the total neutron fluence through the ^{6}Li(n,T)^{4}He reaction, yet it is approximately the same as the resonance neutron measurement. It is suspected that a systematic error is present. The different types of TLD chips were not positioned in exactly the same geometries with regard to the total dosimetry stack. The difference

between the #1 and #2 packet measurements and also some increase in the TLD measurements near the forward edge in packet #2 shows that a considerable amount of attenuation in the incident charged-particle fluences was taking place in the dosimetry stack. It is believed that the differences in attenuation experienced by the different TLD types has created measurement fluctuations nearly as great as the small differences corresponding to resonance neutron interactions.

The errors in the ^{6}LiF/cellulose nitrate plastic detector measurements are much less. The major errors are due to the assumption of the neutron spectral shape and the statistical fluctuations in counted tracks. The limits of error are estimated to be −30% to +50% for these measurements.

High-energy neutrons. The high-energy fluences were calculated from the fission foil/mica detectors. The relevant cross sections of ^{181}Ta, ^{209}Bi, ^{232}Th, and ^{238}U are shown in Figs. 8 and 9. The neutron and proton cross sections for ^{232}Th and ^{238}U are given in the former for energies less than 40 MeV. The ^{232}Th cross sections for the two reactions are comparable above 32 MeV, but for ^{238}U the neutron cross section is considerably higher. Proton cross sections between energies of 10 and 10^{4} are given in Fig. 9 for the four radiator isotopes. The cross sections in both figures were constructed from published measurements (11, 12, 20, 21, 22). Some interpolations have been done to reconcile measurements and fill in gaps in the data. The neutron and proton cross sections converge as nucleon energies increase and the effect of the protons charge becomes relatively less important. Somewhere above 100 MeV, the two cross section curves should become approximately equal. For ^{209}Bi and ^{181}Ta, the (n,f) and (p,f) cross sections have been assumed equal.

The sensitivity of thick fission foil detectors have been measured to be 1.16×10^{-5} tracks/neutron-barn (14). The sensitivity for a nucleon spectrum therefore depends on the effective cross section of the detector to the spec-

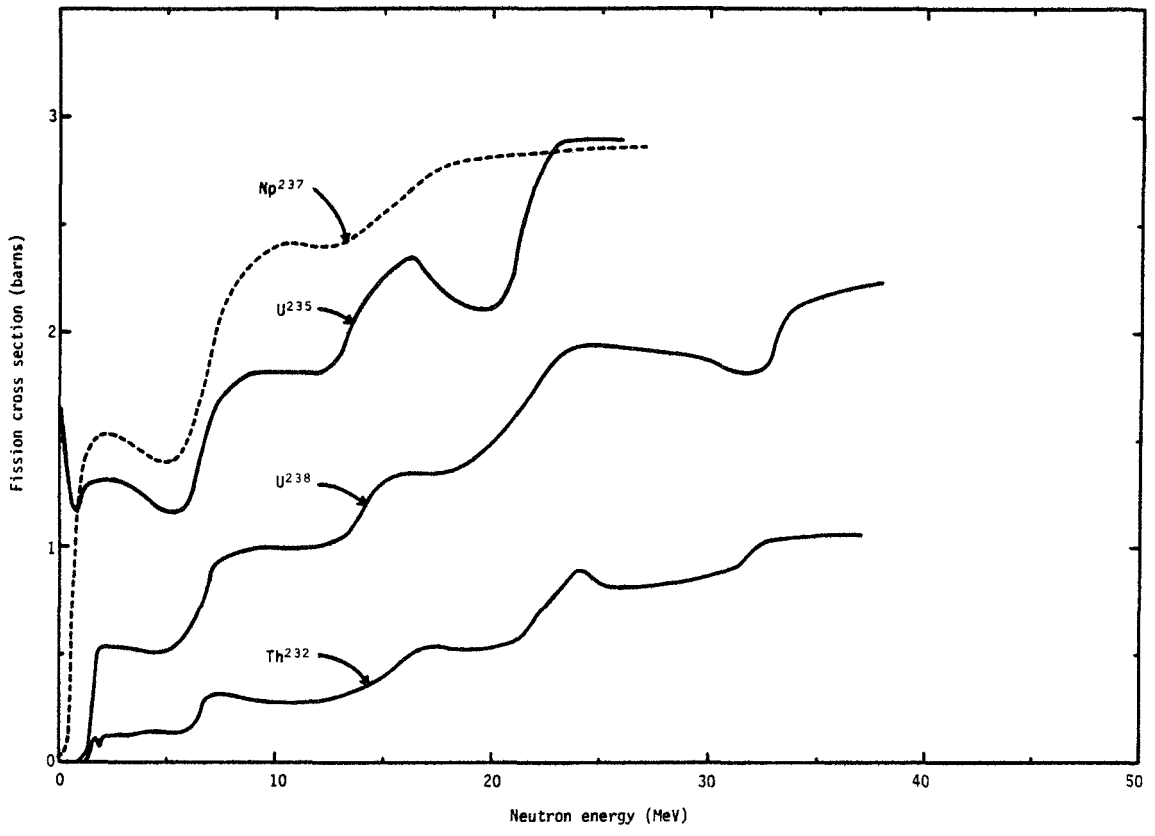

Figure 8

The (n, f) and (p, f) reaction cross sections of ^{232}Th and ^{238}U in the neutron energy region less than 40 MeV.

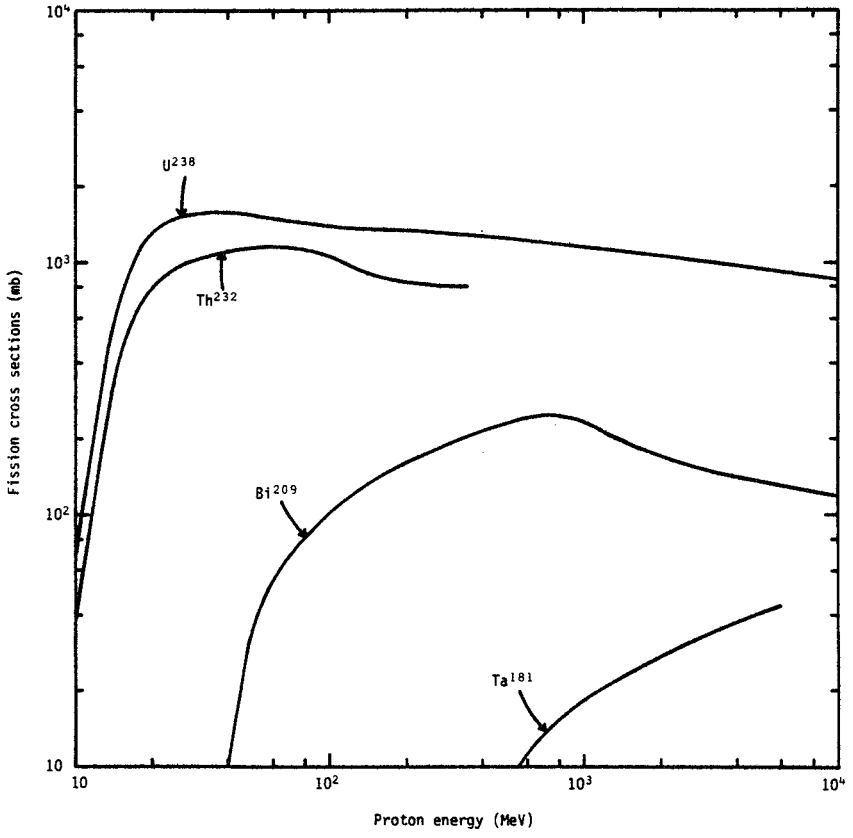

Figure 9

The (p,f) reaction cross sections of ^{181}Ta, ^{209}Bi, ^{232}Th, and ^{238}U in the energy region from 10 to 10^4 MeV.

trum which is given by

$$\sigma_e = \int_0^\infty \sigma(E)\, N(E)\, dE$$

where $\sigma(E)$ is the energy dependent cross section and $N(E)$ is the normalized nucleon spectrum. The exact shapes of the proton and neutron spectra on Cosmos 936 are not known. However, proton spectra have been measured on other Earth orbit missions by nuclear emulsions. A typical example are the Biosatellite III measurements which have been reported (8). For a representative neutron spectrum, a calculated differential spectrum of cosmic-ray-induced atmospheric neutrons has been used (13). The spectra for a series of air pressure altitudes was calculated from 0 to 700 g/cm^2. The 0 g/cm^2 case, which gives the hardest spectrum, was used. This calculation should yield the most reasonable approximation of the situation aboard a spacecraft. The production modes for neutrons are similar in the two cases. The relative proton and neutron spectra are plotted in Fig. 10.

Numerical integrations were made to determine the efficiencies of the ^{209}Bi, ^{232}Th, and ^{238}U detectors for the above neutron spectrum for energies above 1 MeV. This was not done for the ^{181}Ta detectors. The track densities on these detectors were at background levels, or about 0.5 tracks/cm^2. The ^{181}Ta fission cross section can be represented approximately as a constant 30 mb at energies above a nucleon activation threshold energy of 1000 MeV. The sensitivity of the detector is therefore 3.5×10^{-7} tracks/nucleon. The background level was equivalent to 1.5×10^6 nucleons/cm^2 above 1 GeV. The actual fluences in this energy region were much smaller on the Cosmos 936 flight.

Efficiency calculations were also performed for the three more sensitive detectors for the proton spectrum. An effective threshold was assumed at 17 MeV for the ^{232}Th and ^{238}U detectors and the proton spectrum was trun-

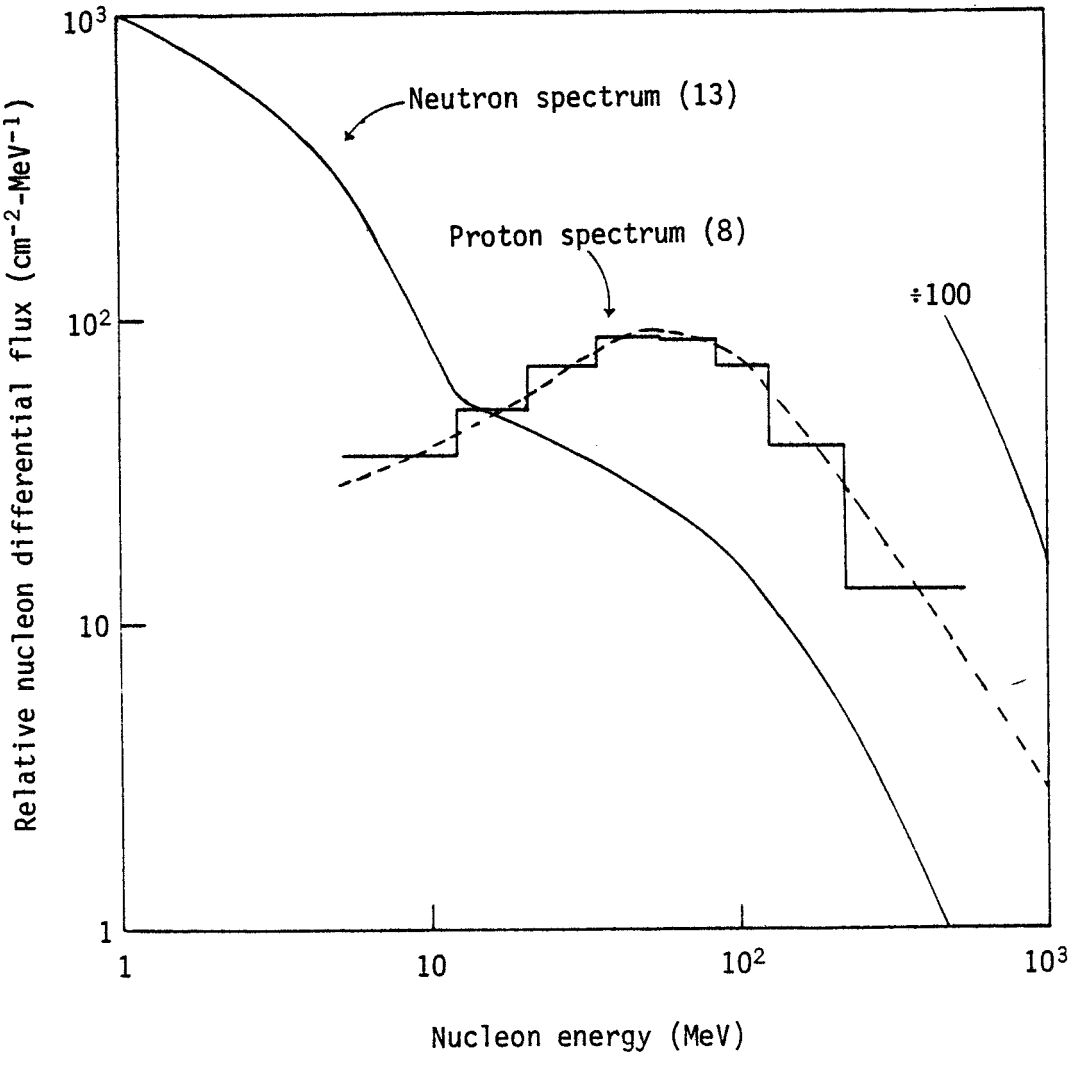

Figure 10

Representative relative neutron and proton spectra for satellites in earth orbit.

cated below this energy. The results of the calculations are given in Table 8. An attempt was made to determine the proton and neutron fluences by, first, calculating track densities expected with different percentages of the total due to neutrons, and then comparing the calculated values with the experimental track densities to get a "best" fit. The results are given in Table 9. The number of detectors was too small and the errors too large for this approach to be fruitful. The errors corresponding to the experimental values are only those due to counting statistics. There are also large errors due to the assumptions made in the efficiency calculations. The best fit occurred for the case of a nucleon fluence composition of 100% protons but this is not meaningful.

In order to make a reasonable calculation of neutron fluence, it was necessary to determine the relative abundances of protons and neutrons by other means. Some Skylab measurements of neutron and proton fluences have been reported (6). These were made simultaneously by activation foil methods on an orbital spaceflight where conditions should approximate those on Cosmos 936. Fluxes of 2.3 protons/cm^2-sec between 30 and 100 MeV and 0.96 neutrons/-cm^2-sec between 3 and 15 MeV were measured. For the spectral shapes of the nucleons assumed in this report, these values would convert into fluxes of 7.85 protons/cm^2-sec > 17 MeV and 3.94 neutrons/cm^2-sec > 1 MeV. Based on this ratio of nucleons, 24% of the weighted track densities were due to neutrons. This yields a value of 2.1×10^6 neutrons/cm^2 for the high energy fluence (>1 MeV) on Cosmos 936. The corresponding proton fluence is 4.2×10^6 protons/cm^2 (>17 MeV). The many assumptions made in the calculations allow much room for error. However, these errors are probably less than an order of magnitude.

TABLE 8. EFFICIENCY FACTORS FOR THE ^{209}Bi, ^{232}Th and ^{238}U FISSION FOIL DETECTORS FOR THE SELECTED NEUTRON (E_n > 1 MeV) AND PROTON (E_p > 17 MeV) SPECTRA-TRACKS/NUCLEON

Radiator foil	Neutron spectrum	Proton spectrum
^{209}Bi	6.95×10^{-7}	1.58×10^{-6}
^{232}Th	7.24×10^{-6}	1.04×10^{-5}
^{238}U	1.50×10^{-5}	1.57×10^{-5}

TABLE 9. CALCULATIONS OF FISSION FOIL DETECTOR TRACK DENSITIES FOR DIFFERENT PERCENTAGES OF NEUTRON-CAUSED TRACKS

Detector	0%	10%	20%	30%	40%	50%	100%	Experimental
^{209}Bi	8.8	8.5	8.3	8.0	7.7	7.5	6.2	8.9 ± 2.6
^{232}Th	57.9	58.6	59.3	59.9	60.5	61.2	64.5	64.4 ± 8.6
^{238}U	87.4	92.0	96.7	101.3	105.8	110.5	133.7	77 ± 24

Total absorbed dose. In addition to neutron measurements, the TLDs were employed to measure the total absorbed dose due to charged particles and gamma rays. The unshielded ^{7}LiF detectors allow this quantity to be measured with relatively small errors. Most of the dose is due to protons during Earth-orbit flights. The thermoluminescent response of protons in LiF, relative to ^{60}Co radiation, has been measured by Jähnert (9). His data are shown in Fig. 11. His measurements, which are given as a function of LET_{∞} of the protons, can be compared with a representative proton spectrum for an earth orbit flight to estimate the overall thermoluminescent efficiency. Flux and dose curves have been generated by Schaefer and Sullivan (18), displayed in Fig. 12, which can be used for this purpose. It can be seen that about 25% of the cumulative dose from this spectrum is due to protons with LET > 10 keV/μm, where the loss of sensitivity becomes appreciable. At the maximum LET for protons, 85 keV/μm, the sensitivity drops to about 0.5. The total dose would be underestimated by ∿7% for this proton spectrum. Assuming that 90% of the dose measured by the TLD-700 chips is due to protons, the correction would be 6%. The errors in the measurements of the absorbed doses are due to readout statistics--given in Table 5, the absolute calibration of the chips--about 5%, and errors due to estimating the efficiency of the unknown LET spectra of the particles measured--less than 3%. The equivalent exposure values were converted to tissue dose by multiplying by the factor, 0.957. In packet #2, the absorbed dose was 424 mrads ±9%. Although there were no ^{7}LiF TLDs in packet #1, a value can be found by scaling between the shielded ^{6}LiF detectors. The absorbed dose in packet #1 is then 523 mrads ± 11%. The 19% decrease in the absorbed dose between the two packets illustrates the shielding effectiveness of the USF dosimetry stack.

Discussion

Neutron fluences in the thermal energy region were found to be 3.64×10^{5} neutrons/cm^{2} (0.228 neutrons/cm^{2}-sec) over the 18.5 day Cosmos 936

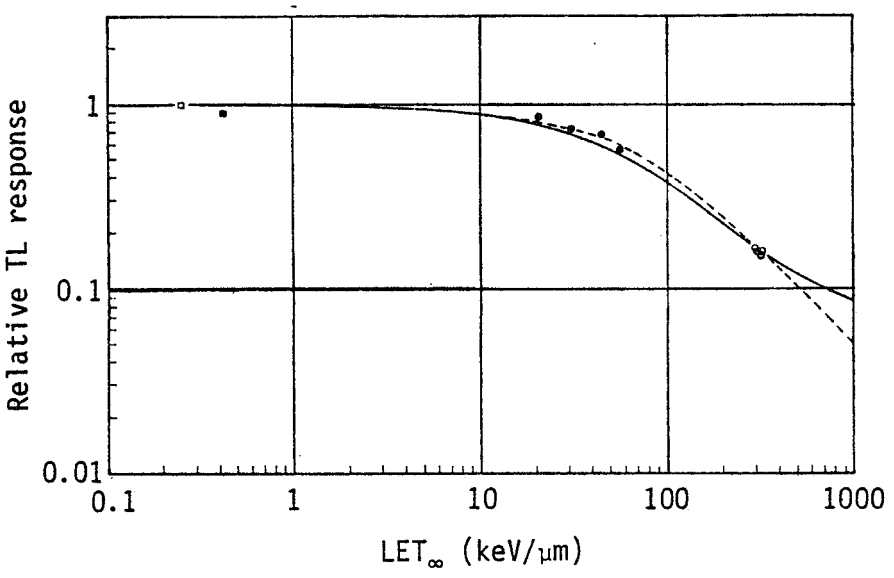

Figure 11

Thermoluminescent response as a function of the average stopping power (LET) for LiF. --- Theory with one type of trap, —— theory with two types of traps. O ^{210}Po-α-rays, ● protons, □ ^{20}Co- -rays, ■ electrons (9).

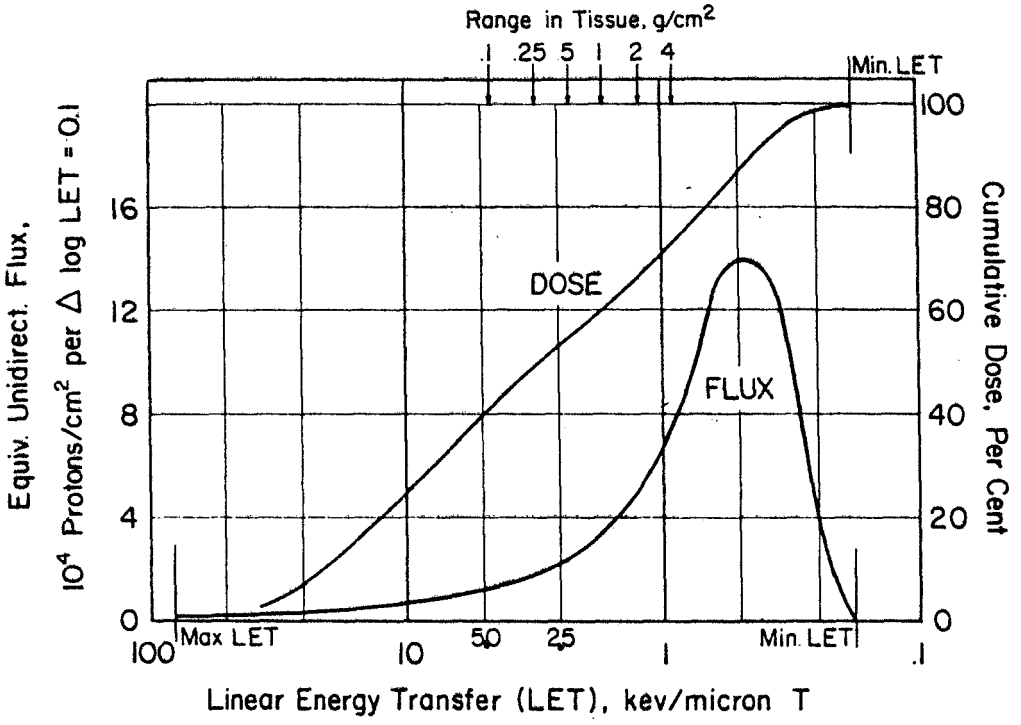

Figure 12

The proton flux and cumulative dose measured during the Gemini VII mission (18).

flight. The associated error is estimated to be ±20%. This corresponds to a dose of 0.37 mrem. Neutron fluences in the resonance region (0.3 eV to 1 MeV) have been found to be 9.5×10^5 neutrons/cm^2 (0.59 neutrons/cm^2-sec) with error limits of −30% to +50%. This fluence corresponds to about 5 mrem. In the high energy region (>1 MeV) the best estimate of the neutron fluence was found to be 2.1×10^6 neutrons/cm^2 (1.3 neutrons/cm^2-sec). The assumptions made in the associated calculations allow an error of an order of magnitude in this number but it compares reasonably well with other measurements made under similar conditions (15). The dose corresponding to this fluence is about 125 mrem. The total charged particle plus gamma-ray absorbed dose was also measured. It varied between 424 and 523 mrads for two positions with several grams/cm^2 difference in shielding between them. The errors associated with these numbers is about 10%.

NUCLEAR EMULSIONS

Monitoring of the proton exposure component of the radiation in Cosmos 936 was carried out by Ilford nuclear emulsions of the G.5 and K.2 types. The original intent was to monitor the LET spectrum from a proton energy range of zero to approximately 100 MeV. The technique used, as discussed by Schaefer and Sullivan (19), requires the use of emulsions of different sensitivities. To this end, the above mentioned emulsion types were arranged in packets (emulsion size 3.8 × 5.1 cm) and placed on all faces of the US-25% part and of the joint-50% part foam cube. The emulsions were deemed a necessary component of the passive monitoring package in that protons did not usually (i.e. under normal etching conditions) register in the then currently available plastic track detectors whereas nuclear emulsions afforded a well-established tool of high sensitivity for high-resolution work on singly charged particles.

Materials and Methods

25 μm and 50 μm G.5 emulsions and 100 μm K.2 emulsions were selected as the proton recording media, the G.5 emulsions being sensitive to all charged particles of any energy while the K.2 emulsions record protons to about 80 MeV. Each emulsion was mounted on a 178 μm Melinex substrate. As usual, the emulsions were kept refrigerated prior to assembly, at which time they were each marked as to emulsion type and thickness, and then one each of each emulsion type was inserted into a 0.006 in. thick black polyethylene bag which was then heat sealed to ensure a light-tight container. All this work was carried out under darkroom conditions. Each such emulsion packet was then inserted, along with several plastic layers, into another heat sealable black plastic bag--this unit forming a single "orthogonal" detector. Twelve US orthogonals and six USSR orthogonals were assembled and, as per the assembly plan, were attached (with Teflon tape) to the joint foam cube part and to the US-25% part.

Upon receipt of the exposed materials, the orthogonals were detached from the cube faces, checked for compliance with the assembly plan, and then the emulsion packets were removed and subsequently put into a refrigerator. Under darkroom conditions, the emulsions were removed from their packets, marked as to the orthogonal number (1F-US through 12F-US and 7F-S through 12F-S), a 3-4 mm diameter circle was scribed on each emulsion, and each emulsions' thickness was measured within the circle. Next, each emulsion was mounted separately on a 4.5 × 7.6 cm Lucite slide, with an Acrylic-1-2,dichloroethane adhesive (this being done for ease in handling the emulsions during processing). Along with the flight emulsions, two backup emulsion packets (1B-US and 2B-US) were also prepared, in the aforementioned manner, for processing.

All the emulsions of a specific thickness and type were developed together with the 25 μm and 50 μm G.5s processed in D-19 developer without a presoak

(they were put immediately into the hot stage), and the 100 μm K.2s developed in Amidol and using a presoak with the hot stage.

After processing, all the emulsions were carefully removed from the Lucite slides and the Melinex substrates were cleaned. Each emulsions' thickness was then measured. Two fiducial holes were drilled in each emulsion and they were all then packaged in light-tight boxes.

Scanning for proton enders was then initiated in the 7F-US and 11F-US K.2 samples. K.2 emulsions, being less sensitive than G.5 emulsions have a greatly reduced developed grain density (for the same exposure as a G.5) and therefore proton enders are easier to find. However, due to the long exposure time of 18.5 days, track crowding became a severe problem, so much so that 100X oil immersion objectives had to be used, along with 10X eyepieces, merely to scan for proton enders. The three selection criteria used for counting enders were the following: the track must intersect one of the emulsion surfaces (i.e. it must not be contained totally within the volume of the emulsion as could be the case with neutron-produced recoil protons); the track could not originate from a star (to avoid these two cases each ender was traced back to make sure it intersected the surface and was not star produced); and tracks of all dip angles should be included.

As stated previously, the extreme track crowding required scanning at high power and in addition only approximately 25% of the field of view could be scanned at once, so as not to miss proton enders. Needless to say, the more sensitive G.5 emulsions proved practically impossible to grain count tracks in, even at 1000X; this precluded evaluating the proton LET spectrum above a proton energy of approximately 10 MeV (10 MeV roughly corresponds to an LET value such that proton tracks cannot be grain counted in G.5 emulsion--i.e., the grain density is so high that the tracks appear to be continuous).

Results

The enders count was determined for the K.2 emulsions in the orthogonal packets 7F-US and 11F-US. The emulsion volume scanned was corrected for shrinkage and then scaled to an equivalent tissue volume by using an average stopping power ratio of 2 for each emulsion (in the interval from zero to 10 MeV, the stopping power ratio of emulsion to tissue for protons varies between 1.7 and 2.2). Using the known values of LET and QF (quality factor) as functions of proton energy in tissue, absorbed dose and dose equivalents were computed. Table 10 summarizes all the pertinent data.

Discussion

The intent of this part of the experiment was to evaluate the contribution of protons to the radiation in the Cosmos 936 flight. G.5 emulsions were to be used to evaluate the exposure in the proton energy region from approximately 10 MeV to approximately 100 MeV by use of the grain count versus LET method. This function can be produced from the calibration curve of grain count versus residual range for a long ender in the particular emulsion being scanned and the known tabulations of LET versus residual range for protons in G.5 emulsions (10). In the region from zero to about 10 MeV, proton tracks in G.5 emulsion are very hard, if not impossible, to grain count. As K.2 emulsions easily record proton enders and, due to their decreased sensitivity as compared to G.5 emulsions, have much fewer developed grains for the same exposure, the distinguishing and counting of proton enders is greatly facilitated. The K.2 component (0-10 MeV) and the G.5 component (10-100 MeV) when put together yield the complete proton spectrum from zero to 100 MeV.

It was known prior to the flight that, for G.5 emulsions, minimum grain density tracks ($g_0 \simeq 19$ grains/100 μm emulsion) and most probably $2g_0$ and $3g_0$ tracks could not be distinguished due to the high track crowding expected in

TABLE 10

Orthogonal	Total enders counted	Volume density $\left(\frac{\text{number}}{\text{cm}^3 \text{ tissue}}\right)$	Dose (millirads)	Dose equivalent (millirem)
7F-US	93 ± 9.6	$(2.56 \pm 0.27) \times 10^5$	44.2 ± 0.5	130.2 ± 13.7
11F-US	39 ± 6.2	$(2.87 \pm 0.46) \times 10^5$	49.6 ± 0.8	145.9 ± 23.4

this long a flight ($3g_0$ corresponds to approximately 100 MeV protons). However, the exposure was such that it was practically impossible to grain count the G.5 emulsions of either 25 μm or 50 μm thickness, and it was very difficult and time consuming to count the enders in the K.2 emulsions. This being the case, the results show only the effects of the zero to 10 MeV protons.

SUPPLEMENTAL REPORTS

Supplemental reports for experiment K-206 will be issued at a later date. These reports will be based on analyses in progress at the present time. The following describes some of the areas presently under investigation.

The results of gamma scan of the Cosmos 936 Vostok satellite, which will yield the distribution of spacecraft shielding with respect to the K-206 experiment container, are required for analysis of the effect of shielding on HZE particle fluence. The results of the gamma scan have not been received.

Comparison of US and Soviet results, a major item in the K-206 experiment, will occur at a future date after exchange of papers.

Studies are being carried out on the efficiency, sensitivity, and response of plastic detectors using accelerator ions of known energy and charge obtained at the Berkeley-Bevalac machine. Results of these studies will be used to improve present calibration relationships for plastic detectors and interpretation of results obtained in the K-206 experiments.

To greatly improve the accuracy of the Z determination and extend the coverage of the Z spectrum through Z = 26, the Lexan portion of the stack will soon be measured. The results from the Lexan layers will then be combined with the results from the CN layers.

Another improvement in the Z spectrum intended in the future is a higher

magnification measurement of the etched-through particle tracks. The present stack was measured with a resolution of approximately 7 μm. A fivefold increase in the resolution is quite possible without a corresponding increase in the measuring time. This will be accomplished by scanning for the tracks at low magnification and measuring at high magnification.

The analysis of the neutron measurement data is still in progress. Thermal neutron calibrations are being performed which will allow a direct calibration of the detectors flown on Cosmos 936 rather than a reliance on published sources which may be less accurate. The self-shielding factors will also be measured. Studies are also being made to determine whether or not approximations made in calculating the high-energy neutron fluence can be improved upon.

ACKNOWLEDGMENTS

Work was partially supported by NASA contract NAS2-9504. We express our thanks to D. Hoffman, J. Wimberley, M. Tran, C. Johnson, P. Farrell, and E. King of the University of San Francisco, and to K. Souza and R. Farrell of NASA for their assistance during the course of this investigation. The authors would also like to thank Dr. E.E. Kovalev and the staff of the Institute of Biomedical Problems for their help in various phases of this work.

REFERENCES

1. Benton, E.V., and M.M. Collver. Registration of heavy ions during the flight of Gemini VI. *Hlth. Phys.* 13: 495-500, 1967.
2. Benton, E.V., and W.D. Nix. The restricted energy loss criteria for registration of charged particles in plastics. *Nucl. Instrum. Meth.* 67: 343-347, 1969.
3. Benton, E.V., R.P. Henke, and D.D. Peterson. Plastic nuclear track detector measurement of high-LET particle radiation on Apollo, Skylab, and ASTP space missions. *Nucl. Track Detection* 1: 27-32, 1977.
4. Benton, E.V., D.D. Peterson, J.V. Bailey, and T. Parnell. High-LET particle exposure of Skylab astronauts. *Hlth. Phys.* 32: 15-19, 1977.
5. Benton, E.V., D.D. Peterson, A.M. Marenny, and V.I. Popov. HZE particle radiation studies aboard Kosmos 782. (To be published in *Hlth. Phys.*)
6. Fishman, G.J. Neutron and proton activation measurements from Skylab. *AIAA Paper No. 74-1227, AIAA/AGU Conference on Scientific Experiments of Skylab*, Huntsville, Alabama, 1974.
7. Fleischer, R.L., P.B. Price, and R.L. Walker. *Nuclear Tracks in Solids*. Berkeley, University of California Press, 1975.
8. Hewitt, J.E., H.J. Schaefer, and J.J. Sullivan. Radiation exposure during the Biosatellite III primate flight. *Hlth. Phys.* 23: 461-468, 1972.
9. Jähnert B. The response of TLD-700 thermoluminescent dosimeters to protons and alpha-particles. *Hlth, Phys.* 23: 112-114, 1972.
10. Janni, J.F. Calculation of energy loss, range, path length, straggling, multiple scattering, and the probability of inelastic nuclear collisions for 0.1- to 1000-MeV protons. *AFWL-TR-65-150*, 1966.

11. Khodai-Joopari, A. Fission properties of some elements below radium. *UCRL-16489*.

12. McCormick, G.H., and B.L. Cohen. Fission and total reaction cross sections for 22-MeV protons on ^{232}Th, ^{235}U, and ^{238}U. *Phys. Rev.* 96: 722-724, 1954.

13. Merker, M. The contribution of galactic cosmic rays to the atmospheric neutron maximum dose equivalent as a function of neutron energy and altitude. *Hlth. Phys.* 25: 524-527, 1973

14. Pretre, S., E. Tochilin, and N. Goldstein. A standardized method for making neutron fluence measurements by fission tracks in plastics. *USNRDL-TR-1089*.

15. Quist, T.C., M. Furst, D.S. Burnett, J.H. Baum, and C.L. Peacock, Jr. Spacecraft-produced neutron fluxes on Skylab--preliminary report. Division of Geological and Planetary Science, California Institute of Technology, Pasadena, California 91125.

16. Roberts, J.H., R.A. Parker, F.J. Congel, J. Kastner, and B.G. Oltman. Environmental neutron measurements with solid state track recorders. *Rad. Effects* 3: 283-285, 1970.

17. Rogers, D.W.O, M.L. Walsh, B.H. Orr, and N. Teekman. Albedo-dosimeter response to monoenergetic neutrons. *Hlth. Phys.* 33: 251-254, 1977.

18. Schaefer, H.J., and J.J. Sullivan. Radiation monitoring with nuclear emulsions on project Gemini. II. Results on the 14-day mission Gemini VII. *NAMI-990*, January, 1967.

19. Schaefer, J.J., and J.J. Sullivan. Nuclear emulsion measurements of the astronauts' radiation exposure on the Apollo Soyuz mission. *NAMRL-1228*, 1976.

20. Stehn, J.R., M.D. Goldberg, B.A. Magurno, and R. Wiener-Chasman. Neutron cross sections, Vol. III. *BNL 325*, 1965.

21. Steiner, R.M., and J.A. Jungerman. Proton induced fission cross sections for ^{235}U, ^{238}U, ^{232}Th, ^{209}Bi, and ^{197}Au at 100 to 340 MeV. *Phys. Rev.* 101: 807-813, 1955.

22. Wollenberg, H.A., and A.R. Smith. Energy and flux determinations of high-energy nucleons. *UCRL-19364*. 1969.

78

N79-11678

COSMIC RAY EFFECTS ON THE EYES OF STATIONARY AND CENTRIFUGED RATS FLOWN ON COSMOS NO 936, EXPERIMENT K-207

PRINCIPAL INVESTIGATOR:

Delbert E. Philpott, Ph.D.
Ultrastructure Research Laboratory
Biomedical Research Division
National Aeronautics and Space Administration
Ames Research Center
Moffett Field, California 94035, U.S.A.

CO-INVESTIGATORS:

Robert Corbett, Charles Turnbill, Sam Black,
Deborah Dayhoff, Jackie McGourty, Robert Lee,
and Gladys Harrison.
Biomedical Research Division
National Aeronautics and Space Administration
Ames Research Center
Moffett Field, California 94035, U.S.A.

This work was done in collaboration with Loya Savick, Ph.D.,
of the Institute for Biomedical Problems, Moscow, U.S.S.R.

ABSTRACT

10 rats 5 centrifuged during flight to simulate gravity and 5 in flight stationary experiencing hypogravity, orbited the earth in a 62.8° orbit for 18.5 days in the Russian satellite Cosmos 936. The animals were sacrificed 25 days post-recovery and the eyes were enucleated and fixed immediately. The tissues were then returned by courier to Ames Research Center. No differences were noted comparing flight stationary to flight centrifuged. While most of the eye tissue appeared normal, the morphological alterations observed in experiment K-007 flown on Cosmos #782 and the response of retinal cells exposed to high energy particles (HZE) of Ne, Ar, and Fe are comparable. Affected cells in the outer nuclear layer, where synthesis of the outer segment takes place, showed swelling, clearing of cytoplasm and disruption of the membranes. Channels were again found similar to those seen in K-007. Preliminary results using the digitizer to quantitate the tissue response indicated an increase in cell size after radiation and decrease in the number of cells in the outer nuclear layer.

INTRODUCTION

In the last experiment, on Cosmos 782, it was reported that ultrastructural changes in the retinas of the flight rats had occurred (20). These changes are thought to be the result of high energy (HZE) particle radiation incurred during spaceflight. This type of radiation has been thought to have caused the light flashes seen by the astronauts on the Apollo 11 mission and subsequent flights (21), confirming a theory voiced by Tobias in 1952 (24). He thought that cosmic rays (nuclei of various atoms stripped of their electrons) present at high altitudes and in space, would pass through the eye and activate the photoreceptors in the retina resulting in a perceived flash of light. The results of the Apollo experiment aroused interest in the biological effect of cosmic ray radiation. In experiments using cyclotron beams, the subjects, whose retinas were exposed, reported seeing light flashes (2, 3, 7, 15, 26). However, when the optic nerve and brain were irradiated, no flashes were seen (3, 25). The flashes were considered to be caused by direct ionization in the retina (25). Cerenkov radiation has also been proposed as a cause, the flashes being perceived as the HZE particles traverse the vitreous humor (8, 11, 12).

The production of HZE particles at the Lawrence Berkeley Laboratory, and the experiments on Apollo 17 (19) provided a chance to study the effects of this radiation on the eye (1, 13, 14, 17, 18, 27). Evidence of photoreceptor activation by HZE particles was obtained with the first electroretinogram (ERG) using rabbit retina and nitrogen nuclei (17, 18). Ultrastructural alterations were also observed in the rods and in the pigment epithelium of irradiated pocket mouse retina (18). Recent neon and argon exposures have also revealed alterations in the outer nuclear layer, rods pigment epithelium and blood vessels (10). The site of sharpest vision is

in the rod-free area of the fovea, the tiny central area of the macula. Cellular damage in this area of best vision, about 26 μm in diameter in humans, could become a severe problem by limiting vision in space travelers. We know that a short term flight causes changes in the retinas of mice and rats (19, 20). In longer spaceflights, long term, low dosage radiation could cause lens changes, leading to cataracts. Although data are lacking in this area of long-term, low-dose response, the possibility of extended flights makes such information vital.

MATERIALS AND METHODS

The Russian Satellite Cosmos 936 was launched August 3, 1977. It circled the earth in a 62.8° orbit and returned to earth on the morning of August 22, 1977, a total of 18.5 days in flight. Included on board the spacecraft for this experiment were 10 white rats, Wistar strain. Five rats were centrifuged to simulate (1.05 G) gravity during the flight and five rats were kept stationary and experienced the effects of hypogravity.

Radiation dosimeters were placed in the Satellite to obtain an average flux and atomic number of the cosmic ray particles (16). Ten rats were kept in Moscow as controls. Five rats in a biosatellite mock-up were subjected to spacecraft temperature and atmosphere conditions 4 days after the information was transmitted from the satellite. These synchronous controls also experienced simulated blast-off and recovery G-forces, noise, and vibration. Five unstressed controls were kept under normal laboratory conditions and fed the same diet. The flight rats were transported to the Institute of Biomedical Problems in Moscow where they

were maintained with the controls. Twenty-five days after recovery of the spacecraft, the flight stationary, flight centrifuge and vivarium control rats were sacrificed. The synchronous control rats were sacrificed 4 days later, 25 days after the simulated landing.

Each rat eye was enucleated immediately after decapitation and placed lens down in a dish of cold "triple-fix" (6). A cup-shaped depression formed in silastic provided support while the back of the eye near the optic nerve was opened with a sharp razor blade. The "triple-fix" immediately entered the eye and the slit was further widened with fine eye scissors. A flow of fresh fixative to the inner eye was accomplished by inserting a pipette into the slit and gently introducing more fixative, carefully directing the flow against the lens to further reduce the velocity. The entire procedure took less than 2 minutes. Each eye was placed into a small specimen bottle; 30 minutes later the bottles were gently agitated to ensure that fresh fixative again reached the retina. The eyes were stored at 4°C and remained at this temperature during the flight from Moscow to Ames Research Center. At Ames the slit in each eye was then enlarged to completely separate the eye into halves. The eyes were post-fixed in 1% osmium tetroxide, then were slowly dehydrated in a graded (25%-100%) series of acetone and each half was then embedded in epoxy plastic. 2 μm serial sections were cut from each hemisphere and observed, unstained, under phase light microscopy. Occasionally, .5 μ m - 1μ m sections were cut and stained with silver stain (4, 5) or AzureII-Methylene Blue (23) to observe greater detail. Sections were cut for electron microscopy and stained with lead citrate and uranylacetate and mounted on 75 x 300 mesh grids. Photomontages were

constructed and large retinal areas from flight and control eyes were compared to each other and to results from previous experiments (20). Some micrographs of the outer nuclear layer of the retina (ONL) from an eye in each group were put on a Ladd digitizer and the cells were counted and measured. Averages for population density, width of the ONL, and nuclear volume were computed for flight stationary, flight centrifuge and vivarium control.

RESULTS

Rapid fixation was provided by slitting the back of the eye with the razor blade, near the optic nerve. However, this can jeopardize the attachment of the soft retinal tissue beneath the sclera. To avoid as much detachment as possible the slit was made with very little pressure on the eye and was further opened with fine eye scissors. By using a pipette to gently bathe the inner eye with "triple-fix" and then slowly dehydrating the tissue, detachment was kept to a minimum. The eyes were transported in the same size bottles and same holders that were successfully used on Cosmos #782. Leaving the lens in place helped to provide support to the inner structures. Movement of the eye within the small bottle and the eye structures themselves were kept to a minimum with this method. No ultrastructural changes were believed to have occurred in the tissue as a result of the jet flight from Moscow to Ames Research Center.

The flux of HZE particles indicated an average of 35 particles/cm^2 for the 18.5-day flight in the area where the dosimeters were placed.

The retinas of pocket mice and C-57 black mice exposed to a Neon beam in the Bevalac at Lawrence Berkeley Laboratories showed definite

ultrastructural changes (Figure 1) and provided a comparison of known radiation-caused changes to the alterations in retinas of Cosmos mice. Both Cosmos and Berkeley exposures produced swollen outer nuclear layer cells. Rod inner segments of these cells also became disrupted and swollen. The cells that appeared damaged or dying were, as in the previous flight, widely scattered throughout the retina. Most of the necrotic cells, characterized by swollen cytoplasm and dense nuclei (Figure 2) seemed to appear in the outer nuclear layer (ONL). A few cells, each surrounded by swollen cytoplasm, were also found in the inner nuclear layer (INL). These cells were visible at the light microscopy level (Figure 3) as well as in the electron microscope (Figure 4). As in the previous flight clear channels in the rod inner and outer areas were found. These were followed for 5-15 μm in the 2 μm serial sections prepared for light microscopy (Figures 5 and 6). The channels appeared to be straight. In the electron microscope these channels were often the diameter of a cell and usually clear but some contained membrane-like debris (Figure 7, 8, 9). Myelin figures and swollen or necrotic mitochondria were also present (Figures 10, 11). The dead or dying cells were surrounded by well-fixed material eliminating the possibility they were fixation artifacts. At the junction between the pigment epithelium and the rods, phagocytotic activity of outer segments appeared to be greater than in control tissue (Figure 12). One cell in the ONL contained outer rod membrane material (Figure 13).

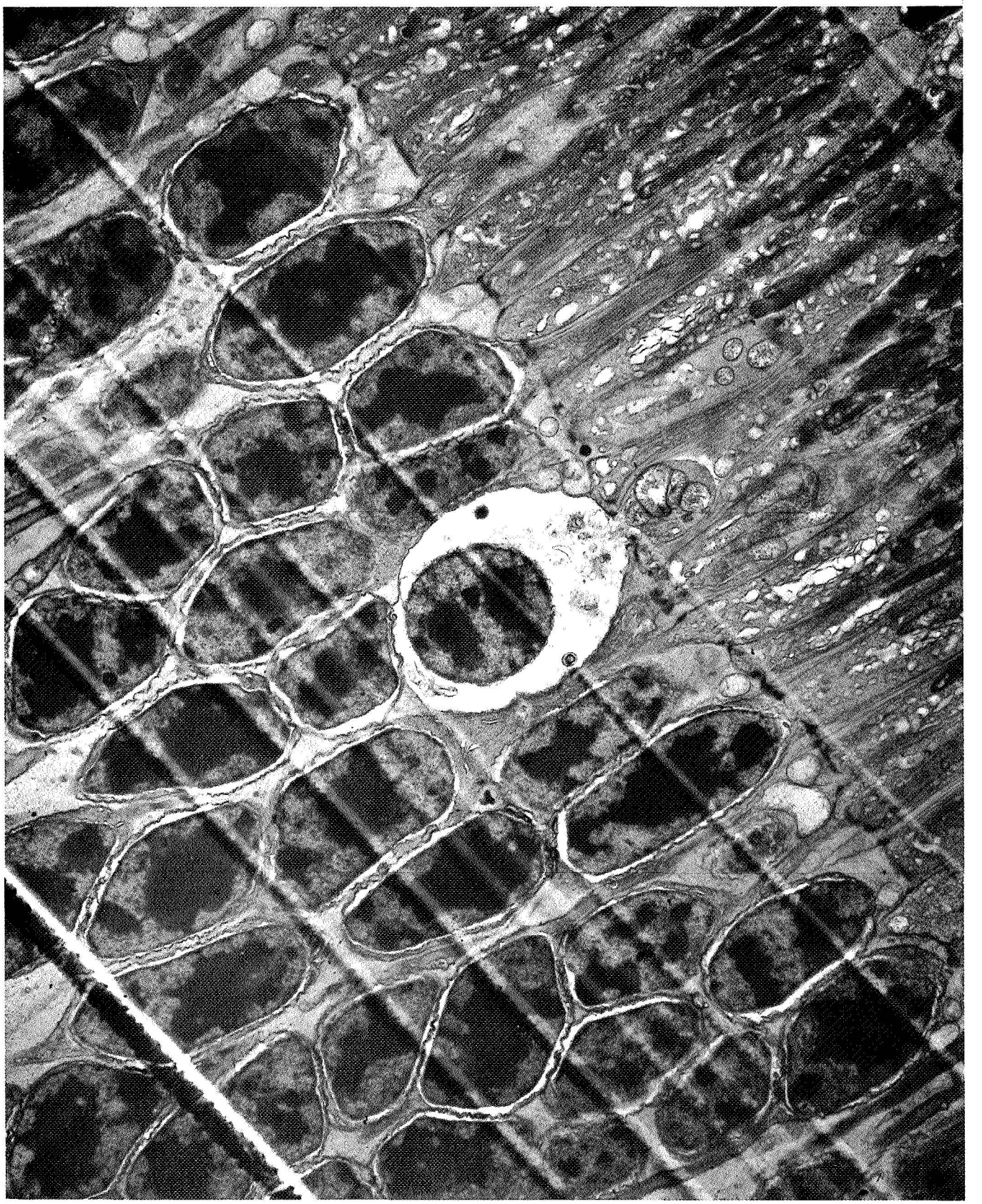

Figure 1 Mouse retina 27 days after exposure to 1000 rad Neon particle beam at Berkeley. Swelling around nucleus and in adjacent inner segment. Note blebbing of membrane surrounding nucleus. 3,400x

Figure 2 Flight stationary. Necrotic cell in ONL. Swelling of cytoplasm and dense nucleus. 17,800x

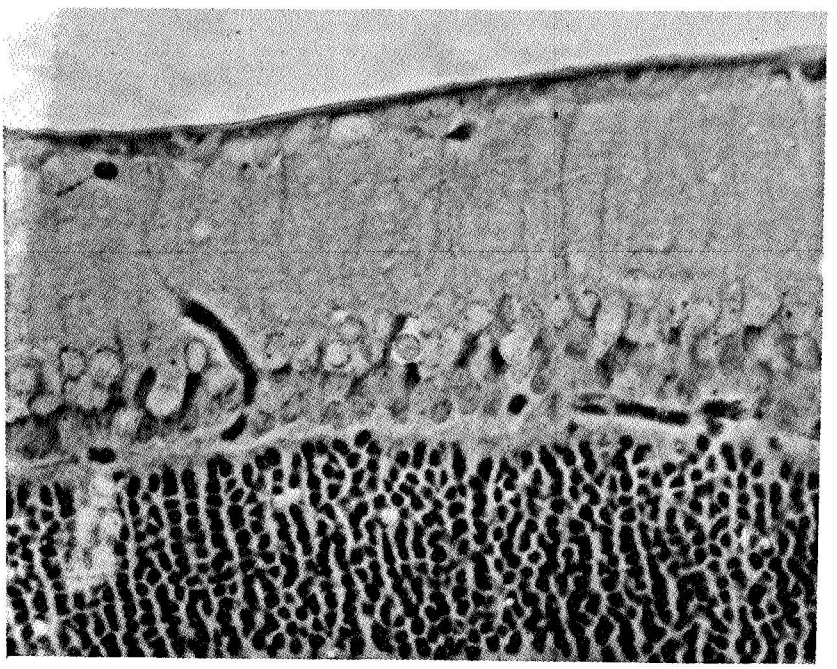

Figure 3 Flight centrifuge. Note swelling and clear area around nucleus in INL. 400x

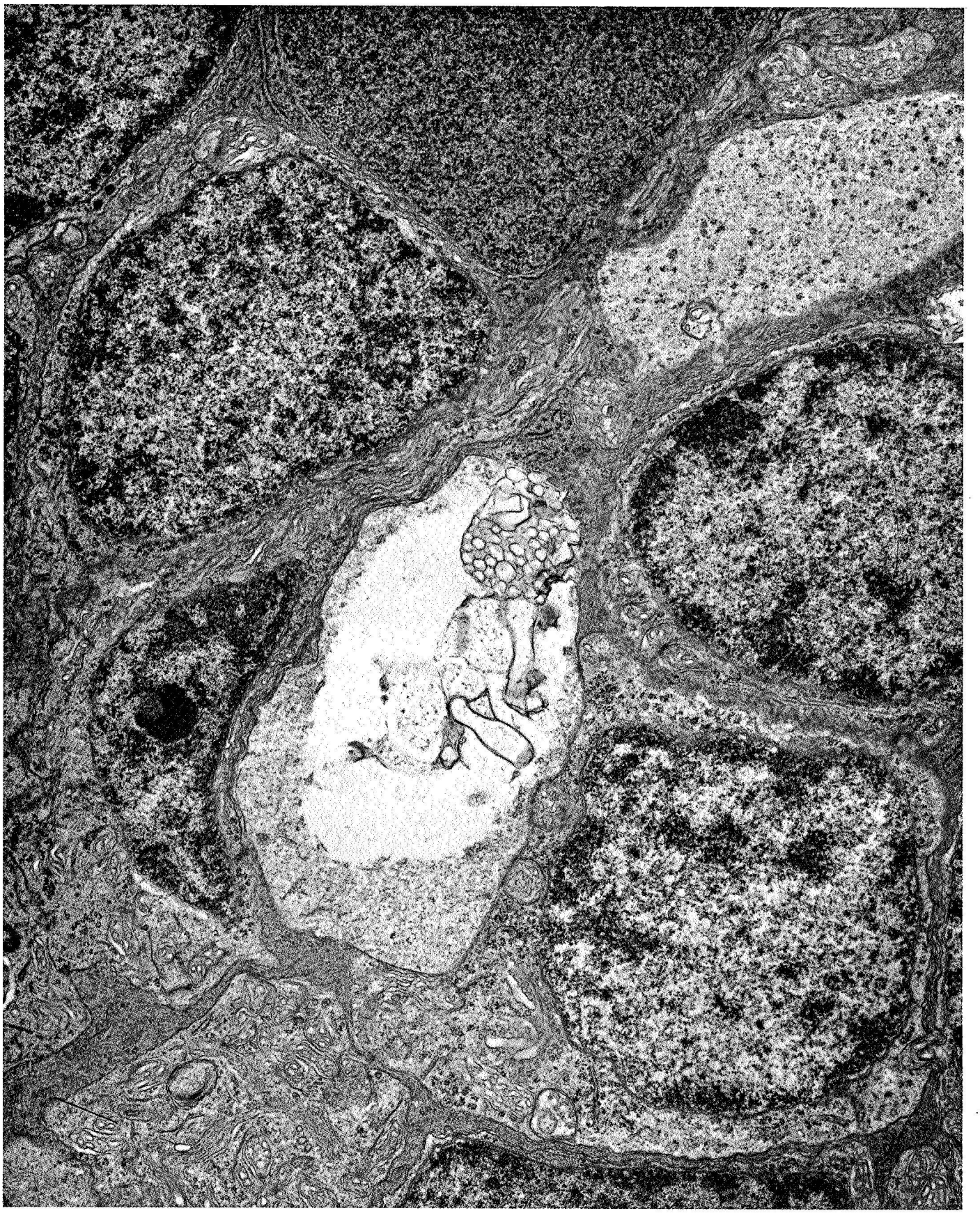

Figure 4 Flight stationary. Swollen cytoplasm surrounding nucleus in INL. 16,400x

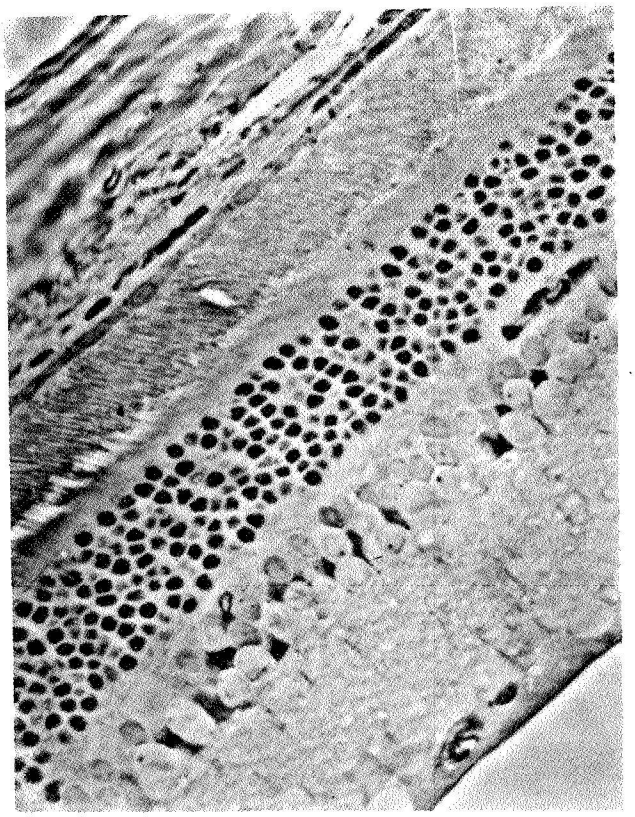

Figure 5 Flight stationary. Channel in outer segments. 400x

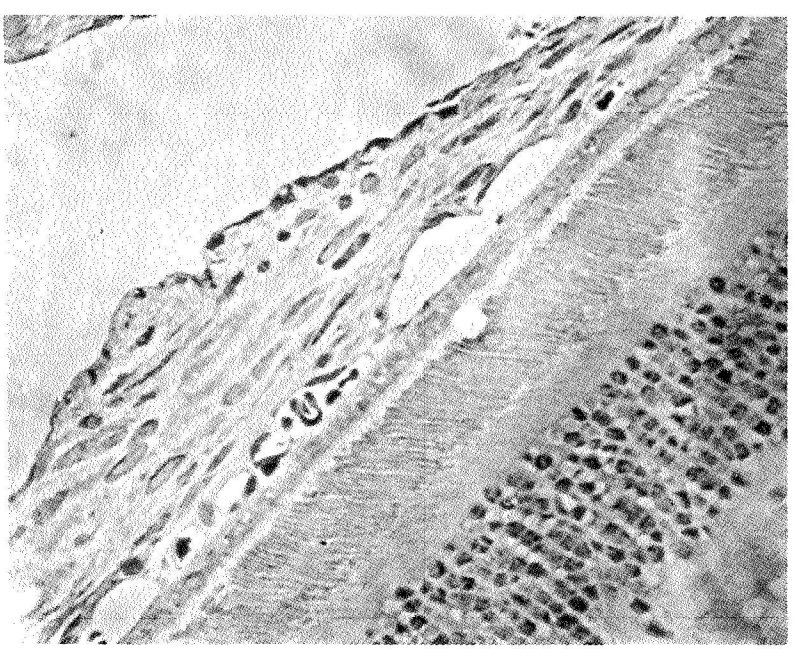

Figure 6 Flight centrifuge. Note clear channel located between pigment epithelium and tips of outer segments. 400x

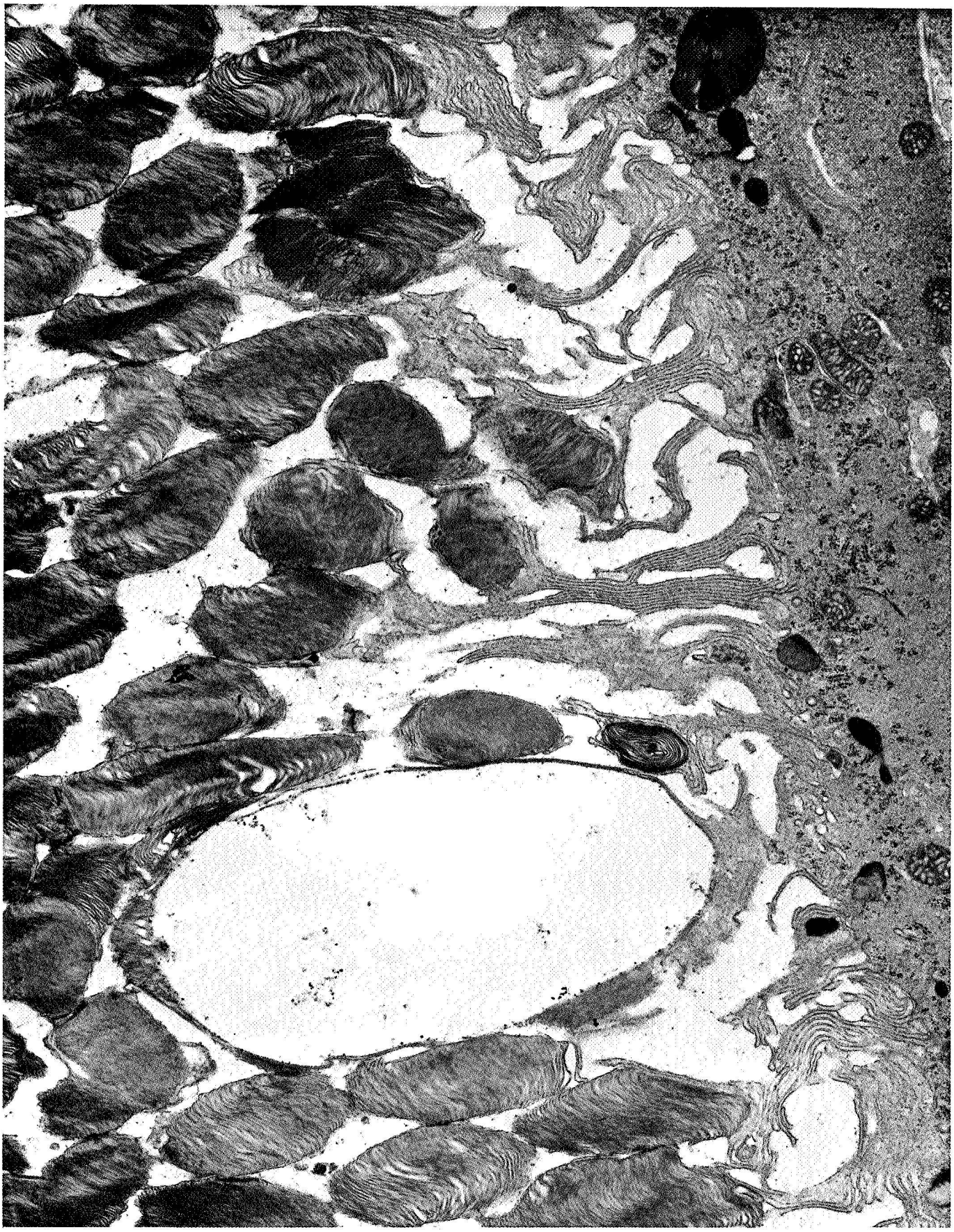

Figure 7 Flight stationary. Electron micrograph showing clear channel between rod tips and pigment epithelium. 16,400x

Figure 8 Flight centrifuge. Note similar clear area between pigment epithelium and outer segments as seen in figure 7. 11,800x

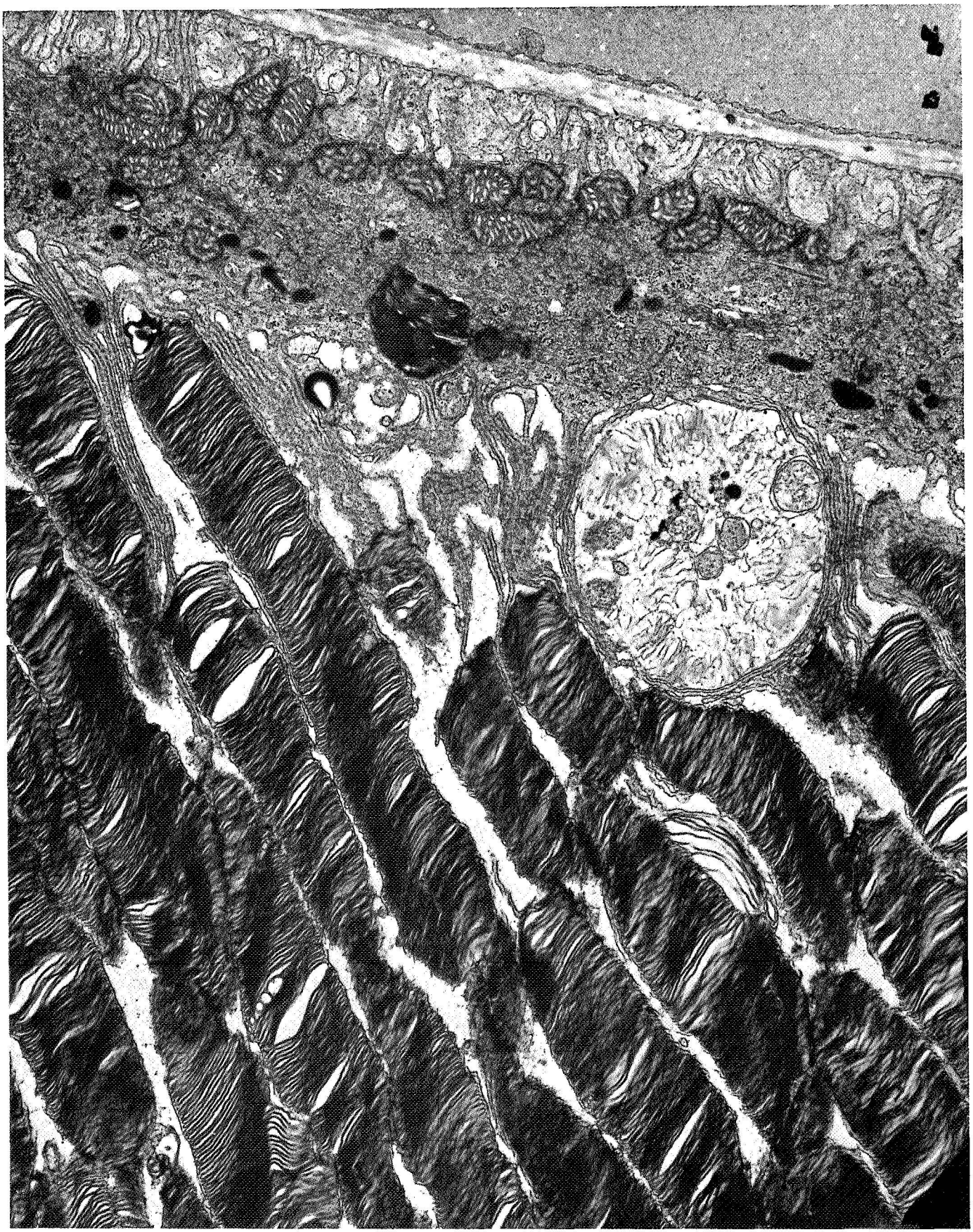

Figure 9 Flight centrifuge. Large debris-filled channel/vesicle at the junction of rods and pigment epithelium. 16,400x

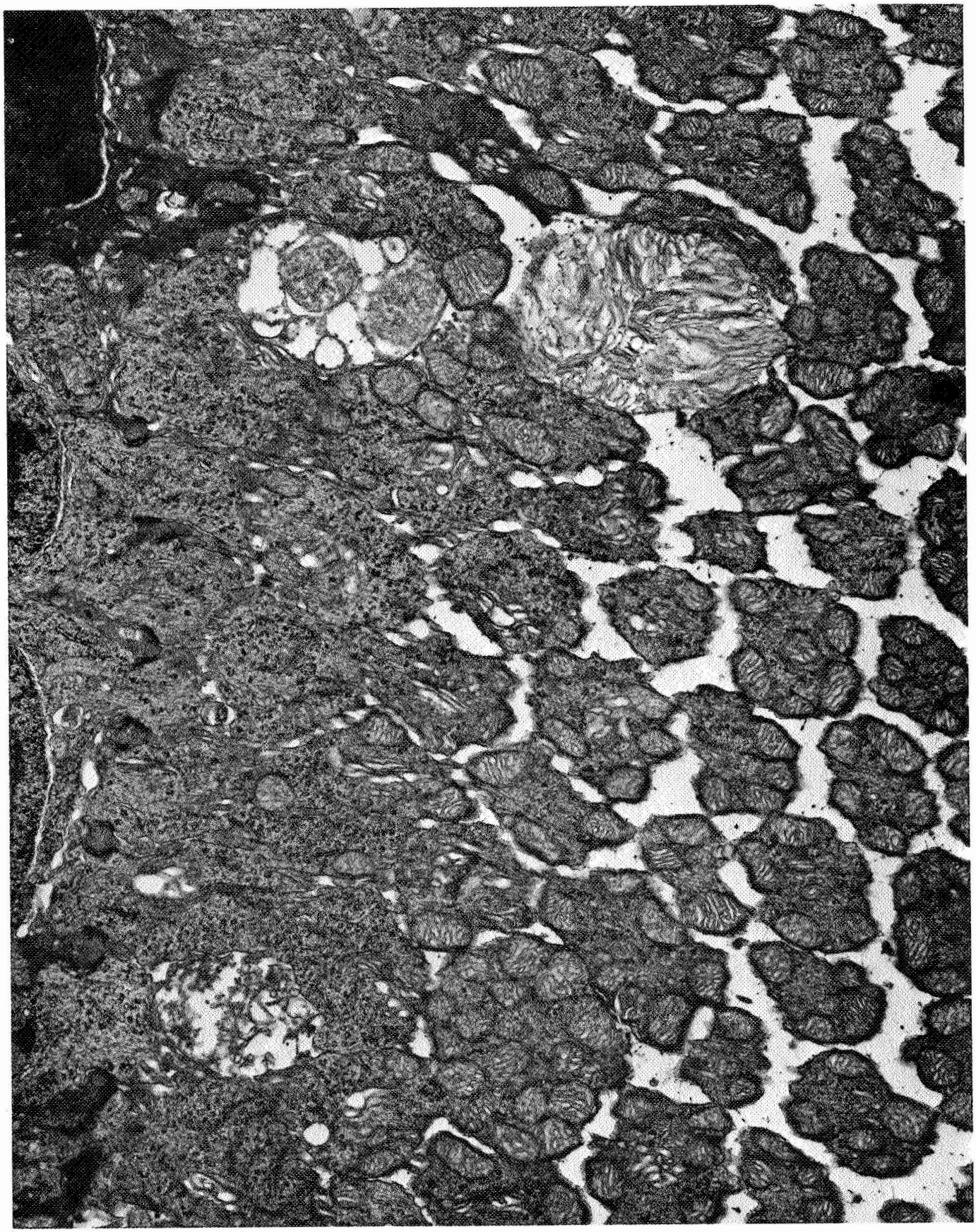

Figure 10 Flight centrifuge. Swollen mitochondria located in inner segment area. Note also the adjacent membrane filled vesicle. 16,400x

Figure 11 Swollen semi-clear mitochondria located in cytoplasm of ONL cell. Note excellent fixation in all adjacent areas. 30,000x

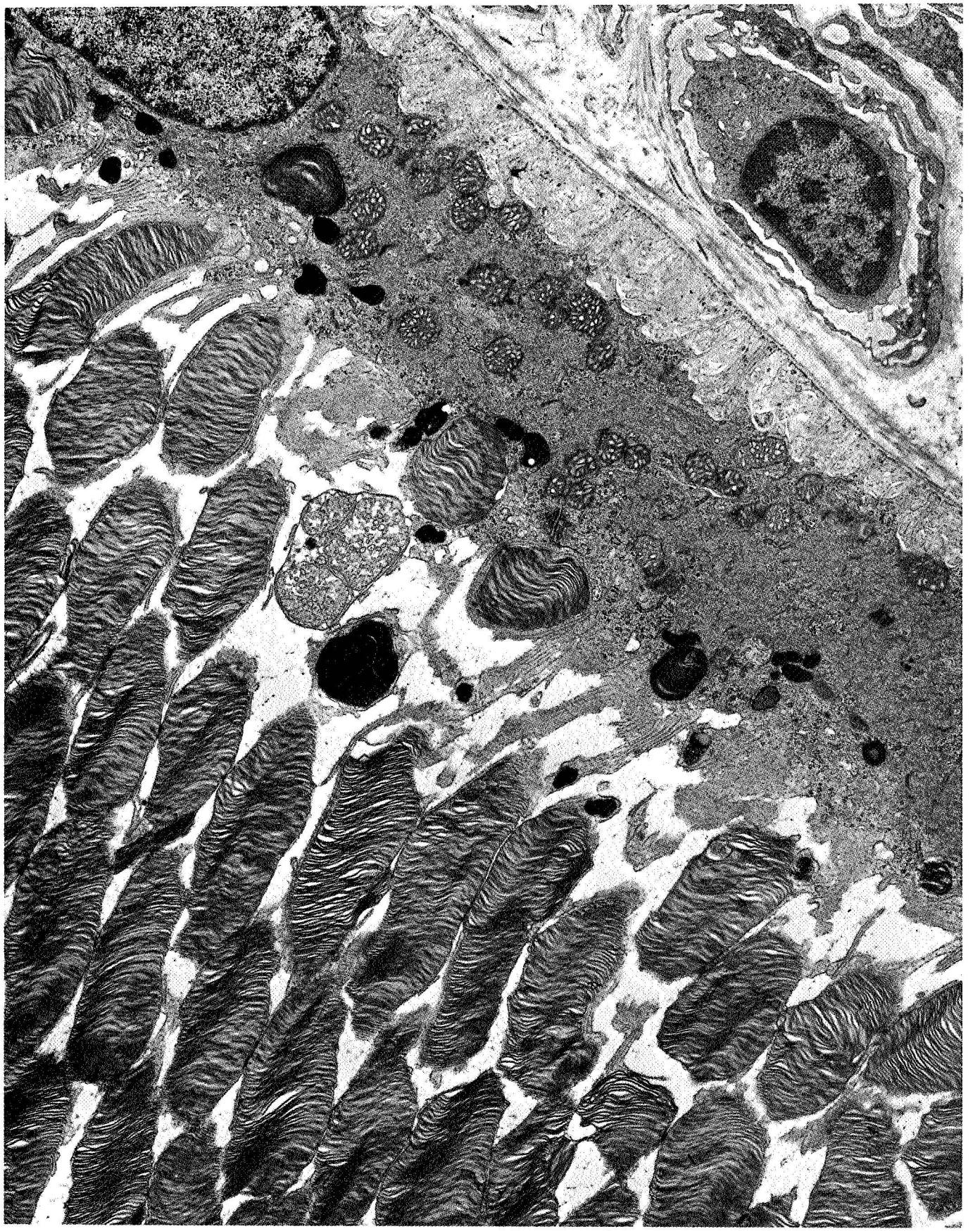

Figure 12 Flight stationary. Increased phagocytotic activity by the pigment epithelium. Note abundance of material being injested and digested. 13,000x

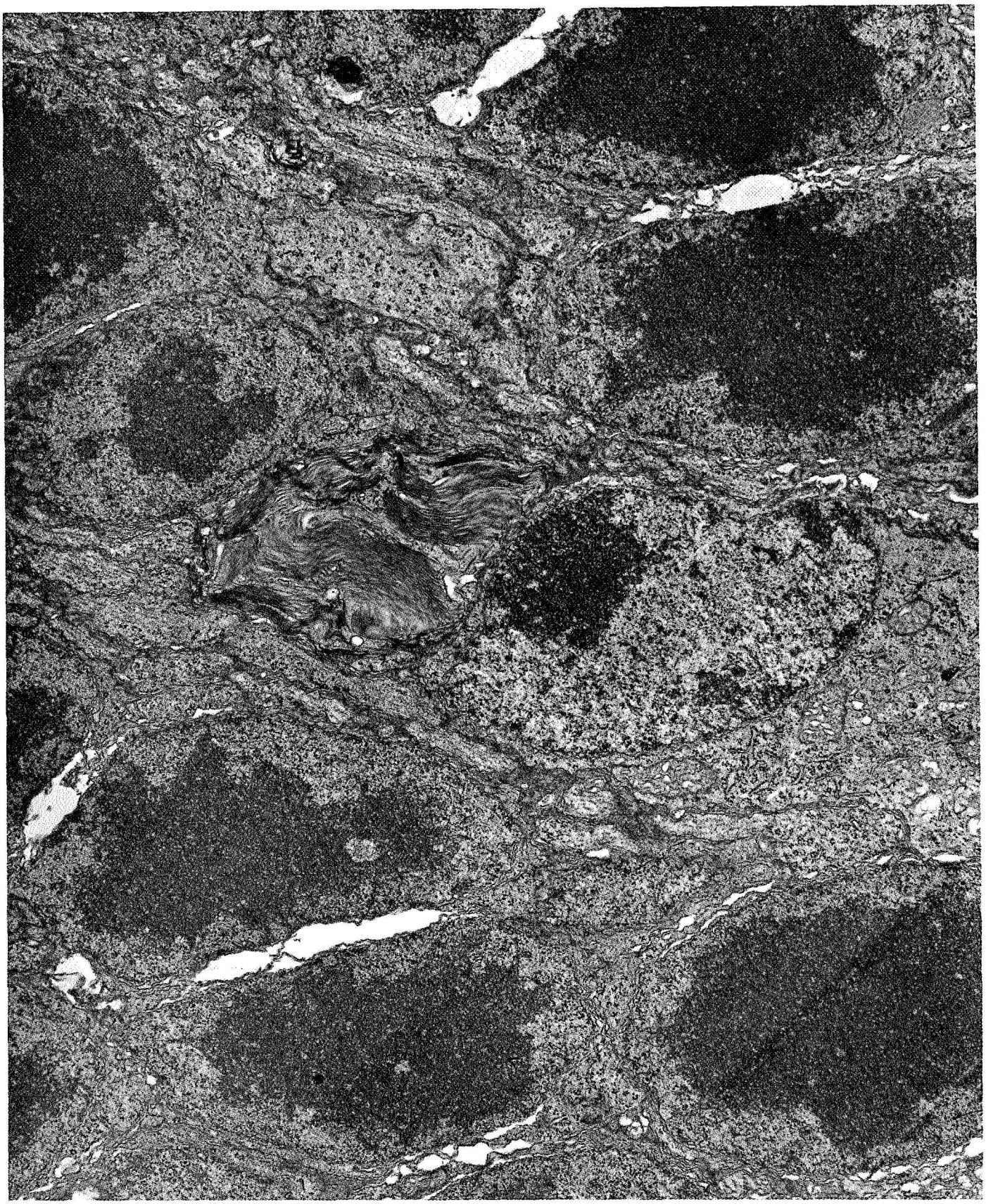

Figure 13 Flight centrifuge. Presence of rod-like membrane material in ONL. This abnormal finding has only been found in retinas exposed to iron particle radiation in the Bevatron at Berkeley. 16,4000x

The control eyes contained some rod disruption between the rod and the pigment epithelium near the area of incision. No macrophages were found and only a few altered mitochondria were seen.

One flight eye showed a filamentous, clustered tubular arrangement not seen in any other eyes examined. This same structure was seen in one cell after argon exposures at Berkeley (Figures 14 and 15).

Preliminary results from digitizing cells indicated a difference in the three groups. The greatest density of cells in the ONL was in the control group while the least number of cells were found in the flight stationary group; the width of the ONL was greatest in the control group and least in the flight stationary group; the average volume of an ONL cell was found to be greatest in the flight stationary group and the least in the flight centrifuge group.

DISCUSSION

Again, as on Cosmos #782, the method for preserving eye tissue had to be modified from routine perfusion of the animal, because the rest of the rat was needed for the many other experiments associated with this flight. Hence rapid enucleation and the sclera incision, as developed for the Cosmos #782 flight was necessary and again, it provided excellent fixation.

All the eyes were embedded in plastic for electron microscopy. 2 µm sections were taken from these blocks and viewed unstained under phase contrast light microscopy. This method allowed a large amount of tissue to be evaluated, but the silver stained 1 µm sections provided better resolution. Areas of interest were noted and ultra-thin sectioning per-

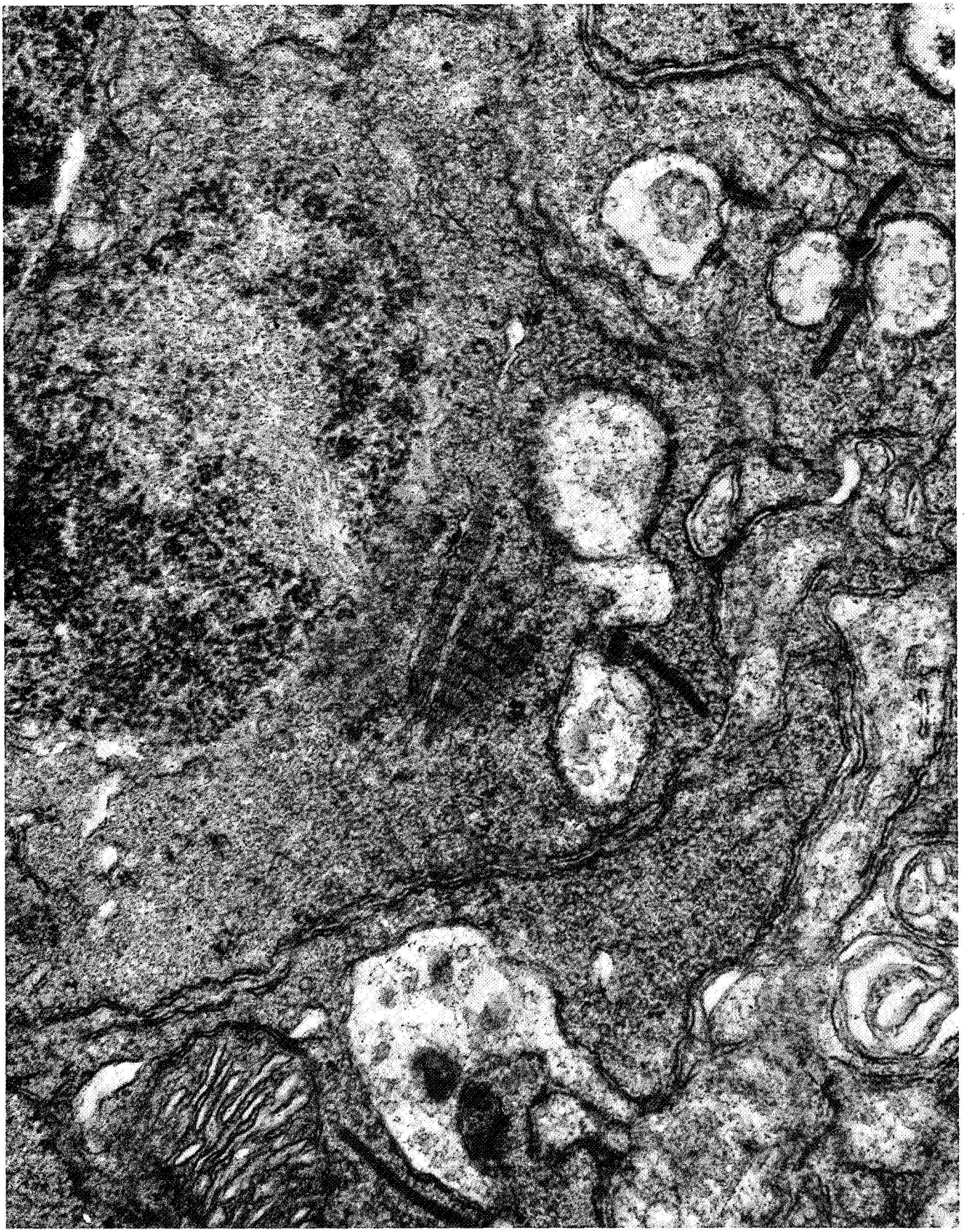

Figure 14 Flight stationary. The synaptic ribbon area at base of the ONL. Abnormal filamentous structure. Loose chromatin packing in adjacent nucleus is also evident. 57,200x

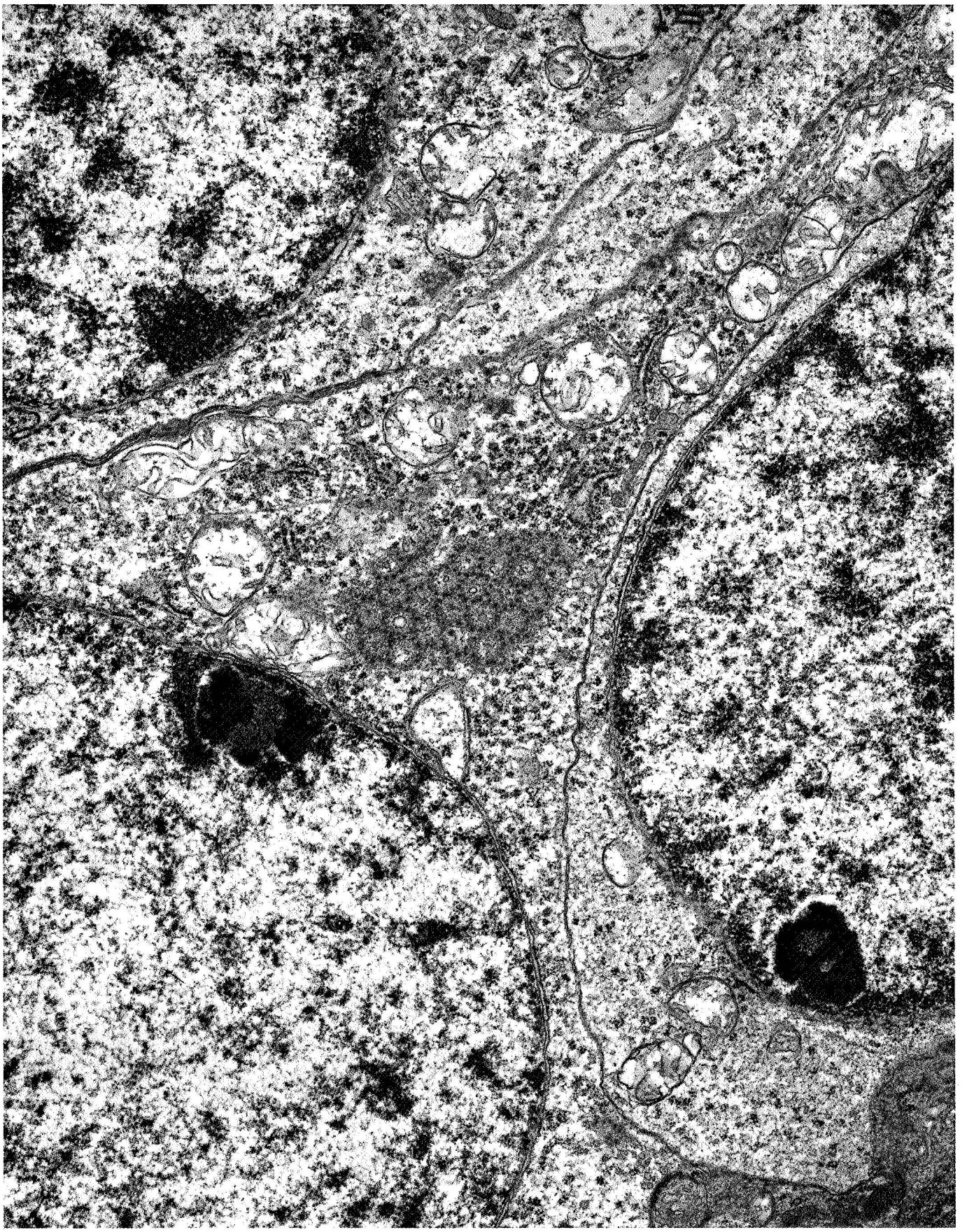

Figure 15 Flight stationary. Same eye. Filamentous, clustered, tubular structure in INL. May be a cross section of structure observed in figure 14. 20,300x

formed for electron microscopy. The sections were mounted on large mesh grids to enable viewing of the maximum amount of retina.

Besides the control eyes used for comparison, each eye also acted as its own control. Since the number of particles/cm^2 was fairly low, much of the retina in the flight eyes would be expected to be normal due to the low dose and uniqueness of particle radiation. The damaged cells were found to be widely scattered thoughout the retina. Areas adjacent to the alterations were examined for inadequate fixation and all were found to be normal.

It appears that some areas of the retina are particularly susceptible to radiation damage. Earlier predictions in our group (20) held that the ONL, packed with nuclei, would be a good area to study for radiation effects because a particle must pass through several nuclei in order to traverse this layer. This prediction now seems to be correct as many of the cellular alterations observed were in this layer. Here active synthesis occurs thoughout life. Membrane material is synthesized in the ONL cell and moves up to become part of the outer segment. As the outer segments are renewed their outer tips are phagocytized by the pigment epithelium. This active synthesis magnifies any pathological insult to ONL cells. An alteration of the synthesis process appears to manifest itself as vesiculated membranes and swollen ONL cells. The vesiculated membranes found in the rods may be due to improper synthesis of membrane material. The swelling in the inner segments and in the rods may be caused by this or it may be a response to direct damage to their structure. Cell necrosis in the retina seems to follow the same pattern after exposure to HZE particles at both Berkeley and during space flight. The cell swells and the cytoplasm breaks down, becoming

less dense. The double trilaminar membrane around the nucleus shows swelling between the membranes. This cellular enlargement is probably an osmotic response to molecular breakdown as the cell injests fluid. This is followed by cellular collapse which may be due to membrane dysfunction as active transport ceases.

In this experiment R+25 eyes were examined, whereas in experiment K-007 both R+0 and R+25 eyes were available for study. In experiment K-007 macrophages were seen at R+0 but none were found in the R+25 eyes. There were no macrophages in these R+25 flight eyes, but as in experiment K-007, there was increased phagocytotic activity in the pigment epithelium. It would seem that the macrophages form when a large amount of cellular debris is present and disappear when the pigment epithelium can ingest the excess. At the time of sacrifice, R+25, it seemed that the rate of phagocytotic activity had adjusted to the new load and the need for macrophages to aid in removal of debris was not necessary (9).

The pattern of cell necrosis in the retinas from the flight centrifuge group showed the same response to radiation as the flight stationary retinas from K-007 and K-207. This would indicate that hypogravity was not a factor in the observed results. Also the cellular response in the retinas exposed in the Berkeley accelerator again matched both the flight stationary and flight centrifuged retinas. Thus all three conditions provide comparable changes and this again indicates HZE particles as the possible cause of the channels, cellular alterations, and breakdown. Channels are also believed to be an osmotic response to molecular breakdown following damage to that area.

Even though DNA undergoes some repair (22) it is generally believed

that HZE particles break both stands of DNA. Correctly repairing a double break is more difficult and the nuclear damage could result in transcriptional or translational defects or even cell death. This provides a possible explanation for the altered membrane material seen in the outer segments and especially the membrane material seen (Figure 13) in a cell in the outer nuclear layer. The abnormal assembly of the membranes could be a consequence of the altered DNA.

Morphometrics has been implemented in an attempt to quantitate the response of the ONL. After dead cells are removed, they of course cannot be observed. Therefore, the digitizer was used to quantify the number of cells per unit area and the width of the ONL. Also, knowing that injured cells swell, the volume and the area were measured. Preliminary results indicate a narrowing of the ONL in the flight eyes and a decrease in total number of cells. This would indicate there were fewer cells in the flight eyes. This change was not observable by just looking at the pictures and could only be detected with the digitizer. The average nuclear volume also increased in the flight eyes again indicating an abnormal cellular response compared to the controls. Although these results are only preliminary, this method shows real promise for quantification of cell response. Further work is planned on these retinas and on the Berkeley-exposed tissue.

ACKNOWLEDGEMENT

The assistance of Katharine Kato, Andrea Baloun, and Marjorie Wilke for preparing slides, prints and technical assistance is greatly appreciated.

REFERENCES

1. Beckman, F. N., D. M. Hunter, and C. H. Bonney. 1973. Effects of heavy-ion, high energy particles upon the retinal vasculature of the Rhesus monkey. Lawrence Berkeley Laboratory, Document LBL-2016, pp. 63-74.

2. Benson, R. E., and L. S. Pinsky. 1972. Visual light flash phenomenon. NASA SP-315, pp. 17-27.

3. Budinger, T. F., J. T. Lyman, and C. A. Tobias. 1971. Visual perception of accelerated nitrogen nuclei interacting with the human retina. Lawrence Berkeley Laboratory, Document LBL-529, pp. 49-65.

4. Corbett, R. L. 1971. Modification for electron microscopy of the Corbett Ammoniacal Silver Stain. Proc. 29th Ann. Meeting Electron Microscopy Soc. Amer., pp.484-485.

5. Corbett, R. L. 1972. Rapid silver-formalin staining of epon-embedded sections for light microscopy. J. Ultrastructure Res. 38:214.

6. Corbett, R., D. E. Philpott, and S. Black. 1973. Prolonged fixation studies for spaceflight. Proceeding Electron Microscope Soc. Amer. 31:332.

7. Demirchoglyan, G. G. 1974. Visual effects of the eye-penetrating cosmic rays and high-enery particles. Biofizika 19:314-318.

8. Fazio, G. G., J. V. Jelley, and W. N. Charman. 1970. Generation of Cerenkov light flashes by cosmic radiation within the eyes of the Apollo astronauts. Nature 228:260-264.

9. Gurovskiy, N. N., O. G. Gazenko, A. W. Genin, Y. A. Ilyin, B. A. Adamovich, and A. A. Zlatorunskiy. 1976 Preliminary results of an experiment with mammals on the Kosmos-782 Biological Satellite. Institute of Medical and Biological Problems of the U.S.S.R., Ministry of Public Health, U.S.S.R., Moscow: Unpublished Report.

10. Kraft, L. M., M. A. Kelly, J. E. Johnson, Jr., E. V. Benton, R. P. Hence, D. E. Philpott, F. S. Vogel and W. Zeman. 1977. High-LET Neon (^{20}Ne) particle irradiation of the Pocket Mouse. (Perognathus longimembris). Effects on the brain, eyes and other head structures. (In preparation)

11, Mady, R., and P. J. McNulty. 1972. Frequency of light flashes induced by Cerenkov radiation from heavy cosmic-ray nuclei. Proc. Natl. Symposium on Natural and Man-made Radiation in Space, pp. 757-766.

12. Madey, R., and P. J. McNulty. 1970. Visual sensations induced in the dark-adapted eye by Cerenkov radiation from heavy cosmic-ray nuclei. Bull. Amer. Phys. Soc. 15:1671.

13. Malachowski, M. J., F. Abrams, J. T. Leith, and C. A. Tobias. 1975. Animal radio-biology-morphological damage. Progress Report, NASA P.O. T7163 B.

14. Malachowski, M. J., C. A. Tobias, and J. T. Leith. 1976. Effects of radiation upon light-sensing elements of the retina as characterized by scanning electron microscopy. Presented at 19th Plenary Meeting Cospar, June 16, 1976, Philadelphia, Pa, (to be published).

15. McNulty, P. J., V. P. Pease, L. S. Pinsky, V. P. Bond, W. Schimmerling, and K. G. Vosburgh. 1972. Visual sensations induced by relativistic nitrogen nuclei. Science 178:160-162.

16. Peterson, D. D., E. V. Benton, and M. Tran. 1976. HZE-Particle Dosimetry, Experiment K-103 for Kosmos 782. Technical Rept. 42, Department of Physics, University of San Francisco, San Francisco, CA.

17. Philpott, D. E., R. L. Corbett, S. Black, and C. Turnbill. 1973. Ultrastructural investigation of the "light flash" phenomenon seen by our astronauts, through exposure of pocket mouse and rabbit retina to X-ray, nitrogen, and oxygen irradidation. Lawrence Berkeley Laboratory, Document LBL-2016, pp. 172-178.

18. Philpott, D. E., R. Corbett, S. Black, and C. Turnbill. 1972. Ultrastructural investigation of the "light flash" phenomenon seen by our astronauts. Proc. Electron Microsc. Soc. Amer. 30:52.

19 Philpott, D. E., R. Corbett, and A. Takahashi. 1974. Histological examination of five pocket mice retinas after the flight of Apollo XVII. Aerospace Med. 45:352.

20. Philpott, D. E., R. Corbett, C. Turnbill, G. Harrison, D. Leaffer, S. Black, W. Sapp, G. Klein, and L. Savki. 1978. Cosmic ray effects of the eyes of rats flown on Cosmos No. 782, experiment K-007. Aviation Space and Environmental Medicine. Jan. 1978 pp.19.

21. Pinsky, L. S., W. Z. Osborne, J. V. Bailey, R. E. Benson, and L. F. Thompson. 1974 Light flashes observed by astronauts on Apollo 11 through Apollo 17. Science 183:957-959.

22. Powers, G. E., P. Keng and J. T. Lett. 1976. Damage to tissues of the central nervous system from heavy ions. NASA Progress Report.

23. Richardson, K. C., L. Jarett, and E. H. Finke. Embedding in epoxy resins for ultrathin sections in electron microscopy. Stain Tech. 35,313 (1960)

24. Tobias, C. A. 1952. Radiation hazards in high-altitude aviation. J. Aviat. Med. 23:345-372.

25. Tobias, C. A., T. F. Budinger, and J. T. Lyman. 1972 Human visual response to nuclear particle exposures. NASA TM X-2440, pp. 416-422.

26. Wick, G. L. 1972. Cosmic rays: Detection with the eye. Science 175:615-616.

27. Zeevi, Y. Y., C. A. Tobias, and E. R. Lewis. 1971 Initial studies on vertebrate retinal interaction with the nitrogen beam. Lawrence Berkeley Laboratory Rept. 529, pp. 67-73.

79.

N79-11679

COSMOS - 936

EXPERIMENT K-208

SPACEFLIGHT EFFECTS ON MUSCLE FIBERS

Kenneth R. Castleman, Ph. D.

Jet Propulsion Laboratory
Pasadena, California

Luis A. Chui, M. D.
Joseph P. Van Der Meulen, M. D.

USC School of Medicine
Los Angeles, California

ABSTRACT

Muscle fiber size and type distribution have been studied in the extensor digitorium longus (e.d.l.) muscle of fifteen COSMOS-936 rats. The groups studied include five flight stationary, five synchronous stationary, and five vivarium control animals. Of the three groups, average fiber diameter was largest in the vivarium control animals and smallest in the flight animals. Flight muscles appeared to be shorter than those of the other groups. Fiber number showed no significant difference. The e.d.l. contains predominantly "fast twitch" fibers. The "slow" fiber percentage was quite variable in these animals, and no statistically significant fiber type conversion was noted.

INTRODUCTION

Skeletal muscle is capable of two basic types of contraction. The so-called "Type I" fibers employ an oxidative type of energy metabolism and thus require an available oxygen supply. The "Type II" fibers utilize a glycolytic anaerobic energy metabolism. These fibers contract rapidly but are readily fatigued. Type I fibers contract more slowly but are quite fatigue resistant. It is widely believed that the slow fibers are particularly important in maintaining posture against gravity, while the fast fibers are required for quick, forceful movements.

Whether a muscle fiber employs an oxidative or glycolytic energy mechanism is not immutably fixed, but can be influenced by external factors. The factors which determine fiber type include (1) the type of innervation the fiber has, (2) the type and amount of exercise the fiber is called upon to perform, and (3) the occurrence and nature of electrical stimulation. Fiber types are also known to change during fetal development. It is well known that exercise causes the fiber size to increase while lack of exercise has the opposite effect. Furthermore, certain types of exercise produce more hypertrophy in one fiber type, while different activities are more effective on the other type.

Since space flight drastically alters the stimulus patterns to which skeletal muscle is exposed, it is relevant to investigate the changes which take place, not only in muscle fiber size, but also in the energy mechanism. This experiment uses histochemical preparation techniques and computer image analysis to quantify the space flight induced changes in muscle fiber size, number and energy metabolism. Rather than sampling each muscle only at a few positions along its length, this experiment seeks a quantitative total ascertainment of fiber size, number and type.

Material and Methods

Tissue Preparation. The extensor digitorium longus (e.d.l.) muscle was removed from the right leg at the time of sacrifice, placed in individual glass vials, and frozen in liquid nitrogen. Specimens were shipped at dry ice temperature to the USC Department of Neurology in Los Angeles, California. There the frozen muscles were embedded in OCT (optimal cryostat temperature) mounting medium and sectioned in a cryostat microtome. Every eleventh 10 micron thick section was mounted on a microscope slide with approximately nine sections per slide. Thus, each slide accounts for about 1 mm of muscle length.

Every fourth slide, starting with the first (i.e. 1,5,9,13,17, etc) was prepared with the 9.4. pH ATPase reaction[1] to distinguish fast from slow fibers. Every fourth slide, from the second, (i.e. 2,6,10,14, etc) was prepared with the NADH reaction.[2] Every fourth slide, from the third, (i.e. 3,7,11,15, etc) was prepared with the PAS reaction.[3] Every fourth slide, from the fourth, (i.e. 4,8,16, etc.) was prepared with 4.6 pH ATPase reaction.[4]

Quantitative Analysis. The slides from the first group (9.4 pH ATPase), numbering about 75 in all, were analyzed in the Medical Image Analysis Facility at the Jet Propulsion Laboratory. This facility includes a microscope mounted television camera capable of converting the specimen image into numerical form and feeding it into a computer for analysis. The digital image is a rectagular array of 512 by 512 optical density measurements.

If M is the power of the objective lens, the sample point spacing is 34.5/M microns and the sampled image field covers a 17.66/M milimeter square at the specimen.

Using a 16X or 20X objective lens, the operator selects for analysis a portion of the center section on the slide. The specimen image is digitized and processed in a PDP-11 minicomputer. The computer program isolates the individual fibers and measures the area, perimeter and average optical density of each.[5,6] The operator corrects any inaccuracies in the automatic fiber isolation step. Fiber diameter D is computed as the diameter of that circle having the same area A by the formula $D = 2\sqrt{A/\pi}$ This assumes that basically cylindrical fibers have to be pushed into polygonal cross sectional shape by close packing, and it assumes all fibers are cut normal to their axis. The fiber diameter measurement error is less than 3%.

The computer program produces a scatter plot showing how the fibers are distributed in diameter and optical density. The operator selects a density threshold which separates light (slow) from dark (fast) fibers and the program plots fiber diameter histograms (distribution curves) for both dark and light fibers. It also prints individual and mean fiber area and diameter measurements.

Several non-overlapping fields are processed on the central section from each slide until from 200 to 500 fibers have been measured. Then mean fiber diameter, mean fiber area, and light fiber percentage are tabulated for each slide. Also the total area of the central section is measured.

This is divided by the mean area of a single fiber in that section to estimate total fiber number. Section area is also used to compute e.d.l. diameter, assuming circular cross section, by the previous equation. The standard t-test of statistical significance is used to establish within what confidence limits the groupwise differences are significant.

Results

Histopathology. Upon histological examination, all slides appeared essentially normal. The PAS specimens showed no major accumulation of glycogen. Loss of mitochondria in the NADH specimens was not observed. There were no major cytoarchitectural changes, and necrotic changes and "moth eaten" fibers were not seen.

Muscle Size. Muscle diameter curves, averaged within each of the three rat groups, are presented in Figure 1. Each muscle cross sectional area has been converted to the diameter in mm which the e.d.l. would have if its cross sectional shape were circular. This quantity is used because it can be interpreted more easily than the directly measured cross sectional area from which it was derived. The curves for individual muscles were averaged within groups and the averages plotted versus length along the muscle from insertion (distal end) on the left, to origin (proximal end) on the right. Since the muscle sectioning process did not start at exactly the same position on each muscle, several of the curves from individual animals were shifted right or left before averaging by as much as a milimeter to effect approximate agreement at the left (distal)end. Over the major portion of muscle length, the vivarium animal muscles are the largest and the flight animal muscles are the

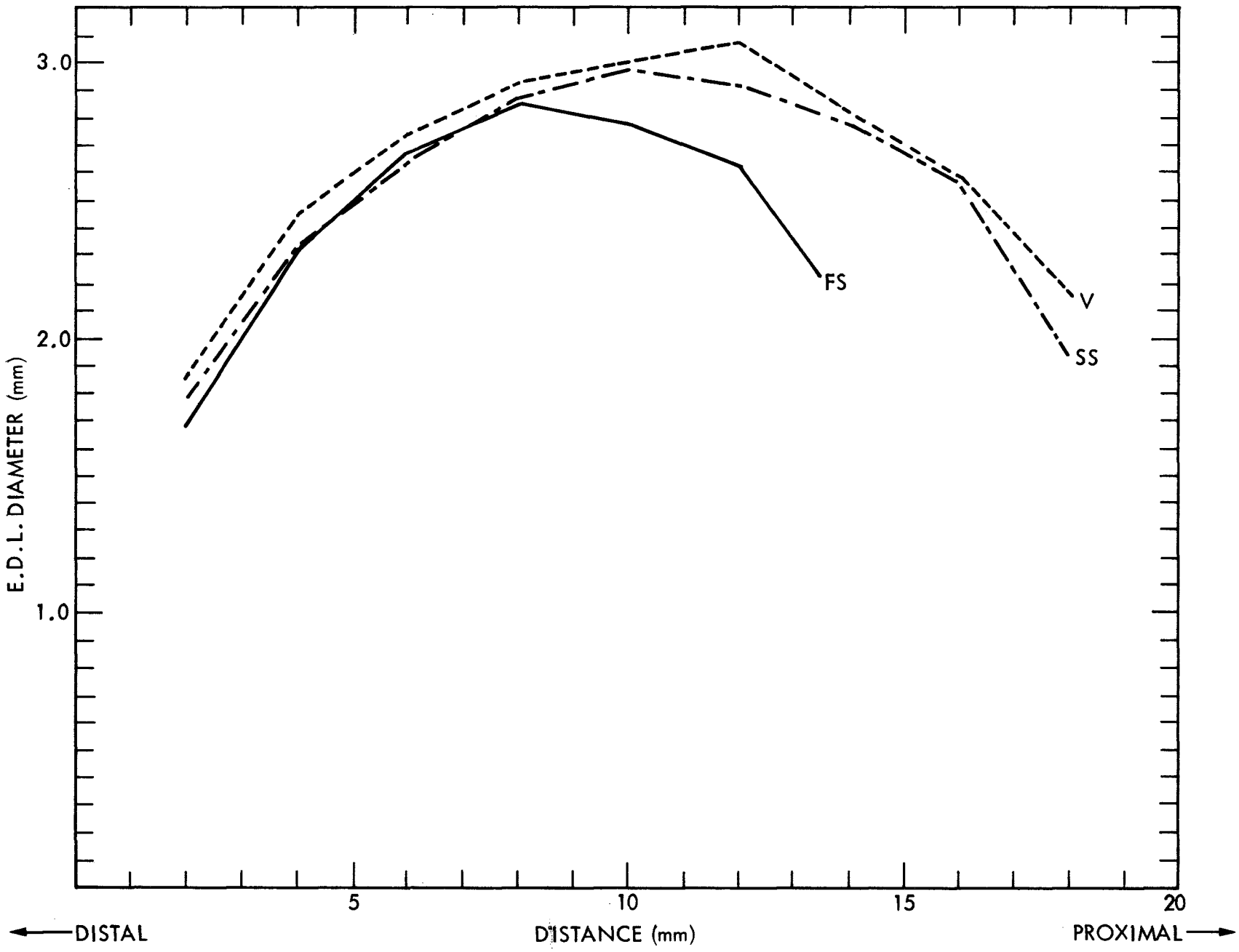

Figure 1. Average Muscle Diameter. This graph shows how e.d.l. diameter varies along its length. Diameter curves from individual animals have been averaged together by experimental group. FS: Flight Stationary, SS: Synchronous Stationary, V: Vivarium Control. Diameter differences of 0.24 mm or more are significant at the 95% confidence level ($p < 5\%$).

smallest. However, the variances are such that only differences greater than 0.24 mm are significant at the 95% confidence level. Table 1 presents data on individual animals.

Fiber Size. Figure 2 illustrates the groupwise averages of mean muscle fiber diameter versus distance along the muscle using the same horizontal scale as before. Again, diameter is computed as the diameter of that circle having the same area as the fiber. The differences among the three groups bear an extremely high degree of statistical significance. Here it is clear that, throughout the muscle, the vivarium animals have the largest, and the flight animals the smallest fibers.

Number of Fibers. Figure 3 shows the groupwise averages of the estimated number of fibers versus distance along the e.d.l. muscle for each animal. While the curves suggest that the flight animals have the most fibers and the vivarium animals the least, the within-group variances are high, and the differences are not statistically significant.

Fiber Type Conversion. Table 2 shows the percentage of light (slow twitch) fibers in the animals. The within-group variance is quite high and the groupwise differences are not statistically significant.

Discussion

Background. Previous flights in the COSMOS biosatellite series, involving similar exposures of rats to spaceflight conditions, have demonstrated atrophic and dystrophic changes in various muscles due to hypokinesis

TABLE 1, Rat Data

Rat Number		Launch Weight (grams)	Recovery Weight (grams)	E.D.L. Length (mm)	Mean E.D.L. Diameter (mm)	Mean Fiber Diameter (μm)
USA	USSR					
FS01*	6	212	300	16.17	2.30	41.78
FS02	7	208	246	15.07	2.23	42.23
FS03	8	199	290	19.25	2.26	43.70
FS04	9	208	286	13.53	2.60	39.64
FS05*	10	207	306	14.41	2.41	41.78
SS01	31	202	296	24.09	2.06	45.95
SS02	32	218	338	18.70	2.44	47.38
SS03	33	220	341	18.70	2.63	43.22
SS04	34	202	308	20.46	2.38	48.46
SS05	35	212	318	20.68	2.36	50.96
V01	56	214	306	18.92	2.65	49.40
V02	57	198	310	17.71	2.51	52.03
V03	58	190	276	20.57	2.48	49.48
V04	59	212	296	18.48	2.44	51.58
V05	60	210	300	19.58	2.56	47.58

* Fractured right femar 12 hr. before sacrifice.

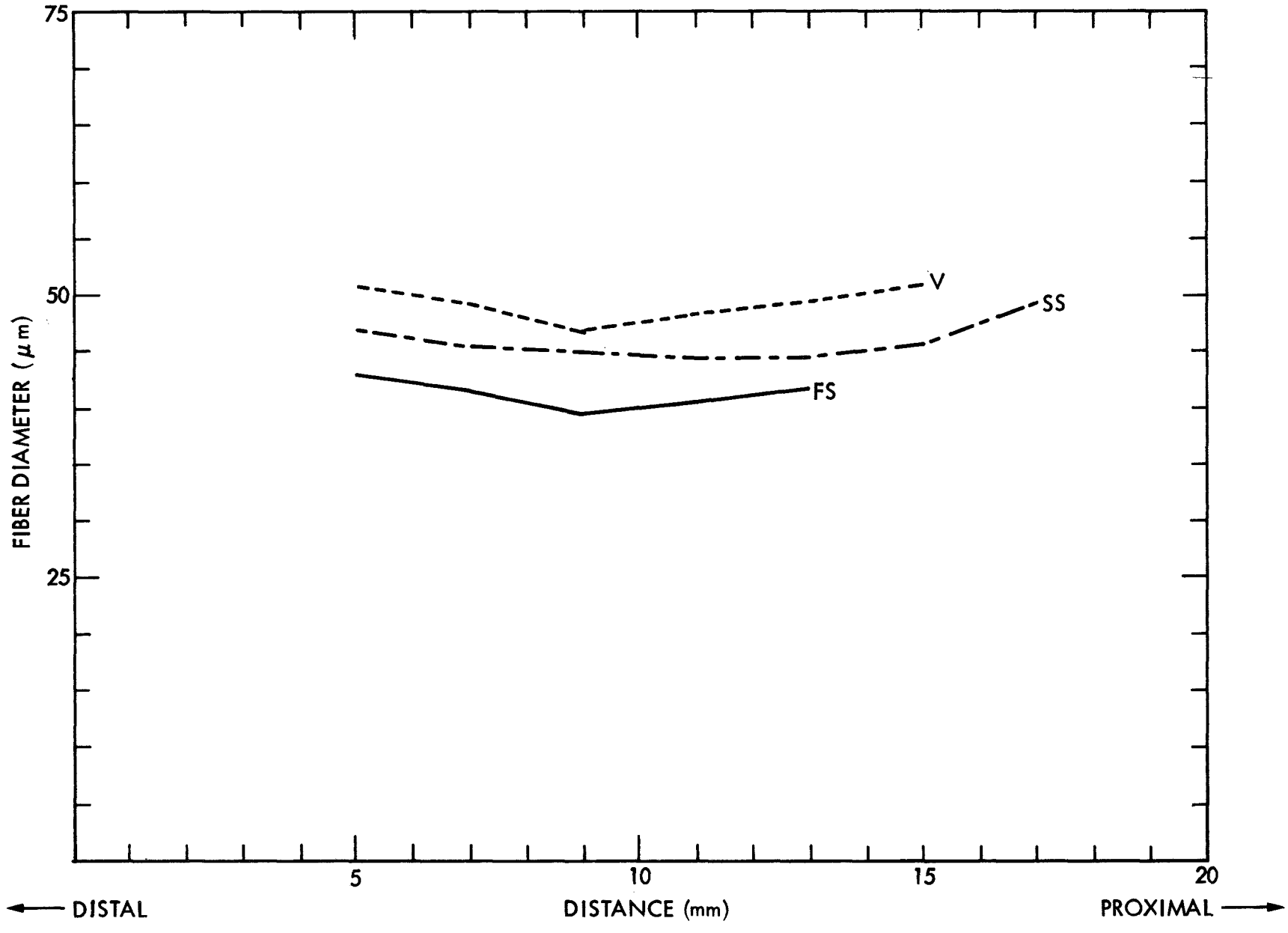

Figure 2. Average Fiber Diameter. The mean diameter of muscle fibers are plotted versus distance along the e. d. l. muscle as in Figure 1. Again, groupwise averages are presented. Statistically, the groupwise differences are highly significant.

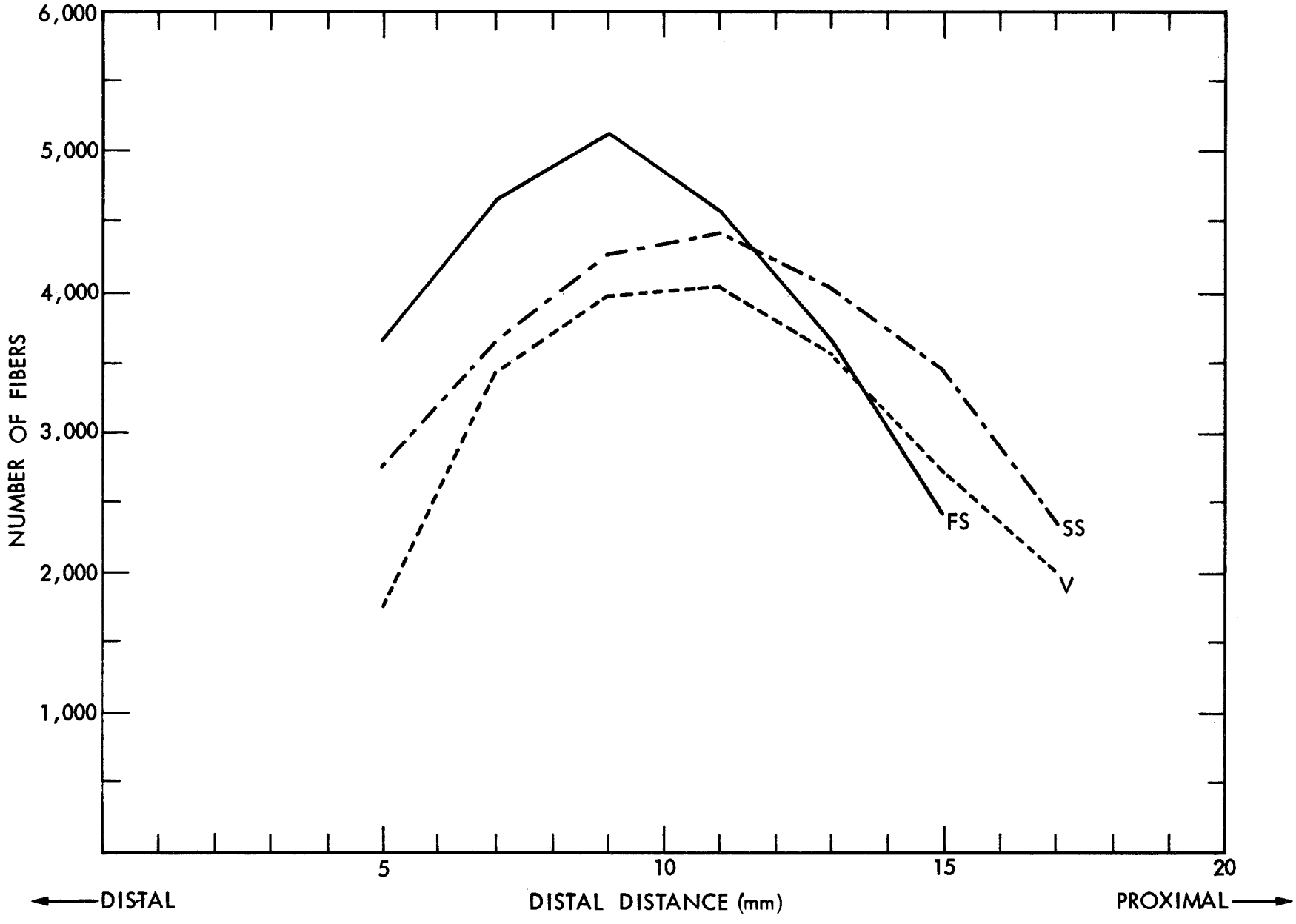

Figure 3. Average Number of Fibers. The estimated total number of fibers is plotted versus distance along the e. d. l. Fiber number is estimated as the ratio of tissue section area to mean fiber area. While this graph suggests that flight muscles are shorter and have more fibers, the variance within groups is so high that none of these differences is statistically significant.

TABLE 2

Rat Data Averaged by Experimental Group

GROUP	Age at Sacrifice (days)	Weight at Sacrifice (grams)	Feed Rate* (grams/day)	Fibers Counted	Mean Fiber** Diameter (μm)	% Slow*** Fibers	E.D.L.** Length (mm)	E.D.L.*** Diameter (mm)
Flight Stationary	82	286	51.4	8808	41.34	1.83	15.69	2.36
Synchronous Stationary	83	320	54.8	5728	46.32	0.59	20.53	2.37
Vivarium Control	89	298	40.0	4107	49.90	1.00	19.05	2.53

* During 18.5 day experiment.

** Statistically Significant Differences.

*** No Statistically Significant Differences.

and hypogravity. On the 22-day COSMOS-605 flight the weight of the e.d.l. muscle was 12% lower in flight than vivarium animals, and fiber area was down by 13%.[7] Changes in the soleus muscle were more pronounced, 32% down in weight and 22% down in fiber area. On those rats used in the radioisotope experiment the muscle weight changes were slightly larger: 18% for the e.d.l. and 37% for the soleus.[8] Both muscles exibited a decrease in strength and a slowing of the twitch response. In the soleus, contraction time was shorter in the flight animals.[9]

On the 20.5 day COSMOS-690 flight, which included a 24 hour exposure to an 800 rad dose of radiation, the soleus showed a 25% weight deficit, and the gastrocnemius a 19% weight deficit when flight animals were compared with vivarium controls.[10] In this experiment the e.d.l. showed no significant weight change. In the soleus the area of "red" fibers showed a 28.7% decrease while "intermediate" fiber area went down by 36.4%.

On COSMOS-782, the weight of the soleus was 38% lower in flight animals and 17% lower in the synchronous experiment than in vivarium controls.[11] In all previous flights the large mixed-fiber muscles (quadriceps, biceps and, except as noted above, gastrocnemius) failed to show significant weight changes.

The effects of hypergravity have been studied in rats which spent the first 3 months of life in a 2g centrifuge. Fiber type conversion was observed in the soleus muscle which went from 84% slow fibers in controls (16% intermediate fibers) to 100% slow fibers in experimental animals.[12] The soleus also showed a fiber diameter decrease in males. The plantaris

muscle showed statistically significant fiber diameter increases in females and decreases in males.

Muscle Size. Figure 1 suggests that the e.d.l. muscles from flight animals are shorter than those of the other two groups. The diameter differences are statistically significant to the right of the 10 mm point. If this length difference is not an artifact of dissection, it could be the result of chronic extension of the foot and/or toes during spaceflight. This would result if the opposing muscles (flexer digitorium longus, plantaris and soleus) lost tonus during flight. This figure also suggests that the total mass of the flight muscle is considerably lower than that of the other two groups.

Fiber Size. Figure 2 illustrates fiber diameter differences having extremely high levels of statistical significance. This strongly supports the contention that hypogravity aggravates the atrophic effects of hypokinesis. It also tends to confirm that the muscle weight losses observed in previous flights are due primarily to fiber atrophy. The groupwise grand mean fiber diameters in Table 2 show 17% and 7% fiber diameter reductions for the flight and synchronous control groups respectively when compared to the vivarium controls. Assuming uniform muscle length and number of fibers this would suggest 31% and 13.5% weight reductions in flight and synchronous muscles respectively — somewhat more than the 12 to 20% weight reductions of previous flights. However, muscle diameter (Fig. 1), length (Table 1) and number of fibers (Fig. 3) are rather variable from animal to animal. Hence, these differences do not represent a statistically significant departure from the results of earlier flights.

While reduced activity may be the major cause of fiber atrophy in spaceflight animals, other factors may contribute. For example, the stress of negotiating the near weightless environment could produce an ACTH-cortisol response. This could contribute to reduced fiber size.

It would be interesting to study fast, slow and mixed-fiber muscles from the same rats for fiber type conversion and fiber size changes. The results of these experiments would give a more complete picture of adaptation to spaceflight conditions.

Acknowledgements

The authors wish to thank Joan Higgins, who performed the histological preparation, Rick Gordon, who made helpful modifications to the muscle biopsy computer programs, and Cheryl Mills who collected the data using the automated system for muscle biopsy analysis.

References

1. Padykula, H. A. and E. Herman: The specificity of the histochemical method for ATPase. J. Histochem. Cytochem. 3:170, 1955.
2. Barka, T and P. J. Anderson: Histochemistry: Theory, Practice and Bibliography, New York; New York, 1963.
3. Manual of Histologic Stain Method of the Armed Forces Institute of Pathology, 3rd Edition, New York, McGraw-Hill Book Co., 1968.
4. Dubowitz, V. and M. H. Brooke: Histological and histochemical stains and reactions, in Muscle Biopsy: A modern approach; London; W. B. Saunders Co., Ltd., 1973, p. 20.

5. Castleman, K. R., J. P. Van Der Meulen, T. L. Munsat, H. J. Frieden and J. Higgins: Quantitative muscle biopsy analysis. Proceedings of the SPIE 89:119, 1976.

6. Van Der Meulen, J. P., L. A. Chui, T. L. Munsat and K. R. Castleman: Computer assisted quantitative analysis of muscle biopsy, preliminary observations. Neurology: 27:355, 1977.

7. E. I. Ilyina Kakueva, V. V. Portugalov, and N. P. Krivenkova, "Space Flight Effects on the Skeletal Muscles of Rats", Aviation, Space, and Environmental Medicine, Vol. 47, No. 7, pp. 700-703, July, 1976.

8. V. A. Kazaryan, E. A. Rapoport, L. A. Goncharova, and S. Ya. Bulycheva, "Effect of Prolonged Weightlessness on Metabolism of Proteins in Red and White Skeletal Muscles of Rats", Kosmicheskaya Biologiya I Aviakosmicheskaya Meditsina", No. 6, pp. 19-23, Moscow, 1977.

9. V. S. Oganov, and A. N. Potapov, "On the Mechanisms of Changes in Skeletal Muscles in the Weightless Environment", Life Scienes on Space Research, Vol. XIV, Akademie-Verlag, Berlin, 1976.

10. E. I. Ilyina-Kakueva, and V. V. Portugalov, "Combined Effect of Space Flight and Radiation on Skeletal Muscles of Rats", Aviation, Space, and Environmental Medicine, Vol. 48, No. 2, pp. 115-119, February, 1977.

11. V. V. Portugalov, "Morphological and Cytochemical Study of the Organs and Tissues of Animals on Cosmos-782", Academy of Sciences of the USSR Report, Moscow, October, 1975 (NASA Technical Translation F-17257, October, 1976).

12. W. D. Martin, and E. H. Romond, "Effects of Chronic Rotation and Hypergravity on Muscle Fibers of Soleus and Plantaris Muscles of the Rat", Experimental Neurology, Vol. 49, pp. 758-771, 1975.

1. Report No.	2. Government Accession No.	3. Recipient's Catalog No.
NASA TM-78526		

4. Title and Subtitle	5. Report Date
FINAL REPORTS OF U.S. EXPERIMENTS FLOWN ON THE SOVIET SATELLITE COSMOS 936	6. Performing Organization Code

7. Author(s)	8. Performing Organization Report No.
Susan Rosenzweig* and Kenneth A. Souza	A-7616
	10. Work Unit No. 199-91

9. Performing Organization Name and Address	11. Contract or Grant No.
NASA - Ames Research Center Moffett Field, Calif. 94035	

12. Sponsoring Agency Name and Address	13. Type of Report and Period Covered
National Aeronautics and Space Administration Washington, D.C. 20546	Technical Memorandum
	14. Sponsoring Agency Code

15. Supplementary Notes

*Northrop Services, Inc., 500 East Orangethorpe Avenue
Anaheim, Calif. 92801

16. Abstract

On August 3, 1977, the Soviet Union launched Cosmos 936, an unmanned spacecraft carrying biology and physics experiments from 9 countries, including both the Soviet Union and the U.S. The launch marked the second time the Soviet Union has flown U.S. experiments aboard one of its unmanned spacecraft, the first being Cosmos 782 launched Nov. 25, 1975, which remained in orbit 19.5 days. Aboard Cosmos 936 were: 1) 30 young male Wistar SPF rats, 20 of which were exposed to hypogravity during flight while the remainder were subjected to a 1 x g acceleration by continuous centrifugation; 2) experiments with plants and fruit flies; 3) radiation physics experiments; and 4) a heat convection experiment. After 18.5 days in orbit, the spacecraft landed in central Asia where a Soviet recovery team began experiment operations, including animal autopsies, within 4.5 hr of landing. Half of the animals were autopsied at the recovery site and the remainder returned to Moscow and allowed to readapt to terrestrial gravity for 25 days after which they, too, were autopsied. Specimens for U.S. experiments were initially prepared at the recovery site or Soviet laboratories and transferred to U.S. laboratories for complete analyses. An overview of the mission focusing on preflight, on-orbit, and postflight activities, and the final reports of the seven U.S. experiments flown on Cosmos 936 are presented.

17. Key Words (Suggested by Author(s))	18. Distribution Statement
Space biology Weightlessness Aerospace medicine	Unlimited STAR Category - 51

19. Security Classif. (of this report)	20. Security Classif. (of this page)	21. No. of Pages	22. Price*
Unclassified	Unclassified	296	$9.25

*For sale by the National Technical Information Service, Springfield, Virginia 22161